TESE DE DOUTORAMENTO

MECHANISTIC UNDERSTANDING OF MIXED-CULTURE FERMENTATIONS BY METABOLIC MODELLING

Alberte Regueira López

ESCOLA DE DOUTORAMENTO INTERNACIONAL

PROGRAMA DE DOUTORAMENTO EN ENXEÑARÍA QUÍMICA E AMBIENTAL

SANTIAGO DE COMPSOTELA

2020

USC
UNIVERSIDADE
DE SANTIAGO
DE COMPOSTELA

DECLARACIÓN DO AUTOR DA TESE

Mechanistic understanding of mixed-culture fermentations by metabolic modelling

D. Alberte Regueira López

Presento a miña tese, seguindo o procedemento axeitado ó Regulamento, e declaro que:

1) A tese abarca os resultados da elaboración do meu traballo.
2) De selo caso, na tese faise referencia ás colaboracións que tivo este traballo.
3) A tese é a versión definitiva presentada para a súa defensa e coincide coa versión enviada en formato electrónico.
4) Confirmo que a tese non incorre en ningún tipo de plaxio doutros autores nin de traballo presentados por min para a obtención doutros títulos.

Santiago de Compostela, a 16 de marzo de 2020

Asdo. Alberte Regueira López

USC
UNIVERSIDADE
DE SANTIAGO
DE COMPOSTELA

AUTORIZACIÓN DOS DIRECTORES DA TESE

Mechanistic understanding of mixed-culture fermentations by metabolic modelling

D. Juan M. Lema Rodicio, Profesor Emérito de Enxeñaría Química e Miguel Mauricio Iglesias, Investigador Posdoutoral do Departamento de Enxeñaría Química

INFORMAN

Que a presente tese, correspóndese co traballo realizado por D. ***Alberte Regueira López****, baixo a nosa dirección, e autorizamos a súa presentación, considerando que reúne os requisitos esixidos no Regulamento de Estudos de Doutoramento da USC, e que como directores desta non incorre nas causas de abstención establecidas na Lei 40/2015.*

Santiago de Compostela, 16 de marzo de 2020

Asdo. Juan M. Lema Rodicio Asdo. Miguel Mauricio Iglesias

USC
UNIVERSIDADE
DE SANTIAGO
DE COMPOSTELA

From elephant to butyric acid bacterium,

it is all the same!

Albert Kluyver

USC
UNIVERSIDADE
DE SANTIAGO
DE COMPOSTELA

Abstract

The biorefinery carboxylate platform is set to have a key role in the establishment of a more circular economy since in this production scheme organic wastes are transformed into added-value products such as bioplastics or biofuels. The first step is the production in anaerobic mixed-culture fermentations (MCF) of volatile fatty acids (VFA), a family of valuable compounds that are also used as substrate in subsequent processes to yield the final biorefinery products. One of the main issues of MCFs is their characteristic poor and variable product selectivity. The product spectrum is substantially influenced by environmental conditions without a systematic and mechanistic understanding or control. As a consequence, designing MCF processes targeting specific products is a challenging task and limits significantly the progress of the carboxylate platform. Therefore, the aim of this thesis is to develop predictive tools to gain insight of the mechanisms governing the stoichiometry of MCF under different environmental conditions and to use that knowledge to design MCF processes that allow for the selective production of the desired products.

The work performed in this thesis led to a more comprehensive and wider knowledge of MCF metabolism. In the case of glucose MCF, the inclusion of the biochemical mechanism electron bifurcation in the metabolic network and the consideration of the resource allocation theory in the mathematical models allowed to fully understand its metabolism and stoichiometry. For the first time, lactate production occurring only under a narrow operational condition space could mechanistically understood. The stoichiometry of VFA production from protein mono-fermentation and from its co-fermentation with carbohydrates can now be predicted at different operational conditions.

The mathematical models contributed in gaining insight of the mechanisms linking the environmental conditions of the reactor and the product selectivity of the MCF processes. The substrate composition and the reactor configuration and pH were identified as the operational conditions with the highest influence on the product spectrum. The models shown that the different substrates may interact in the fermentation and compete for shared resources. These relationships are directly correlated with the concentration of the substrates involved and therefore the proportions between the substrates have an impact on the global stoichiometry of the process. The reactor configuration proved to exert an influence on the outcome of microbial competition. Discontinuous

processes foment the domination of the microorganisms that consume fast the substrate, while continuous processes with low residual substrate concentration favour the prevalence of energetically efficient microorganisms. The reactor pH was shown by the models to have a strong connection with the energy harvesting of the different metabolic pathways, favouring, in this way, the production of certain VFA depending on its value.

In this thesis mathematic models proved to be excellent tools for gaining insight into the mechanisms governing MCF. However, they also present a strong potential as tools to design MCF processes targeting the production of specific VFA with a high productivity, as shown in several examples throughout the thesis. We believe that the knowledge gained and the models developed in this thesis will be of great help to pave the way to the establishment of the biorefinery as a sound and viable production scheme for the transition towards a circular economy.

Keywords: mixed-culture fermentation, volatile fatty acids, mathematical models, product selectivity, bioprocess design, mechanistic insight.

LIST OF CONTENTS

ABBREVIATIONS AND ACRONYMS

AA	Amino acid
ADP	Adenosine 5'-diphosphate
Ala	Alanine
Arg	Arginine
Asn	Asparagine
Asp	Aspartate
ATP	Adenosine 5'-triphosphate
BPB	Butyrate-producing bacteria
COD	Chemical oxygen demand
CSTR	Continuous stirred tank reactor
CV	Coefficient of variation
Cys	Cysteine
D	Dilution rate
E	Redox potential
EB	Electron bifurcation
EC	Electron carrier
FBA	Flux balance analysis
Fd_{ox}	Oxidised ferredoxin
Fd_{red}	Reduced ferredoxin
ΔG	Gibbs free energy of reaction
Gln	Glutamine
Glu	Glutamate
Gly	Glycine
HA	Homoacetogenesis
His	Histidine
HRT	Hydraulic retention time
Ile	Isoleucine
LAB	Lactic acid bacteria
Leu	Leucine

L_{liq}	Liter of liquid (excluding biomass)
L_r	Liter of reactor
L_X	Liter of biomass
Lys	Lysine
MCF	Mixed-culture fermentation
Met	Methionine
NAD(H)	Nicotinamide adenine dinucleotide
OD	Optic density
OLR	Organic loading rate
PHA	Polyhydroxyalkanoates
pmf	Proton motive force
Pro	Proline
R_i	Reaction rate (mol/L·h)
RMSD	Root-square-mean deviation
R_T	Transport rate (mol/L·h)
SBR	Sequential batch reactor (SBR)
Ser	Serine
Sex	Extracellular concentration (mol/L)
Sin	Intracellular concentration (mol/L)
SIR	Substrate-to-inoculum ratio
SLP	Substrate-level phosphorylation
SRT	Solids retention time
S_X	Biomass concentration (mol/L)
TAN	Total ammonia nitrogen
Thr	Threonine
Val	Valine
VFA	Volatile fatty acid

RESUMO

USC
UNIVERSIDADE
DE SANTIAGO
DE COMPOSTELA

Capítulo 1. Introdución e contexto

O actual modelo económico baseado no uso masivo de recursos fósiles está comezando a súa transición cara un esquema socioeconómico máis circular en resposta a un futuro escenario de altos e inestables prezos de petróleo e á demanda da sociedade de apostar por este tipo de modelos. Neste contexto enmárcase o concepto de biorrefinería, un esquema de produción no que a biomasa (residuos orgánicos ou madeira) é transformada nun espectro de produtos e enerxía con valor de mercado como plásticos, combustibles ou electricidade. As biorrefinerías pretenden ser tan flexibles como as tradicionais refinerías de petróleo e producir baixo demanda un abano de produtos dende un número reducido de materias primas.

Dentro dos diferentes tipos de biorrefinería, destaca a plataforma dos ácidos carboxílicos xa que se centra en empregar residuos orgánicos como substratos. Neste esquema de biorrefinería o substrato é transformado nunha primeira etapa de fermentación anaerobia a unha mestura de ácidos carboxílicos ou ácidos graxos volátiles (AGV), coma o acético ou butírico, e alcois que son finalmente convertidos en produtos de alto valor engadido como bioplásticos ou biocombustibles. Os AGV actúan de nexo entre os residuos orgánicos e os compostos finais e, polo tanto, o proceso de fermentación anaerobia é primordial para o esquema da plataforma dos ácidos carboxílicos. Porén, un dos principais problemas das fermentacións anaerobias é que o seu espectro de produtos adoita ser unha mestura de AGV cunha composición que depende tanto dos parámetros de operación como do substrato empregado.

No contexto da plataforma dos ácidos carboxílicos, as fermentacións anaerobias adoitan ser realizadas por unha comunidade microbiana mixta e non definida e xeralmente denomínanse fermentacións en cultivo mixto (FCM). En contraposición co uso de cultivos puros, os cultivos mixtos permiten empregar substratos non esterilizados como os residuos orgánicos, o que diminúe notablemente os custos de operación e permite procesos en réxime continuo. Ademais, os cultivos mixtos conteñen unha ampla variedade de funcións metabólicas, o que lles permite consumir substratos complexos que precisan varias transformacións e ser máis resistentes a cambios nas condicións ambientais.

Nas FCM, un cambio nas condicións ambientais adoita provocar un cambio no espectro de produtos. Isto abre a porta a poder dirixir que AGV se producen no

proceso variando parámetros de operación. Na literatura científica téñense identificado certos parámetros que inflúen notablemente no espectro de produtos. Entre eles destacan a composición do substrato e en maior medida o pH do reactor. As proporcións entre os distintos substratos dunha fermentación inflúen sobre as estequiometrías individuais dos substratos xa que existen interaccións entre eles. O pH do reactor ten un alto impacto no espectro de produtos e un valor pode facer desaparecer produtos que son maioritarios noutras condicións. Ademais, esta variable ten o atractivo adicional de que é moi sinxela de manipular en calquera montaxe experimental. Polo tanto, unha das principais preguntas que trata de responder esta tese é ata que punto se pode controlar e dirixir a selectividade do proceso coas condicións de operación. Dado que o coñecemento mecanístico sobre a influencia destes parámetros é limitado, cómpre desenvolver ferramentas preditivas para coñecer os mecanismos que ligan as condicións ambientais e a estequiometría do proceso. Este coñecemento, ademais, proporcionaranos a capacidade de deseñar procesos altamente selectivos naqueles produtos desexados.

Os modelos matemáticos son ferramentas que permiten interpretar e predicir diversos fenómenos naturais. Poden ser empregados para validar novas hipóteses ou para predicir e deseñar procesos, un aspecto cun gran atractivo xa que reducen notablemente a necesidade de traballo experimental. Deste xeito, o seu potencial para seren empregados en sistemas biolóxicos e, en particular, nas FCM é moi elevado. Na literatura científica xa existe un coñecemento axeitado, aínda que non completo, sobre a modelaxe da FCM de carbohidratos como a glicosa. Porén, o coñecemento sobre a FCM doutros tipos de substratos como as proteínas é moito máis limitado.

O obxectivo principal desta tese é comprender os mecanismos que controlan as FCM e como están afectadas polas condicións ambientais empregando modelos matemáticos. O coñecemento adquirido e as ferramentas desenvolvidas tamén se empregarán co obxectivo de deseñar procesos de FCM cunha alta selectividade nos compostos desexados para facilitar o establecemento da biorrefinería como un esquema de produción viable técnica e economicamente.

En particular, nesta tese, preténdese responder ás seguintes preguntas científicas:

- **Cal é o efecto da composición do substrato nas FCM?** Cal é o espectro de produtos na fermentación de proteínas? Quedaría afectado no caso de cofermentar a proteína con outros substratos?

- **Como afectan os parámetros de operación no resultado das FCM?** Como se comporta o espectro de produtos a diferentes condicións de operación?
- **É posible dirixir o espectro de produtos das FCM cara produtos específicos?** Ata que punto se pode modificar o espectro de produtos variando as condicións de operación e a composición dos substratos?

Capítulo 2. Desenvolvemento do modelo

Este capítulo céntrase na descrición detallada dos modelos matemáticos desenvolvidos nesta tese. Pódense distinguir pola súa estrutura e obxectivo dous tipos de modelo: modelos bioenerxéticos e modelos cinéticos.

Os modelos bioenerxéticos teñen como obxectivo a predición da estequiometría do sistema a diferentes condicións de operación. O seu cometido é determinar cal é o espectro de produtos máis probable tendo en conta o substrato e as condicións ambientais do reactor. Para seleccionar os produtos óptimos, asumen que os microorganismos producen aqueles AGV que lles permiten obter a maior enerxía posible do substrato en forma de ATP. Son modelos baseados en primeiros principios e polo tanto teñen un número moi limitado de parámetros que depende do sistema en particular a simular.

Os modelos cinéticos son aqueles que se centran en describir as dinámicas do proceso (a velocidade de produción dos diferentes AGV, as posibles inhibicións por produtos, etc.). Ó contrario que os modelos bioenerxéticos, a maioría dos seus parámetros son específicos para cada proceso e polo tanto necesitan ser calibrados con datos experimentais en cada sistema a simular (p. ex. se a proteína a simular é diferente ou mesmo se o pH do reactor é modificado).

Capítulo 3. O mecanismo de bifurcación de electróns e a homoacetoxénese explican a produción en fermentacións anaerobias en cultivo mixto.

A fermentación de glicosa en cultivos mixtos está estudada en profundidade na literatura científica tanto dende un punto de vista experimental como de modelaxe. En particular, o efecto do pH do reactor no espectro de produtos resulta de interese xa que exerce unha gran influencia. Os modelos matemáticos máis recentes para a predición da estequiometría do proceso son capaces de capturar correctamente os cambios observados experimentalmente no espectro

de produtos co pH. Deste xeito, predín unha transición dende ácido butírico a etanol e ácido acético cando o pH cambio de ácido a alcalino. Porén, aínda non son capaces de predicir con precisión o espectro observado experimentalmente. A pH baixos os modelos predín que a gran maioría da glicosa é transformada a ácido butírico, mentres que os experimentos mostran un espectro dominado por unha mestura equimolar de ácido butírico e acético. Este desfase nas predicións pode estar debido a que a rede metabólica que empregan os modelos non estea completa e actualizada. Neste capítulo inclúese na rede metabólica o mecanismo bioquímico bifurcación de electróns co obxectivo de comprobar se permite aumentar a precisión das predicións do modelo.

Unha nova rede incluíndo este mecanismo comparouse coa rede que empregaban os modelos actuais. Para isto, desenvolveuse unha metodoloxía baseada en realizar balances de NADH a diferentes series de resultados experimentais na literatura, xa que unha rede correcta debe producir balances pechados de NADH. Os resultados indican inequivocamente que a inclusión da bifurcación de electróns na ruta de produción do butírico permite pechar mellor o balance de NADH en todos os datos analizados, indicando claramente que a nova rede é máis completa e precisa.

A inclusión da bifurcación de electróns na rede da glicosa implica tamén que a relación predito polo modelo entre H_2 e CO_2 deixe de ser equimolar, xa que hai unha produción adicional de H_2 na nova ruta do ácido butírico. Para conciliar este feito coas medidas experimentais gasosas que mostran unha relación equimolar, proponse que o proceso de homoacetoxénese (o consumo de H_2 e CO_2 para producir ácido acético) é a causa máis probable para explicar cuantitativamente os datos experimentais.

Os resultados deste traballo indican que todas as rutas de produción de ácido butírico, independentemente do substrato do que partan, deben considerar a inclusión deste mecanismo bioquímico para poder predicir correctamente o espectro de produtos.

Capítulo 4. A teoría de asignación de recursos explica a produción de ácido láctico en fermentacións anaerobias en cultivo mixto.

O traballo deste capítulo céntrase na predición da produción en FCM de glicosa de ácido láctico, un dos ácidos carboxílicos máis producidos con aplicacións no eido da industria farmacéutica e alimentaria. Experimentalmente só se observou

a súa produción en FCM en condicións de operación moi específicas. O reactor ten que ser operado en modo descontinuo e no medio de cultivo cómpre que haxa aminoácidos e certas vitaminas presentes, xa que as bacterias acidolácticas son auxotróficas para estes compostos. Os modelos de predición de estequiometría en FCM asumen que os microorganismos xeran aqueles produtos que lles permiten obter a máxima produción de ATP por unidade de substrato. O lactato só produce 2 moléculas de ATP por cada molécula de glicosa convertida en comparación coas 3 ou 4 que se producen cando o produto é o ácido butírico ou acético, respectivamente. Dado o seu baixo rendemento en ATP, os modelos non o predín baixo ningunha circunstancia e non son capaces de reproducir o observado experimentalmente. Polo tanto, é obvio que ademais de motivos enerxéticos (rendemento en ATP) se necesitan outros argumentos para explicar mecanisticamente por que se produce lactato nesas condicións experimentais.

Neste capítulo desenvolveuse un modelo matemático que inclúe conceptos da teoría de asignación de recursos (usualmente coñecida pola súa denominación en inglés: *resource allocation*). Esta teoría establece que os distintos procesos celulares (crecemento ou catabolismo) compiten por unha cantidade finita de recursos, entre os cales o máis limitado é a capacidade proteica ou encimática. O modelo predí que a produción de ácido láctico se favorece naqueles escenarios nos que a selección microbiana se fai de acordo á velocidade máxima de crecemento, é dicir, naqueles ambientes nos que hai unha concentración elevada de substrato, como en reactores en descontinuo ou en reactores en continuo cun tempo de dilución moi elevado, sempre e cando o medio de cultivo conteña aminoácidos e vitaminas. En calquera outras condicións ambientais, como nun reactor en continuo limitado por substrato, a produción doutros AGV como o ácido acético ou butírico é o resultado esperado da FCM de glicosa. O modelo é quen de identificar que a auxotrofía para aminoácidos das bacterias acidolácticas resulta ser unha vantaxe competitiva xa que lles permite atinxir unha velocidade de consumo de substrato específica máis elevada ó poder reasignar os recursos da produción de aminoácidos a outras tarefas.

As conclusións deste capítulo permiten delimitar as condicións nas que optimizar exclusivamente en base ó rendemento en ATP dos produtos é unha estratexia correcta.

Capítulo 5. Modelo bioenerxético para a predición da estequiometría de fermentación de proteína.

Unha serie de residuos orgánicos axeitados para ser usados na plataforma dos ácidos carboxílicos teñen unha concentración elevada de proteínas, como, por exemplo, residuos da industria conserveira ou cárnica. O espectro de produtos da FCM de proteínas tamén é moi sensible a condicións de operación como o pH, tal como mostra a literatura científica, pero a nosa comprensión sobre o comportamento do sistema é aínda moi limitado. Ademais, non hai ningunha ferramenta preditiva para a comprensión e predición da estequiometría destes procesos, o que dificulta o deseño procesos de produción selectiva de AGVs a partir de residuos ricos en proteínas no contexto da plataforma dos ácidos carboxílicos. O obxectivo deste capítulo é desenvolver un modelo bioenerxético para a conversión de proteínas a AGV con especial fincapé en entendermos como afecta o pH do reactor á estequiometría do sistema.

O modelo considera as proteínas como unha mestura de aminoácidos e simula a acidificación de 17 aminoácidos a etanol e ácido carboxílicos de cadeas de 1 a 6 átomos de carbono. Os resultados do modelo para a proteína xelatina indican que o espectro de produtos está dominado polo xeral por ácido acético e propiónico a pH neutros e alcalinos. A medida que se acidifica o reactor (a valores do pH inferiores a 6), a produción de ácido butírico comeza a incrementarse e a valores de pH máis baixos que 5, acaba por ser un dos produtos dominantes do espectro, cunha produción másica semellante á do ácido acético e propiónico. Cando se comparan estas predicións con experimentos de literatura, compróbase que o modelo é capaz de predicir correctamente a estequiometría de produción de AGVs a pH 7 e 5.3 e que ademais captura correctamente os cambios observados na estequiometría ó cambiar o pH.

Pola natureza mecanística do modelo desenvolto neste traballo, puidéronse identificar os posibles mecanismos que provocan estes cambios na estequiometría do proceso. Unha baixada do pH do reactor provoca un aumento da enerxía que se pode conservar en forma de ATP nas rutas de produción de ácido butírico dalgúns aminoácidos, como o glutamato. Ademais, o modelo tamén propón que algúns aminoácidos interaccionan entre si principalmente a través do consumo ou produción de poder redutor (NADH). Isto indica que a estequiometría de acidificación individual destes aminoácidos pode verse modificada se se modifican as concentracións relativas de aminoácidos, é dicir, se a proteína fermentada é outra.

Capítulo 6. Modelo bioenerxético para a predición de estequiometría de co-fermentación de proteínas e carbohidratos.

Este capítulo continúa o traballo realizado no anterior capítulo e aborda a co-fermentación de proteínas con carbohidratos. A maioría de residuos con potencial uso en esquemas de biorrefinería presentan concentracións significativas de proteínas e carbohidratos, como o soro láctico ou certos residuos da industria conserveira. Polo de agora non existen ferramentas de predición da estequiometría que teñan en contas as posibles interaccións entre substrato nun proceso de cofermentación. Polo tanto, este capítulo céntrase na comprensión e predición da estequiometría de co-fermentacións de proteínas e carbohidratos en cultivos mixtos mediante o uso de modelos matemáticos. É de especial interese o efecto que o pH do reactor e as proporcións entre proteína e carbohidrato teñen sobre o espectro de produtos do proceso.

O modelo simula a conversión conxunta de 17 aminoácidos e glicosa e considera as posibles interaccións entre todos os substratos. Os resultados indican claramente que a estequiometría está moi ligada tanto ó pH do reactor como ás proporcións entre os co-substratos. Para a co-fermentación de xelatina e glicosa, as mesturas ricas na proteína favorecen, a produción de ácido acético independentemente do pH do reactor, e as mesturas ricas en glicosa a produción de ácido butírico. Outros AGV teñen comportamentos distintos. Por exemplo, a produción de ácido propiónico é máxima a valores de pH intermedios mentres que as proporcións entre co-substratos non lle afectan moito. O modelo é capaz de reproducir os poucos resultados experimentais da literatura científica e é quen de capturar correctamente o efecto na estequiometría do proceso de engadir glicosa a un mono-fermentación de xelatina.

A variación do espectro de produtos está debida a que cada substrato aporta a súa estequiometría específica de acidificación e que, ademais, os co-substratos (é dicir, a glicosa e cada un dos aminoácidos) interaccionan entre si, o que modifica parcialmente as súas estequiometrías individuais. Coma no caso da monofermentación de xelatina no anterior capítulo, as interaccións entre co-substratos tamén acontecen en torno ó consumo e produción de poder redutor (NADH). As rutas máis favorables enerxeticamente dalgúns substratos veñen acompañadas por unha produción neta de NADH, o que forza a outros substratos a ser convertidos en rutas menos favorables, xa que globalmente a produción de ATP se ve incrementada.

Ademais, exemplifícase a potencialidade deste modelo á hora de deseñar procesos que permitan a produción selectiva dos AGV desexados cunha serie de casos de estudo, como a optimización da produción de AGV nunha co-fermentación de xelatina e glicosa para ser utilizados como substrato na produción biolóxica de bioplásticos.

Capítulo 7. Modelo cinético da fermentación anaerobia en cultivo mixto de proteína.

Os anteriores capítulos estiveron centrados na comprensión e predición da estequiometría de acidificación a diferentes condicións de operación (pH do reactor e proporcións entre co-substratos). Este capítulo aborda o estudo do comportamento cinético e como se ve afectado por variacións nas condicións de operación.

Os modelos cinéticos dispoñibles na literatura non se adaptan ás características do proceso de fermentación polo que non poden ser usados con esta fin. Empregan parámetros cinéticos estimados en ambientes metanoxénicos (que son diferentes ós fermentativos) e non consideran a variabilidade da estequiometría do proceso coas condicións ambientais. Neste capítulo, construíuse e calibrouse un modelo cinético para a FCM de proteínas, empregando datos de experimentos expresamente deseñados para a ocasión con dúas proteínas, caseína e xelatina. Os parámetros estimados mostran que tanto o pH do reactor como o substrato (que proteína se fermenta) afectan o comportamento cinético do proceso.

Neste capítulo proponse un esquema de simulación de fermentación de proteínas en cultivos mixtos integrando datos experimentais e os modelos desenvoltos nesta tese para a predición da estequiometría e do comportamento cinético. Coas directrices presentadas, pódese simular a produción de AGV a partir de distintas proteínas a diferentes valores de pH. A finalidade é mostrar a utilidade das ferramentas preditivas desta tese máis aló de proporcionarmos coñecemento sobre os fenómenos que rexen o proceso.

Capítulo 8. Discusión e conclusións xerais.

Neste capítulo intégranse os principais resultados e conclusións do traballo desenvolto na tese co obxectivo de responder as preguntas presentadas na introdución desta tese: cal é o efecto da composición do substratos e dos parámetros de operación no resultado das FCM? É posible dirixir o espectro de produtos cara certos produtos?

Os resultados desta tese indican que tanto a selectividade do sistema como o seu comportamento cinético están ligados á composición do substrato. No relativo á selectividade, os modelos conclúen que os co-substratos que compoñen a alimentación interaccionan entre si e que as súas estequiometrías individuais de conversión a AGV se poden ver afectadas pola abundancia relativa dos co-substratos. Identificouse que as interaccións son debidas ó consumo e produción de poder redutivo (NADH), xa que en sistemas anaerobios o seu balance ten que ser nulo. Aínda así, os efectos das interaccións son limitados e, polo xeral, a estequiometría final depende en boa medida das estequiometrías individuais dos co-substratos. No estudo cinético de fermentacións de proteína, concluíse que a composición do substrato (é dicir, o perfil de aminoácidos das proteínas) inflúe no comportamento cinético do sistema. En xeral, a caseína mostrouse como un substrato que se consome sensiblemente máis rápido que a xelatina e que permite unha maior velocidade de crecemento ás poboacións que a consomen respecto ás que consomen xelatina.

Os parámetros de operación amosaron aínda unha maior influencia no resultados das FCM. O pH do reactor exerce unha notable influencia no espectro de produtos, en especial na fermentación de glicosa, e segundo o seu valor AGV como o ácido butírico poden pasar de ser produtos dominantes a non producirse. Como normal xeral, valores ácidos do pH incrementan a presenza de ácido butírico no espectro de produtos tanto na mono-fermentación de proteínas como na súa co-fermentación. A través dos modelos, púidose identificar o aumento da enerxía conservada nas translocacións de protóns na ruta do ácido butírico como o mecanismo responsable deste cambio na selectividade. O pH tamén demostrou a súa influencia no comportamento cinético do proceso, independentemente da proteína a fermentar. Como regra xeral, observouse que a valores neutros do pH a velocidade de consumo do substrato e crecemento é máxima, diminuíndo máis en caso de pH acedos que básicos. A configuración do reactor tamén ten unha influencia notable na selección das poboacións dominantes na fermentación de glicosa. Reactores que operan en descontinuo favorecen que bacterias acidolácticas dominen a comunidade. Pola contra, os reactores en continuo favorecen a presenza de bacterias que producen ácido acético ou butírico ou etanol. Cun modelo desenvolto nesta tese e baseado na teoría de asignación de recursos, identificouse que a auxotrofía típica das bacterias acidolácticas lles permite ter unha maior capacidade de consumo do substrato que as outras especies. Así, son capaces de desprazar outras especies naqueles ambientes nos que prima ser o máis eficaz en consumir o substrato e

non o máis eficiente, como naqueles reactores con elevadas concentracións de substrato.

Os resultados da tese permiten concluír que si é posible controlar a selectividade das FCM mediante as condicións de operación. En concreto, identificáronse tres variables de deseño cun alto potencial para esta fin: o pH do reactor, a composición do substrato e a configuración do reactor (esta última variable só foi estudada no caso de glicosa). De entre eles destaca o pH do reactor xa que é unha variable de fácil manipulación en calquera instalación experimental e porque é capaz de alterar radicalmente o espectro de produtos resultante.

A presente tese contribúe, pois, ó coñecemento dos mecanismos que rexen as fermentacións en cultivo mixto prestando unha especial atención a aqueles que determinan a estequiometría de produción de AGVs. Este coñecemento foi adquirido mediante o desenvolvemento de ferramentas preditivas (modelos matemáticos). Ademais, estas ferramentas posúen un potencial de cara ó deseño de bioprocesos, para deste xeito poder desenvolver FCM cunha alta selectividade e produtividade nos AGV desexados, axudando así ó establecemento das biorrefinerías como esquema de produción válido para a transición a unha economía circular.

CHAPTER 1

Introduction and context

USC
UNIVERSIDADE
DE SANTIAGO
DE COMPOSTELA

1.1. BIOREFINERIES FOR A CIRCULAR ECONOMY

The economic and social era based on the massive use of fossils fuels that started in the industrial revolution is beginning its transformation in response to a future scenario of high prices, scarcity and geopolitical instability related with oil reserves (Landeweerd et al., 2011). In addition, social awareness of the effects of indiscriminate use of fossil fuels in the climate is steadily increasing and the society is already demanding alternatives. It is clear then that our production model should shift towards long-term sustainable options, among which, microbial production processes could play an important and primordial role. The current socioeconomical model is also eminently linear: raw materials are transformed into products that are disposed to the environment at the end of their lifespan, at best after treatment. Disposing endlessly wastes represents an equally worrying problem and it also concerns society. New models aiming at using fewer resources and at reusing wastes are desired and demanded.

The biorefinery concept was created in this context of demand of a more circular society and economy. A biorefinery can be defined as "the sustainable processing of biomass into a spectrum of marketable products and energy" (de Jong and Jungmeier, 2015). In this production scheme, organic wastes or renewable feedstocks (e.g. wood) are used as substrates in different microbial processes to produce the final products (e.g. plastics, fuels, chemicals, electricity, etc.). In this sense, renewable raw materials are used creating effectively a matter and energy loop and imitating one of the many biogeochemical cycles of nature. Moreover, using organic wastes instead of crops or other agricultural products avoids competition with food purposes, avoiding any ethical conflict of the biorefinery concept. Including the word refinery in the term envisions one of the target characteristics of the process: flexibility. Biorefineries are conceived to be as flexible as oil refineries and produce a variety of final products from a reduced array of feedstocks through different processes upon demand.

Several types of biorefinery can be distinguished among which the three most noteworthy are: the sugar biorefinery in which biomass is firstly hydrolysed chemically or enzymatically to sugars, the thermochemical biorefinery, in which synthesis gas is produced by biomass thermal gasification and the so-called carboxylate platform, in which biomass is firstly converted to short carboxylates by anaerobic fermentation. After an initial start, the sugar and thermochemical biorefinery are now focused on the use of lignocellulosic biomass as substrate (Octave and Thomas, 2009; Rasmussen et al., 2014), while the most recent

carboxylate platform is centred in treating organic wastes such as food waste or the organic fraction of the municipal waste (Lee et al., 2014; Strazzera et al., 2018; Venkata Mohan et al., 2016). In this sense, the carboxylate platform is a very attractive option since i) it can valorise those organic wastes and thus close the matter loop and ii) it can complement the other platforms by using their wastes, increasing thus their efficiency (Bastidas-Oyanedel et al., 2015). However, because of its shorter lifespan and due to the variability of the substrates used, the carboxylate platform is still a less mature technology than the other biorefinery types.

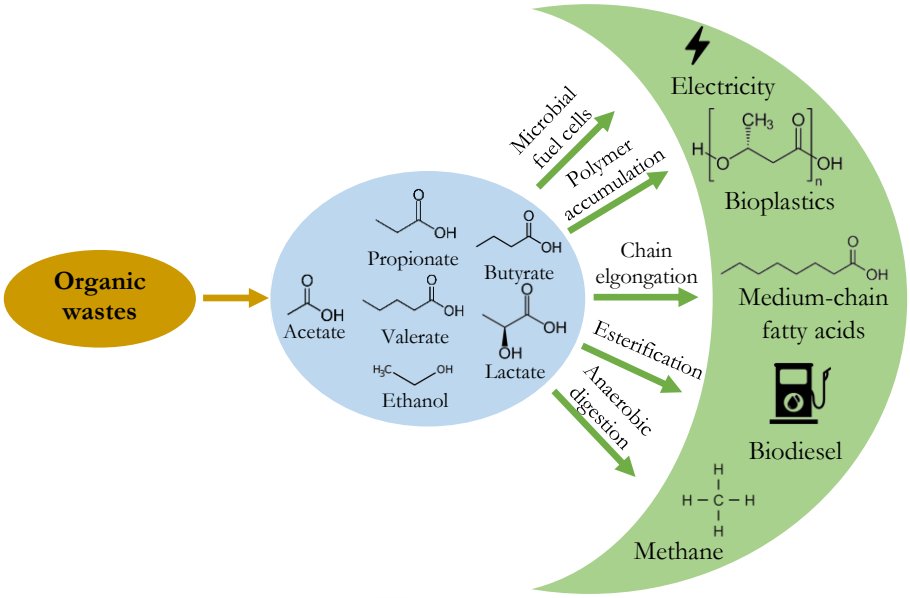

Figure 1.1. Carboxylate platform biorefinery scheme. Organic wastes are converted to short carboxylates via anaerobic fermentation (gold arrow), which are further converted to the final high added-value products in subsequent processes (green arrows).

In the carboxylate platform (Figure 1.1), the catabolic products of anaerobic fermentation can be further transformed in subsequent microbial processes to produce higher added-value products. For instance, VFA are used as substrate for the production of polyhydroxyalkanoates (PHA), a bioplastic family with some members (polyhydroxybutyrate) presenting mechanical properties similar to polypropylene (Kumar et al., 2019). Another example is the medium chain fatty acids (carboxylic acids of 6-12 carbon atoms) production in chain elongation processes using VFA and alcohols or lactate (Carvajal-Arroyo et al., 2019; Spirito

et al., 2014). These carboxylates are valuable products and have application that include antimicrobial agents (Reddy et al., 2018), precursors of biofuels (Shilling et al., 2013) or monomers in bioplastics (medium-chain PHA) that can be used in medical applications (Rai et al., 2011). Moreover, the resultant longer carboxylates are easier to separate from the fermentation broth than VFA as they can be produced in concentrations close to the solubility of their undissociated form in water (Steinbusch et al., 2011). In this regard, short carboxylates act as a nexus between the organic wastes used as feedstock and the final biorefinery high added-value products. The process of anaerobic fermentation is pivotal within the carboxylate platform and forms part of the core of the biorefinery philosophy, as it allows the transformation of a waste into valuable chemicals which could be further transformed in subsequent processes to high added-value products.

One of the main drawbacks of anaerobic fermentation is that usually the product spectrum consists of a mixture of VFA with a variable composition depending on both the operational conditions and the substrate composition. Therefore, developing predictive tools to understand the connection between operational conditions and stoichiometry and to design processes targeting specific VFA is a key element for the success of the carboxylate platform and is the main objective of this thesis.

1.2. ANAEROBIC FERMENTATIONS TO PRODUCE ENERGY-DENSE COMPOUNDS

Anaerobic fermentation is a process forming part of the anaerobic food chain transforming organic matter into methane, carbon dioxide and ammonia, the final products of decomposition (Figure 1.2). In particular, anaerobic fermentation transforms the monomers (i.e. amino acids, glucose and long-chain fatty acids) of the organic polymers that compose organic matter (i.e. proteins, carbohydrates and lipids, respectively) into volatile fatty acids (VFA), alcohols, ammonia, hydrogen and carbon dioxide.

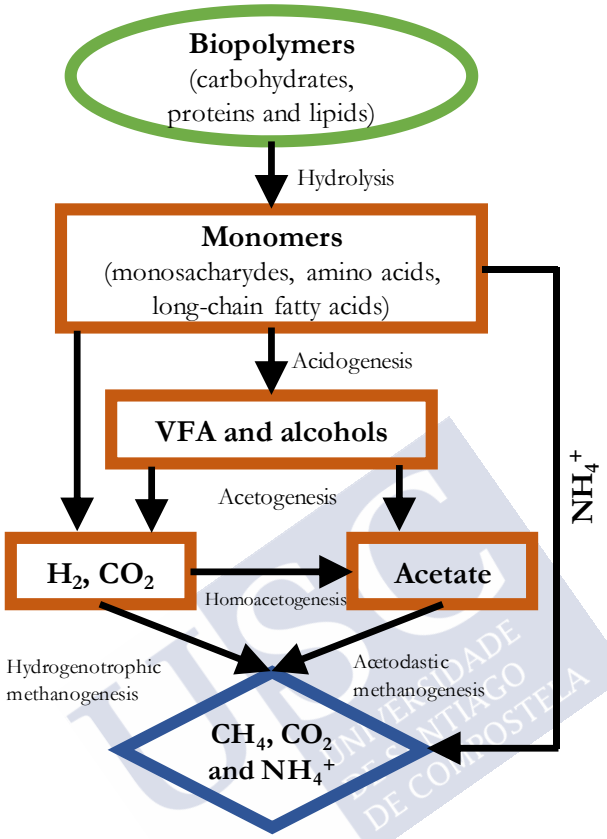

Figure 1.2. Anaerobic food chain.

In aerobic processes microorganisms generally oxidise the substrate completely in their catabolism to carbon dioxide and water and transfer the electrons to oxygen, a strong electron acceptor (Figure 1.3). This electron transfer is very exergonic (i.e. releases Gibbs free energy) which allows microorganisms to harvest large amounts of energy from the substrate. As a result, biomass production is high and up to half of the substrate can be converted into biomass (Kleerebezem et al., 2015). Usually, there are no energetic barriers in the catabolism of aerobic microorganisms and the substrate is transformed to non-valuable products. Therefore, aerobic processes are used when the desired product is produced in their anabolism, as for example alginate (Sabra et al., 2001), exopolysaccharides (Lin et al., 2010; Satpute et al., 2010), biosurfactants (Mnif et al., 2011; Satpute et al., 2010) or antibodies (Lee and Jeong, 2015).

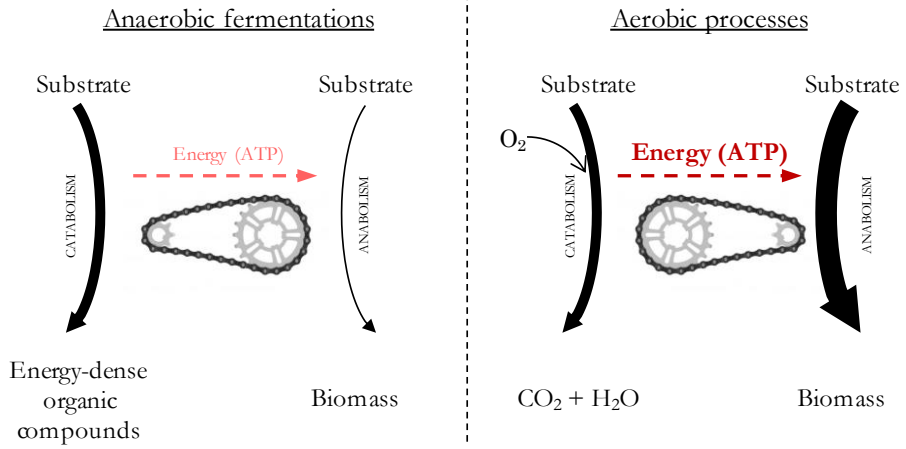

Figure 1.3. Anaerobic and aerobic processes differ in the biomass yield from substrate due to the difference in energy production in catabolism. For a same substrate conversion flux, aerobic processes biomass flux is much higher than that of anaerobic processes.

On the contrary, anaerobic fermentation processes are characterised by the lack of external and strong electron acceptors, which forces the substrate to be both the electron donor and acceptor. The driving force of the reactions is thus smaller, as the redox potential of the catabolic reactions is lower, and therefore microorganisms can harvest much less energy from the same substrate. In consequence, a larger amount of substrate is needed to harvest the energy required for biomass production (Figure 1.3). Catabolism in anaerobic fermentations takes place usually at conditions not far from the thermodynamic equilibrium, which leads to partial transformations of the substrate in which limited energy can be harvested (Jackson and McInerney, 2002a; Oh and Martin, 2007). These strong constraints led evolution to produce a plethora of possible catabolic reaction combinations to extract energy from the surroundings in the most efficient possible way. Therefore, anaerobic processes are more attractive when the targeted compounds form part of its catabolism (Borodina and Nielsen, 2014; Dharmadi et al., 2006; Jansen et al., 2017; Mans et al., 2018; Shen et al., 2011). Specifically, in anaerobic fermentation, the typical catabolic end-products are a mixture of energy-dense compounds consisting mainly of VFA and also alcohols and hydrogen (Agler et al., 2011; Angenent et al., 2004; Kleerebezem and van Loosdrecht, 2007).

1.2.1. Volatile fatty acids as main products of anaerobic fermentations

Anaerobic fermentation main products range from alcohols such as ethanol or butanol to medium-chain fatty acids as for example caproate; however, the main products are fundamentally VFA (Atasoy et al., 2018; Hoelzle et al., 2014). The term VFA refers to the carboxylic acids with a carbon-chain length between two and five carbons, that could also be referred as short carboxylates.

Currently at an industrial level, VFA are usually produced from oil in the petrochemical industry and feature a wide variety of applications from polymer production to food preservatives and fuel additives (Table 1.1). The market price of the different anaerobic fermentation products is roughly proportional to the carbon chain length, being butyrate and caproate the most valuable products. In comparison, producing methane in anaerobic digestion from the same substrate appears as a less attractive option due to its lower market price and for being a gas (it hinders its transport). It is worth mentioning that anaerobic fermentation by pure cultures of microorganisms is already the principal method for producing at industrial level lactate and ethanol, highlighting the industrial and economic viability of microbial production processes. In the case of lactate, 90% of its production comes from bacterial fermentation (Alves de Oliveira et al., 2018) while more than 96% of the ethanol global market was fulfilled by fermentation in 2008 (Taherzadeh and Keikhosro, 2008).

VFA production in anaerobic fermentation processes faces two main issues. First of all, the selectivity of the process for specific products is often low as VFA are usually produced in a mixture and at variable proportions with different operational conditions. In second place, separating the products from the broth is a challenging task due to typical low VFA concentrations encountered in anaerobic fermentations and because of the very similar chemical properties of VFAs (Zacharof and Lovitt, 2014). In fact, the separation and purification steps are considered to be the main contributors to the production cost of VFA in biological processes (Alkaya et al., 2009; Singhania et al., 2013).

Table 1.1. Market price and size, applications and production methods of typical products of anaerobic processes.

Compound	Market Price[a] (USD/tonne)	Overall market size[b] (ktonne/y)	Applications	Main production methods
Methane	200-600		Fuel, chemical industry.	Natural deposits
Acetic acid	400-800	14,000-17,000[c]	Production of vinyl acetate and derivates, pharmaceuticals[b], food additive[c]	Petrochemical derivative (carboxylation of methanol)[b,c]
Ethanol	700-900	51,000	Solvent, antifreeze, fuel (supplement), raw chemical[b]	Industrial fermentation (>95%)[b] and petrochemical derivate (ethylene oxidation, <5%)
Propionic acid	1500-1700	350-470[c]	Cellulose-based plastics, food preservative[b], precursor of chemicals	Petrochemical derivative (oxidation of butyraldehyde)[c]
Lactic acid	1000-1600	1,220[b]	Polylactate production[d]	Industrial fermentation (pure culture)[b]
Butyric acid	2000-2500	90-105[c]	Cellulose-based plastics, feed preservative	Petrochemical derivate (ethylene hydro formylation, carboxylation of ethylene)[b, c]

Table 1.1 (continued). Market price and size, applications and current production method of typical products of anaerobic processes.

Compound	Market Price[a] (USD/tonne)	Market size[b] (ktonne/y)	Applications	Current production methods
Butanol	1800[e]	2,800[e]	Solvent (paints, dyes), chemical industry (methacrylate esters)[f]	Petrochemical derivative (from propylene in the oxo process)[f]
Valeric acid (pentanoic acid)	-	-	Ester-type lubricant, plasticizers, perfumes and cosmetics[g], synthetic flavour[h]	Petrochemical derivative (oxidation of n -pentanal)[h]
Caproic acid (hexanoic acid)	2000-2500	25	Precursor of pharmaceuticals and flavours[b]	Oleo-chemistry (from coconut or palm kernel oil)[h]

[a] Bastidas-Oyanedel and Schmidt (2018); [b] Bastidas-Oyanedel et al. (2015); [c] Atasoy et al. (2018); [d] Alves de Oliveira et al. (2018), [e] (Liu et al., 2015), [f] (Dürre, 2008), [g] (Jänisch et al., 2019), [h] (Kubitschke et al., 2014)

1.3. MIXED-CULTURE FERMENTATIONS FOR VALORISING WASTES

Anaerobic fermentations can be performed by pure cultures of microorganisms (commonly just one single species) or use a mixed microbial consortium. In this last case, the process is usually open (i.e. the system is open to the entry of microorganisms e.g. in the feeding), the microbial community is undefined and is referred to as mixed-culture fermentation (MCF).

Pure single culture processes are characterised for their high product selectivity and good control with operational parameters (Bastidas-Oyanedel et al., 2015) (Figure 1.4). Owing to these advantages, well-established industrial bioprocesses usually employ pure of microorganisms. For example, in the ethanol and lactate industrial bioproduction pure cultures of the yeast *Saccharomyces cerevisiae* (Klein et al., 2019) and bacteria of the genus *Lactobacillus* or *Lactococcus* (Alves de Oliveira et al., 2018) are employed, respectively.

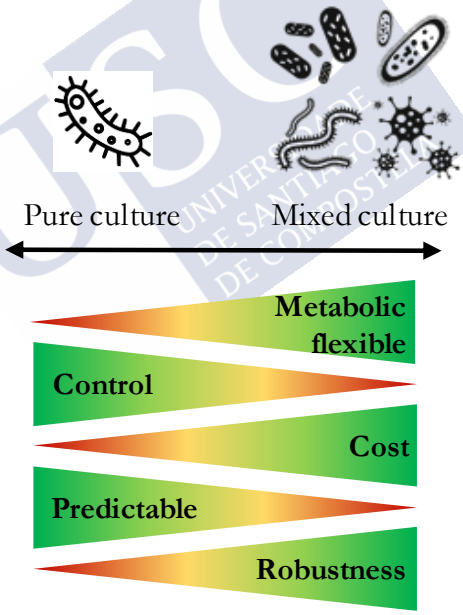

Figure 1.4. Main characteristic of processes using pure and mixed cultures of microorganisms from an operational perspective. Adapted from Smid and Lacroix (2013).

On the contrary, mixed cultures of microorganisms are more difficult to control accurately using operational parameters and the process outcome usually

depends substantially on the environmental conditions, remaining the factors that determine this dependency still unclarified (Hoelzle et al., 2014).

However, when organic wastes are to be used as feedstock mixed cultures can provide several and substantial advantages to the system (Figure 1.4). Firstly, there is no need for an aseptic environment in the reactor to avoid microbial contamination, which makes feedstock sterilisation unnecessary, bringing down significantly the capital and operational costs and opening at the same the possibility of continuous processes (Hoelzle et al., 2014; Kleerebezem and van Loosdrecht, 2007). This is particularly important for the carboxylate platform, since some of the most interesting industrial wastes are very diluted and microbially unstable as, for example, the wastewater of canning or dairy industries. Secondly, processes using mixed cultures can use as feedstock variable mixtures of substrate since the microbiome counts with a very rich functional diversity (Temudo et al., 2008a). This aspect is also key when complicated conversions need to be performed requiring, for example, several transformation stages as in anaerobic digestion (Perez-Garcia et al., 2016). Finally, mixed cultures are more robust than pure cultures because anaerobic microbiomes are typically functionally redundant (i.e. there is more than one guild in the microbiome for each function) and therefore can withstand to a greater extent changes in operational conditions or feeding characteristics, owing to their greater metabolic flexibility (Carballa et al., 2015).

Hence, the use of MCF is usually preferred in the context of the carboxylate platform biorefinery (Bastidas-Oyanedel et al., 2015; Bastidas-Oyanedel and Schmidt, 2018; Lee et al., 2014; Strazzera et al., 2018; Venkata Mohan et al., 2016). Pure culture systems should be only employed when the value of the product is high enough to justify the use of pure feedstocks and the additional costs of pure cultures (e.g. pharmaceutical industry).

1.3.1. Environmental conditions determine mixed-culture fermentation selectivity

In mixed-culture systems, a modification of the environmental conditions will, in most of the cases, alter the outcome of the process. This environmental modification can affect the anabolism and hamper the growth of a particular microorganism (e.g. if some enzymes are incompatible with the new environmental conditions). Alternatively, the effect of the new conditions may be limited to the catabolism by favouring the production of other product. In

this case, the present microorganisms can adapt their catabolic strategy and survive, or it can be replaced by other microorganisms performing the same or another catabolic route, and then change the composition of the microbiome.

Therefore, changing the environmental conditions of a reactor has the potential of selecting different catabolic routes, of changing the microbial community and ultimately to drive the process towards desired products. The main variables studied in literature are related with the feeding (its regime, concentration or composition) or with reactor conditions such as its pH or temperature (Table 1.2).

Table 1.2. Influence of different design parameters on product selectivity. If no substrate is specified, the effect observed should be interpreted as a general effect in MCF.

Parameter studied	Substrate	Change in condition	Effect observed	Ref.
T	-	From mesophilic to thermophilic range	Influence in selectivity is minimal	A
	-	Different	Contradictory results	B
HRT	-	Increase	Contradictory results	A
	FW	Increase from 8 to 12 d	Switch from acetate to propionate	C
	Sucrose-rich WW	Increase from 3 to 30 h	Favours caproate	D
SRT	-	Increase	Varied results	A
OLR	-	Increase (theoretical consideration)	Favours lactate	E, F, I
	Synthetic dairy WW	Increase	Favours propionate	G
	FW	Decrease	Favours butyrate	C
Culture medium	Glucose	Mineral vs rich	Favours lactate	H
AA composition	Protein	Comparison of casein and gelatine MCF	Acetate slightly favoured in gelatine in detriment of butyrate	J

Table 1.2 (continued). Influence of different design parameters on product selectivity. If no substrate is specified, the effect observed should be interpreted as a general effect in MCF.

CH composition	Carbohydrates	Comparison of glucose and xylose MCF	Glucose favours butyrate and xylose ethanol and acetate (CSTR)	K
pH	Glucose	Acidic values	Favours butyrate	L, M, N
		Alkaline values	Favours ethanol	L, N
			Favours propionate	O
	Casein/ Gelatine	Acidic values	Favours butyrate and valerate but disfavours acetate	P
		Alkaline	No effect/ favours acetate	
	WAS	Acidic values	Favours butyrate and valerate	Q
	Synthetic dairy WW	Acidic values	Favours propionate and ethanol	R

T: Temperature; HRT: Hydraulic retention time; SRT: Solids retention time; OLR: Organic loading rate, AA: Amino acids, CH: Carbohydrates; FW: Food waste; WW: wastewater.

References. A: (Lee et al., 2014); B: (Arslan et al., 2016), C: (Lim et al., 2008), D: (Yu and Mu, 2006), E: (Hoelzle et al., 2014), F: (Angenent and Kleerebezem, 2011), G: (Yu et al., 2002), H: (Rombouts et al., 2020); I: (Agler et al., 2011), J: (Bevilacqua et al., 2020a), K: (Rombouts et al., 2019a), L: (Temudo et al., 2007); M: (Fang and Liu, 2002); N: (Zoetemeyer et al., 1982); O: (Horiuchi et al., 2002); P: (Bevilacqua et al., 2020b); Q: (Chen et al., 2007), R: (Yu and Fang, 2002).

Temperature, the hydraulic retention time (HRT) and solids retention time (SRT) present a limited and sometimes contradictory influence on product selectivity. Therefore, they are not interesting parameters for controlling product selectivity, as already suggested in literature (Arslan et al., 2016).

Lactate production was identified, from a theoretical perspective (Agler et al., 2011; Angenent and Kleerebezem, 2011; Hoelzle et al., 2014), to be favoured at high organic loading rate (OLR) values, since its production enables cells to

rapidly consume the reducing equivalent produced in glycolysis. Experimental evidences support this consideration as in a glucose fermentation using a pure culture of *Streptococcus lactis*, a switch in the product spectrum from acetate and ethanol to lactate was observed when the OLR increased (Thomas et al., 1979). Also, experimentation with mixed cultures reported at higher OLR an increase in the production of propionate, which is a typical product of lactate fermentation (Seeliger et al., 2002). Regarding lactate production, the cultivation medium also affects its production since lactic acid bacteria (LAB) are known for being auxotrophic for amino acids (i.e. they cannot synthesise them from inorganic compounds). Thus, cultivation media providing amino acids (in the form of peptides or yeast extract) allows for lactate production while its absence foments the presence of prototrophic (i.e. they can grow on inorganic nitrogen) bacteria (e.g. of the genus *Clostridium*) that produce VFA such as butyrate or propionate (Wang et al., 2015).

Reactor pH is the parameter best studied both in terms of the number of relevant publications and of the quality of the analysis of the observations proposed. This parameter has a great influence on the product spectrum and is capable of provoking large shifts in product selectivity, especially for carbohydrate fermentations, which makes it an attractive parameter for selectivity control. For example, Temudo et al. (2007) in a study on acidification of glucose, reported a close to equimolar ratio of butyrate and acetate at pH values below 5.5 but butyrate was absent at neutral and alkaline values, where ethanol and acetate dominated the product spectrum. This complete shift in butyrate selectivity was also observed in other studies using glucose as substrate (Horiuchi et al., 2002; Zoetemeyer et al., 1982). Likewise, an acidic pH in protein MCF also led to an increased butyrate production, albeit to a much lesser extent. For instance, Bevilacqua et al. (2020b) reported an increase in the molar fraction of butyrate only from 10 to 20% when shifting the pH from 9 to 5 in casein MCF. Accordingly, experiments with complex substrate consisting partially of protein, show a narrower variability of the product spectrum with pH than cases with substrate mainly composed of carbohydrates.

Therefore, pH stands as one of the most interesting parameters to control to control product selectivity on MCF since, on the one hand, increases the flexibility of the system due to its remarkable on the product spectrum and, on the other hand, is one of the easiest operational parameters to manipulate independently and control in an experimental setup. This potential as a product

design tool was identified by several authors (Atasoy et al., 2018; González-Cabaleiro et al., 2015; Strazzera et al., 2018; Temudo et al., 2007). Substrate composition is also a parameter with capabilities for directing the production of MCF in a scenario with a wide array of organic wastes available that have varied compositions, as a mixture of them could be tailored to favour specific products.

Hence, one of the main research questions of this thesis is to evaluate to what extent product selectivity in MCF can be controlled by means of the operational conditions, paying an especial attention to the reactor pH and composition and characteristic of the substrate.

In some of the reported studies, the understanding of the factors influencing product selectivity is limited by the concurrence of several steps in complex substrate conversion to VFA: disintegration, hydrolysis and acidification. Some changes in the product spectrum reported by Lee et al. (2014) or Arslan et al. (2016) are likely to be caused by the temperature, HRT or pH enhancement of hydrolysis that may modify the substrate to acidify, rather than changes in the fermentative process itself. Processes consuming VFA could also be favoured at longer HRT, as chain elongation to produce medium chain fatty acids, as reported by Yu and Mu (2006). Failing to isolate the effect of these parameters individually on substrate acidification leads to confusing information with very limited applicability. Moreover, studying the effect of a parameter with real substrates composed by an undefined mixture of compounds only increases the complexity of interpreting the information. Experiments should be conceived expressly to study the effect of individual operational parameters on product selectivity using single or known mixtures of substrates.

1.3.2. Experimental studies to study product selectivity variability

The link between operational conditions and product selectivity was especially tackled for carbohydrate MCF, mainly with glucose as substrate, both from an experimental (Rombouts et al., 2020, 2019b; Temudo et al., 2007) and modelling (González-Cabaleiro et al., 2015; Kleerebezem et al., 2008; Zhang et al., 2013) perspective in good detail. Although different environmental factors were studied, the study of the pH effect on the process was their main focus.

Protein MCF was addressed at a lesser extent and mostly from an experimental and descriptive point of view (Breure et al., 1986a, 1986b, 1985; Breure and van Andel, 1984; Yu and Fang, 2003). The only modelling approach was done by Ramsay and Pullammanappallil (2001), who developed a stoichiometry predictor

for protein fermentation taking into account the amino acid composition. However, pH influence was ignored in this work even though there are enough experimental evidence suggesting the opposite. Only recently, some works tried to study systematically and mechanistically the influence of both pH and amino acid composition in the performance of protein MCF and in particular in its product selectivity (Bevilacqua et al., 2020a, 2020b; Duong et al., 2019). Protein cofermentation with carbohydrates was barely studied with works centred in just describing the changes in product spectrum at different substrate proportions (Alibardi and Cossu, 2016; Breure et al., 1986a, 1986b).

The fate of lipids in MCF was barely addressed in literature and only a few works can be found (Alves et al., 2009; Cavaleiro et al., 2016; Gonçalves et al., 2014). The common conclusion is the partial and incomplete degradation of long-chain fatty acids and the identification of thermodynamic (long-chain fatty acid degradation in the absence of a hydrogen scavenger is an endergonic process) and inhibition issues (lipids adhere on cell walls) as the main barriers for lipid fermentation. The fate of lipids in MCF should be further investigated since they could be used in cofermentation scenarios to steer the process towards more reduced and valuable VFA due to their high reduction degree.

Most of the abovementioned works only describe phenomenologically experimental observations without analysing them systematically. More works with a clear focus on understanding mechanistically the interactions between the environmental conditions and cellular metabolism are needed because empirical black-box-like knowledge is not enough for this challenging goal.

1.4. ENGINEERING MIXED-CULTURE FERMENTATIONS

The latest hypotheses regarding the origin of life locate it in alkaline hydrothermal vents at the bottom of the ocean (Lane, 2015). Microscopically thin vent walls formed by iron minerals separated two different environments with quite different concentration of hydrogen, carbon dioxide and protons. These concentration gradients and their respective energy gradients were the spark that ignited life in the depths of the ocean. Curiously enough, some catalytic centres of well-known enzymes are still formed by minerals present in alkaline hydrothermal vents, such as the iron sulphide clusters of ferredoxin, an enzyme participating in the Wood-Ljungdahl pathway, one of the allegedly most antique microbial pathways (Martin, 2012). From there on, life evolved to build cell membranes to actively create customizable and changeable environments and to

control the energy and matter exchanges with the surroundings. In this way, cells isolate and modify aliquots of the environment to allow reactions that otherwise would not be possible or to avoid harmful conditions incompatible with life.

The task of a bioprocess engineer is somehow a bit similar to that of cell membranes: to create specific environments to modify and guide intentionally cellular metabolism towards the production of specific products. The only way of domesticating cells in such a way without genomic modifications, and especially in open systems as MCF, is to modify the boundary conditions where cells live. In this way, the optimal strategy of survival may differ and could involve the production of other products. Following the well-known postulate of Bas Beckel "everything is everywhere but, the environment selects" (O'Malley, 2008), it is clear that the focus should be set in the operational conditions rather than in the microbial inoculum.

Hence, to successfully engineer microbial communities the desired product must have a metabolic function or a selective trait that increases cellular fitness under some environmental conditions. If so, it will be theoretically possible to design a process in which the community produces substantially that desired product. For example, the driving force to storage carbon in the form of a biopolymer (i.e. bioplastic) is to consume, before other, all the available substrate when the conditions do not allow growth. In this sense, when the conditions allow again to grow, all the substrate is captured intracellularly and not available for competitors (Jiang et al., 2011). If bioplastic is the target compound, the system should be designed to enrich the mixed-culture with bioplastic-forming bacteria, with can be accomplished with feast and famine cycles, as bacteria storing the bioplastic have a fitness advantage.

To establish the biorefinery scheme as a sound technology alternative, we need to understand and guide the microbial community of anaerobic fermentations at our own will. **Therefore, one of objectives of this thesis is to develop predictive tools to i) understand the mechanisms linking environmental conditions and cellular metabolism (i.e. its stoichiometry) and with that insight ii) design processes targeting the production of the desired compounds.**

1.5. MATHEMATICAL MODELS FOR UNDERSTANDING AND PREDICTING MICROBIAL METABOLISM

A mathematical model is an abstract description of a system using mathematical language, aiming at understanding a system or predicting its behaviour (Ningthoujam et al., 2018). The use of mathematical models has spread in all branches of science as they are powerful tools for interpreting and predicting diverse natural phenomena and empirical observations (Gombert and Nielsen, 2000). Mathematical models can be employed to validate new hypotheses or can be used for their predictive capacity, in other words, for their design capabilities. In the latter case, mathematical models are especially attractive since they may be helpful to screen *a priori* operational conditions, thus reducing substantially the need of experimental work, which is usually time-consuming and expensive.

All models are simplified visions of the reality, but this is a matter of necessity and convenience. In the case of mathematical models of living systems, this is already intuitive even for the simplest life forms (e.g. bacteria) as it is not possible to capture all possible processes due to our limited knowledge. However, the key element is that although models are conceptually wrong, in the sense that they cannot describe reality perfectly, they are built with the purpose of being useful for a particular task. Models should be developed for specific ranges of environmental conditions and, very importantly, with the adequate level of accuracy for each occasion, since adding additional layers complexity could difficult the identification of the cause-effect relationships. It is the task of the model developer to find a balance between model complexity and the applicability of the model and decide what mechanisms should be include depending on the purpose of the model. In this regard, the statistician George Box stated (Box, 1976):

> Since all models are wrong the scientist cannot obtain a "correct" one by excessive elaboration. On the contrary following William of Occam he should seek an economical description of natural phenomena. Just as the ability to devise simple but evocative models is the signature of the great scientist so over-elaboration and overparameterization is often the mark of mediocrity.

He then perfectly synthesised his own words to create the well-known statement: "All models are wrong, but some are useful" (Box, 1979). Naturally, model use should be accompanied by a strong conscience of their range of application,

especially when extrapolating. Failing to identify the limits of model application imposed by assumptions or the non-inclusion of certain mechanism could lead to far greater inaccuracies than the oversimplification of reality themselves. Again, in words of George Box (Box, 1976):

> Since all models are wrong the scientist must be alert to what is importantly wrong. It is inappropriate to be concerned about mice when there are tigers abroad.

1.5.1. Modelling cellular metabolism

In general, cellular metabolism can be schematically divided into anabolism and catabolism (Figure 1.5). In anabolism, new biomass is formed from the substrates in an energy-consuming process which decreases the entropy of the system as complex and ordered molecules are formed from simpler building blocks. The needed energy is provided in form of ATP by catabolism, which is the process in which cells obtain energy by converting the substrate to other simpler and more disordered compounds.

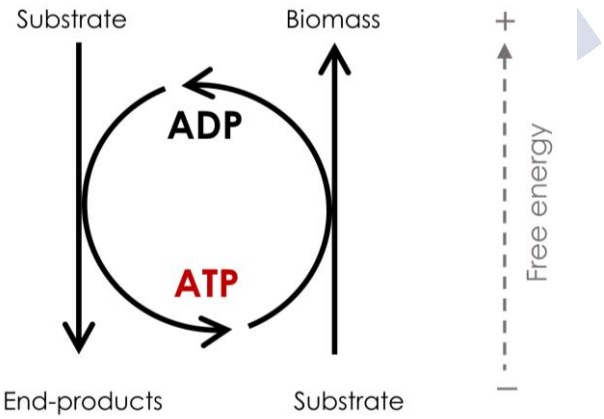

Figure 1.5. Cellular metabolism is composed of catabolism and anabolism. The ATP produced in catabolism is consumed in anabolism to produce biomass from the substrate. Adapted from Kleerebezem and Van Loosdrecht (2010).

The word anabolism means literally in Greek *to throw upwards* and was coined by physiologist W. H. Gaskell for the first time in 1876 with the interpretation of building up biomass compounds or a constructive metabolism (Gaskell, 1886). Catabolism, on the contrary, means *to throw down* and should be interpreted as breaking down the substrate or a destructive metabolism. Therefore, the

energetic and entropic nature of both processes is already perfectly captured in their etymology. Catabolism destroys or breaks down the substrate in smaller units to gain the energy that is needed to construct the complex biomass compounds from the substrate.

In anaerobic environments, catabolic reactions are thermodynamically, and hence energetically, limited which leads to reduced biomass production, as mentioned in section 1.2. Additionally, different substrate conversions are usually very similar in terms of energy (González-Cabaleiro et al., 2015), which could explain the quite high variability of catabolic end-products found in MCF under different environmental conditions. This provides a great flexibility to the system as it allows it to produce different products from the same substrate. If a given end-product, e.g. propionate, provided significantly more energy to microorganisms, it would probably be more difficult to steer microbial production towards other end-products. Therefore, when modelling MCF the main focus should be set in catabolism and more specifically in the mechanisms responsible of the changes in production strategies.

1.5.2. Cells face an optimisation problem

Cellular metabolism is assumed to be the result of adaptation to the environmental conditions and cellular surroundings. It could be assumed that only those microbial groups performing the optimal metabolic strategy prevail as only the fittest survive (Koonin and Wolf, 2012). Focusing on MCF, it could be argued then that the end-products representing the optimal catabolic strategy are likely to dominate the product spectrum of the process, since they allow the microorganisms that produce them to dominate the microbial community.

Empirical observations indeed indicate that MCF global catabolism adapts to changing environmental conditions and, as a result, different end-products are produced by the mixed microbial community (section 1.3.1). The community dominant species may adapt to the new conditions and change their catabolic strategy or different species with a more suitable strategy can outcompete them and become the new dominant species. The adaptation and selection of microbial groups has been represented in mathematical models as an optimisation problem where the objective is to maximise the growth rate, or an equivalent expression, and the decision variable are the metabolic fluxes performed (Table 1.3). Physical and biological restrictions would act as constraints of the model and limit the possible solutions. For example, thermodynamics dictate what processes are

possible to occur (physical constraint) or an overall maximum intracellular concentration could be set to reflect a limit to osmotic pressure (biological constraint).

Table 1.3. Cellular metabolism can be translated into a mathematical optimisation problem with a maximisation objective (to maximise growth rate) and additional constraints.

	Empirical observation	Mechanistic interpretation	Mathematical expression
		Growth rate is maximised	$\max(\mu)$
	The fittest survive	Biomass yield is maximised	$\max(Y_X)$
		ATP production is maximised while catabolic fluxes minimised	$\max(r_{ATP}/\sum r_i)$
Physical constraints	No external electron acceptor	Electron balance in the system is zero	$\sum(r_{ELECTRON}) = 0$
	Second law of thermodynamics	Globally endergonic reactions (*j*) are not possible	If $\Delta G_j \geq 0$, then $r_j = 0$
Biological constraints	Some intracellular compounds are at quasi steady state conditions	Net fluxes of those compounds (*i*) are null	$N_i \cdot r = 0$
	Intracellular osmotic pressure has a maximum	Maximum intracellular concentration allowed	If $\sum C_i > C^{max}$ $r_{TRANSPORT} = r_{PRODUCTION}$
	Kinetics dictate a minimum substrate concentration for a reaction to occur	Minimum concentration of reactants	If $C_i < C^{min}$ $r_j = 0$

Usually the strategy maximising growth rate is interpreted to also provide the highest ATP yield with respect to the substrate and it is commonly used as optimisation factor (González-Cabaleiro et al., 2015; Rodriguez et al., 2006; Zhang et al., 2013). Nevertheless, there are other interpretations of what provides the highest possible growth rate (Schuetz et al., 2007). Biomass yield on the substrate is also proposed under the reasoning that evolution would have driven

cells to optimise the production of biomass per unit of substrate. Other approaches consider also kinetic arguments and propose that pathway length should be minimised (Melendez-Hevia, 1990) or that cells maximise the ATP production rate while minimising the overall catabolic fluxes (Dauner and Sauer, 2001).

1.5.3. Types of metabolic models

Metabolic models can be classified depending on the description of the microbial community as unsegregated or segregated (Figure 1.6). Most of the models are unsegregated and considered each microbial group as a homogeneous population. On the contrary, segregated models, such as individual-based models, contemplate differences among individuals from the same population in, for example, size, shape or phenotype (Li et al., 2019; Millat et al., 2013).The application of these models is of interest when spatial distribution may influence metabolism as in biomass aggregates (e.g. biofilms) or when cells can adopt different states (e.g. vegetative or sporulated) as in ABE fermentations.

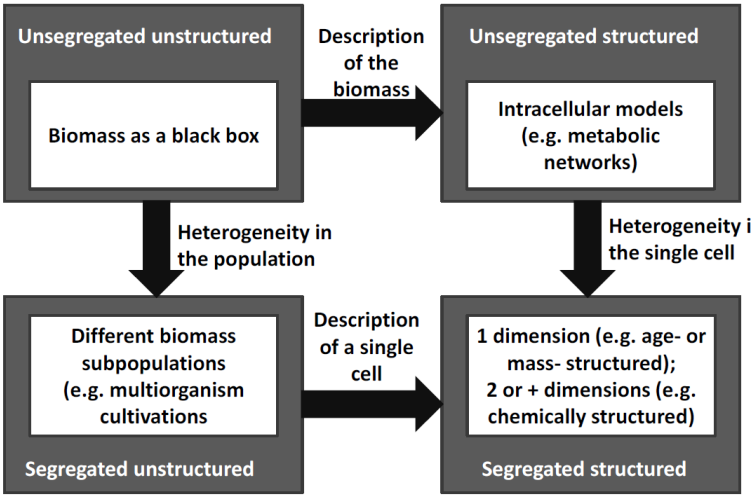

Figure 1.6. Classification of metabolic models according to their structure and biomass description. Taken from Gernaey (2015) with permission from Elsevier Books.

If in the system to model, more than one microbial species is present, there are distinct ways of describing the community and the interactions between species. Models can describe the mixed community as different compartments representing each group (with individual metabolic networks), in which case the

optimisation strategy is usually referred to the global community (Zhuang et al., 2011; Zomorrodi and Maranas, 2012). This approach is well suited to describe microbial communities consisting of up to a handful of different species and it particularly well-suited to capture microbial interactions beyond competition such as commensalism, parasitism or mutualism (Perez-Garcia et al., 2016; Zomorrodi et al., 2014). However, a precise knowledge about the metabolism (i.e. identifying the substrates and possible products of each of the species) is mandatory for applying a compartmentalised approach, which makes it an unattractive option for describing MCFs.

An *enzyme soup* or *lumped* network approach ignores completely species boundaries and it assumes that all metabolites are shared equally among all community members (Biggs et al., 2015). This is equivalent to describing the microbiome as a single virtual microorganism owning all its metabolic functions and capabilities, which are condensed in a single lumped metabolic network. For its characteristics, this method was identified as being specifically appropriate for those occasions in which there is scarce knowledge about the community and the main objective is to explore the metabolic capacity of a specific microbial community and the interactions among community members are irrelevant (Biggs et al., 2015; Perez-Garcia et al., 2016; Taffs et al., 2009). These characteristics make the enzyme soup approach to be much more in line with the system of study, open MCFs, and with the main objectives of this work.

Metabolic models can also be classified according to the level of detail with which microbial metabolism is described (Figure 1.6). On the one hand, unstructured models consider cells as black boxes and treat microorganisms just as another chemical compounds, albeit with (auto)catalytic properties. A good example is the well-known and widely-applied Anaerobic Digestion Model No. 1 (ADM1) for the simulation of the anaerobic digestion process (Batstone et al., 2002a). On the other hand, structured models describe intracellular compounds and kinetic processes separately from the reactor dynamics and may provide a greater level of mechanistic knowledge. However, as discussed at the beginning of this section, each model should have the needed degree of complexity for the purpose it was developed. Unstructured models are computationally much simpler and their level of detail is usually enough to describe accurately the kinetic behaviour of many microbial processes of interest such as anaerobic digestion.

1.5.4. State of the art

The existing modelling works in literature concerning MCF can be classified into bioenergetic or kinetics models, according to the complexity and aim of the model

Bioenergetics models have as central assumption that cellular metabolism is strongly shaped by bioenergetics. These models consider that cells pursue the maximisation ATP yield per substrate unit, as anaerobic fermentations are energy-scarce environments (González-Cabaleiro et al., 2013), and tune their catabolism accordingly. Their main objective is to predict the stoichiometry of the system under different environmental conditions and to understand the mechanisms that promote them. Consequently, they give great emphasis to describing with detail the different intracellular mechanisms (e.g. transport, homeostasis or energy conservation) and thus their predictions could be in principle extrapolated since they require a limited number of environment-specific parameters. They are unsegregated but structured and describe the microbial community following the enzyme soup approach, as it is an appropriate description of poorly defined microbial communities as the microbiome of MCF.

Kinetic models are unsegregated, unstructured and their objective is to describe and predict the general kinetic dynamics of a system. These models usually describe cellular metabolism in a simple way and do not consider possible changes in the stoichiometry with the operational conditions. Contrary to bioenergetic models, different parameters for different environments are needed and consequently they depend on calibration with experimental information in each condition.

Scientific literature on MCF modelling (Table 1.4) has dedicated much more attention to carbohydrates, in special to glucose, and the number of bioenergetics models is significantly more reduced than kinetic models. While all bioenergetics models available in literature, to the best of my knowledge, are listed in Table 1.4, the kinetic models featured are just a selection.

Table 1.4. Previous modelling works. Bioenergetic models.

Description	Comments	Ref
First and seminal work on glucose MCF bioenergetic model ling for stoichiometry prediction.	pH effect on VFA and H_2 selectivity is not well captured. Only one EC is considered. VFA undissociated form is used for transport calculations.	A
Modification of the previous model considering correctly the different EC.	Gaseous compounds prediction is improved. Butyrate shift at acidic pH is well captured but it is predicted to be the only products, which is not seen experimentally.	B
Modification of the first model (Ref. A) with updated metabolic network, including electron bifurcating mechanism. EC ratios are set by the H_2 partial pressure.	It captures well the shift towards butyrate at acidic pH but ethanol production is never predicted at all, while reported experimentally. Transport energy cost considers only the dissociated form of VFA.	C
Most recent model for stoichiometry prediction of glucose MCF.	It captures the observed shift from acetate-ethanol towards butyrate from alkaline to acidic pH values. However, at low pH butyrate is predicted to be the only product, when experiments show an equimolar production of butyrate and	D

Table 1.4 (continued). Previous modelling works. Kinetic models.

Description	Comments	Ref
Modification of ADM1 to simulate sucrose MCF with variable stoichiometry, which depends on the H_2 partial pressure.	Only one EC is considered. It uses kinetic parameters estimated in methanogenic conditions.	E
Modification of ADM1 to simulate high-solid sludge MCF, focusing on ammonia inhibition.	Methanogenesis cannot be ruled out. Operational conditions are poorly defined.	F
Kinetic model for the MCF of protein and its cofermentation with carbohydrates.	Methanogenesis was not successfully inhibited.	G
Kinetic model for glucose MCF studying the effect of pH, total undissociated acid concentration and temperature.	The stoichiometry is not considered to vary with the operational conditions	H
Kinetic model for glucose and fructose MCF to analyse the differences in kinetic behaviour	Product selectivity is not considered	I

EC: Electron carrier.

A: (Rodriguez et al., 2006); B: (Kleerebezem et al., 2008), C: (Zhang et al., 2013); D: (González-Cabaleiro et al., 2015); E: (Shi et al., 2019); F: (Bai et al., 2017); G: (Tommaso et al., 2013); H: (Infantes et al., 2012); I: (Fernández et al., 2011).

Regarding available bioenergetic models (Table 1.4), glucose was the only substrate addressed. The most recent model of González-Cabaleiro et al. (2015), captures the changes experimentally observed in product spectrum with the pH, but fails to correctly predict the stoichiometry at acidic pH values. The model predicts that butyrate is almost the sole product (more than 90% in molar basis) while the experimental evidence reports the production of butyrate and acetate at an equimolar ratio at acidic conditions (Fang and Liu, 2002; Temudo et al., 2007; Zoetemeyer et al., 1982). One common feature of all bioenergetic models is that none of them can predict lactate production in the conditions experimentally observed, limiting thus the design of processes targeting it. Due to their optimisation formulation, lactate is never predicted due to its low ATP yield in comparison with other possible products (e.g. butyrate or acetate).

Concerning the kinetics models available in literature, models for glucose and protein were found. In the case of protein, however, the existing models present significant limitations in comparison with the works dedicated to carbohydrates: the parameters were often estimated in methanogenic environments and they consider VFA production stoichiometry as independent of the environmental conditions. Hence, the scope of substrates that can be simulated in MCF is mainly constrained to carbohydrates. The production of VFA from lipids was not addressed from a modelling point of view since the experimental knowledge on the process is still very limited as discussed in section 1.3.1.

1.6. OBJECTIVES AND STRUCTURE

This section presents the main objective of this thesis followed by the identification of the research questions and objectives that guided the research throughout this work. Finally, the structure of the thesis and its relationship with the research questions and objectives is shown.

1.6.1. Main objective

The main objective of this thesis is to **understand the mechanisms** governing anaerobic MCF and their connection with the environmental conditions by means of predictive tools (i.e. mathematical models). The new insight is also used with the objective of **designing MCF processes** with high productivity for desired compounds to facilitate the establishment of the biorefinery concept as a viable industrial process.

1.6.2. Research questions

In literature, several gaps were detected for accomplishing this objective, which are summarised here. Mechanistic knowledge on protein MCF is limited and there is a lack of capacity to predict its product spectrum under different operational conditions. In the case of glucose, its MCF modelling has already been addressed but, the product spectrum is still not correctly predicted and the possible lactate production, a product of industrial interest, from glucose is neither predicted nor understood.

Considering the main objective of the thesis and the gaps detected in literature, the following research questions (RQ) were identified:

- **What is the effect of substrate composition on MCF?** How to improve the accuracy of prediction in glucose MCF? What is the product spectrum of the MCF of different proteins? How is it affected by cofermenting protein with other substrates? Are protein MCF kinetics affected by the amino profile of protein? What is the fate of lipids in anaerobic fermentation? Is it possible to convert them in cofermentation scenarios?
- **How do operational parameters affect the outcome of MCF?** How do different operational parameters affect protein MCF or its cofermentation with glucose? Why is lactate only produced under certain environmental conditions?
- **Can MCF be steered towards specific products?** Is it possible to maximise the production of desired compounds by altering operational parameters and modifying the substrate composition?

1.6.3. Research objectives

To guide the research throughout the thesis, the former research questions are transformed in several research objectives (RO).

- To update the metabolic network of glucose fermentation to describe the experimental results.
- To develop a glucose MCF metabolic model for lactic acid production.
- To developed models for protein mono and cofermentation stoichiometry prediction.
- To develop a kinetic model for protein MCF using experimental data and including the stoichiometry proposed by the previous models.

- To propose an early-stage methodology for designing MCF processes targeting specific VFA with high productivity.

1.6.4. Structure

The connection between the research questions and objectives and the different chapters of this thesis is shown in **Figure 1.7**.

The discrepancies between the model predictions and experimental results could be caused by the use of an incomplete metabolic network that does not include all relevant biochemical mechanisms. In **Chapter 3** the metabolic network of glucose MCF is updated with the inclusion of EB to check whether it helps improving the prediction capacity of models. The role of homoacetogenesis (HA) in anaerobic fermentations is also tackled in order to understand the reported experimental H_2 and CO_2 yields.

A metabolic model with an amended optimisation procedure based on the resource allocation theory is developed in **Chapter 4** to understand mechanistically the production of lactate in glucose MCF under the environmental conditions experimentally observed. The resource allocation theory was used successfully in modelling to predict the production of other compounds that are not compatible with an ATP maximisation framework. In this chapter, the boundaries on the application of ATP maximisation as a suitable optimisation strategy are also investigated.

Due to the lack of modelling approaches for the stoichiometry prediction of protein MCF, bioenergetic models for the mixed-culture monofermentation of protein and the mixed-culture cofermentation of proteins with glucose are developed in **Chapter 5** and **Chapter 6**, respectively. The main goal of these models is to understand the link between environmental conditions (pH and substrate composition) and the variable stoichiometry.

Chapter 7 is centred in developing a kinetic model to using experimental data on protein MCF. The kinetic behaviour of the system is evaluated under different operational conditions and protein amino acid profiles.

As culmination of the thesis, all the insight on MCF gained in accomplishing the previous objectives is condensed from a process design perspective to propose an early-stage design methodology in **Chapter 8**.

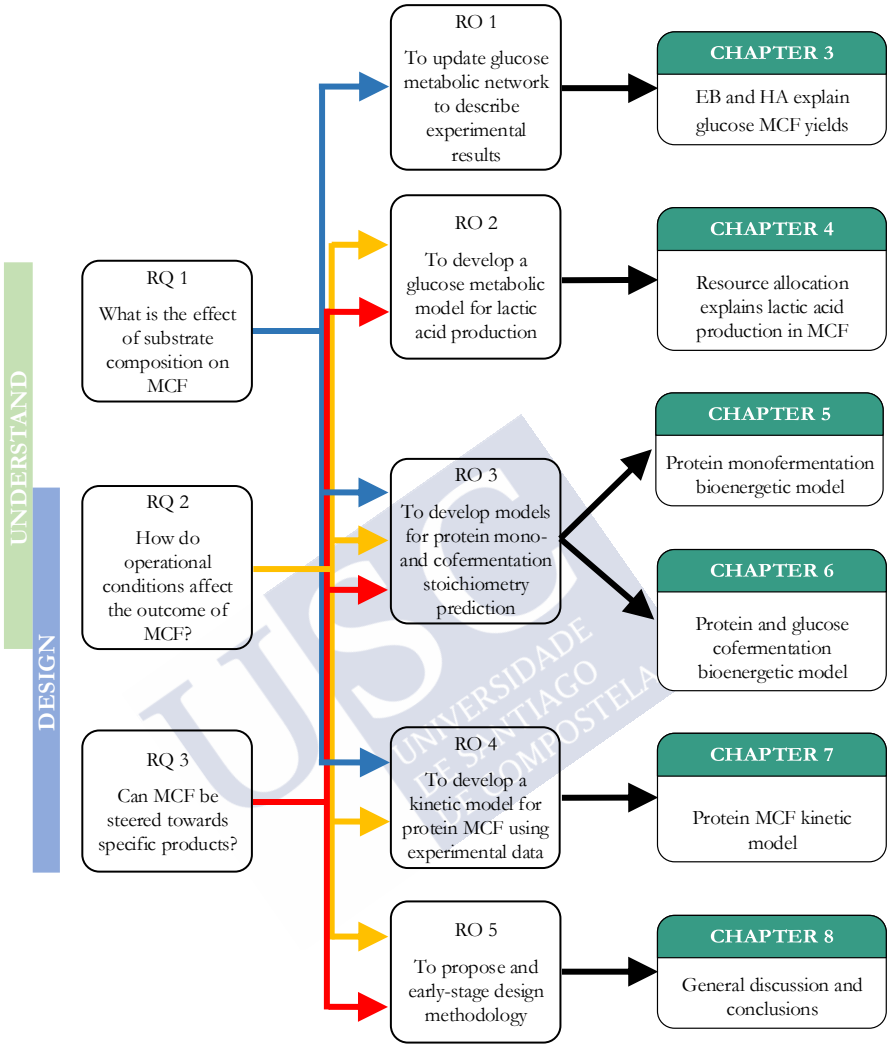

Figure 1.7. Thesis structure and connection with the research questions (RQ) and research objectives

USC
UNIVERSIDADE
DE SANTIAGO
DE COMPOSTELA

CHAPTER 2

Model development

USC
UNIVERSIDADE
DE SANTIAGO
DE COMPOSTELA

2.1. INTRODUCTION

In this section, the main predictive tools developed throughout the thesis are described. These mathematic models respond to different objectives: bioenergetic models have the purpose of predicting the process stoichiometry under different environmental conditions and kinetic models are responsible of describing the process the kinetic behaviour. Bioenergetic models are used in Chapter 5 and Chapter 6 and kinetic models in Chapter 7.

In both cases the system to model is a continuous stirred tank reactor (CSTR) in which up to 3 compartments can be distinguished. The kinetic model considers the reactor bulk and gas headspace of the reactor. Bioenergetic models consider additionally the intracellular space, as they model in detail intracellular processes and transport processes between the bulk reactor and the intracellular matrix (Figure 2.1).

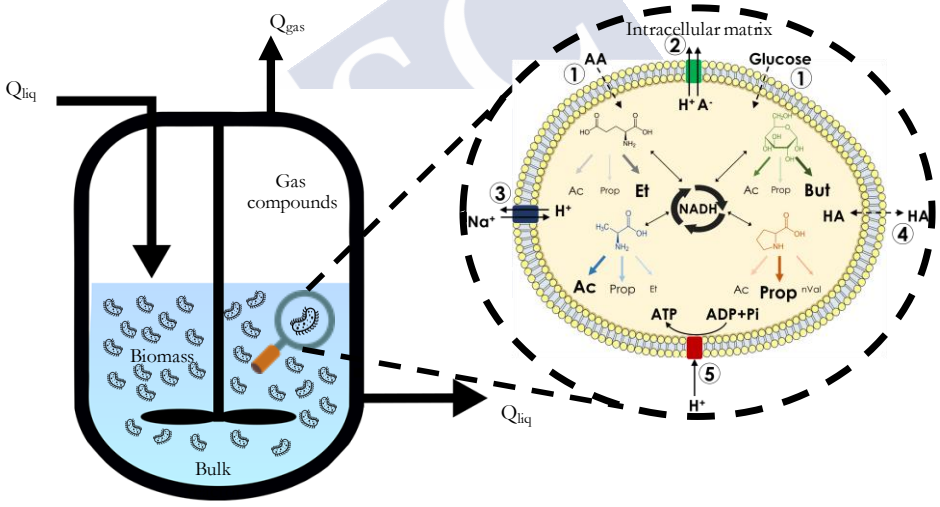

Figure 2.1. System modelled with the four considered compartments: reactor headspace (gaseous compounds), bulk reactor, biomass and intracellular space. In the bioenergetic model the following intracellular processes are modelled: 1: Substrate transport from the bulk reactor to the intracellular space; 2: Active transport of products; 3: Homeostasis via sodium-proton pump; 4: Passive transport of products; 5: ATP production via proton translocation.

The development of the bioenergetic models of this thesis (Chapter 5 and Chapter 6) follows the framework established in a previous contribution of a bioenergetic model for glucose MCF (González-Cabaleiro et al., 2015). The

description of the main cellular processes (e.g. metabolite transport, reaction rate determination) is based on this previous approach with some substantial modifications in the implementation in MATLAB. The building of the metabolic network for protein fermentation and all the consideration regarding the structure of the microbial community and interaction among substrates in co-fermentation scenarios are novel contributions of this thesis.

In this section, firstly the bioenergetic model is described in detail. The mass balances of the system are presented followed by a discussion of the most relevant hypotheses of the model. Then the metabolic network for glucose and AAs is presented and its construction (e.g. electron carrier election, energy conservation methods) explained. Finally, the architecture of the model is described and the optimisation problem defined. The processes included in the kinetic model and their description are discussed at the end of this section.

2.2. BIOENERGETIC MODEL

2.2.1. Model structure and mass balances

The model development is based on the approach used by González-Cabaleiro et al. (2015) for building a glucose fermentation model. The model is built on the mass balances in a continuous stirred tank reactor (CSTR) of the different compounds (states) (Eq. 2.1-2.4). The model defines three compartments: intracellular (where the reactions occur), extracellular (i.e. reactor bulk) and gas phase. The intracellular and extracellular compartments exchange compounds through passive and active transport, and the transfer between the bulk reactor and the gas phase occurs via liquid-gas transfer. Among the states, 3 are moieties related with ATP (ATP, ADP and Pi). The rest represent the concentration of different intracellular compounds (24), extracellular compounds in the bulk reactor (40), gaseous compounds (3) and biomass. NAD^+ to NADH ratio is set fixed to a value of 10 and the intracellular substrate concentrations are assumed constant at a value of 0.1 mM and therefore they are not states.

The mass balances of the system are defined by the following equations (Eq. 2.1-2.4).

Intracellular compounds

$$\frac{dS_{in}}{dt} = R_i + R_{T,in} \quad (2.1)$$

where S_{in} is the intracellular concentration (mol L_X^{-1}), R_i and $R_{T,i}$ are, respectively, the reaction rate and intra-extra cellular transport rate (mol L_x^{-1} h^{-1}). Intracellular concentrations and processes are referred with respect to the biomass volume (L_X).

Extracellular compounds

$$\frac{dS_{ex}}{dt} = D_{liq} \cdot \left(S_{ex,inlet} - S_{ex}\right) + R_{T,\mathrm{ex}} \quad (2.2)$$

where S_{ex} is the extracellular concentration (mol L_{liq}^{-1}), D_{liq} is the dilution rate of the liquid fraction (h^{-1}), $S_{ex,inlet}$ is the concentration on the inlet (mol L^{-1}) and $R_{T,i}$ is the intra-extra cellular transport rate (mol L_{liq}^{-1} h^{-1}). Extracellular concentrations and processes are referred with respect to the liquid volume of the reactor (L_{liq}), i.e. not considering the biomass volume.

Biomass

$$\frac{dS_X}{dt} = -D_{liq} \cdot S_X + R_{ana} - R_{decay} \quad (2.3)$$

where S_X is the biomass concentration (mol L_r^{-1}), R_{ana} is the anabolism rate and R_{decay} the decay rate. The biomass-related concentration and processes are referred with respect to the complete working reactor volume (L_r).

Gas compounds

$$\frac{dG_m}{dt} = -D_{gas} \cdot G_m + R_{T,m} \quad (2.4)$$

where G_m is the concentration (mol L_{gas}^{-1}), D_{gas} is the gas space dilution rate (h^{-1}) and $R_{T,m}$ is liquid-gas transport rate (mol L_{gas}^{-1} h^{-1}). Gas-related concentrations and processes are referred with respect to the headspace volume of the reactor (L_{gas}).

Hereafter, in the next section, the determination of the reaction and transport rates is described in detail.

2.2.2. Model Hypotheses

2.2.2.1. Fermenters are efficiency-driven systems

Anaerobic fermentations carried out in conditions of substrate scarcity (as in a properly operated continuous reactor) are low-energy environments (González-Cabaleiro et al., 2013; Hoehler and Jørgensen, 2013; Jackson and McInerney,

2002b; LaRowe et al., 2012). Under these conditions, microorganisms behave as efficient energy scavengers and microbial groups capable of harvesting the most energy from the substrate (as ATP) will likely dominate the community. In other words, the microbial competition in substrate limitation conditions is set on efficiency rather than on speed. It is expected then that kinetic differences among the branches consuming a particular substrate (e.g. glucose or the different amino acids of a protein) do not play an important role in cellular metabolism and, in consequence, their kinetic description is alike.

2.2.2.2. The microbial community of mixed-culture fermentations is described as an enzyme soup

It is considered that there is a population of one virtual microorganism capable of performing all the theoretical metabolic pathways. This approach assumes that all intracellular metabolites are always available for all routes or, equivalently, that the ability of performing determined pathways is equally distributed across the microbial populations. This approach was termed as *enzyme soup* in opposition to compartmentalized approaches that model the different microorganisms separately and where the boundaries between community members shape the model solution (Bauer and Thiele, 2018; Biggs et al., 2015). The enzyme soup approach is appropriate for those systems in which there is limited *a priori* knowledge about the microbial consortia, such as MCF. Moreover, the communities of such systems are changing continuously (even when the system is at macroscopic steady state) as a result of function redundancy among the species and due to the supply of new microorganisms in the feeding (Carballa et al., 2015; Fernández et al., 1999). In this model, the emphasis is set on exploring the metabolic potential of complex microorganism consortia and not on the interactions between species or with the environment.

2.2.2.3. Some amino acids may be consumed incompletely

Substrate conversion can be limited when its consumption is not energetically feasible or beneficial to the microbial consortia. Although in glucose fermentation the substrate is usually fully converted, protein conversion may be incomplete. Some AA may reach thermodynamic barriers and their degradation pathways result in endergonic reactions under typical intracellular conditions. Experimental evidence indeed shows that it is frequent that proteins are not fully degraded in fermentations (Breure et al., 1985; Breure and van Andel, 1984; Fang and Yu, 2002; Ramsay, 1997; Yin et al., 2016). Consequently, the model can choose to not

consume specific AA completely or partially. Cells will not consume a particular AA if all degradation pathways are overall endergonic. Also, an AA could be not completely consumed even if its degradation is exergonic just because cells cannot conserve energy from its degradation.

2.2.3. Metabolic network

2.2.3.1. Electron carriers

Reduction and oxidation reactions happening in the metabolic network involve different electron carriers (ECs). In the proposed network we consider two of them: ferredoxin (Fd_{red}/Fd_{ox}) and NADH ($NADH/NAD^+$). The couple Fd_{red}/Fd_{ox} is characterized by its low redox potential –$E^{0'} \approx$ - 400 mV[1] and $E' \approx$ - 500 mV[2] (Buckel and Thauer, 2013)– and because it is the only EC capable of reducing protons to H_2. It is only considered to be reduced in high exergonic reactions due to its low reduction potential as, for example, decarboxylations. To regenerate the oxidised form (Fd_{ox}) two options are possible: either the Fd_{red} is oxidised reducing protons to produce H_2 by cytoplasmic ferredoxin:proton reductases (Ech) or formate is produced when CO_2 is reduced instead by ferredoxin:CO_2 oxidoreductases. The production of H_2 and CO_2 versus formate is in a thermodynamic equilibrium ruled only by the pH (González-Cabaleiro et al., 2015; Hoelzle et al., 2014; Temudo et al., 2007). The couple $NADH/NAD^+$ has a higher redox potential than Fd_{red}/Fd_{ox} –$E^{0'}$ = - 320 mV (White et al., 2012), E' = - 280 mV (Buckel and Thauer, 2013)– and it is involved in most of the redox reactions occurring in the metabolic network (González-Cabaleiro et al., 2015; Kleerebezem et al., 2008).

2.2.3.2. Energy conservation

It is assumed that microorganisms conserve energy in two ways. Through substrate level phosphorylation (SLP) microorganisms can yield ATP, transferring a phosphoryl group (PO_4^{3-}) from a metabolite to ADP. Alternatively, microorganisms can extrude one proton outside the cells against its electrochemical gradient -also termed proton motive force (pmf), when coupled to sufficiently exergonic reactions. That same proton will be used to produce

[1] $E^{0'}$ is the redox potential of a reaction at biological standard conditions, i.e. at pH 7 and metabolic concentrations of 1 mM.

[2] E' is the redox potential of a reaction corrected to the typical concentrations found in microorganisms.

ATP when returning to the cytoplasm down its electrochemical gradient. Nevertheless, extruding a proton requires a complex enzymatic machinery, meaning that there is not a proton extrusion in all the steps that energetics would theoretically allow for it. Proton extrusions are only allocated in the metabolic network is places where experimental evidence was found.

Usually, to introduce a phosphoryl group in an organic molecule, it must be previously activated with the cofactor coenzyme-A (CoA-SH), forming a thioester. Then the CoA cofactor is swapped by a phosphoryl group and is eventually transferred to an ADP molecule to give ATP (the SLP process). However, the activation reaction is endergonic (+30-50 kJ/mol) and therefore must be linked to exergonic reactions, as for example decarboxylations. When there is no exergonic reaction to link the CoA activation, the CoA group is transferred directly from other metabolite containing it. In this case the donor molecule loses the possibility of conserving energy by SLP. This consideration is important when constructing the network as the number of ATP molecules yielded in each pathway has a big impact in the model solution.

2.2.3.3. Glucose metabolic network

The metabolic pathways of the major products observed when glucose is fermented by open microbial communities are included in the network (Figure 3.1). The products considered in the glucose metabolic network are: acetate, ethanol, propionate, lactate and butyrate (Angenent et al., 2004; Fang and Liu, 2002; González-Cabaleiro et al., 2015; Hoelzle et al., 2014; Horiuchi et al., 2002; Lengeler et al., 1999; Mohd-Zaki et al., 2016; Rodriguez et al., 2006; Temudo et al., 2008b, 2007; Zhang et al., 2013; Zoetemeyer et al., 1982). All these products derive from a common glycolytic process (glucose conversion to pyruvate), in which the conversion of glucose starts with the *Embden-Meyerhof-Parnas* pathway (EMP) producing two moles of pyruvate per mole of glucose. Two other degradation pathways of glucose can be found in prokaryotes microorganisms: *Entner-Doudoroff* (ED) and *Pentose-Phosphate pathway* (PPP). ED pathway is reported to be related with aerobic environments and to be used to mainly metabolise sugar acids (Peekhaus and Conway, 1998). PPP pathway is mainly used for anabolic purposes (i.e. to obtain the needed metabolites in biomass generation) (Kruger and Von Schaewen, 2003). But the fact that EMP pathway has an ATP yield twice as big as the ED pathway strongly suggests selecting EMP as the glycolysis route in our metabolic network. These reasons, and the fact that in literature the EMP pathway for describing glycolysis is ubiquitous (Buckel and

Thauer, 2013; González-Cabaleiro et al., 2015; Hoelzle et al., 2014; Kleerebezem et al., 2008; Mosey, 1983; Rodriguez et al., 2006; Temudo et al., 2009, 2008b, 2007; Zhang et al., 2013; Zoetemeyer et al., 1982), led us to only consider the EMP pathway.

The three-carbon compounds, propionate and lactate, are directly yielded from pyruvate. Acetate, ethanol and butyrate (compounds with an even number of carbons) need a first decarboxylation of pyruvate to yield acetyl-CoA, in which an equimolar mixture of H_2 and CO_2 or formate is produced via Fd_{red}.

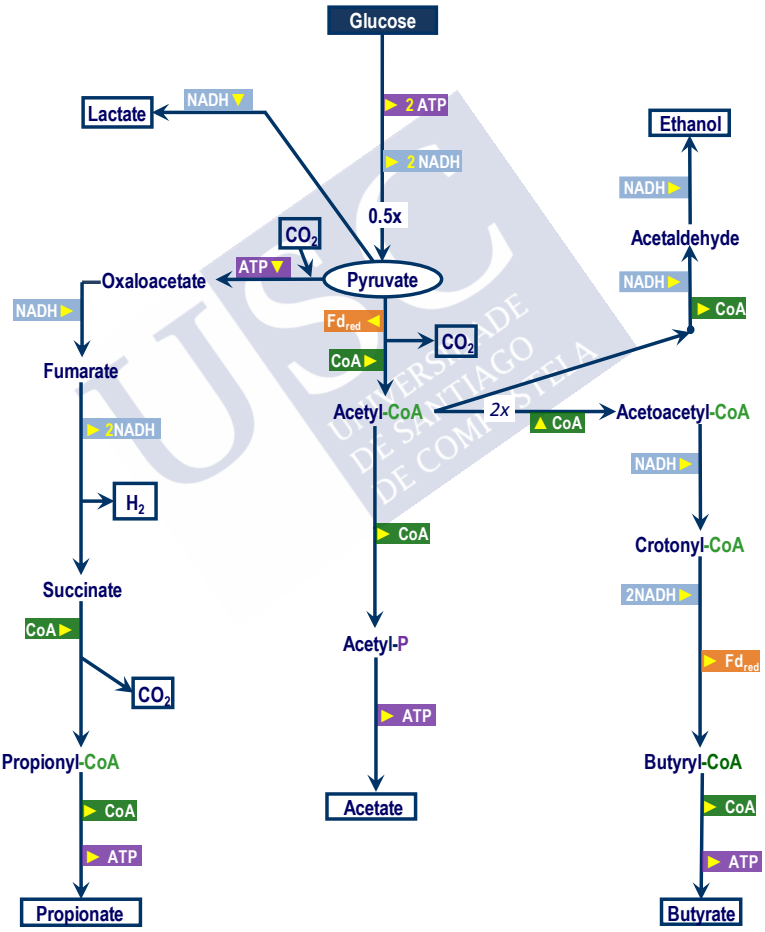

Figure 2.2. Selected metabolic network of glucose fermentation for mixed cultures under fermentative environmental conditions.

Crotonyl-CoA is an intermediate in the butyrate yielding pathway. The crotonyl-CoA reduction with NADH to butyryl-CoA is a very exergonic step ($\Delta G'^{m}$=-57 kJ/mol), indicating that it is probable that energy is conserved in this step. Literature indeed reports energy conservation via proton translocation (Buckel and Thauer, 2013; González-Cabaleiro et al., 2015; Li et al., 2008), but also indicates that another biochemical mechanism might take place: electron bifurcation (EB). EB is a mechanism by which cells can couple endergonic reactions with sufficiently exergonic ones (Buckel and Thauer, 2018; Peters et al., 2016). It was experimentally detected that in this step the exergonic crotonyl-CoA reduction is coupled to the endergonic reduction of Fd_{ox} by NADH, which eventually will yield H_2 (Li et al., 2008). Both possibilities are included in all the crotonyl-CoA reductions featured in the metabolic network. In chapter 3 the inclusion of EB in the metabolic network is studied and the results prove indeed that the consideration of EB reduces the discrepancies between the predicted and experiments results of glucose MCF.

Fumarate reduction to succinate is a similar metabolic step to crotonyl-CoA reduction in terms of energetics and reaction mechanisms (a hydrogenation of a double carbon bond). However, only energy conservation via proton translocation is reported in literature and therefore EB is not placed as an option in this step (Buckel, 2001; Herrmann et al., 2008).

2.2.3.4. Protein metabolic network

The protein bioenergetic model is the first attempt to describe in detail the fermentation of all the AA that conform proteins, to the best of my knowledge. As a consequence, its metabolic network had to be built from scratch integrating many different literature sources for each considered AA. In all cases, only reactions likely to occur in fermentative environments were included in the metabolic network

The metabolic network used in the model is formed by the degradation pathways of 17 amino acids (AAs): alanine, arginine, asparagine, aspartate, cysteine, glutamate, glutamine, glycine, histidine, isoleucine, leucine, lysine, methionine, proline, serine, threonine and valine. AA containing aromatic side chains were not included in the metabolic network (phenylalanine, tyrosine and tryptophan) because their degradation pathways are not sufficiently clear on literature (Andreesen et al., 1989; Barker et al., 1987). Besides, these AA do not account for more than 10% (molar basis) in the usual proteins found in wastes (9.2% in

casein, 9.4% in gelatine, 8.8% in albumin, 7.4% in gluten, 3.7% in keratin and 6.9% in zein). The products covered are fatty acids from C1 to C6, ethanol, formate, methanethiol, hydrogen sulphide, CO_2 and H_2. Butyrate and valerate are present in both their linear and branched form and in the case of caproate only the branched appears as a possible product in the metabolic network. Most of the routes are adapted from Andreesen et al. (1989), Barker (1981) and Fonknechten et al. (2010).

Some AAs are interconverted to others instead of being converted to VFA. This is the case, for example, of glutamine and asparagine, that are the amides of glutamate and aspartate, respectively. In this case we considered that the common AA acts like a node, and the degradation pathways of these AA end in another AA and not in the final products (i.e. VFA). Other AAs have pyruvate as an intermediate in their conversion to VFA. In these cases, the conversion of pyruvate is assumed to follow the metabolic network of glucose from pyruvate on (Figure 2.2).

Alanine (Ala)

Alanine is deaminated to pyruvate by direct oxidation via NAD-dependent alanine dehydrogenase. Pyruvate is then converted following Figure 2.2.

Aspartate (Asp)

Aspartate can be oxidatively deaminated with NAD^+ to yield oxaloacetate, which is then decarboxylated to pyruvate. Aspartate can be as well deaminated to yield fumarate, which is further reduced with NADH to succinate (Unden et al., 2013). Succinate can be either an end product or further catabolised to yield propionate and CO_2 with concomitant ATP formation.

Arginine (Arg)

Arginine is first deaminated to citrulline, which is decomposed into carbamoyl-P and L-ornithine (Figure 2.3). Carbomoyl-P is a compound that releases bicarbonate, ammonium and ATP when decomposed enzymatically, providing the cell with ATP in the hydrolytic step. L-ornithine is as well an AA but, as it only acts as an intermediate in Arginine degradation, it is not considered as a starting AA in the network. L-ornithine has two possible degradation pathways. The first one consists in a deamination to L-proline, racemization to D-proline and then it follows the proline usual degradation pathway (described later). The other option yields D-alanine, acetyl-CoA and NADH (Uematsu et al., 2003).

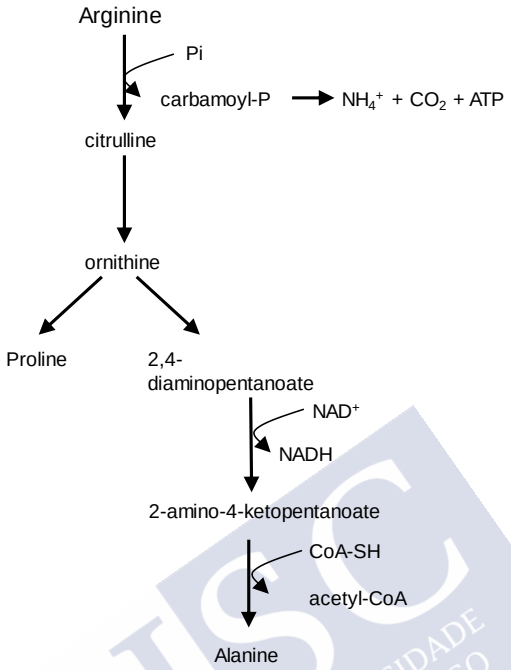

Figure 2.3. Arginine (Arg) degradation pathways considered in the metabolic network.

Cysteine (Cys)

Cysteine is converted to pyruvate and releases one molecule of hydrogen sulphide from the thiol group in carbon 3 (Loddeke et al., 2017). Hydrogen sulphide is a weak acid and is considered to be excreted to the bulk reactor without further transformation.

Glutamate (Glu)

Glutamate is mainly reported to be degraded in two ways (Buckel, 2001; Buckel and Barker, 1974). It might be converted to pyruvate and one acetate (not acetyl-CoA) or, alternatively, glutamate might be transformed to glutaconyl-CoA and then decarboxylated to crotonyl-CoA, which is considered to be completely converted to butyrate. In this pathway, the decarboxylation of glutaconyl-CoA is reported to conserve energy in form of a proton translocation. Other reported degradation pathways yield 4-aminovalerate and 5-aminovalerate but, they are not included in the metabolic network as they are reported to be performed as a reaction to an internal pH drop and against osmotic stress, respectively.

Glycine (Gly)

The most accepted degradation pathway for glycine is reduction and deamination to acetyl-P with NADH to yield acetate and ATP in a subsequent step (Andreesen, 1994). Other options include oxidation to CO_2 and ammonium (discarded as this pathway is reported when glycine is the only carbon source for microorganisms) (Andreesen et al., 1989) and production of methylene-THF, CO_2 and ammonium (which occurs simultaneous to autotrophic pathways).

Glutamine (Gln) and Asparagine (Asn)

These two AA are the amides of Glutamate and Asparagate, respectively. They are deaminated in one step to their respective AA without the generation of reductive power.

Histidine (His)

This AA is converted in several steps to yield glutamate and formamide (the amide of formic acid). Formamide is considered to be split into formate and ammonium without producing energy (Kaminskas et al., 1970; Prusiner and Milner, 1970; Sims et al., 1986).

Lysine (Lys)

This AA has only one reported degradation pathway (Kreimeyer et al., 2007; Ramsay and Pullammanappallil, 2001). Lysine is oxidised with NAD+ to yield butyrate and acetate. One ATP molecule is yielded concomitantly.

Methionine (Met)

Methionine is initially transformed to 2-oxobutyrate and methanethiol (methionine has a sulfur-containing functional group such as Cysteine but in this case is a thioester, not a thiol) (Bonnarme et al., 2001, 2000). Methanethiol is considered to be excreted without further transformation. However, it is not reported whether 2-oxobutyrate is excreted in this way or it is further transformed. It is proposed here that, in analogy with valine, isoleucine and leucine; 2-oxobutyrate is decarboxylated oxidatively in a reaction similar to pyruvate dehydrogenase, by the enzyme 2-oxobutanoate synthase. The products of this reaction are propionyl-CoA, CO_2 and Fd_{red}. Propionyl-CoA is proposed as well to yield ATP at the end of the pathway. 2-oxobutyrate could be also reduced to crotonate, in a reaction scheme equal to leucine reduction to isocaproate (2-oxobutyrate has a hydrogen atom in position 3). Crotonate is then

reduced to butyrate as in the butyrate yielding pathway from pyruvate. As in this last case, we consider that this highly exergonic step can lead via EB to H_2 production or to a proton translocation (section 2.2.3.3).

Proline (Pro)

This AA has only one reported option of anaerobic degradation. It consists in the reduction of two molecules of proline to give two molecules of 5-aminovalerate, which react with themselves to finally yield acetate, propionate and n-valerate. The reaction is a dismutation reaction because one molecule of 5-aminovalerate acts as electron donor while the other as electron acceptor. One ATP is reported to be produced for each two molecules of 5-aminovalerate, giving a ratio of 0.5 ATP produced for each proline converted (Barker et al., 1987).

Serine (Ser)

Serine is reported to have only one catabolic degradation possibility, deamination to yield pyruvate and ammonium (Sawers, 1998). Andreesen et al. (1989) also reports its conversion to glycine and tetrahydrofuran (THF) but this option is related only with anabolic purposes and therefore not included.

Threonine (Thr)

This AA could potentially be degraded via five options, of which only two were retained (Figure 2.4) (Sawers, 1998). On the one hand, deamination to 2-oxobutyrate and then either amination to 2-aminobutyrate, which is excreted, or decarboxylation to propionyl-CoA and subsequent propionate and ATP production. In this last option, the enzyme complex in charge of the decarboxylation step is very similar to the pyruvate dehydrogenase complex or it can even be the same enzyme acting on a different substrate. On the other hand, threonine might be oxidised with NAD^+ to 2-amino-3-ketobutyrate, which is afterwards split into acetyl-CoA and glycine. Alternatively, threonine is also reported to be directly split into acetaldehyde and glycine, but this option is not considered as acetaldehyde is not a common product of MCF and because it has a much lower energy yield compared to the other options available.

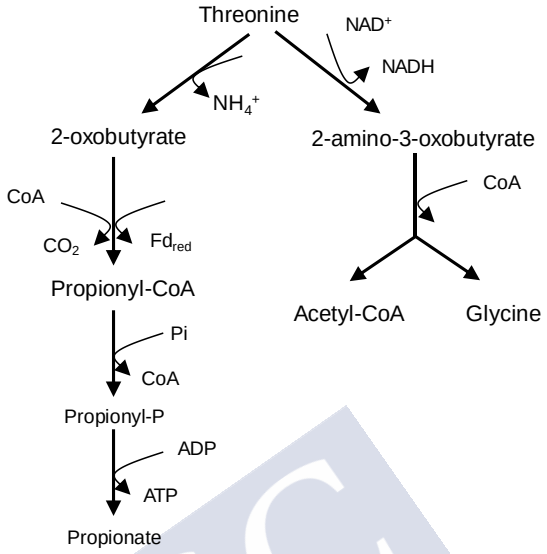

Figure 2.4. Threonine (Thr) degradation pathways considered in the metabolic network.

Valine (Val), Isoleucine (Ile) and Leucine (Leu)

Due to their branched carbon skeleton, the products of these three AAs (Figure 2.5) are branched VFA (isobutyrate, isovalerate and isocaproate, respectively) (Elsden and Hilton, 1978). The pathways and the enzymatic mechanisms of degradation are also similar. All three AA can be oxidised but only one, Leucine, can be reduced.

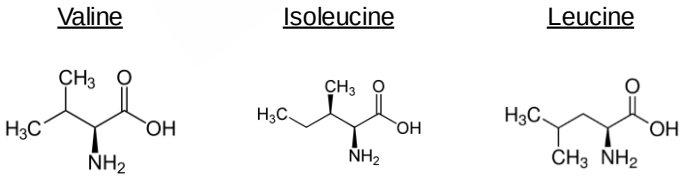

Figure 2.5. AA yielding branched VFA

When oxidised, they are first deaminated oxidatively (i.e. NADH is yielded, reaction 1 in Figure 2.6) to a 2-oxoacid. In the oxidative branch (blue arrows in Figure 2.6) the oxoacid is then decarboxylated with enzymes of the group 2-keto acid oxidoreductase (reaction 2 in Figure 2.6). In this reaction, apart from losing one CO_2 molecule, they produce reduced ferredoxin and one CoA group is added to the carbon skeleton. The reaction scheme is the same as in pyruvate

decarboxylation. In the last step cells conserve energy by SLP. As a result, the resulting VFA has one less carbon than the original AA.

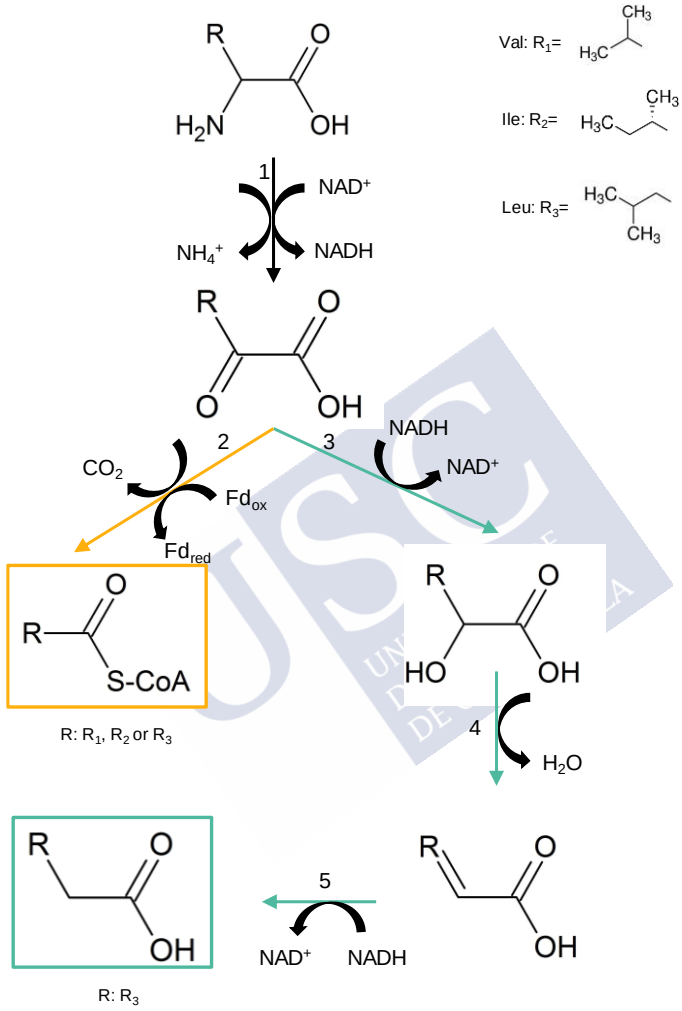

Figure 2.6. Branched-VFA producing AA degradation reaction scheme. Yellow arrows correspond to the oxidative pathway and green arrows to the reductive pathway.

However, as the net ATP production stoichiometry is one mole ATP for each mole AA degraded, the overall reaction will be endergonic and none of the branched AA would be converted to branched VFA. The oxidative branch can be divided in two steps: first an oxidative deamination and then a decarboxylation

with subsequent ATP production. The deamination reaction is significantly endergonic ($\Delta G'_m$=+25.6 kJ/mol for Valine and $\Delta G'_m$=+23.6 kJ/mol for isoleucine), but the decarboxylation is not exergonic enough to make the overall reaction exergonic ($\Delta G'_m$=-8.4 kJ/mol for isobutyrate production and $\Delta G'_m$=-14.2 kJ/mol for isovalerate production). All literature experiments reporting the fermentation of different proteins report branched VFA as a product, indicating that, after all, branched AA consumption does occur in experiments (Breure et al., 1986a, 1986b, 1985; Breure and van Andel, 1984; Fang and Yu, 2002; Tan et al., 2012; Yu and Fang, 2003). To reconcile these two in principle contradictory facts, it is proposed here that part of the ATP generated in the second part of the branch is used to drive the endergonic deamination, in the fashion of the reverse electron transport (RET) mechanism (Elbehti et al., 2000; Stams and Plugge, 2009). A minimal net production of 0.25 ATP was selected to ensure that, even though internal concentrations vary, the global degradation reaction could be exergonic.

The reductive pathway starts after the reduction of the 2-oxo acid generated by deamination to form the corresponding 2-hydroxy acid (reaction 3 in Figure 2.6). This compound is dehydrated, forming an enoate (reaction 4 in Figure 2.6), which can be further reduced to yield a VFA with the same number of carbons as the original AA (reaction 5 in Figure 2.6). However, the enoate reductase, requires a hydrogen atom in position 3, something that only Leucine can satisfy (Figure 2.5) (Simon et al., 1985).

2.2.4. Model description

2.2.4.1. Acid-base speciation

The states of the model are the concentration of the different metabolites that participate in the cell metabolism in the three modelled compartments. They account for all the possible forms of a compound that depend on acid-base equilibria (i.e. with different degrees of protonation). However, to accurately describe some processes, the concentration of a certain form of a compound is needed (e.g. the concentration of the electrically neutral form is needed to describe passive transport).

The speciation of the compounds is determined by their acid-base equilibria, whose equilibrium constants are calculated directly from the Gibbs energy of formation of the compounds involved, which are a parameter of the model.

Acid	$HA \leftrightarrow A^- + H^+$
Base	$B + H^+ \leftrightarrow BH^+$

The charge contribution of each compound is added up in a global charge balance (Eq. 2.5). The resulting non-linear equation is solved following the Newton-Raphson method, thus calculating the proton concentration and pH.

$$F(H^+) = \sum_i f_i(H^+) = 0 \tag{2.5}$$

where, F is the charge balance and f_i are rational functions describing the equilibrium and charge balance of each acid/base compound.

2.2.4.2. Thermodynamic feasibility

The thermodynamic feasibility of the pathways should be addressed, as some pathways may be endergonic under particular environmental conditions. In these cases, the model prevents such pathways using as indicator their change of Gibbs free energy.

The standard Gibbs energy of a reaction (ΔG^0, at standard conditions) is determined with the Gibbs energy of formation of the compounds involved, which are obtained from literature (Alberty, 2010, 2006; Hanselmann, 1991; Thauer et al., 1977) or by using the group contribution method (Flamholz et al., 2012). This value is corrected in each simulation step with the current chemical activities of the compounds involved in the reaction, obtaining thus the actual $\Delta G'$ (Eq. 2.6). To determine the activity the Debye-Hückel law is followed.

$$\Delta G' = \Delta G^0 + RT \cdot \ln Q \tag{2.6}$$

where $\Delta G'$ is the actual Gibbs energy of reaction, ΔG^o is the standard Gibbs energy of reaction, R is the gas constant, T is the temperature and Q is the reaction quotient.

For each of the degradation pathways and at each time step their ΔG is calculated and their feasibility factor (f) is determined. This factor is a step function that varies between 0, when the reaction is endergonic and should not happen, and 1, when the reaction is sufficiently exergonic and can run without limitations. A minimum feasible value for $\Delta G'$ of -2 kJ/mol is assumed to consider a reaction to run, which is a value used previously (González-Cabaleiro et al., 2015).

All step function used in the model are expressed as derivable functions and follow the next general form:

$$f(x) = a \cdot \tanh(x + b) + c \quad (2.7)$$

where *a*, *b* and *c* are constants to modify the shape and limits of the resultant curve and *x* is the function input.

Given that this factor varies continuously between zero and one, there are values of ΔG close to -2 kJ/mol that result in intermediate values, meaning that the reaction does run but at a lower rate. This is in accordance with LaRowe *et al.* (LaRowe et al., 2012).

2.2.4.3. Kinetics

As previously stated (section 2.2.2.1), kinetic differences in the pathways of the same kind of substrate (e.g. carbohydrates or protein), are not expected to shape cellular metabolism in MCF. A tight intracellular regulation is assumed and hence all catabolic reactions arising from a substrate are assumed to have the same rate as the consumption rate of that substrate. The uptake rate of each individual substrate (i.e. glucose and AA) is modelled with a Monod-like equation (Eq. 2.8) with common parameter values for each kind of substrate. Therefore, there are as many independent substrate uptake rates as number of individual substrates in the reactor.

$$r_{S,\mathrm{i}} = {r_{S,\mathrm{i}}}^{max} \cdot \frac{S_{ex,i}}{K_{S,i} + S_{ex,i}} \left(\frac{mol\ i}{mol\ X \cdot h}\right) \quad (2.8)$$

where r_{Si} is the uptake rate of the ith individual substrate, r_{Smax} is its maximum uptake rate, $S_{ex,i}$ is the total bulk concentration of the ith individual substrates and $K_{S,i}$ is the affinity constant.

Subsequent reactions within the pathways of each individual substrate are modelled to have the same rate as the consumption rate of the substrates they originated (Eq. 2.9).

$$R_i = f_i \cdot \nu_i \cdot r_{S,\mathrm{i}} \cdot z_i \cdot S_X \cdot \frac{V_R}{V_X} \left(\frac{mol\ i}{L_x \cdot h}\right) \quad (2.9)$$

where, for the ith reaction, R_i is the reaction rate, fi is the feasibility factor of the reaction, ν_i is the stoichiometry factor between the reaction and the substrate uptake, z_i is the reaction selection parameter (described in section 2.2.5), S_X is the biomass concentration, V_R is the reactor volume and V_X is the biomass volume in the reactor.

2.2.4.4. Anabolism and Decay

The biomass is considered homogeneous and described with a general molecular formula of $CH_{1.8}O_{0.5}N_{0.2}$. It may be formed from glucose, AA and ammonia (when glucose is the only substrate of the system).

Anabolism for glucose follows the stoichiometry of Eq. 2.10. A lumped stoichiometry with a certain degree of decarboxylation is used to describe anabolism (González-Cabaleiro et al., 2015; Tobajas and Garcia-Calvo, 1999). The degree of decarboxylation varies with the substrate and is assumed to be dependent on the heat of combustion of the substrate (Gommers et al., 1988), which in turn can be easily correlated with the degree of reduction (Gary et al., 1995). For glucose the degree of reduction value is 4, which leads to a carboxylation degree of 15% (in terms of moles of carbon of the substrate). The ATP needed to form biomass is set to 2 mol ATP/C-mol biomass, as in previous approaches (González-Cabaleiro et al., 2015).

$$Glucose + 1.02\ NH_4^+ + 9.45\ H_2O + 10.2\ ATP \rightarrow \\ \rightarrow 5.0\ X + 0.90\ CO_2 + 12.1\ H^+ + 10.2\ ADP + 10.2\ P_i \quad (2.10)$$

When protein is the sole substrate, biomass is assumed to be formed from an equimolar mixture of the 17 different AA because any more specific information about AA proportions in typical biomass was not available (Eq. 2.11). To make a general anabolism description that could be used for different proteins as substrate, a mean degree of reduction value of 4 for all AAs was chosen, which leads to the same decarboxylation degree as in the anabolism from glucose (15%). The ATP needed to form biomass is set to 2 mol ATP/C-mol biomass, as in anabolism from glucose, because specific information for biomass growth on protein could not be found (González-Cabaleiro et al., 2015; Tobajas and Garcia-Calvo, 1999).

$$\sum_{i=AA}\left(\frac{1}{17}\cdot AA_i\right) + 9.34\ H_2O + 7.80\ ATP \rightarrow \\ \rightarrow\ 3.90\ X + 0.69\ CO_2 + 0.69\ NH_4^+ + 10.0\ H^+ \\ + 7.80\ \mathrm{ATP} + 7.80\ P_i \quad (2.11)$$

For decay processes the considered stoichiometry is the same but in the forwards direction. If protein is the only substrate, biomass decay is also considered to produce glucose (Eq. 2.10 in the forward direction), since polysaccharides are as well one of the main constituents of biomass (Stouthamer, 1973).

The participation of electron carriers in anabolism and decay is neglected to simplify the modelling procedure but this is not expected to compromise the results of the model due to the generally modest biomass yields in anaerobic processes and because the degree of reduction of biomass and the substrates are very similar.

Anabolism and decay rates are modelled to depend on energy availability, determined by the Gibbs energy of ATP formation (Eq. 2.6) in each simulation step, as an indirect indicator of the availability of ATP. A value higher than 50 kJ/mol ATP indicates that cells have enough energy to grow as it indicates that the ATP concentration is high. If the value is lower than 50 kJ/mol ATP, decay processes take place to regain energy and raise ATP concentration.

Anabolism rate is described with a Monod-like equation (Eq. 2.13), in which the maximum rate term is variable and dependent on energy availability (Eq. 2.12). In the case of anabolism from protein, the substrate is considered to be the sum of the 17 AA in carbon molar basis.

$$k_{ana} = \frac{\Delta G_{ATP} - 50}{5} \quad \left(\frac{mol\ X}{mol\ X \cdot h}\right) \tag{2.12}$$

$$R_{ana} = k_{ana} \cdot \frac{\sum_i S_{ex,i}}{M_{ana} + \sum_i S_{ex,i}} \cdot S_X \quad \left(\frac{mol\ X}{L_r \cdot h}\right) \tag{2.13}$$

where k_{ana} is the anabolism maximum rate, ΔG_{ATP} is the Gibbs energy of ATP formation, R_{ana} is the anabolism rate, $S_{ex,i}$ is the extracellular concentration of the ith substrate (in carbon molar basis) and M_{ana} is the anabolism affinity constant ($6 \cdot 10^{-3}$ Cmol/L).

In cofermentation scenarios, anabolism occurs from glucose and protein and their anabolism rates are determined by Eq. 2.13 using the same parameters. A different rate can only be provoked by a different availability of the substrates through the Monod term.

Decay rate is only controlled by the Gibbs energy of ATP formation (Eq. 2.14).

$$R_{decay} = \frac{50 - \Delta G_{ATP}}{5} \cdot S_X \quad \left(\frac{mol\ X}{L_r \cdot h}\right) \tag{2.14}$$

2.2.4.5. Transport

Cells have evolved semi-permeable membranes that allow for both uncontrolled passive transport and controlled active transport. Uncharged molecules diffuse freely through the membrane, as for example the protonated form of VFA. Charged molecules and big neutral molecules (e.g. glucose or AA) cannot diffuse

across the membrane and must be transported actively by a wide set of channel proteins that are controlled by the cell (White et al., 2012).

Passive transport (Eq. 2.15) is energetically uncoupled to microorganisms and is governed by Fick's Law (i.e. transport follows the concentration gradient of each compound). There is little data available in literature about diffusion coefficients (k_{Diff}) for the different compounds present in the model but values used in previous modelling works are in the same order of magnitude (González-Cabaleiro et al., 2015; Rodriguez et al., 2006; Zhang et al., 2013). Following González-Cabaleiro et al. (2015) approach, all diffusion coefficient are set to 100 $L/mol_X \cdot h$, as the main divergencies among the transport rates will be caused by the differences in their acidification degree (i.e. proportion between the charged and uncharged form of a molecule following acid-base equilibrium), which are already accounted for in the model (section 2.2.4.1).

$$R_{Diff,i} = k_{Diff} \cdot \left({S_{ex,i}}^{uncharged} - {S_{in,i}}^{uncharged} \right) \cdot X \cdot \frac{V_R}{V_X} \left(\frac{mol\ i}{L_x \cdot h} \right) \tag{2.15}$$

where, for the ith compound, $R_{Diff,i}$ is the passive transport rate, k_{Diff} is the diffusion coefficient, ${S_{ex,i}}^{uncharged}$ is the extracellular uncharged concentration and ${S_{in,i}}^{uncharged}$ is the intracellular uncharged concentration.

Active transport, on the contrary, is coupled energetically to metabolism and can be performed against or in favour of the electrochemical gradient and hence be an energy expenditure or gain, respectively. These channel proteins (or ports) are modelled to be coupled to proton translocations. Negatively charged molecules (e.g. anions of organic acids) are transported to the extracellular matrix by a symporter with protons and positively charged molecules (e.g. ammonium) are transported in antiport with protons, to make the process transport electrically neutral.

As an enzymatically controlled process, active transport is also modelled with a Monod-like equation (Eq. 2.16). We assumed that the maximum active transport ratio is equal to the maximum production rate of that compound being transported (Eq. 2.17). Finally, Eq. 2.18 determines the active transport rate.

$$r_{Act,i} = {r_{Act,i}}^{max} \cdot \frac{S_{in,i}}{K_T + S_{in,i}} \quad \left(\frac{mol\ i}{mol\ X \cdot h} \right) \tag{2.16}$$

$${r_{Act,i}}^{max} = \sum_{j=AA} \nu_{i,j} \cdot {r_{S,AA}}^{max} \quad \left(\frac{mol\ i}{mol\ X \cdot h} \right) \tag{2.17}$$

$$R_{Act,i} = r_{Act,i} \cdot X \cdot \frac{V_R}{V_X} \quad \left(\frac{mol\ i}{L_x \cdot h}\right) \tag{2.18}$$

where, for the ith compound, $r_{Act,i}$ is the active transport rate, $r_{Act,i}^{max}$ is the maximum active transport rate, $S_{in,i}$ is the intracellular concentration, K_T is the active transport affinity constant (0.15 M) and $\nu_{i,j}$ is the stoichiometric coefficient of compound i in the degradation reaction of AA j.

Intracellular metabolic concentrations above 10 mM are considered not physiologically compatible (González-Cabaleiro et al., 2013) and rarely measured above this value (Bar-Even et al., 2012). When the concentration of one actively transported compound reaches this value, active transport rate is calculated with Eq. 2.19, preventing thus a higher accumulation.

$$R_{Act,i} = R_i - R_{Diff,i} \quad \left(\frac{mol\ i}{L_x \cdot h}\right) \tag{2.19}$$

Finally, total transport is the sum of both transport mechanisms (Eq. 2.20).

$$R_{T,i} = R_{Diff,i} + R_{Act,i} \quad \left(\frac{mol\ i}{L_x \cdot h}\right) \tag{2.20}$$

where $R_{T,i}$ is the total transport rate.

Substrate molecules are modelled to be transported inwards by active transport because they are either electrically charged and/or are not small enough to freely diffuse across cell membranes. However, it is not clear how their transport is coupled to the energetics of microorganisms. Studies are more focused on describing the characteristic of the ports and how they are controlled than on how transport is coupled with the energetic part of metabolism (Berger, 1973; Guidotti et al., 1978; Heyne et al., 1991; Meister, 2016; Oxender and Christensen, 1963; Poole, 1978). For example, some AA transport mechanisms appear to be stoichiometrically linked to Na^+ or proton intrusion but it is not clear whether they use the energy of those movements or not (Poole, 1978). Substrate intake mechanisms are therefore left uncoupled to cell energetics in the model due to lack of information.

Abiotic transport of H_2 and CO_2 between the liquid phase and the gas head space is modelled assuming phase equilibrium (Henry's Law) and constant atmospheric pressure in the reactor head.

2.2.4.6. Energetics evaluation

The model considers that cell energetics revolve around ATP: the energy gained in catabolism or transport is stored in form of phosphate bonds in ATP and all energetic needs are satisfied by hydrolysing those phosphate bonds to generate ADP, Pi and useable energy. This energy can then be invested in growth, maintenance or fuelling active transport against the electrochemical gradient. The balance of ATP in catabolism is composed of five terms, which are described down below.

Substrate-level phosphorylation (SLP)

ATP can be directly generated by catabolic reactions. The contribution of SLP to the global ATP balance can hence be calculated straightforwardly from the reaction rates and the stoichiometry (Eq. 2.21)

$$R_{ATP,SLP} = \sum_i R_i \cdot \nu_{ATP,i} \tag{2.21}$$

where $R_{ATP,SLP}$ is the production rate of ATP by SLP.

Proton translocation

The cell membrane acts like a capacitor. In some exergonic metabolic steps, microorganisms can extrude a proton from the cytoplasm to the medium, storing thus energy on the membrane as its electric potential difference rises. When that proton re-enters the cell, it does it through a channel protein (ATPase) and lowers the membrane potential as a result. The energy released is stored in ATP molecules, following the chemiosmotic theory (White et al., 2012). Conversely, an ATP molecule can be broken to release energy and extrude protons that will fuel endergonic processes when re-entering the cell.

The energy needed to extrude a single proton and the number of protons needed to yield an ATP molecule depend on the proton motive force (pmf, i.e. the electrochemical potential energy of a proton). The energy needed for translocating a proton is calculated using Eq. 2.22.

$$\Delta\mu_{H^+} = F \cdot \Delta\psi + R \cdot T \cdot ln\left(\frac{S_{ex,H^+}}{S_{in,H^+}}\right) \qquad \left(\frac{kJ}{mol\ H^+}\right) \tag{2.22}$$

where $\Delta\mu_{H+}$ is the pmf, F is the Faraday constant, $\Delta\psi$ is the difference between the extracellular and intracellular electric potential, R is the gas constant, T the temperature, $S_{ex,H+}$ is the extracellular proton concentration and $S_{in,H+}$ the intracellular proton concentration.

The electric potential of the membrane is assumed to be 0 V on the outside and -0.2 V on the inside. In this model, the electric potential is considered to be constant, meaning that processes increasing membrane electrical potential are balanced with processes decreasing it. Intracellular pH is also considered constant at a value of 7, leaving extracellular pH as the only variation source for the pmf. In those reactions where the possibility of a proton extrusion is considered, the model evaluates in each simulation step whether the energy available (i.e. ΔG') is high enough for extruding a proton (i.e. if it is higher that the pmf). In case the reaction is not exergonic enough, the same reaction without a proton extrusion is considered. The energy released by proton intrusion is converted into ATP, as explained before. The rate at which ATP is produced by proton translocations is calculated with Eq. 2.23.

$$R_{ATP,pmf} = R_{H^+,pmf} \cdot \frac{\Delta\mu_{H^+}}{\Delta G_{ATP}} \tag{2.23}$$

where $R_{ATP,pmf}$ is the ATP formation rate due to proton translocations and $R_{H+,pmf}$ is the proton rate across the membrane due to proton translocations.

Transport

Active transport of end products is modelled to occur concomitantly with proton transport inwards or outwards, depending on the electric charge of the product being transported. Logically, protons being transported across the membrane exchange energy with the cell and, accordingly, it should be accounted for. The transport of an end product can be against or in favour of its concentration gradient, consuming or releasing energy, respectively. This energy exchange is coupled to proton extrusion as well, resulting in a net production or consumption of ATP (Eq. 2.24). When the active transport of a compound is an exergonic process, energy is conserved by proton translocations to the cytoplasm, which is converted to ATP as previously explained. On the contrary, if the active transport of a compounds is an endergonic process it is fuelled by ATP (through a proton translocation coupled to ATP hydrolysis).

$$R_{ATP,Transport} = \left(\frac{R \cdot T \cdot ln\left(\frac{S_{in,i}}{S_{ex,i}}\right) - z_i \cdot F \cdot \Delta\psi}{\Delta\mu_{H^+}} + z_i \right) \cdot \frac{\Delta\mu_{H^+}}{\Delta G_{ATP}} \cdot R_{Act,i} \tag{2.24}$$

where $R_{ATP,Transport}$ is the ATP formation rate associated to active transport

Maintenance

Energy requirements for cell maintenance are defined to be directly correlated with the biomass concentration (4.5 kJ/mol_{Cx} h). Therefore, the ATP consumption is calculated with Eq. 2.25.

$$R_{ATP,maintenance} = -\frac{4.5}{\Delta G_{ATP}} \tag{2.25}$$

where $R_{ATP,maintenance}$ is the ATP consumption rate due to maintenance

Homeostasis

Intracellular pH is maintained around a value of 7 with a Na^+/H^+ antiporter (Padan et al., 1981). It is modelled like a proportional controller with a setpoint of an intracellular pH of 7. Extracellular Na^+ concentration is set equal to its intracellular concentration at each simulation step as we consider that microorganisms would choose the cation (e.g. Na^+ or K^+) that requires less energy to be transported (i.e. that has the minimum concentration gradient). To calculate its ATP cost the equation for active transport (Eq. 2.26) is used considering that the intra and extracellular Na^+ concentrations are equal, resulting in Eq. 2.26.

$$R_{ATP,homeostasis} = \frac{R \cdot T \cdot ln\left(\frac{S_{ex,H^+}}{S_{in,H^+}}\right)}{\Delta\mu_{H^+}} \cdot R_{Na^+/H^+} \tag{2.26}$$

where $R_{ATP,homeostasis}$ is the ATP spent in homeostasis.

2.2.5. Solution strategy

The different terms of the balances (section 2.2.1) are determined following the flowchart of Figure 2.7. The initial state values and the feeding properties (flow rate and compound concentrations) are the initial inputs of the model. Firstly, the thermodynamic limitation factor is calculated with the current state values (*thermodynamic limitation* step).

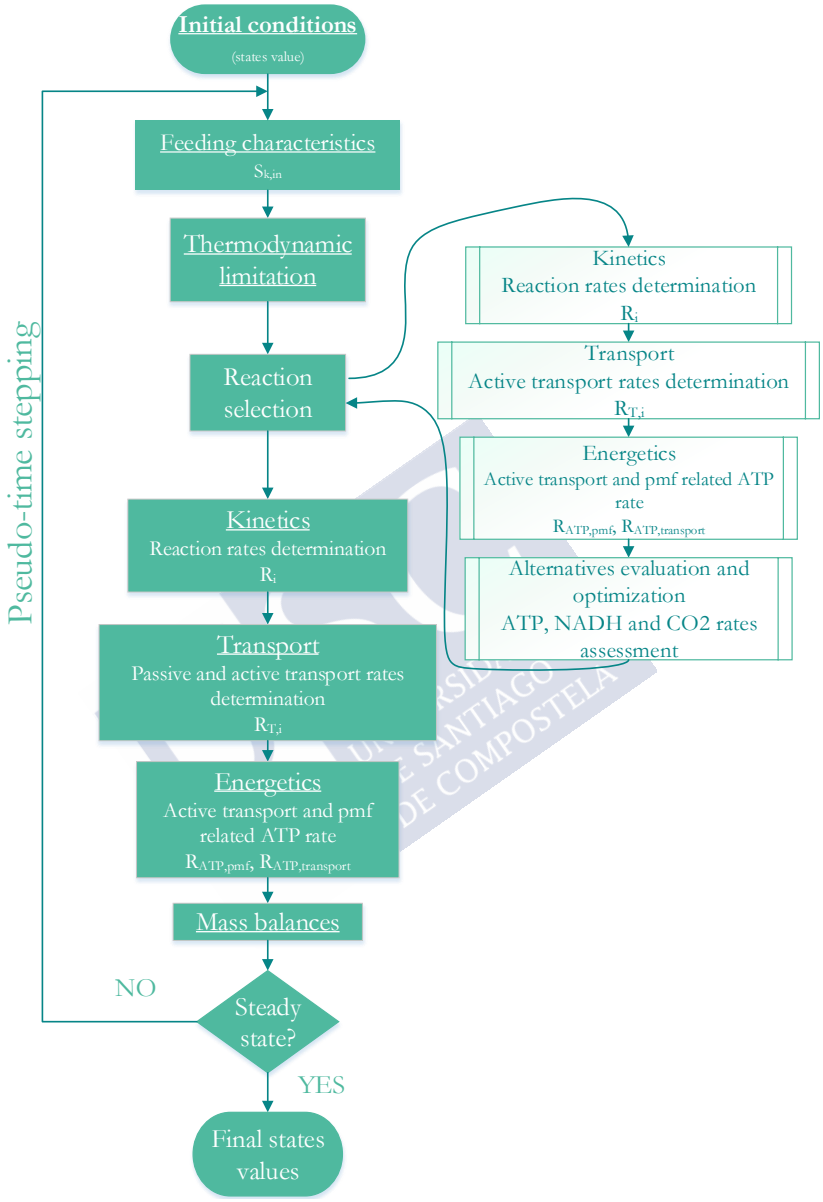

Figure 2.7. Workflow diagram for model solution

Then, in the reaction selection step, the different degradation pathways of the different substrates are first evaluated and then selected by an optimisation procedure (Eq. 2.29-2.30). The reaction evaluation step is divided into several

substeps: determination of the reaction rates (*kinetics*), of the associated transport rates (*transport*) and of the ATP production rate by proton translocations and active transport (*energetics*). Firstly, these tasks are evaluated assuming that each of the substrates is totally and individually converted through each of their possible conversion pathways (*reaction selection step*). Secondly, the optimal set of reactions is selected in the *optimisation* step. The reaction selection step is not performed in each simulation step and the model enters its loop at variable time steps, which are determined depending on the stability of the optimisation problem solution.

Afterwards, the kinetics, transport and energetics substeps are repeated with the set of reactions deemed as optimal in the optimisation program. Finally, the mass balances (Eq. 2.1-2.4) are determined and the steady state condition is evaluated. If it is not yet reached, the state values are updated following a pseudo-time stepping solution procedure, and a new iteration begins.

The objective function aims to maximise ATP production from the substrates. This reflects the hypothesis that the microorganisms capable of harvesting as much energy as possible from the substrate are dominant in an anaerobic mixed microbial community. The net ATP production includes the ATP formed by substrate-level phosphorylation (SLP), the ATP gained through proton translocations and the ATP spent in the active transport of compounds.

Model constraints are related to electron carrier conservation: NADH production and consumption must be balanced within the catabolism because there is no external electron acceptor that could act as an electron sink. Thus, the optimisation problem to be solved can be expressed as follows (Eq. 2.27-2.30):

$$\max_{z} \; r_{ATP}(z) \qquad \text{(mol ATP/L}_X\text{·h)} \qquad (2.27)$$

$$r_{NADH}(z) = 0 \qquad \text{(mol NADH/L}_X\text{·h)} \qquad (2.28)$$

$$0 \leq z_{i,j} \leq 1 \qquad (2.29)$$

$$\sum_{j} z_{i,j} = 1\,, \;\; i = 1, \dots, n_{substrates} \qquad (2.30)$$

where: r_{ATP} and r_{NADH} are the global ATP and NADH production rates, respectively and $z_{i,j}$ are the elements of the matrix of decision variables. They represent the yield of the different metabolic branches of each substrate. Concretely, $z_{i,j}$ is the yield of the metabolic branch *i* of the *jth* substrate and varies continuously between 0 and 1. For each of the AA there is a null reaction available.

The model of the reactor is solved to steady state as a system of nonlinear algebraic equations. A commonly encountered problem in the solution of

moderately large nonlinear algebraic systems is that they tend to get stuck in local solutions or be driven to infeasible states (e.g. negative concentrations). To prevent these issues, we used pseudo-time stepping as heuristic solving method as previously reported by Ceze and Fidkowski (2015), whereby the algebraic system of equations is formulated as a system of ODEs. This system of ODEs was solved until steady state by MATLAB (R2016a) command ode15s. Steady state was assumed when all the state absolute derivatives values were under $1 \cdot 10^{-4}$ mol L^{-1} h^{-1}.

Although based in FBA strategies, our approach differs in how internal concentrations are assumed. Usually in FBA, measured internal concentration values at steady state are used or determined by heuristic (i.e. most probable values based on maximum compatible metabolic concentration, energetics, etc.) (Kleerebezem et al., 2008; Rodriguez et al., 2006; Zhang et al., 2013). This assumption limits the influence of environmental conditions on the product spectrum because it fixes intracellular concentrations to a set value. However, our goal focuses particularly on studying how environmental conditions are linked to the intracellular environment and *vice versa*, in particular by the effect on the energetic cost of transport of products and pH regulation (i.e. how the reactor conditions affect microbial metabolism and how microbial metabolism affects in turn the reactor conditions).

For its solution procedure, the model could be classified as a dynamic flux balance analysis (dFBA) since the reactor state concentration are modelled dynamically and the system stoichiometry is determined by a linear programming optimisation problem (Eq. 2.27-2.30) (Mahadevan et al., 2002; Perez-Garcia et al., 2016; Zhuang et al., 2011). The main difference with standard dFBA models lies on the fact that intracellular concentrations are not assumed to be fixed (e.g. measured values at steady state or assumed values based on heuristic knowledge) and are modelled dynamically as well. In this way, intracellular concentrations are impacted by environmental conditions and vice versa through mechanisms such as active transport, which could have an effect on the solution of the model and on the predicted product spectrum.

2.3. KINETIC MODEL

To complement the bioenergetic model described in the previous sections a kinetic model was also developed in this thesis. The bioenergetic model is centred in determining the stoichiometry of the system but, for design completely a

process the kinetics of processes participating in the system, and how they are affected by the environment, need also to be addressed. Due to the absence of kinetic models for protein MCF, a model for describing the kinetics of protein MCF was developed.

2.3.1. Acidogenesis

As the bioenergetic model considers directly amino acids and the experiments used for its calibration were done using hydrolysates of protein, the kinetic model considers that the feeding is completely hydrolysed and consists of a mixture of individual AA. Furthermore, the aim of this kinetic model is not to follow the conversion kinetics of each of the AA but to describe the protein MCF process as a whole. The consumption of amino acids is described by a Monod equation (Eq. 2.31), in which the half-saturation constant is set to a value of 1.5 g_{AA}/L, as in previous works (Bai et al., 2015; Flotats et al., 2006). The substrate concentration state (S_{AA} in Eq. 2.31) represents the sum of the individual amino acid concentrations in the reactor or, alternatively, the hydrolysed protein. This option was preferred over defining one state for each amino acid, as in the bioenergetic model, since the concentration of individual amino acids was not followed in the experiments and therefore it would add unnecessary complexity to the model while not proving any additional accuracy.

$$r = r_{max} \cdot \frac{S_{AA}}{K_S + S_{AA}} \cdot S_X \tag{2.31}$$

where q is the specific rate, q_{max} is the maximum rate, S_{AA} is the substrate (amino acids) concentration, K_S is the half-saturation constant and S_X is the biomass concentration.

To reflect the non-complete acidification commonly observed in protein and amino acid fermentation experiments in contrast with anaerobic digestion (Bevilacqua et al., 2020b, 2020a; Breure and van Andel, 1984; Duong et al., 2019), the model considers that substrate is converted to VFA (acidification) and to an inert fraction (Table 2.1). Each process has a specific maximum rate value (Table 2.2) and the ratio between these two values indicates the acidification degree of the substrate.

It is assumed that there is only one microbial group utilising amino acids as substrates. Its growth is only modelled to occur due to amino acids acidification (Table 2.1) and its decay is modelled as a first order kinetics with respect to the biomass concentration (Table 2.2).

Table 2.1. Stoichiometric matrix of the different processes considered in the model

	S_{AA}	S_{VAL}	S_{BUT}	S_{PRO}	S_{AC}	S_{ARO}	S_{H2}	S_{inert}	$S_{X,AA}$
Acidification	-1	f_{VA}	f_{BUT}	f_{PRO}	f_{AC}	f_{ARO}	f_{H2}		
Conversion to inerts	-1							1	
Growth	-1								1
Decay								1	-1

Amino acid acidification is modelled to convert amino acids to acetate, propionate, butyrate, valerate, aromatic VFA (which are product of the acidification of aromatic amino acids) and H_2. The stoichiometry of the system is described through stoichiometric factors (*f*) that relate the substrate consumption rate with the production rate of each product. During the batch experiments, the concentration of C2-C5 VFA was followed but aromatic VFA and H_2 were not measured and therefore its stoichiometry cannot be determined from the experimental data.

Table 2.2. Rate equation descriptions of the different processes considered in the model

	Rate equation
Acidification	$r_{Acid} = r_{Acid,max} \cdot \frac{S_{AA}}{K_{S,AA} + S_{AA}} \cdot S_X$
Conversion to inerts	$r_{Inert} = r_{Inert,max} \cdot \frac{S_{AA}}{K_{S,AA} + S_{AA}} \cdot S_X$
Growth	$\mu = r_{Acid} \cdot Y$
Decay	$r_{decay} = k_{decay} \cdot S_X$

To make an estimation of their stoichiometric coefficients, the stoichiometry proposed by Ramsay and Pullammanappallil (2001) is used together with the amino acid composition of the substrates. In this way, and assuming a non-selective conversion of the amino acids, it can be calculated that aromatic VFA account for 10.9% and 4.9% of the products in COD basis for casein and gelatine, respectively. The share of H_2 in the product spectrum for casein is 5.2% (COD basis) while in gelatine fermentation its contribution is negligible. The results of the bioenergetic model generated throughout this thesis cannot be used

for this purpose since the metabolic networks of this model does not include the aromatic AA (section 2.2.3.4).

2.3.2. Methanogenesis

Acetogenesis (conversion of VFA to acetate) and methanogenesis (either from acetate or from H_2) are included in the model (Table 2.3). In first place, the conversion of valerate, butyrate and propionate to acetate (acetogenesis) with concomitant hydrogen production. Valerate and butyrate consumption share biomass group while propionate is converted to acetate by its own biomass group. Methane can be produced either from acetate (acetoclastic methanogenesis) or from hydrogen (hydrogenotrophic methanogenesis). Each conversion is assigned a different microbial group.

Table 2.3. Stoichiometric matrix of the processes related with methane production from VFA.

Process	S_{Val}	S_{But}	S_{Pro}	S_{Ac}	S_{H2}	S_{CH4}	X_{C4-C5}	X_{Pro}	X_{Ac}	X_{H2}	Rate equation
Valerate cons.	-1		$(1-Y_{C4})\cdot 0.54$	$(1-Y_{C4})\cdot 0.31$	$(1-Y_{C4})\cdot 0.15$		Y_{C4-C5}				$q_{Val} = q_{Val,max} \cdot \frac{S_{Val}}{K_{S,Val} + S_{Val}} \cdot X_{C4-C5} \cdot I_{H_2,C4-C5} \cdot I_{pH,acid}$
Butyrate cons.		-1		$(1-Y_{C4})\cdot 0.8$	$(1-Y_{C4})\cdot 0.2$		Y_{C4-C5}				$q_{But} = q_{But,max} \cdot \frac{S_{But}}{K_{S,But} + S_{But}} \cdot X_{C4-C5} \cdot I_{H_2,C4-C5} \cdot I_{pH,acid}$
Propionate cons.			-1	$(1-Y_{Pro})\cdot 0.57$	$(1-Y_{Pro})\cdot 0.43$			Y_{Pro}			$q_{Pro} = q_{Pro,max} \cdot \frac{S_{Pro}}{K_{S,Pro} + S_{Pro}} \cdot X_{Pro}$
Acetate cons.				-1		$(1-Y_{Ac})\cdot 1$			Y_{Ac}		$q_{Ac} = q_{Ac,max} \cdot \frac{S_{Ac}}{K_{S,Ac} + S_{Ac}} \cdot X_{Ac} \cdot I_{pH,aceto}$
Hydrogen cons.					-1	$(1-Y_{H2})\cdot 1$				Y_{H2}	$q_{H_2} = q_{H_2,max} \cdot \frac{S_{H_2}}{K_{S,H_2} + S_{H_2}} \cdot X_{H_2} \cdot I_{pH,hydro}$

The kinetic parameters used are taken from the ADM1 model (Batstone et al., 2002a) and shown in Table S3.

Table 2.4. Kinetic parameter values used for simulating methanogenesis.

Parameter	Value used
$q_{Val,max}$ (g_{COD} Val/g_{COD} BM·h)	0.8
$q_{But,max}$ (g_{COD} But/g_{COD} BM·h)	0.8
$q_{Pro,max}$ (g_{COD} Pro/g_{COD} BM·h)	0.5
$q_{Ac,max}$ (g_{COD} Ac/g_{COD} BM·h)	0.4
$q_{H2,max}$ (g_{COD} H_2/g_{COD} BM·h)	1.0
$K_{S,Val}$ (g_{COD} Val/L)	0.2
$K_{S,But}$ (g_{COD} But/L)	0.2
$K_{S,Pro}$ (g_{COD} Pro/L)	0.1
$K_{S,Ac}$ (g_{COD} Ac/L)	0.15
$K_{S,H2}$ (g_{COD} H_2/L)	$6 \cdot 10^{-4}$
Y_{C4-C5} (g_{COD} BM/g_{COD} C4-C5)	0.06
Y_{Pro} (g_{COD} BM/g_{COD} Pro)	0.04
Y_{Ac} (g_{COD} BM/g_{COD} Ac)	0.05
Y_{H2} (g_{COD} BM/g_{COD} H_2)	0.06

All three processes (acetogenesis and the two methanogenesis) performance is affected negatively by low pH values. The rate of the processes is multiplied by an inhibition function (Eq. 2.32) with two parameters representing the lower and upper limit of the inhibition. The inhibition function and the parameters for each process are taken from the ADM1 model (Table 2.5).

$$I = \frac{1 + 2 \cdot 10^{0.5 \cdot (pH_{LL} - pH_{UL})}}{1 + 10^{(pH - pH_{UL})} + 10^{(pH_{LL} - pH)}} \tag{2.32}$$

Table 2.5. Parameters for the pH inhibition function of the three processes affected by pH inhibition

	pH_{LL}	pH_{UL}
Acetogenesis	4	5.5
Acetate consumption	6	7
Hydrogen consumption	5.8	7

Hydrogen concentration only inhibits acetogenesis and follows the form of a non-competitive inhibition (Eq. 2.33). The values for the three acetogenesis-related processes are shown in Table 2.6 and were taken from the ADM1 model.

$$I_{H_2} = \frac{1}{1 + \frac{S_{H_2}}{K_I}} \tag{2.33}$$

Table 2.6. Parameters of the hydrogen inhibition function for the different acetogenic processes.

	K_I ($g_{COD\text{-}H2}/L$)
Butyrate and valerate consumption (C4-C5)	$1 \cdot 10^{-5}$
Propionate consumption (Pro)	$3.5 \cdot 10^{-6}$

Additional processes (e.g. chain elongation) could be easily added to the model if needed. Also, the kinetic description of the current processes may be modified to reflecting ongoing phenomena such as product inhibition or ammonia toxicity.

USC
UNIVERSIDADE
DE SANTIAGO
DE COMPOSTELA

CHAPTER 3

Electron bifurcation mechanism and homoacetogenesis explain products yields in mixed-culture anaerobic fermentations

Summary

Available mathematical models for the prediction of glucose MCF stoichiometry cannot reproduce the experimental results under some pH conditions. In particular, under acidic conditions the experimentally reporter equimolar production of acetate and butyrate is not well captured, which highlights our incomplete knowledge of the process. The discrepancies between the model and experimental results could be connected to the use of an incomplete or inaccurate metabolic network. To address this issue, in this chapter a new metabolic network of glucose fermentation by microbial mixed cultures incorporating electron bifurcation and homoacetogenesis is proposed. Using a methodology based on NADH balances to analyse published experimental data the new stoichiometry proposed is evaluated. This work proves for the first time that including electron bifurcation in the metabolic network allows for a better description of the experimental results. Homoacetogenesis has been used to explain the discrepancies between observed and theoretically predicted yields of gaseous H_2 and CO_2 and it appears as the best solution among other options studied. Overall, the conclusions of this chapter support the consideration of electron bifurcation as an important biochemical mechanism in microbial mixed cultures fermentations and underline the importance of considering homoacetogenesis when analysing anaerobic fermentations.

3.1. INTRODUCTION

Experimentation on MCFs show that there is a tight relationship between the operational conditions and the products obtained (Fang and Liu, 2002; Horiuchi et al., 2002; Temudo et al., 2007; Zoetemeyer et al., 1982). How this relationship works is not clear enough and for this reason, directing product formation in MCFs is still a challenging task. Most part of the literature is purely an experimental description of the system and the mechanisms causing the shifts in product spectrum are rarely matter of discussion. Only a handful of studies, mostly mathematical models, are truly centred in understanding the connection between the environmental conditions and the changes observed in the product spectrum in glucose MCF (González-Cabaleiro et al., 2015; Groeger et al., 2017; Kleerebezem et al., 2008; Mosey, 1983; Rodriguez et al., 2006; Zhang et al., 2013). However, even though their predictions have improved over time and are able now to capture the main changes observed in the stoichiometry with some operational conditions, there are still some discrepancies when compared with the experiments. For example, in glucose MCF at low pH butyrate is predicted to be the main product in González-Cabaleiro et al. (2015) or Kleerebezem et al. (2008) but experimentally an equimolar mixture of butyrate and acetate is reported (Fang and Liu, 2002; Temudo et al., 2007; Zoetemeyer et al., 1982). These discrepancies might be due to the use of an incomplete metabolic network that does not describe accurately the stoichiometry of the process.

In this chapter, modifications to the most commonly used metabolic network for glucose in MCFs are proposed, with the aim of improving the prediction of experimental results reported in literature. The novel biochemical mechanism of electron bifurcation (EB), fully described elsewhere, was included (Buckel and Thauer, 2013; Herrmann et al., 2008; Li et al., 2008; Peters et al., 2016). Homoacetogenesis (HA) (Dinamarca et al., 2011) is also proposed to be the most reasonable hypothesis for correctly explaining the gaseous species yields.

3.2. MATERIALS AND METHODS

A metabolic network defines the global stoichiometry of the process as a compilation of the pathways that a single microorganism or a microbial population can catalyse. These pathways are described with all the intermediate metabolic steps, including the energetic coupling sites and the coenzymes involved (e.g. coenzyme A or NADH).

To check if including EB in a metabolic network for glucose fermentation helps improving modelling prediction capacity, a *reference* metabolic network is used in this study (Figure 3.1). The construction of this metabolic network is described in detail in chapter 2. This network is equal to the one presented in section 2.2.3.3, but it does not include EB in the butyrate-forming branch and is compared throughout this study with a metabolic network incorporating EB mechanism.

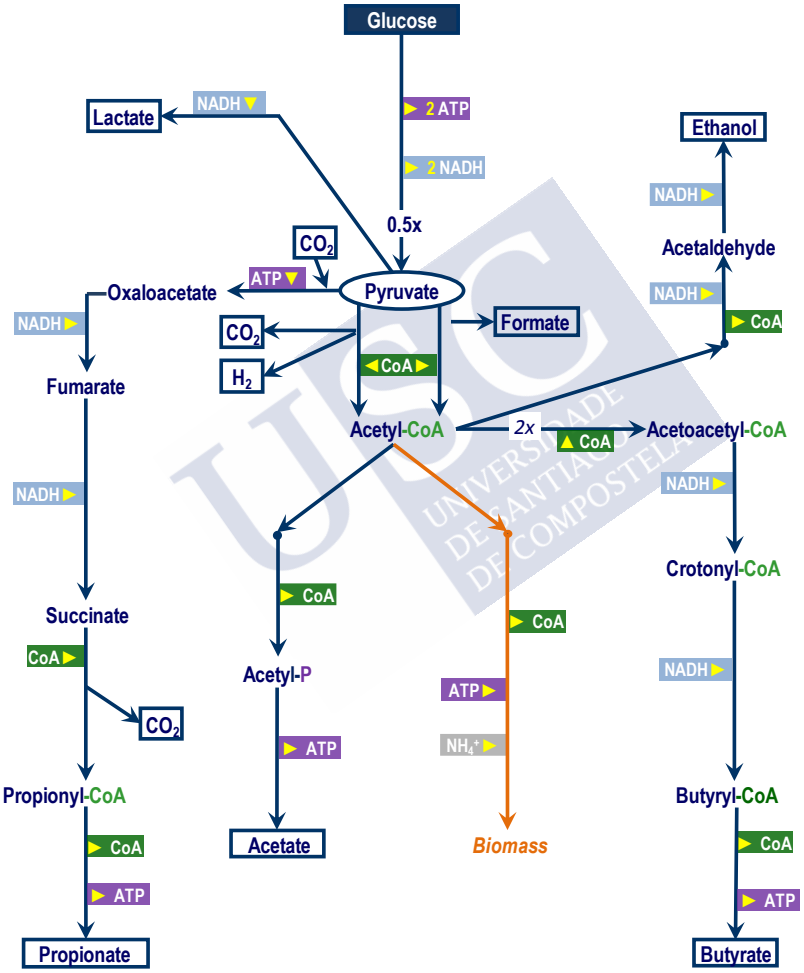

Figure 3.1. Reference metabolic network of glucose fermentation with mixed cultures used in this study.

3.2.1. Anabolism

The metabolic network is closed by including the consumption and production of chemicals in the anabolic process. Following McCarty (2007), it was considered anabolism as a process that uses acetyl-CoA as substrate to produce biomass, which has a lumped chemical formula of $C_5H_7O_2N$ (Eq. 3.1). This biomass formula has the same oxidation state as acetyl-CoA (γ=4), therefore no further redox reactions are needed. However, producing acetyl-CoA from glucose implies that the anabolism carries an extra production of H_2, CO_2 and NADH (Figure 3.1) and this must be considered in the global stoichiometry.

$$2.5\ \text{Acetyl-SCoA} + \text{NH4+} \rightarrow \text{C5H7O2N} + \text{H+} + 0.5\ \text{H2O} + 2.5\ \text{CoA-SH} \quad (3.1)$$

3.2.2. Methodology

At steady state, electron carriers must maintain the balance between oxidised and reduced forms to keep the redox neutrality of the system. Therefore, when an electron carrier is reduced or oxidised, it needs to be regenerated. In fermentations all Fd_{red} is assumed oxidised to produce H_2 (section 2.2.3.1). NADH, on the contrary, cannot produce H_2 directly as the redox potential of the NADH/NAD^+ couple is higher than that of the proton reduction even in the most favourable fermentative conditions (Kleerebezem et al., 2008). Therefore, the NADH produced during glycolysis must be consumed in other places of the metabolic network. In consequence, a complete and accurate metabolic network results in a neutral NADH balance of the data analysed.

To verify the proposed metabolic network, it was compared with the experimental data by calculating the NADH balance (Eq. 3.2). With the stoichiometry given by the network, the amount of corresponded NADH formed and consumed was determined according to the experimental products yields (moles of product formed per mole of substrate consumed in the system). If the NADH balance is neutral, this means that the metabolic network represents accurately the stoichiometry of the process. This can be used to compare different metabolic networks or to check whether a modification in a network improves its accuracy.

$$\sum_{i=N} \vartheta_{NADH,i} \cdot y_i = 0 \quad (3.2)$$

where $\nu_{NADH,\,i}$ is the NADH stoichiometric coefficient associated with the product *i* and y_i is the yield of the product *i* (moles of product *i* per mole of glucose consumed). *N* is the total number of products. The result of the summation at steady state must be zero.

3.2.3. Experimental data used

The experimental work of Temudo *et al.* (2007) (hereafter termed Temudo experiments) was selected, as it is the most comprehensive data set available on glucose fermentation using mixed cultures. It consists in a series of experiments using glucose as substrate (4 g/L) at pH values from 4 to 8.5. The hydraulic retention time (HRT) is 8 h for pH 5.5 to 8.5 and 20 h for pH from 4 to 5.5 (pH 5.5 was tested twice at different HRT values). The volume of the reactor is 2 L with 1 L of heading space and it was operated in continuous mode at 30ºC. To keep an anaerobic environment, N_2 was flushed in the liquid phase at a 200 ml/min. They measured the yields of volatile fatty acids (acetate, propionate, lactate, and butyrate), ethanol, formate, CO_2, H_2, biomass and other minor products, closing the electron and carbon balances within a 10% of confidence (the values of the experimental yields are presented in section 3.5.1). At neutral and high pH, the proportion of inorganic carbon in the form of bicarbonate ion (HCO_3^-) should be considered and it was estimated assuming liquid-gas equilibrium and acid-base equilibrium. The experimental setup was designed to ensure full substrate consumption and that steady state is truly reached. To use these data in this study, formate production was considered equivalent to a sum of H_2 and CO_2 production.

3.3. RESULTS AND DISCUSSION

3.3.1. Incorporation of the electron bifurcation into the metabolic network

EB is an enzymatic mechanism by which an exergonic electron transfer reaction is coupled with a sufficiently endergonic one. In this way, the energy surplus of the exergonic reaction is used to drive the endergonic one (Peters et al., 2016). EB was first hypothesised (Herrmann et al., 2008) in the crotonyl-CoA reduction with NADH in the butyrate synthesis pathway as a possible way for additional energy conservation. The reduction of crotonyl-CoA to butyryl-CoA (E'=-37 mV) when combined with the oxidation of NADH (E'=-280 mV), creates a highly exergonic step that could be used to drive endergonic reactions. The mechanism was then detected (Li et al., 2008) linking the highly exergonic and irreversible NADH-mediated reduction of crotonyl-CoA with the endergonic Fd_{ox} reduction by NADH. Overall, when one mole of crotonyl-CoA is reduced to butyryl-CoA, one mole of Fd_{ox} is reduced and two moles of NADH are oxidized (Figure 3.2).

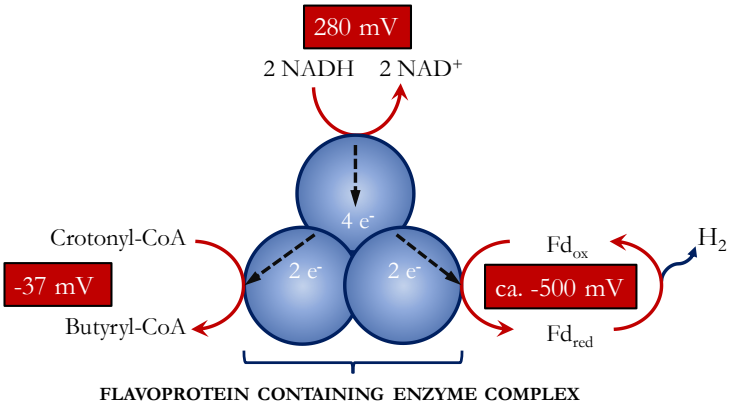

Figure 3.2. Electron Bifurcation mechanism in NADH mediated Crotonyl-CoA reduction in butyrate production pathway

The set of reactions is catalysed by a cytoplasmic enzyme complex (butyryl-Coa dehydrogenase/Etf complex) containing flavoproteins (Buckel and Thauer, 2013). The Fd_{red} yielded is re-oxidised producing H_2 (section 2.2.3.1), increasing thus the global H_2 yields of the system to a theoretical maximum of 2.7 moles of H_2 per mole of glucose (35% more than without EB). Therefore, EB could explain why higher ratios than 2 moles of H_2 per mole of glucose are found in some works (Davila-Vazquez et al., 2008; Hallenbeck and Ghosh, 2009; Jungermann et al., 1973; Kapdan and Kargi, 2006; Petitdemange et al., 1976; Ren et al., 2016). So far, EB was only observed using purified enzymes from *C. kluyveri* (Buckel and Thauer, 2013; Li et al., 2008). However, there is no fundamental impediment to its occurrence in living *C. kluyveri* or *C. pasteurianum*, as proposed by Buckel and Thauer (2013), in MCFs. For these reasons, in the new metabolic network EB is included in the butyrate pathway (Figure 3.3).

The inclusion of EB implies the consumption of one extra mole of NADH. This helps cells to decrease the reducing potential generated by the initial glycolysis. At the same time, it modifies the global stoichiometry of the process, as now the butyrate yielded from glucose requires the production of more oxidised products to close the electron balance of the fermentation. Without considering EB, the two moles of NADH formed in glycolysis were consumed in the butyrate pathway, closing in this way the NADH balance (Figure 3.1).

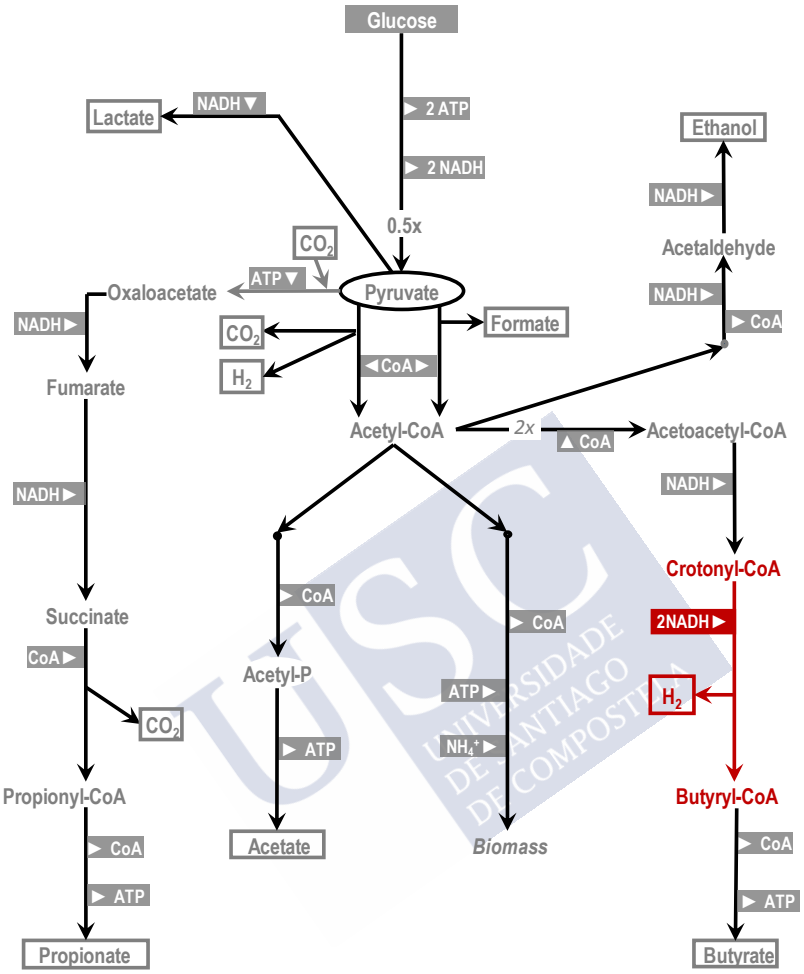

Figure 3.3. Metabolic network including EB in the butyrate pathway

However, with EB three NADH are consumed (Figure 3.3), which means that a higher share of the substrate can be oxidized to *energy rich* intermediates with concomitant substrate level phosphorylation. In essence, EB is an indirect way of conserving energy as reducing protons to H_2 saves substrate as electron acceptor and therefore microbes have the opportunity to harvest more energy from it (Buckel, 1998; Buckel and Thauer, 2013). Table 3.1 shows that ATP yields increases by 11% when considering EB in the butyrate formation pathway.

Table 3.1. Stoichiometry and ATP yield for butyrate pathway with and without EB

	Butyrate stoichiometry	**ATP yield (mol/mol glucose)**
Without EB	Glucose → Butyrate + 2 H_2 + 2 CO_2 + H^+	3
With EB	Glucose → 0.66 Butyrate + 0.66 Acetate + 2.67 H_2 + 2 CO_2	3.33

To determine whether these modifications give a better fit with the experimental data, the methodology described in section 3.2.2 is applied. The NADH balances were calculated as per Eq. 3.2 using the measured products and biomass yields of Temudo experiments and the NADH stoichiometric coefficients given by the metabolic networks for each product. Stoichiometric coefficients for the production and consumption of NADH of both networks and an example of the calculation of the NADH balance are included in the Annexes (Section 3.5.2 and Section 3.5.3, respectively).

The new metabolic network shows improvements in the NADH balance (Figure 3.4) primarily at low pH (pH≤5.5) which correlates with high butyrate production. This likely indicates that without considering EB, the butyrate pathway is not described adequately. Butyrate is produced also at pH 7.75 and again the error without considering EB is sensibly higher than when EB is included in the metabolic network. This suggests that the inclusion of EB explains better the experimental results reported in Temudo experiments. Following the same methodology, other experimental data sets on MCF of glucose available in the literature were analysed (de Kok et al., 2013; Fang and Liu, 2002; Horiuchi et al., 2002; Mohd-Zaki et al., 2016; Temudo et al., 2009, 2008b; Zoetemeyer et al., 1982). These data sets are not as comprehensive as Temudo experiments: in some cases, information on the minor products yields is not available or the gas production information is incomplete. As a result, the application of the methodology only provides partial and qualitative information. Nevertheless, the results confirm the conclusions presented here regarding Temudo experiments and are available in the Annexes (section 3.5.4).

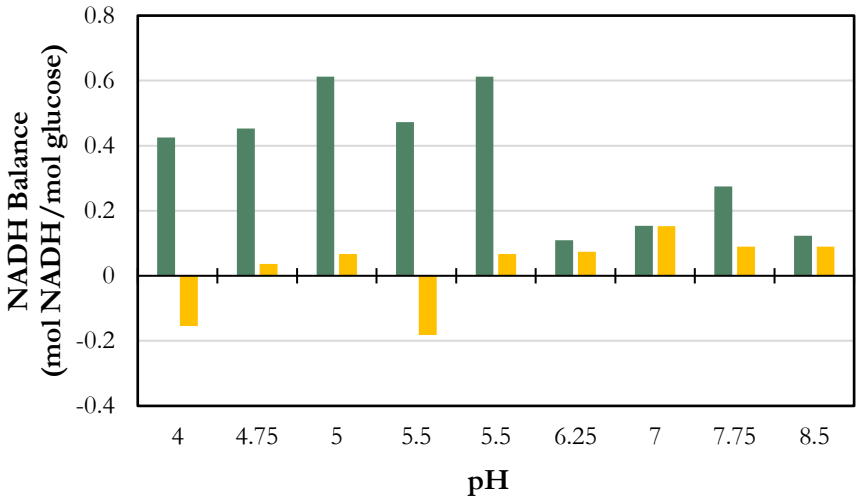

Figure 3.4. Absolute error for the NADH balance with the different metabolic networks considered for the experimental data presented by Temudo et al. (2007). ■ results of the metabolic network without electron bifurcation and ■ results of the metabolic network considering electron bifurcation.

3.3.2. Imbalanced gaseous species

Inclusion of EB alters the NADH balance of the network but also implies a higher overall H_2 yield (section 3.3.1), and therefore a yield ratio of H_2 to CO_2 higher than one. Some authors argue that the H_2 to CO_2 ratio should be equal to 1 because the only step in the metabolic network where H_2 and CO_2 are produced is in the pyruvate decarboxylation (González-Cabaleiro et al., 2015; Kleerebezem et al., 2008; Temudo et al., 2007). This seems to be confirmed by Temudo experiments, and apparently contradicts the EB-inclusion hypothesis.

The theoretical yields of H_2 and CO_2 were calculated and compared with the yields reported in Temudo experiments (Figure 3.5). The theoretical yield values are those calculated considering the product spectrum of the experiment and following the stoichiometry presented in the metabolic network including EB (Figure 3.3). The comparison shows that H_2 theoretical yields (yellow bars) are higher than the experimental ones (grey bars). This can suggest that the difference is because EB is not occurring after all. At the same time, CO_2 theoretical yields (yellow bars) are higher than the measured yields (grey bars) and this cannot be explained by an incorrect assumption of EB. To explain this

imbalance, two hypotheses are proposed: ferredoxin regeneration without H_2 formation and homoacetogenesis.

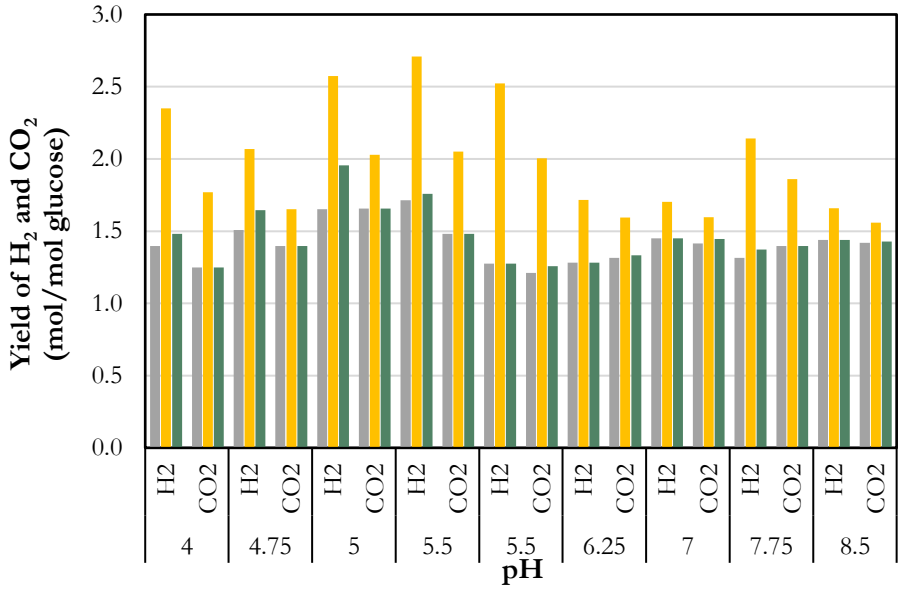

Figure 3.5. H_2 and CO_2 yields experimental and predicted by the different stoichiometries. ■ Experimental values (Temudo et al., 2007) ■ Theoretical yield considering EB but not HA ■ Theoretical yield considering EB and HA

3.3.2.1. Ferredoxin regeneration without H_2 formation.

The yield of H_2 was determined assuming that all the Fd_{red} produced (from the pyruvate decarboxylation step and from the EB mechanism) is re-oxidised by cytoplasmatic hydrogenases (Ech) and produces H_2. This is the most reported form of regenerating Fd_{ox} (Buckel and Thauer, 2013; González-Cabaleiro et al., 2015; Hoelzle et al., 2014; Kleerebezem et al., 2008; Temudo et al., 2007) but Fd_{ox} could also be regenerated in other ways. The two electrons of Fd_{red} can be used in anabolic reactions, presumably in highly endergonic reactions in which NAD(P)H is not a sufficiently strong electron donor (Buchanan and Arnon, 1970). For example, it was reported that some *Clostridia* species lack the enzymes needed to produce the anabolic-related NADPH during glycolysis and their only NADPH source is through ferredoxin-NADPH oxidoreductase (Jungermann et al., 1973). Alternatively, Fd_{red} can participate as electron donor in other catabolic reactions either directly or transferring first its electrons to NAD^+ via the

enzymatic complex ferredoxin-NAD oxidoreductase (RnfA-G enzyme complex), which is usually associated with energy conservation through the creation of an electrochemical Na^+/H^+ gradient (Biesterveld et al., 1994; Buckel and Thauer, 2013; Fonknechten et al., 2010; Herrmann et al., 2008; Hugo et al., 1972; Jungermann et al., 1973; Petitdemange et al., 1976). The latter is typically found in microorganisms that cannot produce NADH by others means because they lack the appropriate enzymes or their substrate does not allow for NADH production (when pyruvate is the main substrate, only Fd_{red} yielded in its decarboxylation into acetyl-CoA is the only electron source available) (Petitdemange et al., 1976).

Any of these options could lower the predicted H_2 production and the predicted H_2 to CO_2 ratio but could not explain why the predicted CO_2 yields are also higher than the ones reported experimentally. Moreover, all these options would imply that the NADH stoichiometric coefficient of the butyrate pathway with EB would be the same as without EB, as the extra NADH consumption is balances with the NAD(P)H production from Fd_{red}. In consequence, the NADH balances including EB would have the exact values as the ones without including it (orange bars in Figure 3.4). Moreover, the EB mechanism described in the butyrate pathway is reported in literature to regenerate $Fd_{(ox)}$ by yielding H_2, as it is the only way to explain the observed H_2 yields in essays with purified enzymes from *C. kluyveri* (Li et al., 2008).

3.3.2.2. Homoacetogenesis

In fermentative conditions HA (Eq. 3.3) is reported to play an important role as H_2 consumer. Partially due to the lack of competitors as usually there are no methanogens or sulphate reducing bacteria (Bundhoo and Mohee, 2016; Dinamarca and Bakke, 2009; Fang and Liu, 2002; Guo et al., 2010; Hallenbeck and Ghosh, 2009; Karadag and Puhakka, 2010; Saady, 2013). Some authors describe HA as persistent in fermentative conditions (Saady, 2013) and it is considered the main barrier for H_2 production via anaerobic fermentation (Dinamarca and Bakke, 2009; Hallenbeck and Ghosh, 2009). Therefore, HA could explain the lower-than-expected H_2 yields found in numerous H_2-oriented fermentations (Hallenbeck and Ghosh, 2009; Ren et al., 2016). Energetic calculations show that HA is highly exergonic considering typical H_2 partial pressures observed in acidogenic fermentations (section 3.5.5).

$$4H_2 + 2\,HCO_3^- + H^+ \rightarrow C_2H_3O_2^- + 4H_2O \qquad (3.3)$$

Like all autotrophs, the growth rate of known homoacetogens is slow. *Acetobacterium woodii* is reported to have growth rates on H_2/CO_2 between 0.024 and 0.050 h^{-1} (Peters et al., 2006; Straub et al., 2014), while *Moorella sp.* was reported to have a growth rate of 0.042 h^{-1} (Sakai et al., 2005). Dilution rates in Temudo experiments are 0.042 h^{-1} for low pH experiments and 0.125 h^{-1} for medium and high pH value experiments, which apparently prevents the presence of homoacetogens. However, homoacetogens can also grow on organic compounds such as glucose, and therefore lower their doubling times down to values of 1.75 h (Saady, 2013). Dinamarca and Bakke (2009) reported homoacetogens presence in continuous experiments with an HRT of 8 h and Saady (2013) discarded lowering HRT as a successful strategy to avoid HA in fermentations. Therefore, it is feasible to hypothesise the presence of homoacetogens in Temudo experiments.

To check if HA could be responsible for the unbalance in H_2 and CO_2 production, it was assumed that HA consumed the difference between the theoretical (Figure 3.5 yellow bars) and the measured yield (Figure 3.5 grey bars) of either H_2 or CO_2. Accordingly, the stoichiometry of HA (Eq. 3.3) defines the correspondent acetate production and CO_2 or H_2 consumption (an example of calculations is included in section 3.5.6). Green bars in Figure 3.5 are the result of the theoretical H_2 and CO_2 yields including HA and show a good fit with the measured gaseous yields. The root-mean-square deviation (RMSD) measures the differences between predicted and observed values (Table 3.2). These results suggest unequivocally that HA provides a much better fit to the experimental data, as values improve by 85% and 95% for H_2 and CO_2, respectively.

Table 3.2. Values of RMSD for H_2 and CO_2 without considering HA and considering HA.

	Without HA (mol/mol glucose)	**With HA (mol/mol glucose)**
RMSD (H_2)	0.789	0.117
RMSD (CO_2)	0.444	0.020

Including HA in the system would also mean that part of the acetate measured did not come through direct glucose degradation but via HA. Consequently, part of the acetate did not produce either the NADH in glycolysis or the CO_2 and H_2 in pyruvate decarboxylation, which alters the NADH balance and the theoretical CO_2 and H_2 calculations. Blue bars in Figure 3.6 represent the NADH balance after considering that part of the acetate was produced via HA.

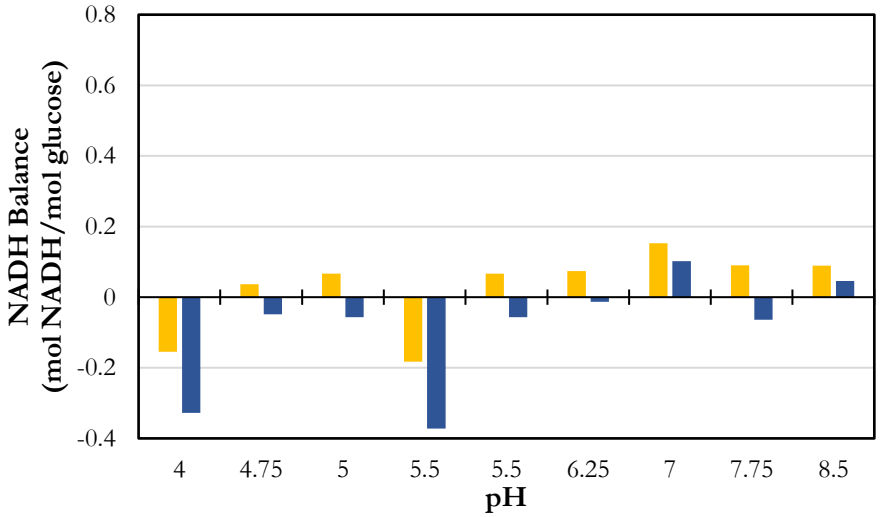

Figure 3.6. Absolute error for the NADH/NAD⁺ balance with the different stoichiometry considered for the experimental data presented by Temudo et al. (2007). NADH/NAD⁺ balances considering: ■ the metabolic network with electron bifurcation ■ the metabolic network with electron bifurcation and assuming homoacetogenesis.

For some of the experiments (especially those at pH 4 and the first at pH 5.5), this consideration implies an increment of the error in the NADH balance. However, these differences might be very well attributed to experimental deviations. For example, carbon recovery in the first experiment at pH 5.5 is around 110%. At the same time, the ratio between butyrate and acetate yields in this experiment is higher than it is in the rest of low-pH experiments (yields are available in section 3.5.1), which might imply that the measurement of the butyrate yield could be deviated. As butyrate consumes NADH, its consumption could be overestimated and explain the negative deviation at this pH (Stoichiometric coefficients are available in section 3.5.2). At pH 4 the butyrate to acetate ratio also seems to be overestimated and a negative deviation in the NADH balance is again observed. Nevertheless, these deviations can be considered relatively small because for every glucose oxidation to pyruvate two mole of NADH are yielded.

3.3.3. EB in the propionate pathway

Fumarate reduction to succinate in the propionate pathway is a similar step to crotonyl-CoA reduction to butyryl-CoA. They are mechanistically alike (hydrogenation of a double carbon bond) and in both cases their energetics

suggest an extra energy conservation ($E'_{Crotonyl\text{-}CoA}$= - 37 mV; $E'_{Fumarate}$ = - 5 mV). However, the EB mechanism was reported in the crotonyl-CoA reduction of the butyrate pathway but not in the fumarate reduction (Buckel and Thauer, 2013; Li et al., 2008). The energy surplus of this metabolic step in the propionate pathway is reported to be conserved extruding a proton from the cytoplasm and therefore creating an electrochemical proton gradient (Buckel, 2001; Herrmann et al., 2008). Even though EB was never detected in this step, it was assumed as feasible since there is no theoretical impediment for it. Using the same methodology as above, the NADH balances were calculated assuming EB in both butyrate and propionate pathways and HA (see section 3.5.7). However, the results show a worse fit when EB is included in the propionate pathway than when it is only included in the butyrate branch (the NADH balances increase the error by 23 %) and therefore the consideration of EB in the fumarate reduction was discarded.

3.4. CONCLUSIONS

This study considers for first time electron bifurcation in mixed-culture fermentation processes yielding butyrate, which provides a better fit between the predicted stoichiometry and the experimental yields measured. Therefore, it is recommended to consider this mechanism in the reduction of crotonyl-CoA to butyryl-CoA in butyrate formation pathways. Including electron bifurcation in the metabolic network allows for the prediction of the production of butyrate accompanied by acetate. This was experimentally observed but not theoretically predicted before. The addition of electron bifurcation revealed an unbalance between the stoichiometry and the observation in the production of the gaseous components, H_2 and CO_2. In this study, it is proposed that the unbalance of H_2 and CO_2 could be explained by the occurrence of homoacetogenesis in the mixed-culture fermentation of glucose.

3.5. ANNEXES

3.5.1. Experimental yields from Temudo *et al.* (2007)

In the Table A3.1 the yields reported by Temudo et al. (2007) are presented. The Hydraulic Retention Time (HRT) was of 20 hours at pH values more acidic than 5.5 and of 8 hours at more basic pH values than 5.5. This avoided biomass washing at low pH. At pH 5.5 the experiment was repeated at both HRT.

Table A3.1. Experimental yields as reported in Temudo et al. (2007).

		pH								
		HRT: 20h				**HRT: 8h**				
		4	**4.75**	**5**	**5.5**	**5.5**	**6.25**	**7**	**7.75**	**8.5**
Product	Butyrate	0.580	0.416	0.546	0.655	0.513	0.036	0.001	0.185	0.034
	Acetate	0.418	0.455	0.366	0.370	0.403	0.619	0.700	0.578	0.680
	Propionate	0.000	0.054	0.000	0.044	0.040	0.007	0.000	0.041	0.020
	Glycerol	0.185	0.116	0.059	0.129	0.094	0.134	0.063	0.058	0.174
	Lactate	0.068	0.165	0.056	0.022	0.005	0.004	0.004	0.098	0.062
	Succinate	0.000	0.000	0.000	0.003	0.004	0.087	0.106	0.097	0.065
	Ethanol	0.000	0.099	0.133	0.048	0.028	0.636	0.689	0.558	0.587
	Biomass	0.385	0.533	0.878	0.653	1.102	0.709	0.625	0.902	0.577
	CO_2	1.249	1.398	1.657	1.481	1.210	1.315	1.414	1.398	1.420
	H_2	1.398	1.508	1.652	1.713	1.276	1.283	1.451	1.315	1.439

3.5.2. NADH, H_2 and CO_2 stoichiometric coefficients

Table A3.2 contains the NADH and H_2 stoichiometric coefficients for each of the pathways considered.

Table A3.2. NADH stoichiometric coefficients for each of the final products

		Stoichiometry			
		NADH		**H_2**	
		Without EB	With EB	Without EB	With EB
Product	Butyrate	0	-1	2	3
	Acetate	1	1	1	1
	Propionate	-1	-2	0	1
	Glycerol	-1	-1	0	0
	Lactate	0	0	0	0
	Succinate	-1	-2	0	1
	Ethanol	-1	-1	1	1
	Biomass (C-mole)	0.5	0.5	0.5	0.5

3.5.3. Calculation example of a NADH balance

Equation A3.1 shows an example of a NADH balance calculation. The product yields used are the ones of the experiment at pH 4 (Table A3.1). No EB is considered.

$$\sum \nu_i \cdot y_i = 0.580 \cdot 0 + 0.418 \cdot 1 + 0 \cdot (-1) + 0.185 \cdot (-1) + 0.068 \cdot 0 + 0 \cdot (-1) + 0 \cdot (-1) + 0.385 \cdot 0.5 = = 0.4255 \ \frac{mol\ NADH}{mol\ glucose} \quad \text{(A3.1)}$$

where ν_i is the NADH stoichiometric factor for each compound (e.g. butyrate, acetate, etc.) and y_i is the yield of that compound per moles of glucose consumed.

3.5.4. Results from other data sets

The analysis with the methodology explained in the main text was repeated using data obtained from other experimental acidogenic fermentations besides the data presented in the main text from Temudo *et al.* (2007). Nevertheless, the other data sets are not as comprehensive and, for example, the mass balances are not closed in most cases. In general, these experiments do not report the yields of minor products (e.g. succinate) therefore the carbon balance is not fully closed, which may have a substantial impact on the NADH balances.

In all the cases, it is observed that the NADH balances fit better the experimental data when electron bifurcation (EB) is considered. Figure A3.1 to Figure A3.6 show the balance results considering and not considering EB in the stoichiometry of the process. Specific comments on the possible causes for the deviations in the balances of some data sets are discussed below.

In some experiments of the data set of Figure A3.1 (Fang and Liu, 2002), glucose consumption was not complete (representing around 20% of the carbon content of the effluent), especially at low pH. At high pH, on the contrary, methane was detected in the gas effluent. This could explain the high NADH balances because part of the reductive equivalents was transferred to methane, which was not considered in the analysis.

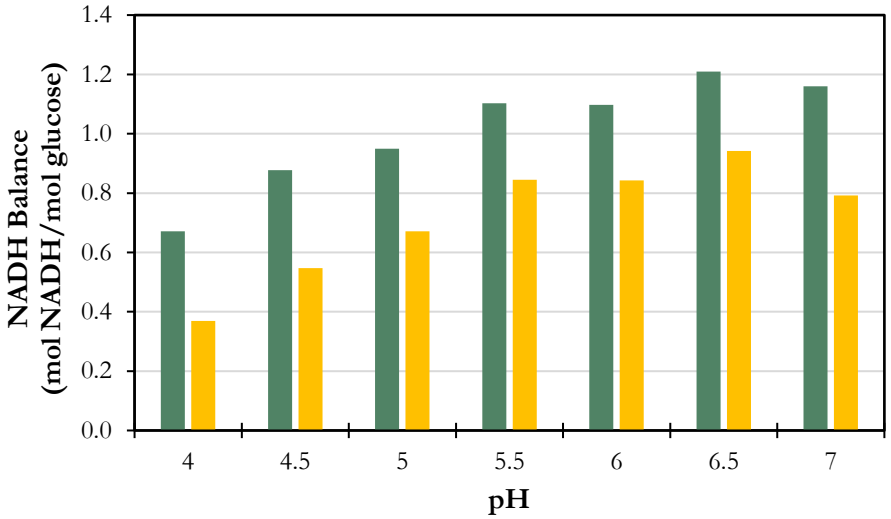

Figure A3.1. NADH balances without and with EB stoichiometry considered for the experimental data presented in Fang and Liu (2002). ■ without EB ■ with EB

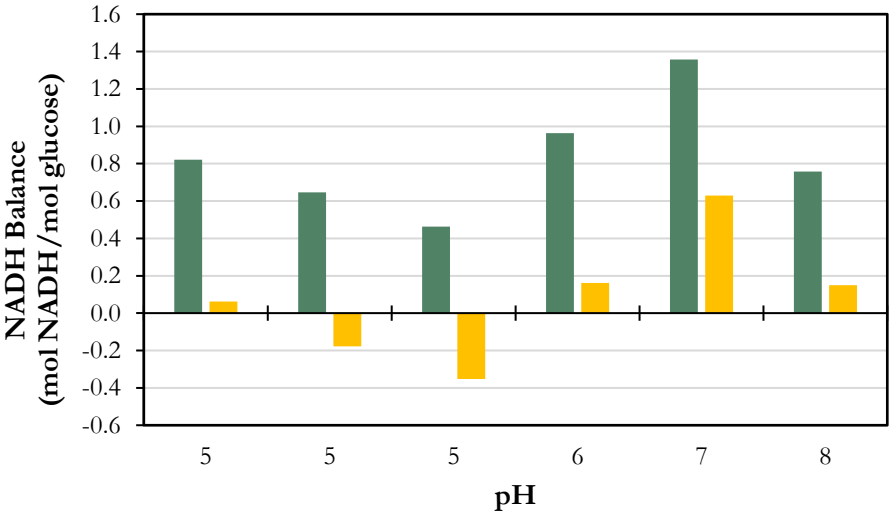

Figure A3.2. NADH balances without and with EB stoichiometry considered for experimental data presented in Horiuchi et al. (2002). ■ without EB ■ with EB

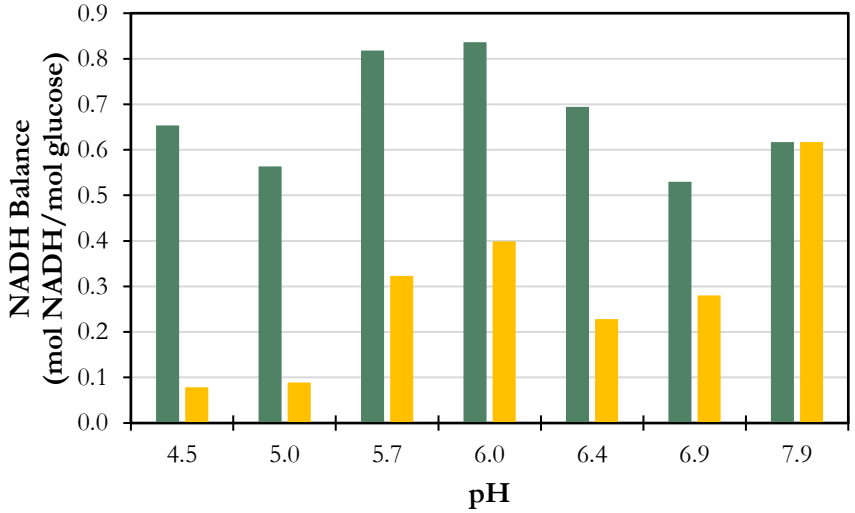

Figure A3.3. NADH balances without and with EB stoichiometry considered for experimental data presented in Zoetemeyer et al. (1982). ■ without EB ■ with EB

In some cases, carbon balances are higher than 100% –e.g. at pH 7.9, (Zoetemeyer et al., 1982) –, which could indicate that some of the concentration values could be overestimated.

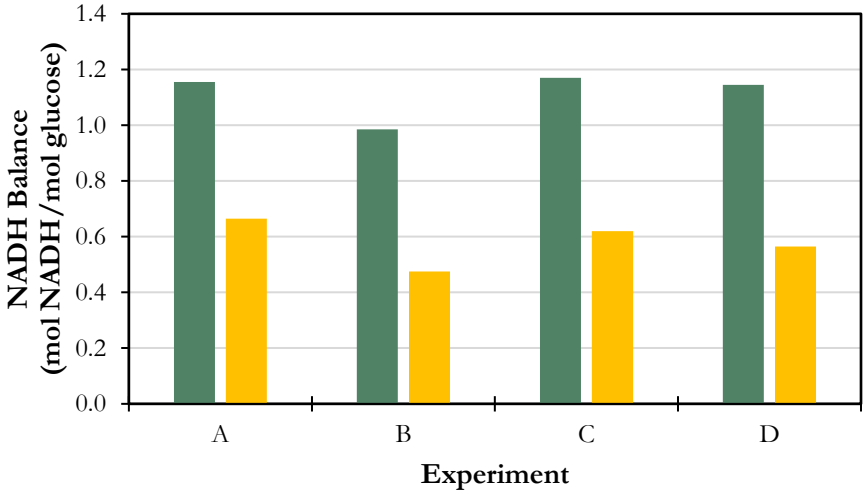

Figure A3.4. NADH balances without and with EB stoichiometry considered for experimental data presented in de Kok et al. (2013) ■ without EB ■ with EB

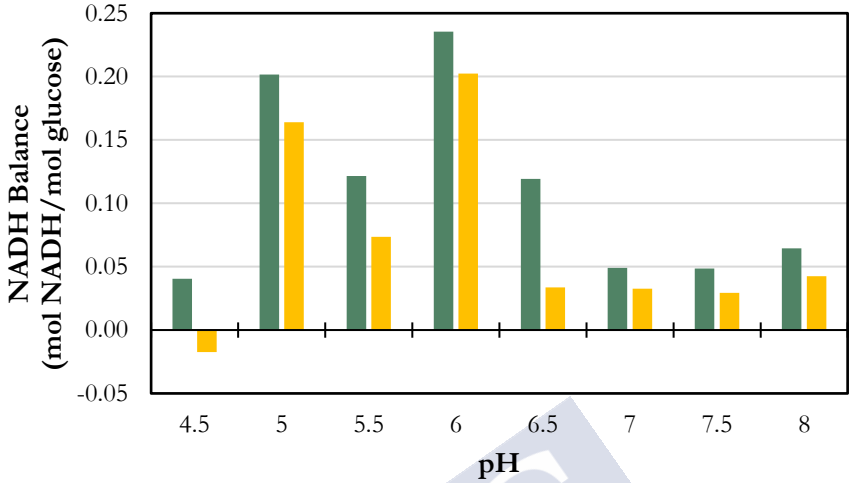

Figure A3.5. NADH balances without and with EB stoichiometry considered for experimental data presented in ■ without EB ■ with EB.

In the data set of Figure A3.5 (Mohd-Zaki et al., 2016) and mostly in those cases where NADH balances are high, carbon recovery is higher than 100%, which would indicate uncertainty in the experimental measurements.

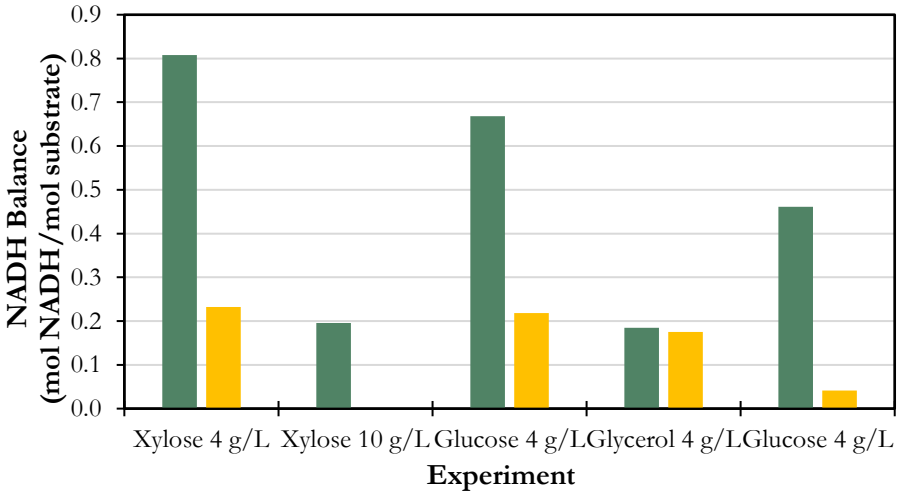

Figure A3.6. NADH balances without and with EB stoichiometry considered for experimental data presented in Temudo et al. (2008) and Temudo et al. (2009) ■ without EB ■ with EB.

3.5.5. Energetics of homoacetogenesis

Figure A3.7 shows the Gibbs energy for HA at different hydrogen partial pressures. The pH is considered constant at 7 and concentrations of acetate and bicarbonate assumed 10 and 2 mM respectively.

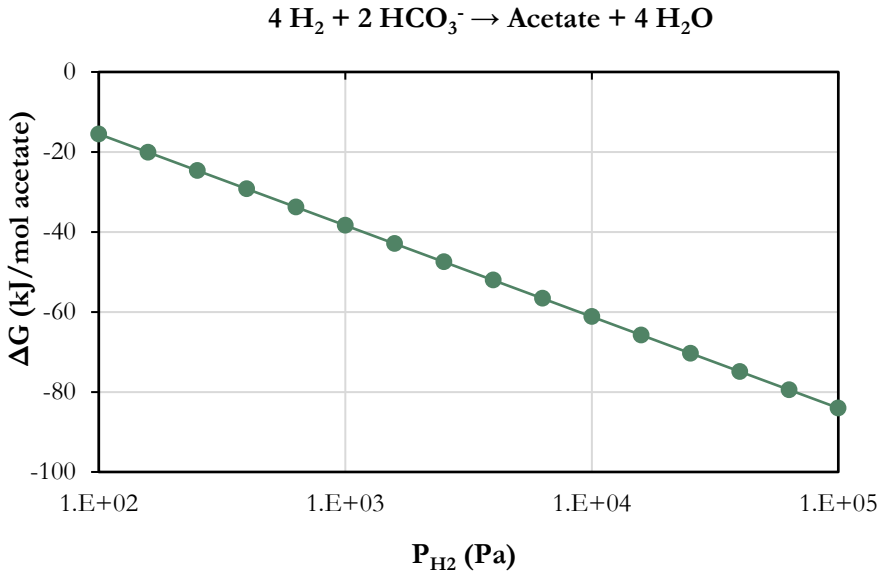

Figure A3.7. Gibbs energy of the HA function of the H_2 partial pressure in the headspace. Assumed ideal liquid-gas equilibrium.

3.5.6. Example of the calculation to include homoacetogenesis

For this example, a simplified fermentation experiment with the following yields is assumed: butyrate (0.6 mol/mol glucose), acetate (0.45 mol/mol glucose), biomass (0.4 C-mol/mol glucose), H_2 (1.7 mol/mol glucose) and CO_2 (1.5 mol/mol glucose). Using the stoichiometric factors provided in Table A3.2, the theoretical H_2 and CO_2 yields are calculated (Eq. A3.2-A3.3).

$$\sum_{i=products} \nu_{i,H2} \cdot y_i = 0.6 \cdot 3 + 0.45 \cdot 1 + 0.4 \cdot 0.5 = 2.45 \ \frac{mol\ H_2}{mol\ glucose} \quad \text{(A3.2)}$$

$$\sum_{i=products} \nu_{i,CO2} \cdot y_i = 0.6 \cdot 2 + 0.45 \cdot 1 + 0.4 \cdot 0.5 = 1.85 \ \frac{mol\ CO_2}{mol\ glucose} \quad \text{(A3.3)}$$

The difference between the theoretical and the measured yields is 0.75 and 0.35 mole for H_2 and CO_2, respectively. It is assumed that HA consumes all the CO_2 yield difference (0.35 mol). Therefore, the amount of extra H_2 consumed (0.7 mol) and extra acetate produced (0.18 mol) are calculated straightforwardly from the stoichiometry of the HA (Eq. 3.2). The new theoretical yields are 1.75 mole for H_2 and 1.5 mole for CO_2 (Table A3.3)

Table A3.3. First iteration of the calculation including HA

	Theoretical yield without HA	Measured yield	Yield difference	Consumed yield in HA
H_2	2.45	1.70	0.75	0.70
CO_2	1.85	1.50	0.35	0.35

However, this result is not completely correct since it was assumed for the calculation of the H_2 and CO_2 theoretical yields that acetate production was contributing to them (0.45 mol/mol glucose). Now, part of this acetate is assumed to come from HA and therefore is not accompanied with H_2 and CO_2 yield. In consequence, the acetate produced by HA (0.18 mol/mol glucose) should be subtracted from the overall yield measured (0.45 mol/mol glucose) recalculating the theoretical yields of H_2 and CO_2 (Eq. A3.4-A3.5).

$$\sum_{i=products} \nu_{i,H2} \cdot y_i = 0.6 \cdot 3 + (0.45 - 0.18) \cdot 1 + 0.4 \cdot 0.5 = 2.28 \frac{mol\ H_2}{mol\ glucose} \quad \text{(A3.4)}$$

$$\sum_{i=products} \nu_{i,CO2} \cdot y_i = 0.6 \cdot 2 + (0.45 - 0.18) \cdot 1 + 0.4 \cdot 0.5 = 1.68 \frac{mol\ CO_2}{mol\ glucose} \quad \text{(A3.5)}$$

With the new theoretical yields, the calculation procedure is repeated (Table A3.4).

Table A3.4. Second iteration of the calculation including HA

	New theoretical yield	Measured yield	Yield difference	Consumed yield in HA
H_2	2.28	1.70	0.58	0.35
CO_2	1.68	1.50	0.18	0.18

The iterations continue until the yield difference between the theoretical values and the measured ones is minimum.

3.5.7. NADH balances considering EB in butyrate and propionate pathways

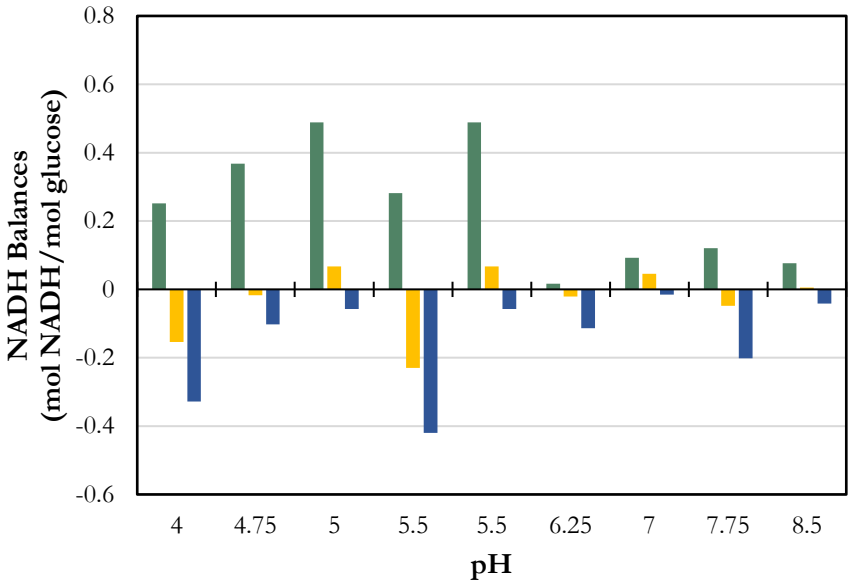

Figure A3.8. Absolute error for the NADH balance with the different metabolic networks considered for the experimental data presented by (Temudo et al., 2007). NADH balances are from: ■ the metabolic network without electron bifurcation and ■ the metabolic network with electron bifurcation in Butyrate and Propionate pathways ■ the metabolic network with electron bifurcation and assuming homoacetogenesis

USC
UNIVERSIDADE
DE SANTIAGO
DE COMPOSTELA

CHAPTER 4

Resource allocation explains lactic acid production in mixed-culture anaerobic fermentations

Summary

Lactate production from glucose in anaerobic carbohydrate fermentations with mixed cultures of microorganisms is generally observed only in very specific conditions: the reactor should be run discontinuously and peptides and some vitamins must be present in the culture medium as lactic acid bacteria are typically auxotrophic for these compounds. The mathematical models for stoichiometry prediction of this thesis assume that microorganisms optimise the ATP yield on substrate and therefore they do not predict the less ATP efficient lactate production. In this work, a metabolic model taking into account cellular resource allocation and limitation is proposed to understand and predict under lactate which conditions lactate production from glucose can be beneficial for microorganisms. The model uses a flux balances analysis approach incorporating additional constraints from the resource allocation theory and simulates glucose fermentation in a continuous reactor. This approach predicts lactate production at high dilution rates, provided that amino acids are in the culture medium. In minimal medium and lower dilution rates, mostly butyrate and no lactate is predicted. Auxotrophy for amino acids of lactic acid bacteria is identified to provide a competitive advantage in rich media because less resources need to be allocated for anabolic machinery and higher specific growth rates can be achieved. The results of this chapter indicate that the optimisation procedure based on ATP yield maximisation used in the stoichiometry prediction models should be limited to those cases in which substrate is in limiting conditions, as in properly operated continuous reactors.

4.1. INTRODUCTION

Lactate is one of the most widely produced carboxylic acids and has annual market growth of over 15%. Unlike other carboxylates (acetate, propionate or butyrate), bacterial fermentations represent 90% of the world production (Alves de Oliveira et al., 2018). It is therefore a good candidate to be produced from organic wastes by open mixed-culture fermentations (MCF) in a cheap and efficient way within the biorefinery paradigm. Recently, it was reported that lactate can dominate the product spectrum in MCF. But this only occurs under very specific operational conditions (Rombouts et al., 2020). A complex medium with peptides and vitamins is needed to grow lactic acid bacteria (LAB) because they are auxotrophic for amino acids and some vitamins meaning that they are not capable of producing these compounds from the primary carbon substrate (Rombouts et al., 2020; Wang et al., 2015). Also environmental conditions that select for maximum specific growth rate, as in batch processes, are a prerequisite for LAB to outcompete other bacterial groups, as shown in (Rombouts et al., 2020). Fermentations carried out under other conditions lead inevitably to the production of a mixture of other carboxylic acids (Rombouts et al., 2020, 2019a; Temudo et al., 2007).

The predictive tools used in this thesis for predicting MCF stoichiometry select the dominant conversion pathways based on the assumption the microorganisms maximise the ATP yield from the substrate (section 2.2.2.1). Other state-of-the-art models for predicting the stoichiometry of glucose MCF also assume this optimisation criterion (González-Cabaleiro et al., 2015; Zhang et al., 2013). However, following this rationale, lactate should never be one of the main products of MCF since it yields 2 ATP molecules per glucose by substrate level phosphorylation (the major contributor to ATP production in fermentations), significantly less than the obtained in the production of other carboxylates such as acetate or butyrate, which yield 4 and 3 ATP molecules per glucose, respectively (section 2.2.3.3). Accordingly, models predict that the product spectrum of glucose MCF can only be dominated by acetate, butyrate and ethanol (González-Cabaleiro et al., 2015). Thus, bioenergetic efficiency-centred arguments are not enough to explain lactate production or, from another perspective, the ATP yield maximisation strategy is not suitable for describing cellular metabolism under all environmental conditions. It is clear that other factors, such as kinetic arguments, should also be considered under particular conditions. Some authors consider that pathway length is minimised by

microorganisms (Melendez-Hevia, 1990) and, in fact, this factor has been proposed to be one of the main aspects explaining cross-feeding between microbial populations in some microbial conversions, as in nitrification or methane production (Costa et al., 2006; Kreft et al., 2020). Another criterion used for prediction of metabolic fluxes is the assumption that cells maximise the ratio between ATP production and the overall fluxes through catabolism (Dauner and Sauer, 2001).

Recently the resource allocation theory has been gaining interest as it can explain different metabolic regulatory strategies that could not be explained from an ATP yield maximisation perspective (Bachmann et al., 2017). Resource allocation theory states that the different cellular processes (e.g. catabolism, growth or transport) compete for a finite protein (i.e. enzymatic) pool. Well-known phenomena, such as ethanol production by yeasts in aerobic conditions, also known as Crabtree effect (Schumacher, 2018), acetate overflow (acetate excretion in aerobic conditions) in bacteria (Zeng and Yang, 2019) or lactate production by cancer or red blood cells in humans (Vazquez and Oltvai, 2011) were correctly reproduced by integrating the resource allocation theory in the metabolic models (Goelzer and Fromion, 2011; Nilsson and Nielsen, 2016; Zeng and Yang, 2019).

The objective of this work is to test if a resource allocation model can provide a plausible line of reasoning to explain the competitive advantage under some environmental conditions of lactate production in anaerobic mixed culture fermentations. The model incorporates constraints from the resource allocation theory to a metabolic network model to provide a mechanistic explanation lactate production under specific operational conditions. Herewith this is a case study that aims to contribute to the clarification of other poorly understood microbial competition dilemmas.

4.2. MODEL DEVELOPMENT

The model simulates the conversion of glucose by two groups of microorganisms –LAB and butyrate-producing bacteria (BPB)– in a CSTR assuming that the system is only limited by the carbon source. The model is focused on central carbon metabolism and includes catabolism, anabolism and transmembrane transport of substrates and products. It follows the approach developed by Schumacher (2018) to simulate the metabolism of the yeast *S. cerevisiae*.

4.2.1. Resource allocation

The resource allocation theory considers the cell as a self-replicating system in which the different growth-related processes (e.g. protein production by the ribosomes, catabolism to obtain energy for growth, etc.) compete for limited resources (Molenaar et al., 2009). The core hypothesis of resource allocation is that the most limiting resource is protein (i.e. enzymes concentration), which is restricted by a maximum content in the cells. The protein pool can be divided schematically in its main different functions: anabolism, catabolism and metabolite transport across the membrane (Figure 4.1). When protein concentration is not limiting, some capacity of the protein pool is unused, which is denoted as free proteome in the pie chart. As the specific growth rate increases, the cell needs more energy to grow (and consequently more catabolic enzymes to extract energy from the substrate) but, at the same time, a higher specific growth rate requires more ribosomes to sustain the cellular protein production rate, and more anabolic enzymes to achieve the higher biomass specific growth rate imposed. In this way, cells face a challenging optimisation problem as they have to allocate the protein pool to the different functions in order to grow as fast as possible and dominate the community.

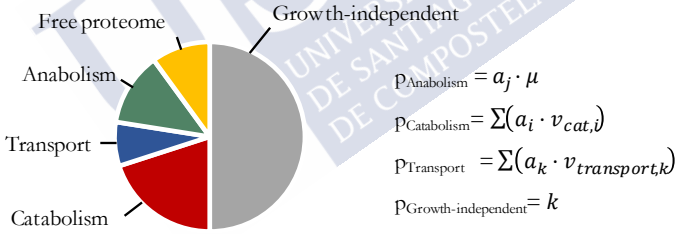

Figure 4.1. Allocation of the cellular protein pool. The share of each fraction is linearly dependent on the flux it catalyses. *p* is the share of the different protein functions, μ is the specific growth rate, *v* represents the fluxes, *a* are the activities of the different groups of enzymes and *k* represent the constant share of the proteome not related with growth tasks.

Each of the enzymes involved in the growth-related functions has a characteristic enzymatic activity (i.e. the catalysed flux per unit of enzyme mass) and thus the different pathways have different enzymatic requirements for catalysing a given flux. Consequently, pathways requiring a low enzymatic concentration are favoured when the total protein concentration is limiting (either because they have few enzymes involved or because the activities of these enzymes are high). On the other hand, when the protein concentration is not

limiting (i.e. at low specific growth rates), pathways with higher enzymatic concentration requirements but also higher ATP yields may be more beneficial and generate a higher growth rate. Thus, there is a trade-off between being efficient in ATP yield and being efficient in terms of enzyme requirements and resource allocation models can predict which strategy prevails under a given conditions and therefore the product spectrum.

For example, in the case of the Crabtree effect resource allocation models predict that, at certain environmental conditions, strategies providing a lower ATP yield but low enzymatic requirements (such as ethanol production in presence of oxygen) can sustain a higher specific growth rate than high ATP yield but high enzymatic requirements options (complete respiration of the substrate).

4.2.2. Model assumptions

- Biomass is divided in two fractions: i) raw biomass (RBM) representing the carbohydrates, lipids, DNA and RNA and ii) protein. The molecular composition of RMB is considered to be constant regardless of the specific growth rate. This has the advantage that the concentration of the different protein fractions (Fig. 1) can be expressed over RBM in the form of a mass ratio (g_{PROT}/g_{RBM}) as a growth-independent measurement. The elemental composition of the two fractions and its ATP requirements are assumed as reported in (Schumacher, 2018).
- Protein is modelled to constitute up to 50% of the total cell weight (i.e. for each gram of protein in the cell, there is one gram of raw biomass resulting in a concentration of 1 $g_{protein}/g_{RBM}$). Values in the same order of magnitude were measured and used in previous resource allocation models (Basan et al., 2015; Mori et al., 2016; Nilsson and Nielsen, 2016; Schumacher, 2018).
- Proteins can be located in the cytoplasm (ribosomes and catabolic enzymes) or in the membrane (transport proteins). The maximum content of membrane proteins is 20% of the total protein pool as experimentally measured in different bacterial species (Liu and Rost, 2001)
- Half of the proteins are not used in growth-related processes and their fraction is constant regardless independent of the specific growth rate. In consequence, of the maximum protein concentration of 1 g_{PROT}/g_{RBM}, 0.5 are not used for growth and the remaining 0.5 may be used for growth purposes, of which a maximum of 0.1 g_{PROT}/g_{RBM} can be located in the membrane. This value is in line with the values used in similar approaches (Basan et al., 2015; Mori et al., 2016).

- The flux catalysed by enzymes follows a first-order kinetics with respect to the enzyme concentration and activity (Eq. 4.1) (Goelzer and Fromion, 2011; Hui et al., 2015; Scott et al., 2014). This assumption was used as well in the previous modelling approaches using the resource allocation theory (Basan et al., 2015; Mori et al., 2016; Nilsson and Nielsen, 2016; Zeng and Yang, 2019).

$$v_i = p_i \cdot \sigma_i \cdot a_i \quad (4.1)$$

where v_i is the flux, p_i is the protein (i.e. enzyme) concentration, σ_i is the saturation coefficient and a_i is the activity of the enzyme catalysing flux i.

- All enzymes are considered to be half-saturated ($\sigma_i = 0.5$), except for the glucose transporters whose kinetics are governed by the extracellular glucose concentration according to the Michaelis-Menten equation. This assumption is based on the previously hypothesised trade-off between low metabolite concentrations and high enzyme saturation (Tepper et al., 2013) and on the observation that most glycolytic enzymes are half saturated in E. coli (Bennett et al., 2009). Previous resource allocation models also followed this hypothesis (Nilsson & Nielsen, 2016; Schumacher, 2018)
- LAB are considered auxotrophic in amino acids (i.e. they cannot synthesise them and need to be transported). The main implication is that LAB do not need to allocate enzymes (ribosomes) to amino acid production from inorganic nitrogen and can dedicate the freed protein fraction to other growth tasks. Experimental measurements revealed that in *E. coli,* the share of amino acid biosynthesis enzymes drops from 20% to 6% when switching from rich to mineral growth medium while the share of other synthetic enzymes increases (Li et al., 2014). This may be interpreted as the enzymatic activity of ribosomes (i.e. the flux of new biomass formed per unit of mass of ribosomal protein) is higher as amino acids are not synthesised. In the model, this observation is represented by a 15% higher enzymatic activity of the ribosomes in LAB with respect to BPB. Information on this subject for LAB or other prokaryotic microorganisms was not available in literature.
- Energy requirements for transport of substrates (glucose, inorganic nitrogen or amino acids) and end-products is not considered as it depends highly on the intracellular concentrations of the substrates and products to be transported, which are not simulated in the model. This assumption does not affect the competition between auxotrophic LAB and BPB since the

energy required for transporting amino acids or inorganic nitrogen is similar (Rombouts et al., 2020; Stouthamer, 1973).

4.2.3. Model description

The model follows the formulation of a flux balance analysis (FBA), in which the different cellular fluxes are optimised by linear programming to maximise the specific growth rate (Eq. 4.2). The optimisation has common FBA constraints of steady state condition (as in a CSTR, Eq. 4.3) and positive fluxes (Eq. 4.4). Additionally, two inequality constraints related with resource allocation are included. As previously stated, the total concentration of growth-related protein (i.e. ribosomes and catabolic and transport enzymes) has an upper limit of 0.5 g_{PROT}/g_{RBM} (Eq. 4.5), of which 20% can be located in the membrane (i.e. transport enzymes), which is expressed in the model by an upper limit on membrane protein concentration of 0.1 g_{PROT}/g_{RBM} (Eq. 4.6). The total and membrane protein concentration are determined by addition of the concentration of all growth-related or membrane enzymes, respectively, for a given set of metabolic fluxes using Eq. 4.1, which relates the needed enzyme mass to catalyse a flux.

$$\max_{v} \mu \qquad h^{-1} \qquad (4.2)$$

$$N \cdot v = 0 \qquad mol/mol_{BM} \cdot h \qquad (4.3)$$

$$v_i > 0 \qquad mol/mol_{BM} \cdot h \qquad (4.4)$$

$$\sum \frac{v_i}{\sigma_i \cdot a_i} \leq p_{max,total} = 0.5 \qquad g_{PROT}/g_{RBM} \qquad (4.5)$$

$$\sum \frac{v_j}{\sigma_j \cdot a_j} \leq p_{max,membrane} = 0.1 \qquad g_{PROT}/g_{RBM} \qquad (4.6)$$

where N is the stoichiometric matrix, v are the fluxes, σ is the saturation degree, which has a value of 0.5 for all enzymes except the glucose transporter, a is the enzymatic activity and p_{max} is the maximum protein concentration. There are i fluxes of which j correspond to membrane-related (i.e. transport) processes.

Since steady state is assumed and glucose is the only substrate, all fluxes depend on the glucose import flux, which in turn depends on the activity of its transporter (Eq. 4.1). As stated in the previous section, the enzymatic activity of this transporter is governed by the Michaelis-Menten equation (Eq. 4.7), depending thus the glucose import flux on the external glucose concentration (Eq. 4.8).

$$\sigma_{GT} = \frac{[lucose]}{K_m + [Glucose]} \tag{4.7}$$

$$v_{Glucose\ transport} = a_{GT} \cdot p_{GT} \cdot \frac{[Glucose]}{K_m + [Glucose]} \tag{4.8}$$

where σ_{GT} is the glucose transporter saturation degree, K_m is the half saturation constant, a_{GT} is the activity of the glucose transporter and p_{GT} is its concentration. The form of Eq. 4.8 is equivalent to a Michaelis-Menten equation in which the maximum rate is represent by $a_{GT} \cdot p_{GT}$.

Three model microorganisms with different catabolic and anabolic characteristics are simulated to discern whether catabolism or anabolism is responsible for the different behaviours of LAB and BPB:

i) An amino acid auxotrophic LAB, i.e. with a higher ribosomal activity.
ii) A hypothetical prototrophic (i.e. non auxotrophic) LAB.
iii) A prototrophic BPB.

4.2.4. Metabolic network

The experiments of Rombouts et al. (2020) show that there is duality in the ecological domination of the microbial consortia in MCF operated in a glucose-fed sequential batch reactor. LAB of the genus *Lactobacillus* and *Lactococcus* dominate the microbial community in rich medium fermentations and bacteria belonging to the genus *Clostridium* dominate the community when mineral medium is used. For the sake of simplicity, the metabolic network used in this model only considers one possible catabolism for each of the microorganisms dominating the culture: acetate and butyrate in the case of BPB and lactate in the case of LAB (Table 4.1).

The glycolytic part of the network (conversion of glucose to pyruvate) is considered equal for both microorganisms and follow the EMP pathway. To produce acetate and butyrate at an equimolar ratio, as observed experimentally with BPB (Temudo et al., 2007), the electron bifurcation mechanism must be included in the butyrate pathway to allow for a closed electron balance in the conversion reaction from glucose (Chapter 3). Biomass is considered to be built from glucose including 10% molar conversion of carbon substrate to carbon dioxide in anabolism and without consumption of electron equivalents. The influx of amino acids or inorganic nitrogen is omitted from the metabolic

network and the model, as glucose is considered to be the only limiting substrate in the system.

Table 4.1. Summarised catabolic reactions considered in the metabolic network.

Microorganism	Conversion reaction	ATP yield
LAB	Glucose → 2 lactate$^-$ + 2 H_2O	2
BPB	Glucose → 0.67 acetate$^-$ + 0.67 butyrate$^-$ + 0.67 H_2O + 2.67 H_2 + 2 HCO_3^-	3.33

4.2.5. Enzymatic activities

The activities of the enzymes involved in the steps described in the metabolic network were collected in the BRENDA database (Schomburg et al., 2002) and in literature (Table 4.2). Glycolysis activity values are referred to enzymes found in *E. coli* as values for the genus of the microorganisms considered in the metabolic network could not be found. These glycolysis enzymatic activity values are used in the catabolism of the two microorganisms considered in the model and, in consequence, the interference in the competition between them is considered to be negligible. For BPB, activity values related with different species belonging to the genus *Clostridium* were chosen. The activity value of the lactate dehydrogenase (the only enzyme needed for converting pyruvate into lactate) was selected from the species *L. plantarum*, a LAB found in dairy, meat and vegetables fermentations involved in food spoilage (de Vries et al., 2006).

Due to lack of available information in literature and databases, some approximations had to be made. Information on the enzymatic activity of any monocarboxylate transporter in bacteria was not available in literature. For the acetate, butyrate and lactate exporter it was decided to use for the three of them the activity value used in Schumacher (2018) for the lactate exporter in *S. cerevisiae*. Glucose importer activity could not be found either and its value was set to reflect a maximum glucose uptake rate of 40 mmol/g_{BM}·h (Batstone et al., 2002a), assuming that glucose is converted to two lactate molecules that have to be transported out of the cell by a system that also occupies space in the membrane. Ribosomes activity was also set to reflect a LAB maximum specific growth rate of 0.35 h^{-1} similar to that observed experimental in lactate producers in Rombouts *et al.* (Rombouts et al., 2020).

Table 4.2. Enzymes considered in the metabolic network and their enzymatic activity.

Enzyme Name	EC Number	Specific activity	Microorganism	Ref
Glycolysis				
HXK	2.7.1.2	158	*E. coli*	
PGI	5.3.1.9	212.6	*E. coli*	
PFK	2.7.1.11	190	*E. coli*	
FBA	4.1.2.13	477	*E. coli*	1
TPI	5.3.1.1	55	*E. coli*	2
GLD	1.2.1.12	40	*E. coli*	3
PGK	2.7.2.3	480	*E. coli*	
GPM	5.4.2.11	124	*E. coli*	
ENO	4.2.1.11	260	*E. coli*	
CDC	2.7.1.40	55	*E. coli*	4
Lactic acid				
LDH	1.1.1.27	2350	*L.plantarum*	
Butyric acid				
PFOR	1.2.7.1	25	*C. acetobutylicum*	5
Acetyl-CoA C-acetyltransferase	2.3.1.9	216	*C. acetobutylicum*	
BHBD	1.1.1.157	445	*C. kluyveri*	
3-hydrobutyrate dehydratase	4.2.1.17		*C. acetobutylicum*	
Etf	1.3.1.109	12	*C. difficile*	
Phosphate butyryltransferase	2.3.1.19	1380	*C. acetobutylicum*	
Butyrate kinase	2.7.2.7	402	*C. acetobutylicum*	
Acetic acid				
PAT	2.3.1.8	7140	*C. kluyveri*	
ACK	2.7.2.1	1087	*C. acetobutylicum*	
Transporters				
Glucose transporter		16.7	Parametrised	
Acid transporter		106	Parametrised	
Anabolism				
Ribosomes		1.7	Parametrised	

1: (Baldwin et al., 1978), 2: (Garza-ramos et al., 1996), 3: (D´Alessio and Josse, 1971), 4: (Waygood and Sanwal, 1974), 5: (Meinecke et al., 1989)

4.2.6. Uncertainty and sensitivity analysis

Given that the model relies on a number of assumptions on parameter values, a global uncertainty and sensitivity analysis of the parameter space was performed. The parameters selected for this analysis (Table 4.3) are assumed to have a uniform probability distribution bounded 25% around the default value, an adequate value for parameters with an intermediate uncertainty (Vangsgaard et al., 2012).

Table 4.3. Parameters whose uncertainly is assessed in the Monte Carlo procedure and their default values.

Parameter	Default value
Total protein concentration	1 $g_{PROTEIN}/g_{RBM}$
Growth-related protein	50%
Protein located in the membrane	20%
Decrease in ribosomal activity in prototrophic BPB	15%
Glucose transporter	1.01 $mg_{PROT}/(mmol_{Glucose}\cdot h)$
Glycolytic enzymes	2.52 $mg_{PROT}/(mmol_{Glucose}\cdot h)$
Butyrate production enzymes	2.91 $mg_{PROT}/(mmol_{Butyrate}\cdot h)$
Acetate production enzymes	0.68 $mg_{PROT}/(mmol_{Acetate}\cdot h)$
Lactate production enzymes	0.007 $mg_{PROT}/(mmol_{Lactate}\cdot h)$
Butyrate transporter	0.16 $mg_{PROT}/(mmol_{Butyrate}\cdot h)$
Acetate transporter	0.16 $mg_{PROT}/(mmol_{Acetate}\cdot h)$
Lactate transporter	0.16 $mg_{PROT}/(mmol_{Lactate}\cdot h)$
Ribosomes	9.30 $mg_{PROT}/(mmol_{Biomass}\cdot h)$

The first four parameters relate to assumptions about the cellular structure and the differences in proteomics between auxotrophic and prototrophic microorganisms. The remaining correspond to the enzyme requirements of different sections of the metabolic network and growth. All the parameters are considered to be uncorrelated to avoid underestimating the uncertainty of the model solution. The parameter space was sampled using the Latin Hypercube Sampling methods to ensure a maximal coverage of the parameter space (Helton and Davis, 2003). Following a Monte Carlo procedure, a total of 1000 samples were taken and used to solve the model at different residual glucose concentration values. The model outputs (specific growth rate values) are the basis for the subsequent sensitivity analysis.

A global sensitivity analysis was carried out to determine what parameters (and assumptions) exert a higher influence in the model output and check the need of refining the model hypotheses. The method of standardised regression coefficients (SRC) was chosen, whereby a first order linear multivariable model relating the model outputs taken from the Monte Carlo procedure (y_k) to the parameter values (θ_i) is fitted with the least squares method (Saltelli et al., 2008):

$$y_k = b_{k,0} + \sum_i b_{k,i} \cdot \theta_i \tag{4.9}$$

where y_k are the model outputs, $b_{k,0}$ and $b_{k,i}$ are the linear regression coefficients and θ_i the parameters. The subscript *k* denotes each of the model outputs and the subscript *i* refers to the parameters analysed.

In this case, only the ratio of the specific growth rates of LAB and BPB is used as model output (denoted as Y) and the parameters included in Table 4.3 were considered. If Eq. 4.9 is made dimensionless by mean-centred sigma-scaling, to make the coefficients directly comparable regardless of their absolute value, the standardised linear regression coefficients, $\beta_{k,I}$, are obtained:

$$\frac{y_k - \mu_{y_k}}{\sigma_{y_k}} = \sum_i \left(\beta_{k,i} \cdot \frac{\theta_i - \mu_{\theta_i}}{\sigma_{\theta_i}} \right) \tag{4.10}$$

where μ_{yk} and $\mu_{\theta i}$ are the mean values and σ_{yk} and $\sigma_{\theta i}$ are the standard deviation of the model outputs and input parameters, respectively.

If the multivariable model of Eq. 4.10 is linearly additive, then $\sum_i \beta_i^2 = 1$ for each of the model outputs should be fulfilled. The parameter β_i^2 represents the contribution to the variance of parameter *i* and can be used as a measure of its importance on the output of the model. To assume the model linear, the squared coefficient of correlation (R^2) between the Monte Carlo simulation output (Y) and the values produced with the regression model with the estimated SRC (Eq. 4.10) regressed linear output should be above 0.7 (Vangsgaard et al., 2012).

4.3. RESULTS AND DISCUSSION

4.3.1. Evaluation of the enzymatic activities for the different strategies

The enzyme requirements (i.e. the mass of enzyme needed to catalyse one unit of flux) for the different sections of the metabolic network and of the different catabolic strategies were determined (Table 4.4). Glycolysis requires a high enzyme mass, similar to butyrate production and, to a lower extent, acetate. In comparison, yielding lactate from pyruvate needs much less enzyme mass

because lactate is only one metabolic step away from pyruvate and the enzyme catalysing that conversion, lactate dehydrogenase, has a remarkable high activity. As a consequence, lactate fermentations only need 3.85 mg of enzyme to catalyse one flux unit while butyrate fermentations need 6.13 mg, which is 40% more, reinforcing the hypothesis that shorter pathways are faster due to lower enzymatic requirements (Kappler et al., 1997; Pfeiffer and Bonhoeffer, 2004). However, lactate formation is energetically less favourable, as the ATP yield is 40% lower (Table 4.1). As a result, the mass of enzymes needed to produce a unit of ATP flux in catabolism, which is proportional to the specific growth rate, is very similar for both strategies (Table 4.4).

Table 4.4. Enzymatic requirements for metabolic fluxes of different pathways.

Pathway	Enzyme requirement
Glucose → 2 Pyruvate	2.52 mg Prot/(mmol glucose/h)
Pyruvate → Lactate	0.007 mg Prot/(mmol pyruvate/h)
Pyruvate → ½ Butyrate	1.46 mg Prot/(mmol pyruvate/h)
Pyruvate → Acetate	0.68 mg Prot/(mmol pyruvate/h)
Complete catabolism	
Glucose → 2 Lactate	3.85 mg Prot/(mmol glucose/h)
Glucose → 2/3 Butyrate + 2/3 Acetate	6.13 mg Prot/(mmol glucose/h)
Catabolism in terms of ATP flux	
Lactate (2 ATP)	1.93 mg Prot/(mmol ATP/h)
Butyrate fermentation (3.33 ATP)	1.86 mg Prot/(mmol ATP/h)

Lactate fermentations cannot be explained through the Crabtree effect, where the differences between fermentation and respiration in terms of enzymatic requirements are noticeable higher than in this case. In this sense, the Crabtree effect can be already explained by only the ATP flux enzymatic requirements. Moreover, if only producing lactate was the key to attain a very high specific growth rate, fermentations dominated by *Clostridium* bacteria potentially could be producing lactate as well, since they have the genes to synthetize lactate dehydrogenase and lactate transporters (Biddle et al., 2014; Geer et al., 2010) and were reported to produce lactate under specific environmental conditions (Payot et al., 1999).

4.3.2. LAB auxotrophic anabolism explains its fast growth

The growth of the three microorganisms presented in section 4.2.3 is modelled at different glucose concentrations and the predicted specific growth rates are

shown in Figure 4.2. Glucose concentration values are divided by the half saturation constant (K_m, Eq. 4.7) to isolate the influence of the value of this parameter on the analysis. Two areas can be clearly identified in the graph. At high glucose concentrations, auxotrophic LAB are the fastest growers and, on the contrary, at low glucose concentrations, BPB can achieve a higher specific growth rate and will likely dominate the microbial community under these conditions. LAB grow slower and at a very similar rate regardless of their anabolism (auxotrophic or prototrophic).

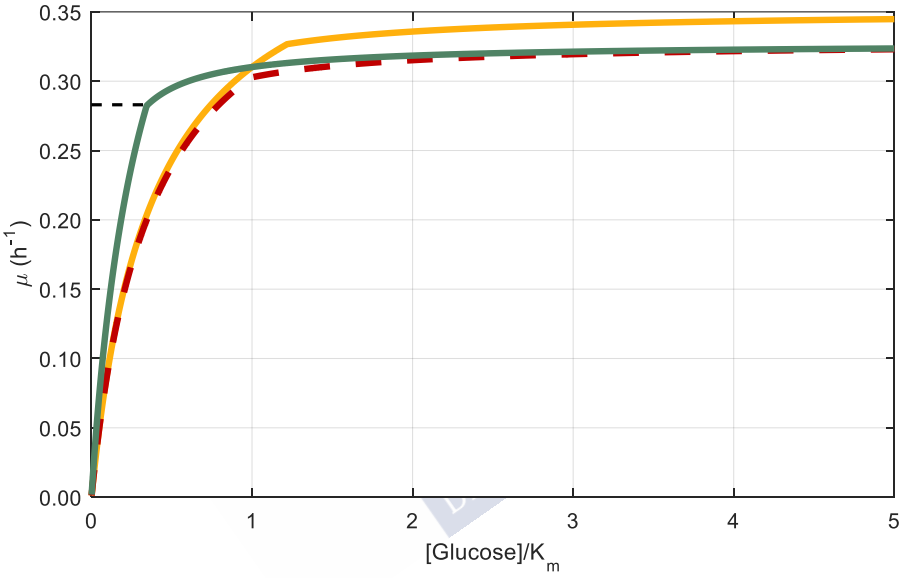

Figure 4.2. Predicted specific growth rate of three model microorganisms at different glucose concentrations. The horizontal axis represents the dimensionless glucose concentration determined by division by K_m ■ Auxotrophic lactic acid bacteria (LAB), ■ prototrophic lactic acid bacteria (LAB) and ■ butyrate-producing bacteria (BPB). The dashed line represents specific growth rate value of 0.28 h^{-1}.

LAB display a maximum specific growth rate of 0.35 h^{-1}, which is 9% higher than that of BPB. This result suggests that auxotrophic LAB outcompete BPB in environments that select for microorganisms with the highest maximum specific growth rate, as for example in sequencing batch reactors. The estimated kinetic parameters of the two microbial communities in the experiments of Rombouts et al. (2020) also show that LAB in rich medium also developed a higher maximum growth rate (0.23 h^{-1}) than BPB in mineral medium. (0.19 h^{-1}), which represent a 20% increase.

Prototrophic LAB behave similarly to auxotrophic LAB at low glucose concentrations but their maximum specific growth rate is lower, which means that an auxotrophic anabolism offers a competitive advantage in terms of maximum specific growth rate. The model predictions also show that the value of the maximum specific growth rate of a hypothetical prototrophic LAB is similar to that of BPB, as already predicted in section 4.3.1 based on the enzyme requirements per ATP flux for the different catabolic strategies. In this way, in a mineral medium, where auxotrophic LAB cannot grow, the two catabolic strategies considered (lactate or butyrate and acetate production) allow cells to attain a similar maximum specific growth rate.

At the low range of glucose concentrations, BPB grow faster or, equivalently, at the same dilution rate (equivalent to the specific growth rate in a CSTR) BPB can achieve lower effluent glucose concentrations, assuming that the affinity for glucose uptake is similar in both types of microorganisms. For example, at a dilution rate of 0.25 h^{-1}, BPB will lower the residual glucose concentration to 0.3 times the affinity constant, while LAB could only lower it to 0.7 (Figure 4.2). Hence, at low specific growth rates catabolism does play an important role as a high ATP yield strategy gives a competitive advantage to BPB. This prediction fully explains the observations of Thomas *et al.* (Thomas et al., 1979) that a pure culture of an homolactic fermenter (*Streptococcus lactic*) produced lactate in a CSTR at high dilution rates but at low dilution rates switched production to acetate and ethanol (Thomas et al., 1979). An auxotrophic anabolism does not appear to offer a competitive advantage at low substrate concentration as both the auxotrophic and prototrophic LAB growth curves overlap in the low glucose concentration area of the graph (Figure 4.2).

Accordingly, a simulation of the competition between the three model microorganisms in a CSTR, at different dilution rates (D), shows that butyrate and acetate would dominate the product spectrum at low dilution rates (Figure 4.3), as for the same growth rate BPB can lower to a higher level the residual substrate concentration and outcompete LAB. In consequence, under these conditions the product spectrum would be well predicted by the ATP yield maximisation perspective. At increasing dilution rates lactate starts to be produced simultaneous with butyrate and acetate and, eventually would dominate the product spectrum at very high dilution rates, as under these conditions only LAB can survive due to their higher maximum uptake rate (Figure 4.2). This behaviour is in close agreement with the observations of Rafrafi et al. (2013) in

CSTR experiments, who reported significant lactate production under high residual glucose concentration, which indicates that the biomass of the reactor was close to being washed out. Therefore, under these conditions of high residual substrate concentration, the ATP yield maximisation as optimisation proxy is not enough to capture the cellular metabolic optimisation and resource allocation concepts help to better describe the cellular behaviour.

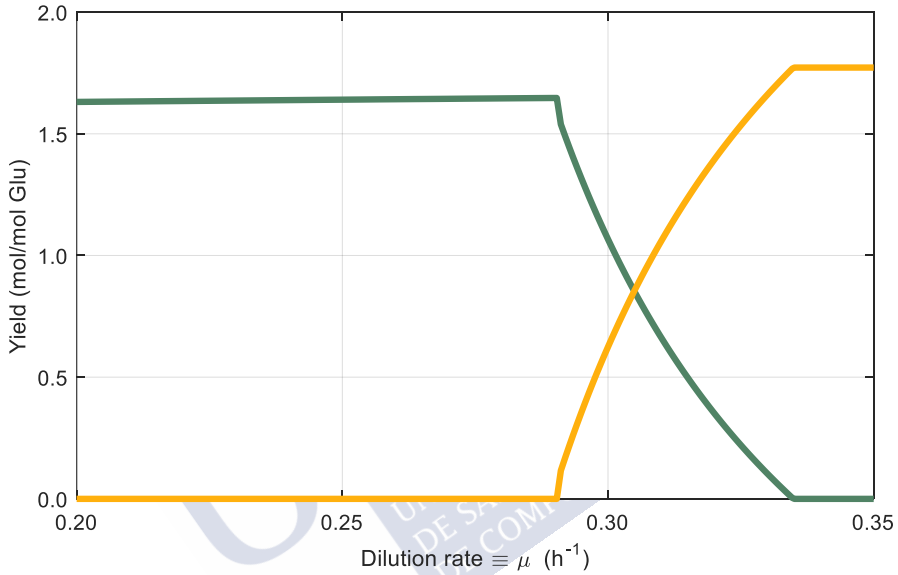

Figure 4.3. Predicted molar product yields resulting from the competition of the three model microorganisms at different dilution rates (D) in a CSTR (equivalent to the growth rate of the populations). ■ lactate ■ butyrate and acetate (sum of the equimolar butyrate and acetate yields).

4.3.3. The maximum protein concentration constraint triggers the change in production strategy.

The behaviour shown in Figure 4.2 and Figure 4.3 can be explained by the total and membrane protein concentration in LAB and BPB attained at different specific growth rates. By using Eq. 4.1, the concentration of the main metabolic enzymatic groups involved in the two studied microorganisms can be calculated using the optimum fluxes determined by the model at different dilution rates (equivalent to the specific growth rate in a CSTR). Figure 4.4A and Figure 4.5A show the concentration of transport enzymes, which are located in the membrane, and Figure 4.4B and Figure 4.5B focus on the concentration of all

the enzymes involved in the metabolism of BPB and LAB, respectively. With that information it can be determined which constraint (membrane or total protein maximum concentration, represented by Eq. 4.5-4.6) shapes the model outcome for each of the microorganisms under different conditions.

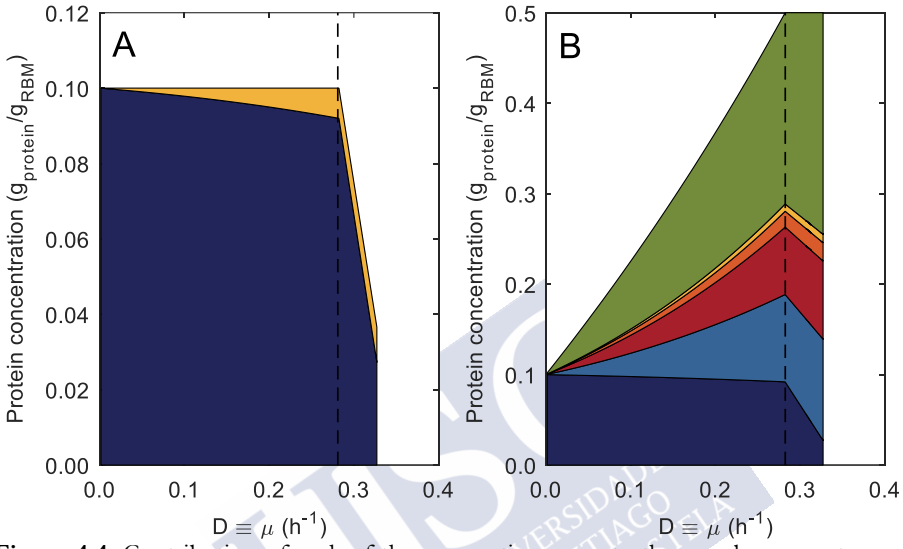

Figure 4.4. Contribution of each of the enzymatic groups to the membrane proteome (A) and to the total proteome (B) of BPB in the model solution at different dilution rates (D) in a CSTR (equivalent to the specific growth rate). ■ Glucose transport, ■ Glycolysis, ■ Butyrate production, ■ Acetate production, ■ Acid transport, ■ Growth. The dashed line represents the growth rate when the maximum proteome space limit is reached at a dilution rate of 0.28 h^{-1}.

In Figure 4.4A it is observed that at low and medium dilution rates, BPB are restricted by the glucose transport capacity, as their membrane protein concentration reaches the maximum allowed value proposed of 0.10 g_{PROT}/g_{RBM} (Eq. 4.6). The increasing specific growth rate observed in Figure 4.2 under these conditions is well justified by the increasing values of glucose concentration (Eq. 4.8). However, at a value of 0.28 h^{-1}, an abrupt change in the specific growth rate slope happens. As observed in Figure 4.4, BPB reach at this point the maximum total protein concentration imposed by the model (Eq. 4.5). From this point on, BPB must optimise enzyme allocation and therefore the opportunities of increasing their specific growth rate at higher glucose concentration are drastically limited. The factor limiting BPB growth at higher dilution rates is the

cytoplasm protein concentration, rather than membrane protein concentration, as shown if Figure 4.4 (A, B).

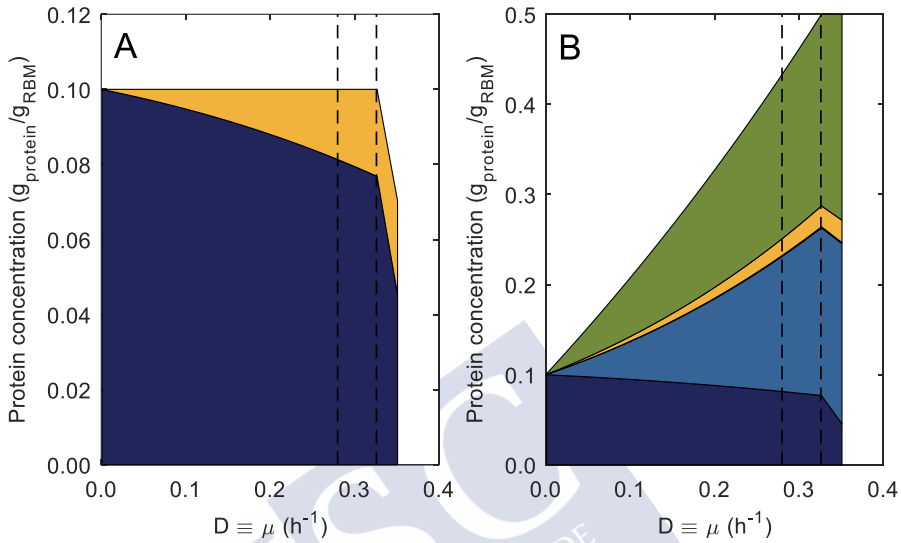

Figure 4.5. Contribution of each of the enzymatic groups to the membrane proteome (A) and to the total proteome (B) of LAB in the model solution at different dilution rates (D) in a CSTR (equivalent to the specific growth rate). ■ Glucose transport, ■ Glycolysis, ■ Lactate production, ■ Acid transport, ■ Growth. The dashed lines represent dilution rates of 0.28 and 0.33 h^{-1}.

LAB display a quite similar behaviour and the factors limiting their growth are also the same as in BPB. However, as observed in Figure 4.5 (A, B), their maximum total protein concentration is attained at a higher dilution rate, highlighting the competitive advantage given by an auxotrophic anabolism, which has a higher ribosomal enzymatic activity. Unlike BPB, the unrestricted LAB do not face enzyme allocation issues in the cytoplasm and can keep increasing the glucose uptake rate between dilution rates of 0.28 to 0.33 h^{-1}. At their maximum specific growth rate, BPB have a concentration of glycolysis-related enzymes of 0.11 g/g_{RBM} (Figure 4.4B) while LAB attain a concentration of 0.20 g/g_{RBM}, indicating that glucose consumption rate almost doubles in LAB (Figure 4.5B). In fact, the observed glucose consumption rate of lactate producers in the experiments of Rombouts et al. (2020) is about twice as much as that of butyrate producers, which is in line with the predictions of the model.

Up to dilution rates of around 0.28 h^{-1}, protein-unrestricted BPB would dominate the microbial community due to their higher ATP yield, as glucose transport is limited in a similar way in both BPB and LAB. Consequently, the predicted product spectrum consists mostly of butyrate and acetate (Figure 4.3). At higher dilution rates, however, LAB eventually overcome their lower ATP yield on glucose and outcompete BPB due to a higher substrate consumption capacity. From dilution rates values of around 0.28 h^{-1}, the product spectrum starts to switch to lactate and eventually it becomes the dominant product (Figure 4.3).

4.3.4. The model captures proteome regulation at different environmental conditions

The model predicts at low substrate concentrations, most of the enzymes are dedicated to substrate transport (Figure 4.6) as the glucose transporter is far from saturation, which, following Eq. 4.7, results in a very low enzymatic activity. Conversely, at high substrate concentrations growth is limited by the cytoplasmatic protein space while the membrane protein concentration constraint is not reached (Figure 4.4 and Figure 4.5).

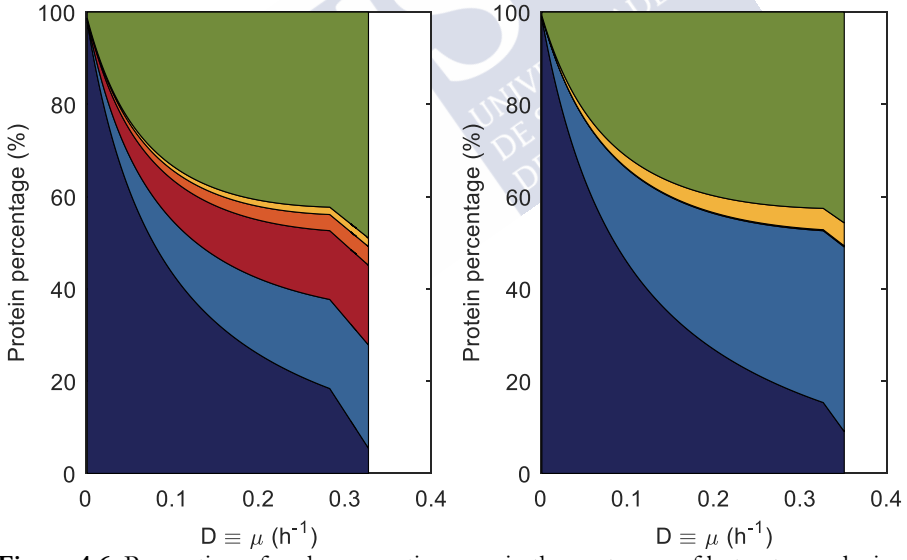

Figure 4.6. Proportion of each enzymatic group in the proteome of butyrate-producing bacteria (BPB, left graph) and lactic acid bacteria (LAB, right graph) at different dilution rates. ■ Glucose transport ■ glycolysis ■ butyrate production ■ acetate production ■ lactate production ■ acid transport ■ growth.

Experimental measurements confirm that cells tune the concentration of the different enzymatic groups depending on the environmental conditions and show that under high substrate concentration conditions cells allocate most of their proteome to ribosomes (Nielsen and Villadsen, 1994). Under these conditions, the model predicts that about 40% of the proteome consists of ribosomes (Figure 4.6), which is in agreement with experimental measurements for E. Coli (Bosdriesz et al., 2015; Hui et al., 2015; Nielsen and Villadsen, 1994).

Experimental evidence also shows that cells modify their morphology as a way of coping and relieving these changing limitations at different environmental conditions (Dennis and Bremer, 2008; Molenaar et al., 2009). At low substrate concentrations, as in a well-operated CSTR, cells tend to shrink as a mean of optimising the surface to volume ratio and of increasing the membrane protein capacity per volume. At high substrate conditions, the opposite trend is observed: cells tend to be larger to maximise their protein capacity in the cytoplasm, in line with the results of section 4.3.3.

4.3.5. Uncertainty and sensitivity analysis

The goal of the uncertainty analysis is to evaluate the influence of different parameter values, especially of those parameters with values set based on assumptions (ribosomal activity, glucose transporter activity, growth-related share of the proteome, etc.), on the model outcome, which is represented by the output Y (the ratio between the specific growth rate of auxotrophic LAB and BPB). For that Monte Carlo simulations with a variability of the input parameters of 25% were carried out (Figure 4.7).

As observed in Figure 4.7, at high glucose concentrations (around 10 times K_m) in 94% of the Monte Carlo simulations the value of the specific growth rate ratio was above 1. Besides, at low glucose concentrations (below 0.5 times K_m), the shaded area in Figure 4.7 lies completely below a ratio value of 1, indicating thus that at low glucose concentrations BPB grow faster for the same glucose residual concentration than LAB. These two results would confirm the robustness of the model outcome.

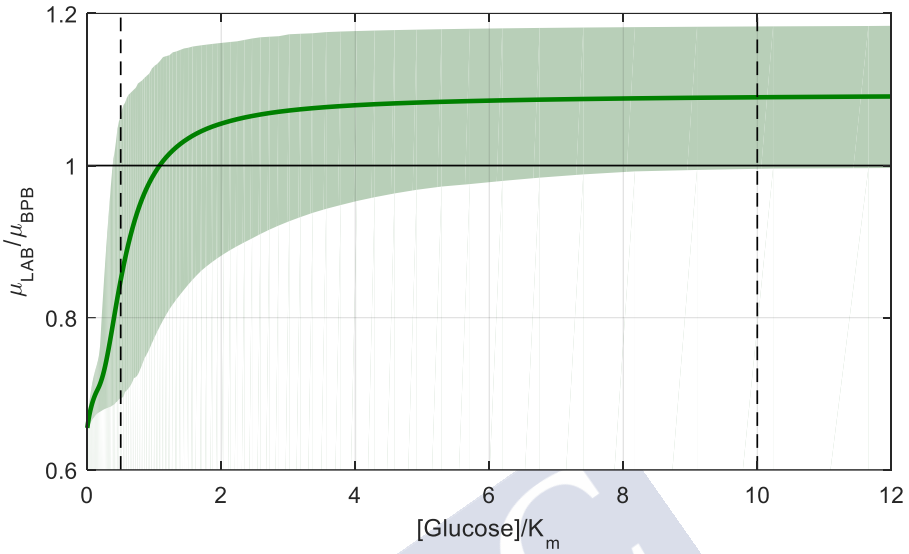

Figure 4.7. Uncertainty analysis results for the ratio between specific growth rate of LAB and BPB at different non-dimensional glucose concentrations. The line represents the mean value of the Monte Carlo simulations and the shaded area the region of ratio values within a 95% confidence interval (percentiles 2.5%-97.5%).

The sensitivity of the model was analysed at two glucose concentrations (0.5 and 10 times K_m) to identify in each case the mechanisms that affect the most the specific growth rate of each microbial group. Table 4.5 features the squared standardised linear coefficients, which represent the contribution of each parameter to the variance of the model outcome at the two points analysed.

At low glucose concentrations, where BPB dominate, membrane-related parameters have the highest influence on the model outcome. The share of the total protein that is located in the membrane represents almost 50% of the variance observed in the model outcome, followed by the enzymatic requirements for glucose transport with 25%. The high sensitivity of these parameters on the model output is in close agreement with section 4.3.3 as transport was already identified to limit growth under these conditions.

Table 4.5. Squared standardised linear coefficients for the parameters varied in the uncertainty analysis.

Parameter	β_i^2	
	[Glucose]=0.5	[Glucose]=10
Glucose transporter	*0.25*	0.03
Glycolytic enzymes	0.01	*0.36*
Butyrate production enzymes	0.03	*0.37*
Acetate production enzymes	0.00	0.02
Lactate production enzymes	0.00	0.00
Butyrate transporter	0.02	0.04
Acetate transporter	0.00	0.00
Lactate transporter	0.00	0.00
Ribosomes	0.10	0.02
Total protein concentration	0.06	0.02
Growth-related protein	0.01	0.00
Protein located in the membrane	*0.47*	0.01
Decrease in ribosomal activity in prototrophic BPB	0.00	0.05
Model linearity (R^2)	0.949	0.935

At high glucose concentrations, where LAB are predicted to dominate the microbial community, the most sensitive parameters are related with cytoplasmatic processes. The enzymatic requirements of glycolysis and butyrate yielding explain 36% and 37% of the variance, respectively. This is in line with the conclusions of section 4.3.3, where it was shown that cytoplasmatic protein capacity was the factor limiting growth at high substrate concentrations.

4.3.6. Resource allocation and process design

Microorganisms strive for energy in their pursuit to grow and dominate their ecosystem. In this sense, strong selective pressures are believed to have been exerted to the ATP-producing pathways (Pfeiffer et al., 2001). Apparently, based on the results of this model, these selective pressures might have led LAB to lose the ability to synthesise amino acids from inorganic compounds as it gives them a competitive advantage, which is in agreement with a previous study regrading auxotrophies prediction. Several auxotrophies for amino acids were predicted in gram-negative bacteria using genome-scale metabolic reconstruction and some of them were postulated to confer a fitness in *in vivo* experiments depending on the environmental conditions (Seif et al., 2020).

According to the results of this work, LAB can dominate the microbial community when the system selects on specific growth rate (as in discontinuous processes or very high dilution rate CSTR) because they are capable of attaining a very high substrate consumption rate. Their anabolism is more enzymatically efficient allowing LAB to allocate a higher share of the proteome to catabolic processes. In consequence, LAB are common in habitats with available peptides as for example wine, milk or grass (Carr et al., 2002), which is in complete agreement with the conclusions of this work.

Resource allocation might also help explaining other metabolic behaviours such as polymer accumulation in some bacteria. In environmental conditions in which growing is limited (e.g. nitrogen is the limiting factor), these bacteria store the substrate in the form of a polymer (e.g. polyhydroxyalkanoate) to use it afterwards when growth is not hampered. Under such conditions, the accumulating bacteria outcompete other non-storing bacteria because they can develop a much higher substrate uptake rate (Jiang et al., 2011; Johnson et al., 2009). From a resource allocation perspective, it could be hypothesised that the hampered anabolism leaves room for additional catabolic enzymes, allowing in this way consuming substrate at a higher rate.

Cross feeding between species is another candidate to be analysed using resource allocation. The most accepted interpretation is that dividing the catabolism in several microbial groups allows for attaining a higher consumption rate and therefore outcompete microorganisms that perform the conversion completely but at a slower rate. In fact, lactate production could also be considered as a case of cross feeding as lactate can be further metabolised to typical fermentation end products. In the experiments of Rombouts *et al.* (Rombouts et al., 2020) lactate is consumed by a non-glucose consumer microbial group (bacteria belonging to the genus *Megasphaera* mainly) producing a mixture of acetate, propionate, butyrate and valerate. In this sense, resource allocation is in line with the most-recent cross feeding interpretations, as it also predicts that in high substrate concentration conditions an association of two microbial groups consuming the substrate faster and in two steps is fitter than one single microbial group converting the substrate to the end products by its own. The faster consumption rate can be given by a more enzymatically efficient catabolism (Crabtree effect or acetate overflow) or anabolism, as shown in this work for lactate fermentation.

This mechanistic knowledge can be applied, for example, in the design of processes aiming at the intermediate compounds in two-step microbial conversions. It was already shown in this work that lactate production is promoted in SBR configurations and butyrate production is favoured in a CSTR (except at very high dilution rates) (Figure 4.3). To avoid lactate consumption the operational conditions should be tuned to avoid the presence of lactate consumers (e.g. at a dilution rate incompatible with the survival of these microbial populations). A similar design case could be the partial nitrification of ammonia to nitrite. If the goal is to achieve a complete partial nitrification, the environmental conditions should favour a two-step process and should avoid nitrite oxidation. Following the resource allocation theory, the longer complete nitrification to nitrate by one microbial group (comammox) would be favoured only at very low substrate concentrations. Indeed experimental evidences show that commamox has a higher biomass yield but lower specific growth rate than a two-step nitrification process and is only observed at low substrate environments (Hu and He, 2017). Thus complete partial nitrification can be achieved with a high ammonia load and low dissolved oxygen concentration as in this way i) the high specific growth rate strategy of two steps is favoured and ii) the second step is discouraged by a low dissolved oxygen concentration, as proved experimentally (Wei et al., 2014).

4.4. CONCLUSIONS

A possible mechanism triggering lactate production in anaerobic mixed-culture fermentations was identified by means of a resource allocation FBA model. Simulation results indicate that the characteristic anabolic auxotrophy on amino acids of lactate acid bacteria is advantageous and enables a higher maximum specific growth rate than butyrate-producing bacteria, provided peptides are available. Maximum total and membrane protein concentration constraints explain the different metabolic strategies and proteome regulation behaviours observed experimentally. The model is in line with empirical observations and predicts lactate production only in rich cultivation medium and at high dilution rates in a CSTR or a (repeated) batch process. On the contrary, prototrophic butyrate-producing bacteria are predicted to dominate the community under any other operational condition. To fully validate the predictions of the model, additional experiments are needed, with a special focus in analysing the meta-proteomics of the microbial community to corroborate the predicted link between proteome and the change in production strategy. In particular, a rich

cultivation medium CSTR experiment at low dilution rate is lacking in the literature to verify that anabolic auxotrophies are only advantageous at high specific growth rates. The model described in this work for the first time uses resource allocation theory to identify and explain an ecological niche for a specific group of microorganisms in a mixed microbial consortium. This chapter also defines boundaries on the application of the ATP maximisation optimisation strategy for stoichiometry prediction. The results shown that when the substrate concentration in the reactor is low (below the affinity constant), ATP efficient pathways dominate and therefore the ATP yield maximisation approach is enough to describe correctly the product spectrum. On the contrary, under high substrate concentrations, as in a batch reactor, being efficient is not enough and optimisations approaches considering also kinetic limitations, as resource allocation, might help to predict the process stoichiometry.

CHAPTER 5

Bioenergetic modelling for stoichiometry prediction of protein fermentation

Summary

Protein-rich organic effluents are suitable substrates to produce VFA in anaerobic mixed-culture fermentations. In these processes, the stoichiometry depends significantly on operational conditions such as pH or feeding characteristics but there are still no predictive tools to predict the stoichiometry of process under different conditions. In this chapter a bioenergetic metabolic model is developed for the prediction of the stoichiometry of VFA production from proteins. In particular, the effect of pH on the product yields is analysed and, for the first time, the observed changes are mechanistically explained. The model reproduces experimental results at both neutral and acidic pH and it is also capable of predicting the tendencies in product yields observed with a pH drop. It also offers mechanistic insight into the interaction among the different amino acids of a particular protein and how an amino acid might yield different products depending on the relative abundance of other amino acids. Particular emphasis is placed on the utility of this mathematical model as a process design tool and different examples are given on how to use the model for this purpose.

5.1. INTRODUCTION

Suitable organic effluents for mixed-culture fermentations (MCF) at industrial scale include the organic fraction of urban waste or agro-industrial residual streams (e.g. cheese whey or canning industry waste). These organic wastes contain carbohydrates, proteins and lipids. While short carbohydrates have been extensively tackled from an experimental (Temudo et al., 2007) and modelling (González-Cabaleiro et al., 2015; Rodriguez et al., 2006) point of view, protein anaerobic fermentation has been barely addressed.

Ramsay and Pullammanappallil (2001) proposed a product spectrum predictor for the MCF of proteins, with the objective of better understanding its anaerobic digestion to methane. In that work it was assumed that the outcome of protein MCF is unaltered by changes in operational conditions (e.g. pH) and that the different amino acids (AA) are degraded always through the same pathway. Protein conversion is also assumed to be complete in all the cases. That means that only the protein composition in AA would affect the product spectrum as their degradation pathways are fixed. However, experimental evidence contradicts most of these assumptions. Protein degradation is not complete and the degradation extent can be affected by pH (Breure and van Andel, 1984; Yu and Fang, 2003), temperature (Yu and Fang, 2003) or dilution rate (Breure et al., 1986b). Moreover, the resulting product spectrum is dependent on operational parameters such as pH (Breure et al., 1986a; Breure and van Andel, 1984).

The objective of this chapter is to develop a bioenergetic metabolic model for the production of VFA from proteins in anaerobic fermentation processes using mixed cultures of microorganisms. This work pretends to give insight for the first time on the degradation mechanisms of the different AA and to predict the stoichiometry of VFA production in protein MCF, the protein conversion and how they are affected by the environmental conditions of the reactor. The influence of pH in the process outcome is specially studied because it is one of the most manipulable design variables and due to its high impact on the energetics of the system.

5.2. MODEL DESCRIPTION

The model is built on the mass balances in a CSTR of the different compounds (states). There are 68 states, of which 3 are moieties related with ATP (ATP, ADP and Pi). The rest represent the concentration of different intracellular compounds (24), extracellular compounds in the bulk reactor (40), gaseous

compounds (3) and biomass. For simplicity, protein hydrolysis is omitted in the model and is directly considered a mixture of AA, as the limiting step in protein fermentation is AA fermentation (Duong et al., 2019). NAD^+ to NADH ratio is set fixed to a value of 10 and the intracellular AA concentrations are assumed constant at a value of 0.1 mM and therefore are not states. Regarding the kinetic parameters, the maximum uptake rate is set to 0.75 mol AA L_X^{-1} h^{-1} and the affinity constant as 1 mM for all AA. There are 99 possible reactions, resulting in a 68x99 metabolic network matrix. Amongst all the reaction rates, 22 of them are independent, i.e. depending solely on extracellular concentrations. The model balances and processes are described in detail in the model development chapter (Chapter 2).

5.2.1. Metabolic network

The metabolic network used in the model is formed by the degradation pathways of 17 AAs: alanine, arginine, asparagine, aspartate, cysteine, glutamate, glutamine, glycine, histidine, isoleucine, leucine, lysine, methionine, proline, serine, threonine and valine. AA containing aromatic side chains were not included in the metabolic network (phenylalanine, tyrosine and tryptophan). The products included in the network are fatty acids from C1 to C6, ethanol, formate, methanethiol, hydrogen sulphide, CO_2 and H_2. Butyrate and valerate are present in both their linear and branched form and in the case of caproate only the branched appears as a product. The considered possible end-products of each AA are shown in Table 5.1. The metabolic network construction and the pathway selection criteria are discussed thoroughly in Chapter 2.

Table 5.1. Summarized amino acid metabolic network.

Amino acid	End products	Comments	Ref.
Alanine (Ala)	Pyruvate, NADH		
Arginine (Arg)	Proline, ATP, CO_2	Via ornithine	
	Alanine, acetyl-CoA, ATP, NADH, CO_2	Via ornithine	1
Aspartate (Asp)	Pyruvate, NADH, CO_2. Succinate, NAD^+	Via oxaloacetate Via fumarate	2
	Propionate, NAD^+, CO_2.	Via fumarate and succinate	
Cysteine (Cys)	Pyruvate, H_2S		3
Glutamate (Glu)	Pyruvate, acetate		4, 5
	Butyrate, NAD^+, CO_2	Via glutaconyl-CoA and crotonyl-CoA with two PT	4, 5
Glycine (Gly)	Acetate, ATP, NAD^+		6
Histidine (His)	Glutamate, formamide		
Lysine (Lys)	Butyrate, acetate, ATP		7
Proline (Pro)	½ acetate, ½ propionate, ½ n-valerate, ½ ATP, ½ NAD^+	Via 5-aminovalerate	8
Serine (Ser)	Pyruvate, ATP		9
Threonine (Thr)	Propionate, ATP, Fd_{red}.	Via 2-oxobutyrate	9
	Glycine, acetyl-CoA, NADH	Via 2-amino-3-oxobutyrate	9
Valine (Val)	Isobutyrate, ATP, NADH, Fd_{red}		10
Isoleucine (Ile)	Isovalerate, ATP, NADH, Fd_{red}		10
Leucine (Leu)	Isovalerate, ATP, NADH, Fd_{red}	Oxidative pathway	10
	Isocaproate, NAD^+	Reductive pathway	11
Methionine (Met)	Propionate, methanethiol, ATP, Fd_{red}		12
	Butyrate, methanethiol, NAD^+	Either H_2 production or a PT	12
Glutamine (Gln)	Glutamate		
Asparagine (Asn)	Aspartate		

Fd_{red}: Reduced ferredoxin; PT: proton translocation; 1: Uematsu et al. (2003); 2:Unden et al. (2013); 3: Loddeke et al. (2017); 4: Buckel (2001); 5: Buckel and Barker (1974); 6: Andreesen (1994); 7: Kreimeyer et al. (2007); 8: Barker et al. (1987); 9: Sawers (1998); 10: Elsden and Hilton (1978); 11: Simon et al. (1985); 12: Bonnarme et al. (2001).

5.3. MODEL RESULTS

5.3.1. Exploring experimental results and their limitations

Most protein fermentation studies available in literature use gelatine as a substrate, due to its presence in agro-industrial effluents (e.g. slaughterhouse and meat-processing wastewater) (Breure et al., 1986a, 1986b, 1985; Breure and van Andel, 1984; Fang and Yu, 2002; Yu and Fang, 2003). A set of works from Breure and co-workers (hereafter Breure experiments) regarding gelatine degradation in CSTR were selected as the best example of experimental results available in literature (Table 5.2). Other available data sets were discarded due to the suspicion that methane could have been produced as hinted by COD balances. If methanogenesis is not completely inhibited it would alter the product distribution as methane production has a net consumption of reducing equivalents.

Table 5.2. Breure experiments characteristics and notation.

Denomination	pH	D (h^{-1})	Inlet concentration (g/L)	Ref.
A	5.3, 7	0.14, 0.23	7.5	1
B	7	0.1	5	2
C	7	0.15	5	2
D	7	0.2	5	2
E	7	0.2	5	2
F	5.3, 7	0.12	7	3

1: (Breure and van Andel, 1984); 2: (Breure et al., 1986b); 3: (Breure et al., 1986a).

The VFA yields reported in the different Breure experiments are overall of good quality and consistent (Figure 5.1 shows yields of the experiments at pH 7). The product order in terms of the yield value is almost identical for the different data sets and the variability of the product yields is generally acceptable. The yields of acetate, propionate and the branched form of butyrate and valerate have coefficients of variation (CV) of 25% or below. On the contrary, n-butyrate and n-valerate yields present a high CV (56% and 44%, respectively). Although the different data sets differ in the dilution rate and the inlet protein concentration, the variations on VFA yields do not follow any tendency with these parameters.

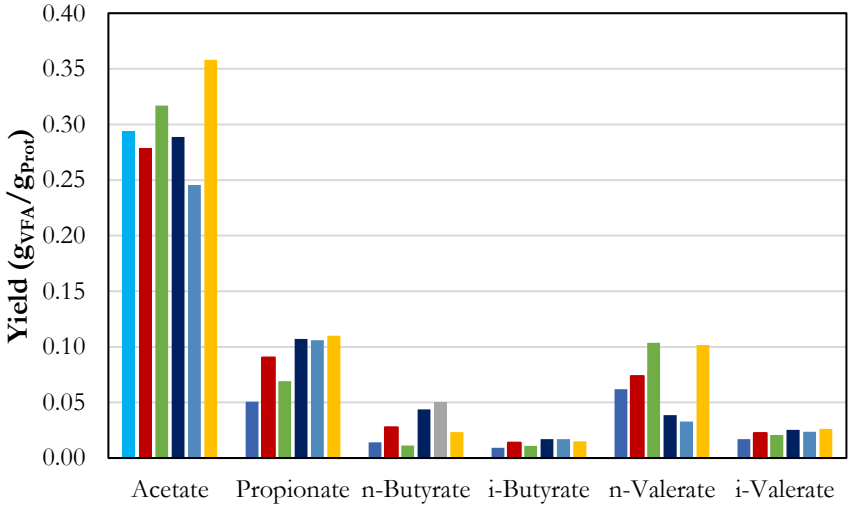

Figure 5.1. VFA yields from gelatine degrading Breure experiments at pH 7. Notation from Table 5.2 is followed: A B C D E F.

Nevertheless, even good quality data are not completely insightful when it comes to understand the process of protein fermentation as there are questions that are hard to clarify with just experimental information. For instance, when protein consumption is not complete, are in this case some AA consumed preferentially or are all of them equally consumed? Moreover, experimental data cannot be extrapolated to other operational conditions than the tested or to other substrates, limiting thus significantly their application for process design. On the contrary, mechanistic models enable us to have detailed knowledge of the mechanisms taking place and therefore they allow extrapolation as the operational parameters set in the model can be easily altered.

5.3.2. Definition of substrate as model input

Gelatine AA composition varies moderately depending on the origin. In Figure 5.2 the average composition and standard deviation in terms of AA of 9 different profiles in the data base of the National Centre for Biotechnology Information is shown (Geer et al., 2010). The AA profile of the protein is one of the main inputs of the model and its outcome is directly correlated with the relative concentration of the different AA. A consequence of this variability is that the origin of the gelatine used in the literature experiments could determine to an extent the observed product yields. For example, proline is the only AA that

usually yields n-valerate, but its relative concentration in Figure 5.2 has a CV of 41.2%, indicating that the characteristics of the specific gelatine selected as substrate will significantly affect the n-valerate yield.

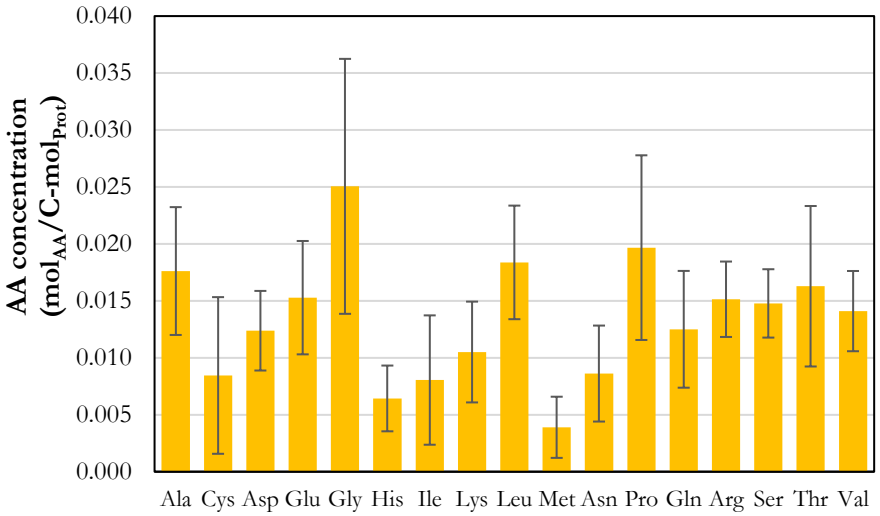

Figure 5.2. Average AA content of 9 different gelatine profiles (Geer et al., 2010).

Unfortunately, the gelatine composition on AA is not reported in Breure experiments and therefore the modelling initial conditions are not fully defined. To fill this knowledge gap, the AA profile used of the simulated had to be assumed. The model was run at pH 7 for each of the 9 gelatine profiles mentioned above and the profile providing the best fit between the model and experimental results at that pH was chosen as the substrate (the chosen profile and results of the analysis are available in the annexes, section 5.6.1). To validate the model, that profile is kept as substrate in all the gelatine simulations and the model results are compared with experimental data at different pH values.

5.3.3. Simulation of continuous gelatine fermentation

5.3.3.1. Effect of pH value on product yields

One of the design parameters more easily manipulated and with a higher impact on product selectivity is pH. Furthermore, its effect has been studied extensively both from an experimental point of view in the case of sugars and proteins (Breure and van Andel, 1984; Fang and Liu, 2002; Temudo et al., 2007; Zoetemeyer et al., 1982) and from a modelling perspective in the case of glucose

(González-Cabaleiro et al., 2015; Rodriguez et al., 2006). Thus, a CSTR was simulated at pH values ranging from 4 to 9, with a dilution rate (D) of 0.12 h^{-1} and an inlet protein concentration of 7 g/L (mimicking experiment F in Table 5.2).

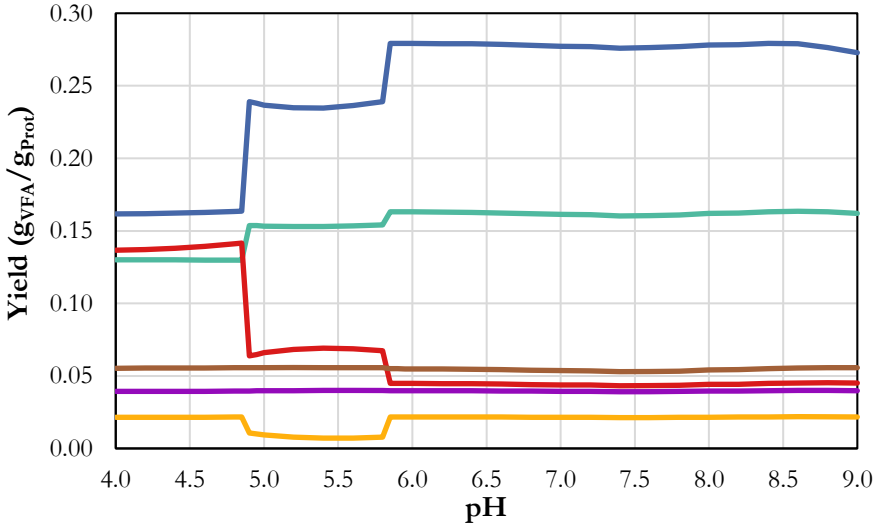

Figure 5.3. Model results (product yields) for gelatine degradation in an CSTR at different pH values. ■ acetate ■ propionate ■ n-butyrate ■ i-butyrate ■ n-valerate ■ i-valerate.

VFA yields are only affected by pH in the acidic region, as increasing the pH from 6 on does not have any relevant effect on selectivity (Figure 5.3). In the acidic region, VFA yields are modified by pH in different ways: while the isoacid yields remain constant, n-valerate, propionate and especially acetate and n-butyrate yields change. For instance, n-butyrate yield triples when pH changes from 6 to 4.5 and acetate yield decreases by approximately 40% for the same pH drop. Protein conversion ranges from 85 to 94% and is maximum at neutral pH values. At acidic or basic pH values, the higher concentrations of non-ionised forms of VFA and ammonia, respectively, are an energetic burden for the cells and limit its yield with respect to the substrate. These conversion values should be interpreted only as the maximum possible values considering the thermodynamic and energetic constrictions at a certain set of conditions.

The information provided by the model simulations at different pH values is of great interest when aiming at designing a process. As the selectivity of the different

VFA changes with pH, it is in principle possible to propose a process targeting a specific VFA with a high selectivity. Admittedly, there are boundaries to how much this parameter affects the selectivity (i.e. acetate is always one of the three major products). The use of predictive models can simulate the joint influence of pH with other design variables (e.g. HRT, substrate nature or concentration) and provide an integral tool for mixed-culture process design.

5.3.3.2. Mechanistic insight

This section shows how mechanistic and exploitable information can be obtained from the proposed model. CSTR experiments at two pH values are simulated to explore why the different AA are converted to their respective final products and how this stoichiometry is affected by pH. A simulation at a neutral value (pH 7) is first described, since most of the Breure experiments were done at this value, followed by a simulation at an acidic pH (value of 5.3) in order to compare with the acidic pH Breure experiments.

Neutral pH

The product yields and the origin of the different VFA (i.e. from which AA they are yielded) are shown in Figure 5.4. According to the model, glycine is not consumed at all because its degradation reaction is endergonic.

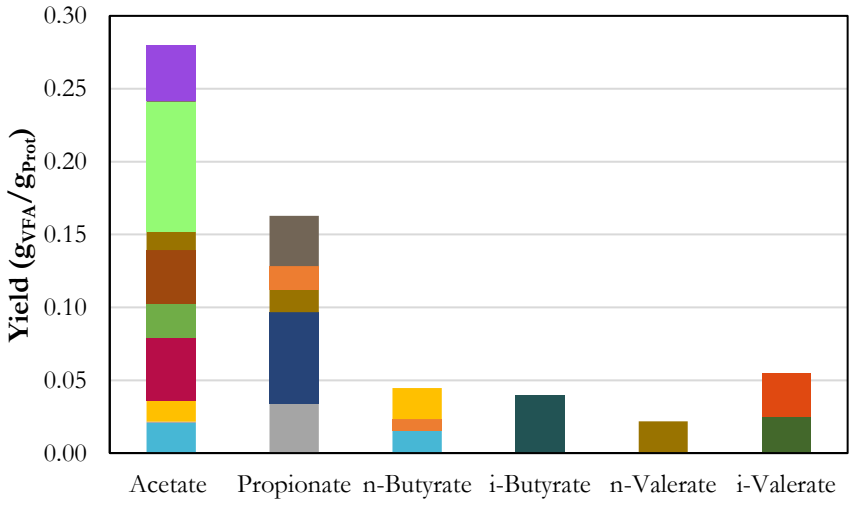

Figure 5.4. Product yields for gelatine degradation in an CSTR at pH 7 predict by the model. Arg Ala Asp Lys Glu Ser Thr Cys Gly Pro Val Ile Leu Met Gln Asn His

The information in Table 5.3 is very useful to explain the model solution. Asp is modelled to be degraded in a 98% to propionate (reaction 1 in Table 5.3) and just a 2% to acetate (reaction 2 in Table 5.3). Both reactions produce net ATP ($r_{ATP}>0$) but reaction 1 consumes NADH ($r_{NADH}<0$) while reaction 2 produces it ($r_{NADH}>0$). However, reaction 2 provides 39% less ATP than reaction 1. Why is then a fraction of aspartate degraded to acetate? The reason is related with the opportunity cost in terms of ATP (i.e. ratio of the ATP rate difference and NADH rate difference or, alternatively, the ATP production rate lost for each unit of NADH production rate unit). Proline (reaction 3 in Table 5.3) consumes NADH, which indicates that to completely degrade proline, other reactions should produce a sufficient NADH rate. This reaction has an ATP to consumed-NADH ratio of 0.26 mol_{ATP}/mol_{NADH}, a value higher than the opportunity cost of degrading aspartate to acetate instead of propionate. Therefore, it is globally worthwhile to sacrifice part of the possible ATP yielded by aspartate as producing enough NADH to fully degrade proline will produce extra ATP. For instance, if aspartate rate increases to use the available NADH in proline degradation and not to increase the propionate yield from aspartate would represent a 4% increase in terms of extra ATP generated.

Table 5.3. Analysis of the steady station solution at pH7.

#	Reaction	r_{NADH}	r_{ATP}	z	r_{ATP}/r_{NADH}	Opportunity cost[1]
1	Asp → Prop	-0.154	0.178	0.976	1.15	
2	Asp → Ac	0.154	0.109	0.024	0.71	0.22
3	Pro → ½ Ac + ½ Prop + ½ n-Val	-0.069	0.018	1	0.26	
4	Ile → i-Val	0.039	-0.006	1	-0.15	
5	Leu → i-Val	0.048	-0.004	1	-0.09	

[1]Opportunity cost is defined as the difference in r_{ATP} divided by the difference in r_{NADH} between two pathways ($\Delta r_{ATP}/\Delta r_{NADH}$). Units: r_{NADH} ($mol_{NADH}/L_X \cdot h$); r_{ATP} ($mol_{ATP}/L_X \cdot h$); r_{ATP}/r_{NADH} (mol_{ATP}/mol_{NADH}); opportunity cost (mol_{ATP}/mol_{NADH}).

This is the case as well of isoleucine and leucine (reactions 4 and 5 in Table 5.3). Both AA produce NADH in their degradation but consume ATP. It seems counterintuitive at first sight to spend ATP degrading an AA when there is always the option of not consuming it. But the ATP to produced-NADH ratio is -0.09 and -0.15 for leucine and isoleucine, respectively, which is lower than the ATP to consumed-NADH ratio of proline, meaning that it is profitable again to spend

energy in degrading AA that produce NADH that will be consumed in the NADH-consuming degradation of proline. For instance, if isoleucine was not consumed at all, only 44% of the proline could be degraded and the ATP produced by these three AA would be an 54% lower.

Acidic pH

The different VFA yields are affected as follows when the pH changes from 7 to 5.3 (Figure 5.5):

- Propionate, isobutyrate and isovalerate yields are basically the same in both cases.
- The yield of n-butyrate increases at pH 5 because there are AA that now yield it that before did not produce butyrate (glutamate, glutamine and histidine).
- The yield of n-valerate yield decreases because proline uptake rate is affected by the low pH value and is not fully consumed at pH 5 (Table 5.4).
- Acetate yield decreases both because part of AA that yield it are affected by the effect of a lower pH and because some AA changed their degradation option.

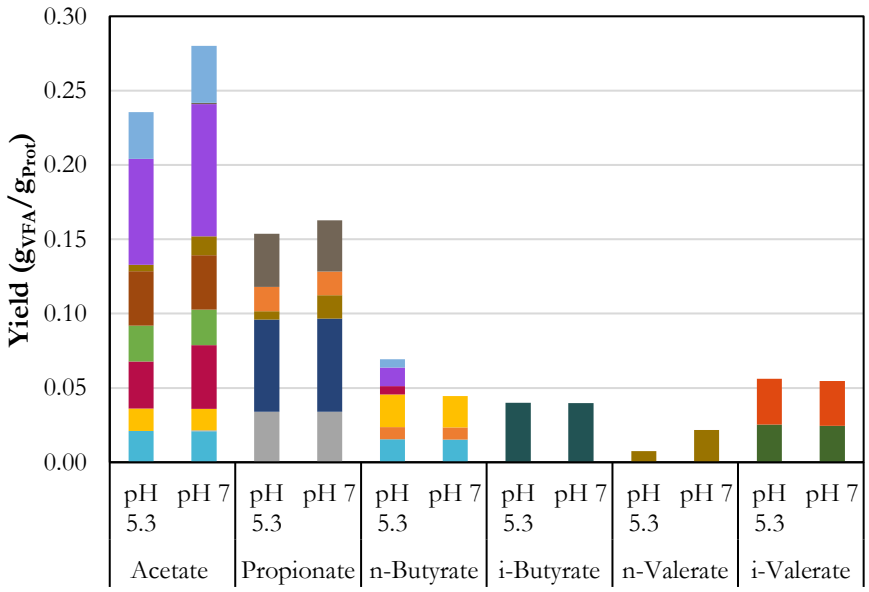

Figure 5.5. Model results for gelatine degradation in an CSTR at pH 7 and pH 5.3. Product yields. Arg Ala Asp Lys Glu Ser Thr Cys Gly Pro Val Ile Leu Met Gln Asn His

At pH 5.3 there are two main products with similar yields (acetate and propionate) and the rest of VFA yields are at a certain distance and with similar values except for n-valerate. The results at a pH of 5.3 show that the biggest change in product spectrum with respect the simulation at pH 7 is the increase of 66% in the n-butyrate share and the 63% decrease of n-valerate product spectrum (Figure 5.5). The acetate share is reduced as well but only in a 11%. Regarding the conversion value the simulation at pH 5.3 indicates a degradation of 86.2%, a decrease of 8% compared to the simulation at pH 7.

Table 5.4. Relevant changes between pH 7 and pH 5.3 model results.

AA	pH 7	NADH balance	Conv.	pH 5.3	NADH balance	Conv.
Asp	0.98 Prop + 0.02 Ac	C	97.7%	Prop	P	90.7%
Glu	2 Ac	-	95.5%	1.61 Ac + 0.19 n-But	C	81.6%
Pro	0.5 Ac + 0.5 Prop + 0.5 n-Val	P	98.9%	0.5 Ac + 0.5 Prop + 0.5 n-Val	P	32.3%
Gln	2 Ac (via Glut)	-	98.9%	1.61 Ac + 0.19 n-But (via Glu)	C	95.2%
Asn	0.98 Prop + 0.02 Ac (via Asp)	C	98.9%	Prop (via Asp)	P	94.8%
His	2 Ac (via Glut)	-	98.9%	1.61 Ac + 0.19 n-But (via Glu)	C	94.2%

Conv: conversion; P: produces NADH; C: consumes NADH.

A change in pH can modify the energetics of the different pathways and the AA uptake kinetics. For example, the energy associated with proton translocations (i.e. pmf) depends on pH and it is higher when the pH is more acidic (Eq. 2.22 and Figure 5.6). In consequence, pathways associated with a proton translocation are favoured when pH drops. This is the case of the glutamate conversion to n-butyrate, which has two proton translocations associated. At pH 7 it is completely degraded into acetate (no proton translocations associated) but at pH 5.3 part of it yields n-butyrate instead because now this pathway yields more ATP (Figure 5.5 and Table 5.5). On the contrary, when pH rises those pathways are disfavoured as its energy production decreases. In the case of the glutamate, changing the pH from 7 to 9 does not

have an effect in its degradation because the pathway without proton translocations was already the preferred at pH 7.

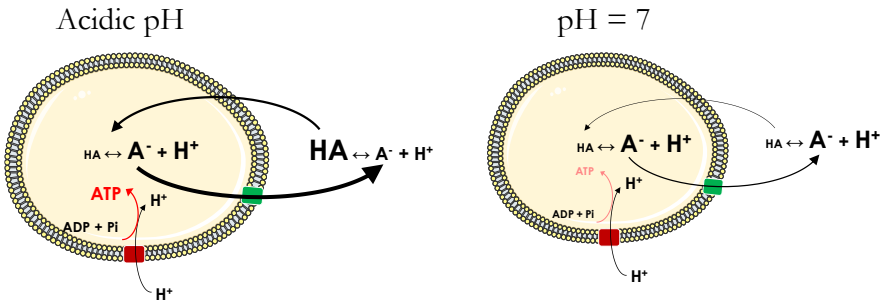

Figure 5.6. Effect of an acidic pH on transport rates and pmf.

Changing the extracellular pH value also modifies the degree of dissociation of VFA (from 99.4% at pH 7 to 77.4% at pH 5.3 for acetate). As the protonated form of acids can freely diffuse towards the cytoplasm of cells, a decrease in pH will increase the diffusion-related transport rate of VFA inwards cells. In consequence cells will be forced to increase the energy-dependent active transport rate to avoid VFA accumulation in the cytoplasm (Figure 5.6). The differences between the degrees of dissociation of the different VFA from pH 7 and a higher value is insignificant (from 99.4% at pH 7 to 100% at pH 9 for acetate). This implicates that changing the pH from 7 to an alkaline value has a very limited impact on transport energy expenditure and therefore also explains why there are no differences in the predicted yields between pH 7 ant higher pH values.

The relation between the energetics and the changes observed in the predicted yields can be understood analysing the model solution at steady state. At pH 7 glutamate was completely transformed into acetate (Table 5.4) in an NADH-neutral reaction as it was the option with the highest ATP production rate associated. However, at pH 5.3 its NADH-consuming degradation into n-butyrate (reaction 1 in Table 5.5) is related with a higher ATP production rate (0.439 against 0.267 $mol_{ATP}/L_X \cdot h$). Why is only 18% of Glu transformed to n-butyrate? Proline conversion also consumes NADH (reaction 3 in Table 5.5) and is in a competitive equilibrium with glutamate: the opportunity cost of degrading glutamate through reaction 2 instead of reaction 1 has the same value as the ATP generated per NADH consumed by proline (Table 5.5). As a result, proline is only degraded to a certain extent ($z<1$) because the global ATP production rate

would be less if all the NADH was invested in degrading proline and not into partially degrading glutamate into n-butyrate.

Table 5.5. Analysis of the steady state solution for pH 5.3.

#	Reaction	r_{NADH}	r_{ATP}	z	r_{ATP}/r_{NADH}	Opportunity cost[1]
1	Glut → n-but	-0.569	0.439	0.19	0.77	
2	Glut → 2 Ac	0.000	0.267	0.87	-	0.30
3	Pro → 0.5 Ac + 0.5 Pro + 0.5 Val	-1.236	0.377	0.05	0.30	
4	Asp → Prop	-0.385	0.474	1	1.23	
5	Asp → Ac	0.385	0.225	0	0.59	0.32

[1]Opportunity cost is defined as the difference in r_{ATP} divided by the difference in r_{NADH} between two pathways ($\Delta r_{ATP}/\Delta r_{NADH}$). Units: r_{NADH} ($mol_{NADH}/L_X \cdot h$); r_{ATP} ($mol_{ATP}/L_X \cdot h$); r_{ATP}/r_{NADH} (mol_{ATP}/mol_{NADH}); opportunity cost (mol_{ATP}/mol_{NADH}).

Aspartate degradation is as well different at pH 5.3 but its effects are less noticeable, because at pH 7 only 2% was degraded to yield acetate (Table 5.4) and not propionate, as both degrading options were in competitive equilibrium with proline. In this case, that equilibrium does not longer exist because the opportunity cost of not degrading aspartate into propionate has increased by 43% to 0.32 mol ATP/mol NADH and is now higher than the ATP to consumed-NADH ratio of proline, meaning that cells would lose ATP if they invested it in degrading proline instead of using it to produce propionate from proline (Table 5.5). This increase of opportunity cost is as well related with the energetics changes when pH is modified. In the propionate-producing pathway from aspartate there is one proton translocation associated and its contribution to the total ATP production rate of the pathway has increased by 41% due to the pH decrease, indicating that at pH 5.3 producing propionate is considerably more attractive than at pH 7.

From the analysis it is observed that AA interact with each other and that the relative presence of one influences the fate of the others, rejecting thus hypothesis that the degradation stoichiometries of the different AA are independent, as proposed in a previous work (Ramsay and Pullammanappallil, 2001). The most explicit interactions are those provoked by NADH competition as its consumption and production must be equal (no external electron acceptor). Some pathways are in equilibrium with others in terms of ATP produced per NADH. In some cases, there are even some AA that are converted through pathways that consume ATP but produce NADH, which is used in high ATP-yield pathways, leading thus to a

net ATP production. Consequently, a change in the relative concentration of some AA would affect the preferred conversion pathways of other AA as these interactions and energetic equilibriums would be modified. For example, if the abundance of AA that produce NADH (e.g. valine, isoleucine or leucine) was higher, it would affect the conversion pathway of AA that might consume NADH (e.g. Asp could yield more propionate or glutamate more butyrate). Varying the pH modifies the energetics of some AA pathways, mainly due to the change in the energy associated with proton translocation (i.e. pmf). If the pH decreases the pmf value increases, favouring thus those pathways associated with proton translocations (Eq. 2.22 and Figure 5.5). This is case of the glutamate conversion to n-butyrate, which has two proton translocations associated. At pH 7 it is completely degraded into acetate and when the pH is lower part of it yields n-butyrate instead because this pathway yields more ATP (Figure 5.5 and Table 5.4).

5.3.4. Sources of uncertainty

The formulation and use of this mathematical model require a number of hypotheses that are effectively sources of uncertainty, namely:

AA profile of the selected protein

As the exact AA composition depends on each specific protein, this uncertainty will be transferred to the VFA yields. To assess this uncertainty, the conversion of the 9 gelatine profiles of Figure 5.2 at pH 5.3 and 7 was simulated(Figure 5.7). The rest of the conditions are equal to experiment F in Table 5.2. Acetate yield shows an acceptable CV value at both pH values (8.5% and 14.4% at pH 5.3 and 7, respectively) when the minimum CV value for all the AA in Figure 5.2 is 20%. As many AAs have convergent pathways leading to the same products, the actual impact on certain VFA yields is decreased. Isocaproate, on the contrary, has a CV value of 60.7%, which is a value much higher than the CV of leucine at pH 7 (27%), the only AA that can yield it, because isocaproate is only yielded with certain AA profiles and only at pH 7. Standard deviations values are similar for all VFA independently of the pH even for those which yield is highly affected by pH (e.g. n-butyrate). It should be also noted that the n-butyrate yield is always higher at pH 5.3 than at pH 7 indicating that regardless of the selected AA profile, a decrease in pH always leads to an increase in n-butyrate yield. However, it should be noted that this uncertainty source is only of concern when the model wants to be compared with experimental data that do not include the AA

composition of the feeding. In a real design application, the AA concentrations in the substrates will be analysed to limit the uncertainty of this issue.

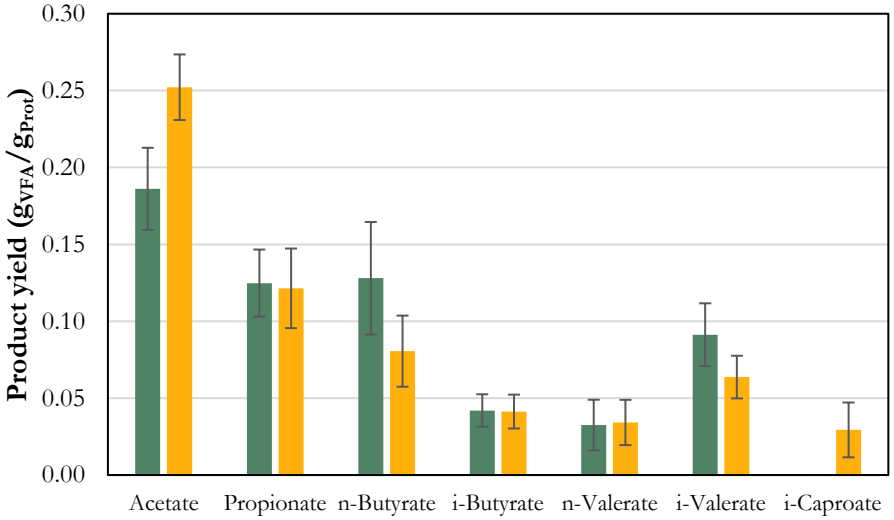

Figure 5.7. Predicted VFA yields variability with 9 different AA profiles of gelatine from NCBI database. ■ Simulations at pH 5.3 ■ Simulations at pH 7.

Metabolic network

Some reported degradation pathways were not included because we did not consider them likely to occur in a fermentative environment. For example, some of them were reported in essays where microorganisms were only provided with an individual AA as carbon source. In this case, and to keep redox homeostasis (i.e. equal NADH consumption and production rates), glycine, for instance, was degraded partially to CO_2 (Andreesen et al., 1989), as a way providing electron equivalents for its reduction to acetate. In this case, it was decided not to include this pathway as it had not been observed in other literature works degrading glycine with other AA and because in the fermentation of a whole protein, the individual AA do not have to be NADH neutral with themselves. Some interconversions between AA (e.g. glutamate to proline) were neither included because these reactions appear not to be significant for AA catabolism (Jones, 1985; Saum and Müller, 2007).

Uncertainty of the Gibbs formation energies (G^o_f)

Their values are used for calculating the Gibbs energy of all the possible reactions ($\Delta G'$) and to determine the thermodynamic feasibility (section 2.2.4.2). The values for G^o_f of some of the compounds, such as AA, are calculated using the Group Contribution Method because there is no avaliable experimental information available (Flamholz et al., 2012; Noor et al., 2013). In some cases, a degradation pathway is above the threshold of the minimum $\Delta G'$ value (-2 kJ/mol) by a narrow margin, and therefore it cannot be selected by the model. In other cases, a reaction is slowed down because its $\Delta G'$ value is very close to the minimum threshold. A variation of 1% in the value of G^o_f would make the pathway exergonic and therefore eligible or increase the degradation rate of the reaction, respectively.

Reducing equivalents consumption in anabolism: NADH production or consumption in anabolism is not assessed in the NADH balance restriction. Proteins might have a different degree reduction than that of biomass and therefore globally produce or consume NADH in the anabolic reactions. However, due to low biomass yield values (0.03-0.05 C-mol biomass/C-mol protein) achieved in the simulations, this assumption is not likely to affect the output of the model.

Simplifications of cell-level mechanisms

For example, intracellular pH and membrane potential are assumed to be constant. However, cells could in occasions modify these physiological characteristic to cope with different external conditions (Booth, 1985; Padan et al., 1981). The energetics of the degradation pathways would be in this case affected and could in turn modify the product spectrum. They were kept constant because any other model of intracellular pH would result in a more complex model structure while the predictive power would not be increased. Other example could be the fact that active transport of AA is considered to be energy neutral in our model. Differences in the energy cost among the different AA could modify their consumption pattern and affect the results of the model. However, in both examples the lack of information regarding both issues made us consider the simplistic option (constant intracellular pH and membrane potential and energy-free active AA transport) as the best solution.

5.3.5. Model validation with literature results

The model is validated using the Breure experiments. The experimental VFA yields are represented in the x-axis of Figure 5.8. Model results mimicking the operational conditions of the experiments from Table 5.2 are the y coordinate of Figure 5.8. To better compare these data with the model results, the yield is referred to grams of protein hydrolysed, since the hydrolysis step is omitted in this model, (i.e. the simulated substrate is directly a mixture of free AA) but is not complete in the literature experiments. The line in Figure 5.8 represents the equation y=x, a perfect match between the model and experimental data. Points that are to the right of this line are underestimated in the model and vice versa.

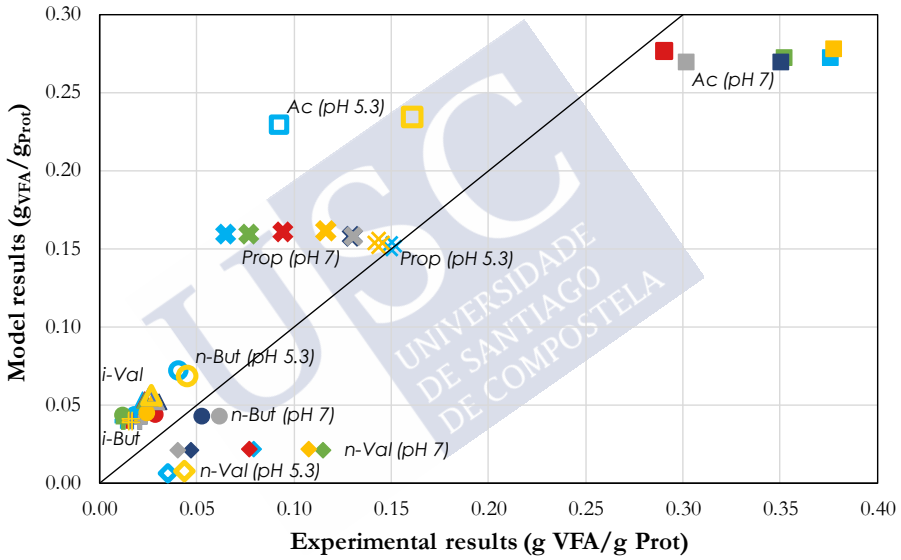

Figure 5.8. Comparison between model results and literature experimental results. Open signs are related with results at pH 5.3. Colours represent the different Breure experiments as follows: A (—) B (—) C (—) D (—) E (—) F (—).

5.3.5.1. Simulations at pH 7

Butyrate is equally distributed around the line, which shows a very good agreement between the model prediction and the experiments. Acetate, propionate and n-valerate are to one or the other side of the line, meaning that are over or underestimated in the model. However, the dispersion of the experimental points, in these two cases, is bigger than the average deviation from the model, suggesting that incomplete knowledge of the substrate composition

on AA and experimental deviations have a significant impact. For instance, the average deviation for propionate is 0.05 g/g_{Prot} and the experimental data range is 0.07 g/g_{Prot}. Moreover, in the model n-valerate is considered only to be yielded by the degradation of proline. This fact, together with the variability of the different gelatines (Section 5.3.2) might indicate that the content in proline in the gelatine used in the model could be lower than the gelatine used in the experiments. The CV value of n-val yields is 51% in Figure 5.7, indicating that the prediction of this VFA is very sensitive to the protein composition input. In sum, given the dispersion observed *inter* experiments, the model satisfactorily reproduces the experimental data with an average root-square-mean deviation (RMSD, Eq. 5.1) between the six model and experimental data yield sets of 0.98.

$$RMSD = \sqrt{\frac{1}{n} \cdot \sum_{i=1}^{n} \left(\frac{\hat{y}_i - y_i}{y_i} \right)^2} \quad (5.1)$$

where n is the number of data pairs, $\hat{y}_i$ is the model yield value and y_i is the experimental yield value. If there happens to be an experimental yield value of zero, the next value in increasing order would be chosen as minimum experimental value.

On average the model predicts a conversion of 92.4% (Cmol basis) of gelatine in the six experiments simulated. This value is higher than the average of the values reported for the same experiments in literature (84.3%), but it should be kept in mind that this model can only consider the non-complete consumption of an AA due to energetic or thermodynamic reasons without considering any specific limitation on substrate consumption (e.g. kinetic inhibition).

5.3.5.2. Simulations at pH 5.3

In the different Breure experiments only two of them (A and F) study the effect of pH and, in both cases, only acidic pH values were tested. In Figure 5.8 the results at a pH value of 5.3 are represented too. Feeding characteristics vary on the data set A, in which the dilution rate is now 0.14 h^{-1}. Protein conversion varies with pH both in model and experimental results. Its value decreased 8% on average in the model while it did so in a 22% in the experimental data. But as previously stated, model conversion values should only be regarded as maximum possible conversion values.

Isobutyrate, n-butyrate and isovalerate yields are overpredicted by the model, as in the results at pH 7 (for this comparison only the yellow and blue points should be

considered). For its part, n-valerate maintains its behaviour and is underpredicted by the model as at pH 7 but at pH 5.3 its experimental results have a smaller dispersion than at pH 7 and its predictions are slightly better. These four VFA have the same behaviour as at pH 7 (i.e. the same VFA are overpredicted and underpredicted), indicating that the discrepancies could be very well caused by differences between the AA profile of the gelatine modelled and the gelatine used in the experiments. Propionate shows an almost perfect fit but acetate, on the contrary, shows a worse fit. However, it is worth mentioning that there is a big difference between the two experimental data (acetate F yield is 73% higher than the yield in A), while the difference in the other VFA between data sets is much more limited.

The pH effect on the transport of the different AA should be also considered when simulating the metabolism of protein degraders. In literature, numerous works show how transport mechanisms are influenced by extracellular conditions (e.g. pH or sodium concentration) in different microorganisms (Broer and kramer, 1990; Driessen et al., 1989, 1987; Excherichia, 1972; Krämer et al., 1990; Poolman et al., 1987). Concerning the effect of a change in the extracellular pH, there is no agreement whether it increases or decreases the uptake rate of AA. For instance, Glu uptake rate is reported to be 3 times slower at pH 5 than at pH 7 in *C. glutamicum* (Krämer et al., 1990) and to be 15 times faster in *S. cremoris* (Poolman et al., 1987). As there is not a more consolidated mechanistic explanation on how pH affects AA uptake and why it seems to be dependent on the microorganisms (the modelled systems are dynamic mixed cultures), we decided to define uptake rates independent from the extracellular pH. This could be very well the reason why acetate yield decreases in a higher degree in the experimental data when the pH decreases, which is in accordance with the overpredicted acetate yields at pH 5.3 in Figure 5.8.

5.3.5.3. Changes in product yields with pH

The ability of the model to predict the changes in yields with the pH is of great interest too and it is an essential feature to be used as a product design tool. The effect of pH in the model and experimental results is compared in Figure 5.9. All VFA except propionate agree on their tendencies with the pH change, indicating that the model performs well in this role. Propionate, however, presents a different behaviour in the experimental data: while in one of the data sets (A) its yield increases notably when the pH drops from 7 to 5.3, in the other data set (F) its value does not increase as much (see the annexes, section 5.6.2, for the

experimental yields data). Acetate behaves equally in the model results and in the experiments: its yield decreases when pH decreases. However, it does it in a significantly higher degree in the experimental data, which is in accordance with the significantly overpredicted acetate yield values at pH 5.3 in Figure 5.8. This issue might be related, as previously discussed, with the effect of pH on AA transport.

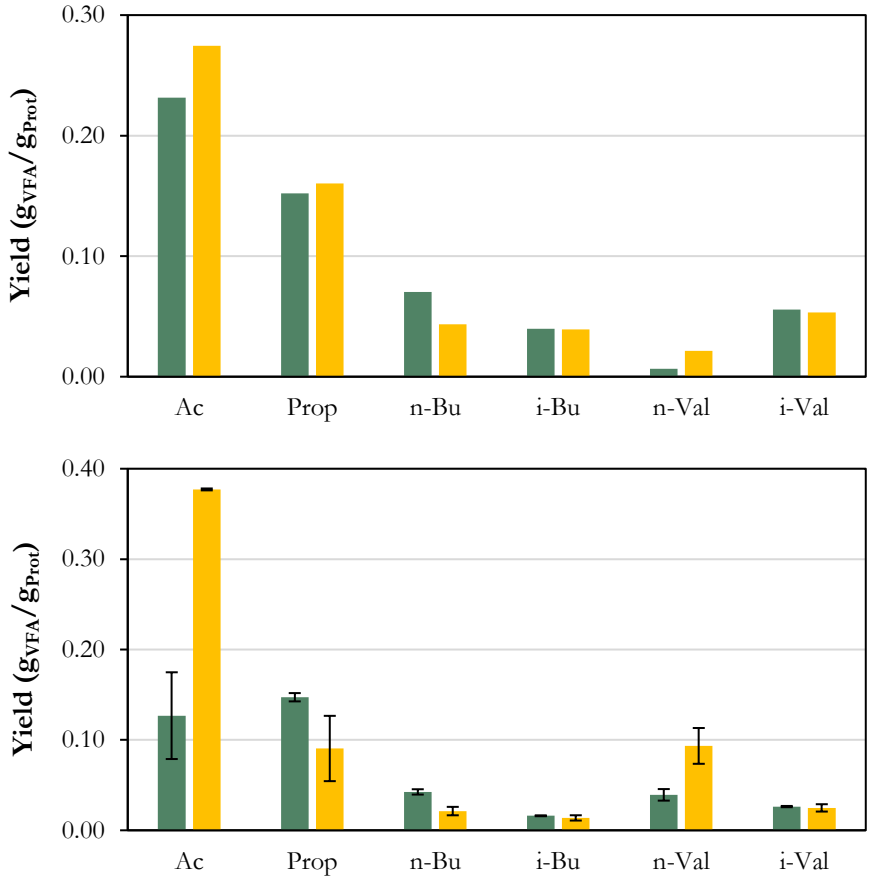

Figure 5.9. Changes in product yields with pH. Upper graph: Model results. Bottom graph: Average experimental results (A, F) (Breure et al., 1986a; Breure and van Andel, 1984). ■ pH 5.3 ■ pH 7.

5.3.6. Comparison with previous studies

In comparison with the only previous work regarding the prediction of VFA yields in protein MCF by Ramsay and Pullammanappallil (2001), the model selected different conversion pathways for 7 AA, representing 61.5% of all AA of the gelatine profile used in the simulations in molar basis (Table 5.6).

Table 5.6. Products of each AA and their role in the NADH balance. Shaded cells correspond to AA where the end-products estimated by this work follow different pathways in comparison with Ramsay and Pullammanappallil (2001).

	Ramsay	NADH balance	Model	NADH balance
Arginine	0.5 Ac + 0.5 Prop + 0.5 n-Val	C	Ac + 0.5 n-But (via Ala)	P
Alanine	Ac	P	0.5 n-But	-
Aspartate	Ac	P	0.98 Prop + 0.02 Ac	C
Lysine	Ac + But	-	Ac + But	-
Glutamate	Ac + 0.5 n-But	C	2 Ac	-
Serine	Ac	-	Ac	-
Threonine	Ac + 0.5 n-But	C	Prop	-
Cysteine	Ac	-	Ac	-
Glycine	Ac	C	-	-
Proline	0.5 Ac + 0.5 Prop + 0.5 n-Val	C	0.5 Ac + 0.5 Prop + 0.5 n-Val	C
Valine	i-But	P	i-But	P
Isoleucine	i-Val	P	i-Val	P
Leucine	i-Val	P	i-Val	P
Methionine	Prop	-	Prop	-
Glutamine	N/C	-	2 Ac (via Glut)	-
Asparagine	N/C	-	Prop (via Asp)	C
Histidine	Ac + 0.5 n-But	-	2 Ac (via Glut)	-

C: Consumes NADH. P: Produces NADH. N/C: not considered

The objective of that work was not to explain mechanistically protein fermentation as it was focused on the anaerobic digestion to methane of proteins. The conversion stoichiometry of the different AA was selected based on literature information and it was considered to be fixed. They did not consider the NADH conservation as a constrain and the redox balance was closed by the production of H_2 from NADH and vice versa. However, it is accepted that H_2 cannot be yielded from NADH as it is clearly an endergonic reaction (see section

2.2.3.1). The model developed in this work, on the contrary, does offer insight on the mechanisms of VFA production from AA and is able to predict how the conversion stoichiometry of the different AA changes with pH. These characteristics make it a more attractive as a design tool than the previous works available.

5.4. USE AND IMPLICATIONS FOR PROCESS DESIGN

The mathematical model developed provides an excellent means to carry out an early stage process design. It allows us to define design parameters, such as pH, that would steer the production towards those desired products, as already shown in previous sections. Furthermore, different wastes have different proteins with diverse AA compositions meaning that they would produce different outcomes. This variability source can also be exploited when designing the process. For example, if VFA production from casein is modelled instead from gelatine, there are considerable changes in the product spectrum at a given pH and in the effect of pH on the VFA yields (Figure 5.10).

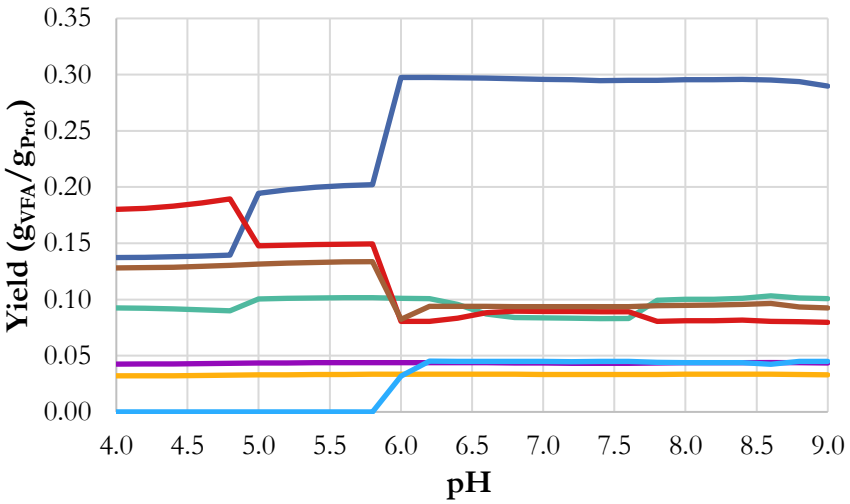

Figure 5.10. Model results for casein degradation in an CSTR at different pH values. Product yields: ■ acetate ■ propionate ■ n-butyrate ■ i-butyrate ■ n-valerate ■ i-valerate ■ i-caproate.

At pH 7 casein shows a different product spectrum than gelatine. For example, propionate yield is 60% lower and now it is the fourth most abundant product when in gelatine degradation it is the second one (Figure 5.3). Isocaproate, which

is not a product of gelatine degradation, has in casein degradation a share of almost 10% in the product spectrum. A change in pH value has a different effect in the degradation of casein than in gelatine degradation. A change in pH from 7 to 4.5 enhances significantly isovalerate yield (+56%), becoming the third most abundant product. Isobutyrate and n-valerate remained constant in gelatine degradation regardless of the pH value (Figure 5.3).

This opens the possibility of choosing beforehand the most interesting waste and operational conditions depending on the targeted VFA. For instance, if we were interested in a process with a high selectivity for propionate, degrading gelatine at neutral pH would be the best choice. But if on the contrary a high butyrate yield is preferred, choosing a casein-rich waste at low pH would be a much better choice. If the number of proteins present in the different available wastes is high enough, we could go a step forward and tailor a blend of wastes that produced a particular AA profile that yielded a specific VFA spectrum when degraded.

The model potential as a process design tool includes too the possibility of modifying synthetically the feeding. An effluent rich in a specific AA could be added to the feeding to boost the process selectivity for a particular VFA. For example, if threonine was supplemented to the feeding it would be expected that the propionate yield increased as threonine only produces propionate. As the production of propionate from threonine is NADH-neutral (it does not produce or consume NADH), it is not expected to interfere with the degradation reactions of others AA. A simulation with doubled threonine concentration at pH 7 was run and the resulting yields are shown in Figure 5.11. In this case the inlet substrate concentration is 7.7 g/L due to the increased threonine content. Propionate yield increased by 39% with respect to the standard gelatine degradation due to the increased content of threonine, which did not change its preferential degradation pathway (i.e. it is still fully degraded into propionate). The other VFA yields were not affected, as predicted. Aspartate and asparagine are other AA yielding propionate (Figure 5.5) but its degradation pathways are not NADH neutral. It is probable that their addition to gelatine would provoke changes in other VFA yields (e.g. less proline consumption, as it also consumes NADH, with a concomitant n-valerate yield decrease), which makes the addition of threonine a more attractive option. This strategy could be successfully used if large amounts of isolated AA from waste-derived proteins are available, as forecasted (Tuck et al., 2012).

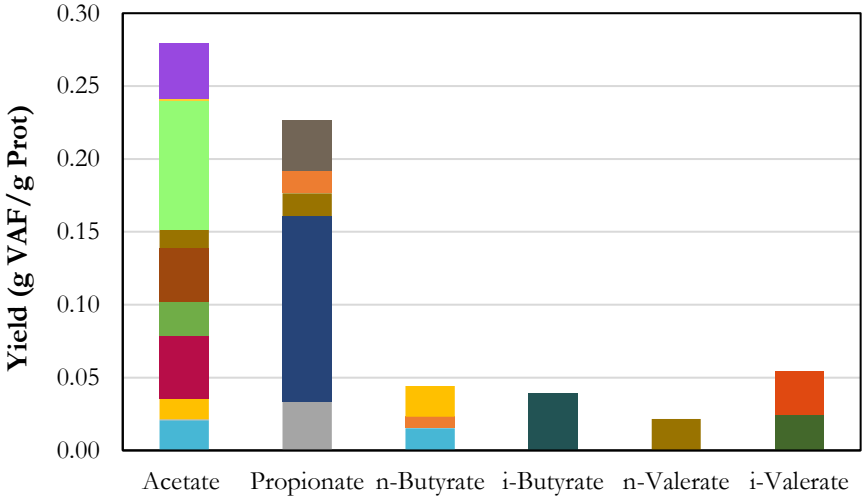

Figure 5.11. Model results for gelatine degradation in an CSTR at pH 7 with supplemented Thr. Product yields. Arg Ala Asp Lys Glu Ser Thr Cys Gly Pro Val Ile Leu Met Gln Asn His

Co-fermenting protein-rich wastes with others that have a high content in carbohydrates could be very well another strategy to allow for flexibility when seeking a particular product spectrum. Carbohydrates degradation is as well highly constrained by NADH conservation and it is expected that proteins and carbohydrates product yields are modified when degraded together, as already shown experimentally (Breure et al., 1986b).

5.5. Conclusions

A mechanistic metabolic model for the degradation of proteins by mixed cultures was developed and reproduces satisfactorily available literature experimental results at pH 7 and 5.3. Moreover, it can predict with a good level of accuracy the effect of lowering the pH value and, for the first time, offers a mechanistic explanation of the changes observed. In this study, it was shown that protein degradation does not have a fixed stoichiometry. Changes in some operational conditions, such as pH, modify the preferred degradation pathways of different AA and consequently affect the product spectrum predicted by the model. It is proposed that amino acids might interact with each other and influence the degradation of others and, as a result, some AA might have different conversion stoichiometries depending on the AA profile of the protein.

Degradation reactions of different AA that both produce or consume NADH are an explicit example of this competition. However, the changes in product spectrum with the operational conditions are not as extreme as for glucose degradation, in which some end product might disappear from the product spectrum with a pH change of one unit (Temudo et al., 2007).

Model validation was partially hindered by the variability of the experimental results and by the lack of knowledge regarding the AA composition of the degraded gelatine. Experiments expressly conceived to validate the mechanisms proposed in the model (e.g. knowing the protein AA profile and the individual AA concentrations in the outlet or measuring gaseous species concentrations) are needed to fully validate the model. For instance, some of the assumptions made during the construction of the metabolic network could be proven (e.g. proton translocation in glutaconyl-CoA decarboxylation) or information regarding the impact of pH on AA uptake could be gathered for incorporation into the model. The potential of the model for being used as a design tool was explored with several examples on how to drive the process towards desired compounds of interests.

5.6. ANNEXES

5.6.1. Amino Acid profile of the simulated gelatine

Simulations with the 9 different gelatine profiles of Figure 5.2 were done at pH 7, and at the conditions of experiments A to F in Table 5.2, and compared with the experimental values. The root-square mean deviation (RMSD, Eq. A5.1) was used as a parameter to select the profile proving a best fit between the simulations and the experimental data.

$$RMSD = \sqrt{\frac{1}{n} \cdot \sum_{i=1}^{n} \left(\frac{\hat{y}_i - y_i}{y_i} \right)^2} \qquad \text{(A5.1)}$$

where n is the number of data pairs, $\hat{y}_i$ is the model yield value and y_i is the experimental yield value. If there happens to be an experimental yield value of zero, the next value in increasing order would be chosen as minimum experimental value.

In Table A5.1 the RMSD values between the simulations with the different profiles and the experimental data are presented. Profile 5 provides the lowest average RMSD value for all the experimental data sets among the 9 different profiles.

Table A5.1. RMSD values between the different Breure experiments and the different AA profiles. The nomenclature of Table 5.2 is followed for naming the experiments.

	Experiment						
	A	**B**	**C**	**D**	**E**	**F**	**Average**
Profile 1	1.89	1.38	2.50	0.72	0.73	1.34	1.43
Profile 2	1.93	1.39	2.52	0.71	0.70	1.35	1.43
Profile 3	1.69	1.21	2.44	0.58	0.57	1.24	1.29
Profile 4	1.92	1.40	2.52	0.72	0.71	1.36	1.44
Profile 5	1.42	0.99	1.53	0.53	0.53	0.87	0.98
Profile 6	1.64	1.49	2.27	0.83	0.81	1.37	1.40
Profile 7	2.42	1.93	3.94	1.01	1.00	2.04	2.05
Profile 8	1.67	1.42	2.71	0.70	0.67	1.43	1.43
Profile 9	1.69	1.10	2.55	0.45	0.41	1.22	1.24

The comparison between the simulated yield values with AA profile 5 and the different experiment yields is shown in Figure A5.1.

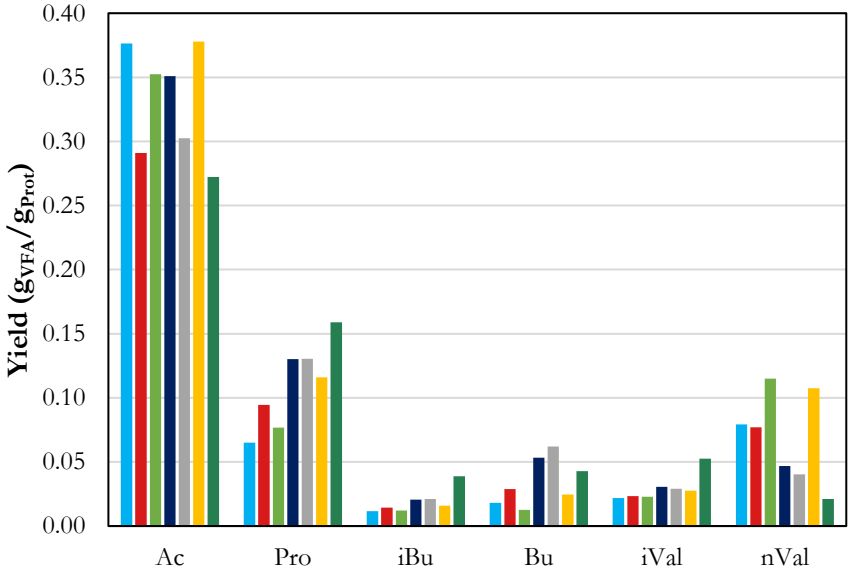

Figure A5.1. Breure experimental results (Table 5.2 in the main text) at pH 7 and model results using Profile 5 gelatine (average value for the different experimental conditions of A-F). A B C D E F Model results.

Profile 5 composition in AA, used in all the simulations, is shown in Table A5.2. The molecular weight of this profile is 29.0 g/C-mol.

Table A5.2. AA spectrum of gelatine profile 5 using in the simulations (molar basis) and molecular weight of a C-mol of that protein.

Amino acid	Molar fraction	Amino acid	Molar fraction
Arg	4.7%	Val	6.0%
Ala	2.7%	Ile	3.3%
Asp	6.3%	Leu	4.0%
Lys	3.3%	Met	3.0%
Glu	5.0%	Gln	9.6%
Ser	5.3%	Asn	6.3%
Thr	11.0%	His	4.3%
Cys	8.0%		
Gly	11.6%		
Pro	5.6%		

5.6.2. Experimental yields from literature

The experimental data used to validate the model is shown in Table A5.3. Values are referred to grams of protein hydrolysed to better compare them with the model results, as the hydrolysis step is omitted in the model.

Table A5.3. VFA yields and operational conditions of the experiments used for the model validation. The nomenclature of Table 5.2 is followed for naming the experiments.

		D	**[Protein]**	**VFA Yields (g_{VFA}/g_{Prot})**					
Exp.	pH	(h^{-1})	(g/L)	C2	C3	i-C4	C4	i-C5	C5
A	5.3	0.14	7.5	0.093	0.150	0.016	0.040	0.026	0.035
	7	0.23	7.5	0.376	0.065	0.018	0.012	0.079	0.022
B	7	0.10	5	0.291	0.095	0.029	0.014	0.077	0.023
C	7	0.15	5	0.352	0.077	0.013	0.012	0.115	0.023
D	7	0.20	5	0.351	0.130	0.053	0.021	0.047	0.031
E	7	0.20	5	0.302	0.131	0.062	0.021	0.040	0.029
F	5.3	0.12	7	0.161	0.144	0.016	0.045	0.027	0.044
	7	0.12	7	0.378	0.116	0.025	0.016	0.107	0.028

CHAPTER 6

Bioenergetic modelling for stoichiometry prediction of protein and carbohydrate cofermentation

Summary

Real wastes with potential of being valorised in the carboxylate platform often consist of mixtures of carbohydrates and proteins as, for instance, effluents from the dairy or canning industry. However, our knowledge regarding the influence of substrate composition in the product selectivity of mixed-culture co-fermentations is still limited. Currently, the stoichiometry predictive tools do not consider the characteristic features of co-fermentation processes, which limits the design of processes producing VFA from interesting industrial organic wastes. In this chapter a mathematical model was developed for the prediction of the stoichiometry of VFA production from the co-fermentation of proteins and glucose. The effect of different glucose to protein ratio and reactor pH values on the process stoichiometry was studied with the model and both design parameters showed a solid potential to direct the process towards the desired VFAs. The model reproduces satisfactorily experimental results and is also able of giving mechanistic insight into the interactions between carbohydrates and proteins that explain the observed changes in the product spectrum. The bioprocess design capabilities of the model are shown in a series of examples within the carboxylate platform biorefinery.

6.1. INTRODUCTION

Real organic wastes with potential to be used as substrates in MCF are usually composed of more than one component (carbohydrates and proteins mainly) as for example dairy or certain canning industry wastewaters. In Chapter 5 it was shown that the different amino acids (AA) of a protein compete for shared resources (i.e. reductive power) and that their individual conversion stoichiometries to VFA depend on the relative concentrations among AA and on environmental conditions (e.g. pH). It is then hypothesised that the addition of a different substrate (glucose) would change these VFA conversion stoichiometries since it provides an extra source of reductive power. For example, acetate is the product associated with the highest ATP yield on glucose fermentation, but not all glucose can be converted to acetate since the electron balance would not be closed (acetate pathway has a net NADH production) and as a consequence other VFA are always produced together with acetate (Temudo et al., 2007). But if glucose was fermented together with proteins, glucose fermentation could be shifted largely to acetate as the NADH produced in its fermentation could be consumed in some of the AA fermentation pathways. In this way, the product spectra of both glucose and protein fermentations would likely change in response to the different ways of allocating the reductive power in their catabolism. As a result, the stoichiometry of cofermentation processes is likely to differ from the addition of the monofermentation stoichiometries of glucose and protein.

Cofermentation processes feature then an extra degree of freedom that can be exploited to drive the process towards the desired products. Carbohydrates and proteins cofermentation has already been studied from an experimental point of view but only in a descriptive manner and without seeking for a mechanistic explanation of the changes observed in product spectrum (Alibardi and Cossu, 2016; Arslan et al., 2016; Breure et al., 1986b, 1986a). Previous modelling works in literature focused on the production of methane and dismissed interactions between proteins and carbohydrates in their fermentation to VFA (Angelidaki et al., 1999; Batstone et al., 2002b).

The objective of this chapter is to develop a metabolic model for the targeted production of VFA by mixed culture cofermentation of carbohydrates and proteins. The aim of the model is twofold: i) to predict the stoichiometry of the process at different operational conditions, with a special focus on pH and the proportion between carbohydrates and proteins in the feeding, and ii) to give

insight on the interaction mechanisms between substrates in cofermentation scenarios and their effect on the stoichiometry of the process.

6.2. MODEL DESCRIPTION

The model is based on the dynamic mass balances of the different compounds (states) in a CSTR and it was developed extending the framework described in Chapter 5 for protein MCF. It encompasses 68 states: 24 intracellular compounds, 40 extracellular compounds in the bulk reactor, 4 gaseous compounds and biomass. For simplicity, protein hydrolysis is omitted in the model and is directly considered a mixture of AA, as the limiting step in protein fermentation is AA fermentation (Duong et al., 2019). Intracellular substrate concentrations are assumed constant at a value of 0.1 mM. There are 99 possible reactions, resulting in a 68x99 metabolic network matrix. Amongst all the reaction rates 22 of them are independent, i.e. depending solely on model states, that represent compound concentrations. It is assumed that the substrate for the system consists of glucose as carbohydrate and gelatine as protein, although simulating other protein sources is straightforward if their AA compositions are known. The AA profile selected for the gelatine is the same as in the protein monofermentation model and can be found in section 5.6.1.

6.2.1. Microbial community structure in cofermentation scenarios

The microbial competition a two-substrate reactor can have two outcomes: either a group of generalists consuming both substrates or a group of two specialists dominate the community. The structure of the microbial community has profound implications in the modelling of the consumption of two substrates (e.g. whether carbohydrates and proteins interact and share metabolites in their conversion to VFA) and hence is likely to have a strong impact on the model solution.

Specialist microorganisms can only consume one of the substrates available but have the advantage that they often their uptake rate is higher than that of generalist microorganisms. However, following the chemostat theory, in a CSTR reactor, the microbial competition is ruled largely by the affinity constant and not by the uptake rate capacity. In this way, assuming that the generalist and specialists populations have similar affinities for the substrates, a generalist population may outcompete the two-specialist community as it can thrive at a lower residual concentration of the two substrates due to obtaining energy from both substrates (Kuenen, 1983; Rombouts et al., 2019b).

The limited experimental evidence also suggests that a generalist population is likely to dominate the community in a substrate limited CSTR. Kuenen (1983) showed in CSTR experiments with mixtures of two pure substrates that generalists can compete successfully with specialist microorganisms for growth and that they consume most of the substrate. Rombouts et al. (2019b) studied the structure of the microbial community of the fermentation of mixtures of glucose and xylose in a CSTR and a sequential batch reactor (SBR). They found that a generalist microorganism dominated the enrichment in the CSTR and even in the SBR, against their initial hypothesis. Therefore, it is assumed that for the conditions for which the model is intended (substrate limited CSTRs), the most likely microbial community structure is a group of generalists due to their advantage in substrate-limited environments. To investigate to which extent this assumption holds true, a simplistic model to study microbial competition was built.

In this model the competition between a generalist microorganism or two specialist microorganisms is modelled in a CSTR. The generalist microorganism can consume all the substrates: a carbohydrate (CH) and protein (PR), in this case. Each of the specialist microorganisms can only consume one substrate but faster than the generalist. In this regard, the model assumes that all microorganisms can consume glucose (the CH used in this model) since the ability to metabolise it is ubiquitous in nature. In this way, the PR specialist microorganism can also consume CH and is, in consequence, a generalist and no longer a specialist. Therefore, this model simulates the competition between a) a generalist consuming both substrates and b) a generalist consuming both substrates co-existing with a CH specialist.

The kinetics of the two groups of microorganisms are modelled with Monod equations. In the case of the generalist, its growth rate depends on the CH and PR concentration, as it consumes both (Eq. 6.1). The CH specialist growth rate only depends on CH concentration (Eq. 6.2).

$$\mu_{Generalist} = \mu_{Gen,CH}^{max} \cdot \frac{[CH]}{[CH] + K_{S,Gen,CH}} + \\ + \mu_{Gen,Prot}^{max} \cdot \frac{[PR]}{[PR] + K_{S,Gen,PR}} \tag{6.1}$$

$$\mu_{Specialist} = \mu_{Spe,CH}^{max} \cdot \frac{[CH]}{[CH] + K_{S,Spe,CH}} \tag{6.2}$$

The parameters of the Monod equations are set differently for the two microorganisms and depending as well on the substrates (Table 6.1). The generalist maximum growth rate on CH is set twice as high as the maximum growth rate on PR. The CH specialist maximum growth rate is considered always higher than that of the generalist, as specialist are normally faster in consuming the substrate than generalist microorganisms. The affinity constant for PR is set higher than for CH, which has the same value for both microorganisms. The biomass yield of PR is defined to be 0.15 g_{BM}/g_{PR} and CH biomass yield is set to 0.2 g_{BM}/g_{CH}.

Table 6.1. Parameter values for the competition model.

Parameter	Value
$\mu^{max}_{Gen,CH}$ (h^{-1})	1
$\mu^{max}_{Gen,PR}$ (h^{-1})	0.5
$\mu^{max}_{Spe,CH}$ (h^{-1})	1-2
$K_{S,Gen,CH}$ (g_{CH}/L)	0.1
$K_{S,Gen,PR}$ (g_{PR}/L)	0.2
$K_{S,Spe,CH}$ (g_{CH}/L)	0.1
$Y_{Gen,CH}$ ($g_{BM,Gen}/g_{CH}$)	0.2
$Y_{Gen,PR}$ ($g_{BM,Gen}/g_{PR}$)	0.15
$Y_{Spe,CH}$ ($g_{BM,Spe}/g_{CH}$)	0.2

To determine under which conditions each outcome of the competition is likely to dominate, a series of simulations were done varying two parameters: i) the ratio between the CH specialist and the generalist maximum growth rate on CH (denoted from now on α) and ii) the ratio between PR and CH concentration in the feeding. The parameter α was varied between 1 and 2 (at 0.05 intervals) and PR concentration in the feeding was varied between 0.5 and 10 g_{PR}/L (at intervals of 0.1 g_{PR}/L), which covers a range of ratios between 0.1 and 2. The rest of the simulation parameters were kept constant and are defined in Table 6.2.

Table 6.2. Simulation parameters

Parameter	Value
D (h^{-1})	0.2
α	1-2
Protein concentration (g_{PR}/L)	0.5-10
Carbohydrate concentration (g_{CH}/L)	5

The model results show that the CH specialist is washed in the majority of the conditions simulations (Figure 6.1 left). Only at low PR to CH concentration

ratios and very high α values the CH specialist is able to thrive. On the contrary, the generalist concentration is significantly higher in the great majority of the conditions simulated, as it can grow on the two substrates (Figure 6.1 right). Only at very low PR to CH concentration ratio values is its concentration lower than the specialist concentration, since in these conditions the PR contribution to the generalist growth is very low and most part of the CH are consumed by the specialist, which can benefit here of its higher maximum uptake rate (Figure 6.2 left).

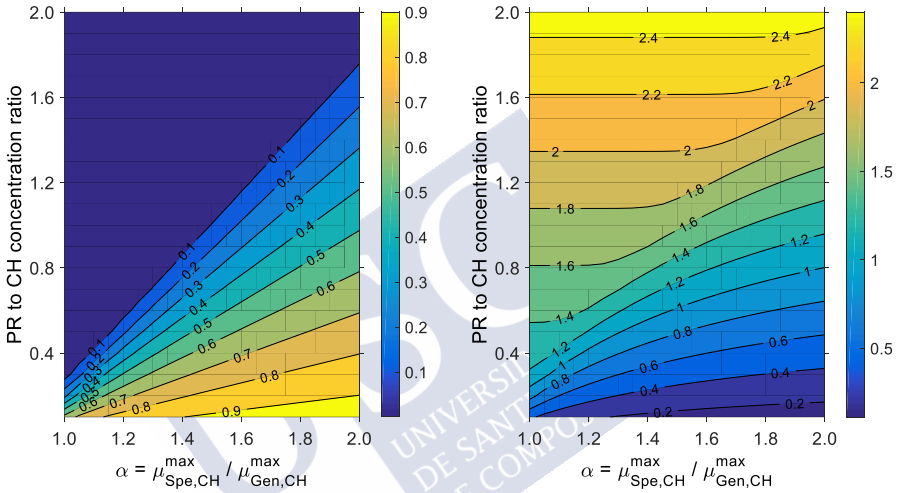

Figure 6.1. CH specialist (left) and generalist (right) biomass concentration (g/L).

As the model is intended to simulate the conversion to VFA of protein-rich effluents, the microbial community is likely to be more accurately described as dominated by generalists. Moreover, α values over 1.5 (meaning CH specialist maximum growth rates 50% higher or more than the generalist maximum growth rate) are needed in order to notice an important presence of the CH specialists, even at low PR to CH ratios. It is believed that in a constantly evolving microbial community the difference in kinetic properties will not be as pronounced. In such conditions, most part of the CH are consumed by the generalists (Figure 6.2 right) and it is likely that specialists are completely absent in the microbial community.

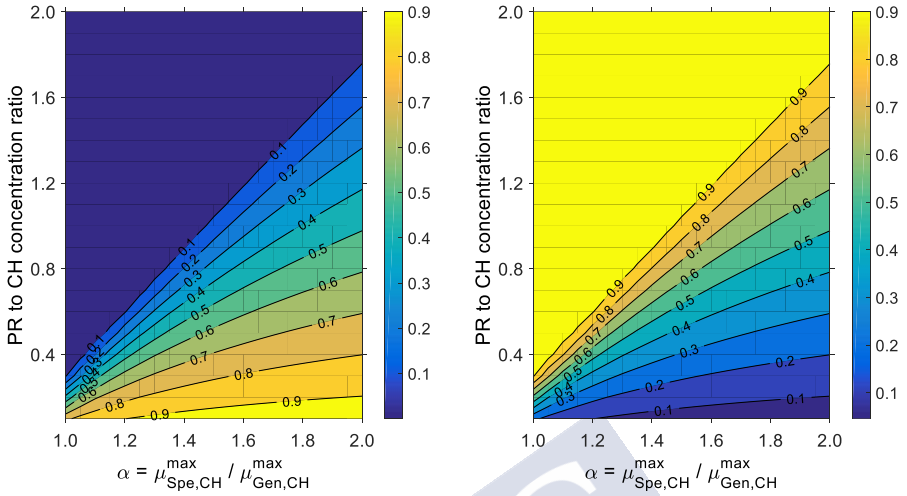

Figure 6.2. Mass fraction of CH consumed by the CH specialist (left) and of CH consumed by the generalist (right).

In conclusion, and taking into account the considerations regarding the chemostat theory, the experimental evidences and the results of the simplistic model; the microbial community is modelled in this work as composed by a generalist group that is able of consuming both glucose and protein simultaneously.

6.2.2. Protein is modelled to be consumed slower

Experimental evidence shows that protein consumption is generally slower than glucose consumption (Batstone et al., 2002a; Breure et al., 1986b, 1986a), which could influence the process stoichiometry as protein and glucose catabolism is modelled to share metabolites (e.g. NADH). To define the ratio between the protein and glucose consumption rate, it was decided to use the Gibbs free energy (ΔG) of the conversion reactions as an indirect indicator, since other information was not available. In environments with reactions close to the thermodynamic equilibrium the rate of a reaction is positively correlated with the ΔG of the reaction (LaRowe et al., 2012). The ratio between the maximum consumption rate of glucose and of each AA was set equal to the ratio between the average ΔG at standard biological conditions (pH 7 and compound concentrations of 1 mM) of all the featured glucose and all the AA conversion pathways, normalised by the number of steps on each pathway (Eq. 6.3).

$$\frac{q_{Glucse}^{max}}{q_{AA}^{max}} = \frac{\frac{1}{n_{Glucose}} \cdot \sum_i \frac{\Delta G'^m_{glucose,i}}{k_{glucose,i}}}{\frac{1}{n_{AA}} \cdot \sum_{j,k} \frac{\Delta G'^m_{AA\ j,k}}{k_{AA\ j,k}}} = 1.5 \quad (6.3)$$

where q^{max} is the maximum consumption rate, $\Delta G'^m$ is the reaction Gibbs free energy at standard biological conditions, k is the number of metabolic steps of pathway i and n is the number of pathways. The subscript i, j and k denote the different glucose conversion pathways, the different AA and their different conversion pathways, respectively.

Glucose pathways have on average almost a 50% higher absolute value of ΔG than those of AA degradation. Therefore, glucose maximum consumption rate coefficient in the Monod equation was set 50% higher than that of the AA. For glucose the maximum uptake rate was set to 0.75 mol L_x^{-1} h^{-1} and to 0.50 mol L_x^{-1} h^{-1} for all the AA, which are close to experimentally observed values (Fernández et al., 2011; Pavlostathis and Giraldo-Gomez, 1991; Ramsay, 1997). The affinity constant is set equal for all substrates at 1 mM.

6.2.3. Metabolic network

Glucose consumption pathways cover the conversion to the most typical end products observed experimentally: acetate, propionate, butyrate, ethanol, succinate and lactate. There are 17 AA considered in the metabolic network: alanine (Ala), arginine (Arg), asparagine (Asn), aspartate (Asp), cysteine (Cys), glutamate (Glu), glutamine (Gln), glycine (Gly), histidine (His), isoleucine (Ile), leucine (Leu), lysine (Lys), methionine (Met), proline (Pro), serine (Ser), threonine (Thr) and valine (Val). The end products in this network are acetate, propionate, isobutyrate, n-butyrate, isovalerate, n-valerate, isocaproate and ethanol. Among all the possible conversion pathways for each of the different AA, those most often reported in literature for anaerobic AA degraders and most likely to occur in fermentative environments were included in the metabolic network. The glucose and AA metabolic network construction as well as the pathway selection criteria are discussed thoroughly in Chapter 2.

6.3. Results and Discussion

Firstly, how the model simulates the dependency of the different VFA yields on substrate composition and reactor pH is presented. Then, these results are analysed to obtain a deeper mechanistic insight on substrate interactions in cofermentation

processes. Finally, the model is tested against the few currently available experimental data and the sources of uncertainty of the model are identified.

6.3.1. Influence of pH and substrate composition on product spectrum

The proportion between the different substrates (glucose and gelatine in this case) is a characteristic design parameter of cofermentation processes and it is expected to affect importantly the global stoichiometry of the system, as previously reasoned. Additionally, pH is one of the design parameters with the highest impact on product spectrum (as shown in Chapter 3 and 5) and it is as well one of the easiest to manipulate in a reactor. Thus, a CSTR was simulated with a dilution rate of 0.1 h^{-1} for a range of pH values (from 4 to 8.5 with 0.25 increments) and for a range of concentrations of a protein (gelatine) and a carbohydrate (glucose) in the feeding from 0 to 10 g/L (with 0.5 g/l increments, keeping a total substrate concentration of 10 g/L).

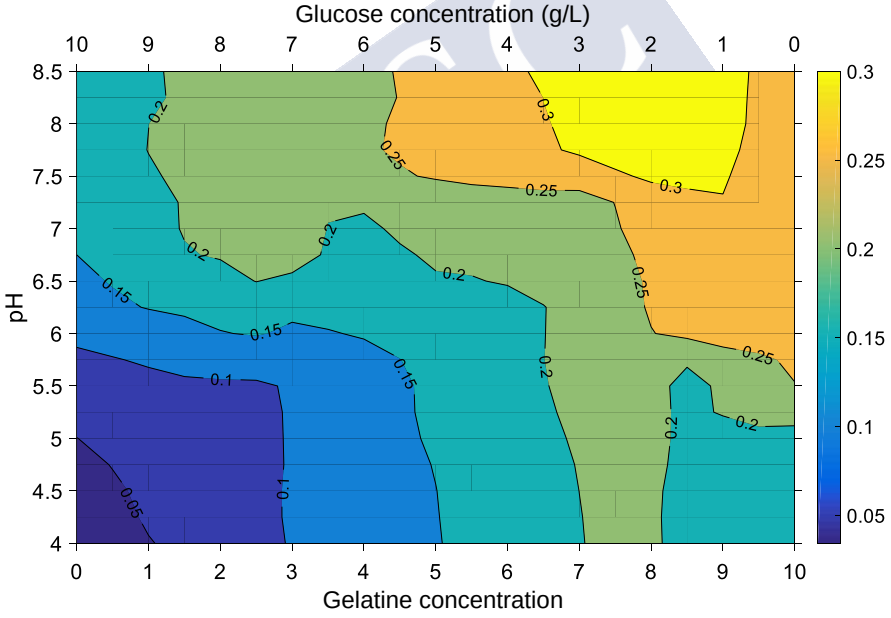

Figure 6.3. Predicted acetate yield ($g_{VFA}/g_{Substrate}$) at different pH values (vertical axis) and at different glucose and gelatine concentrations in the feeding (horizontal axis).

Simulation results indeed show that both design parameters affect the yields of the different VFA (Figure 6.3, Figure 6.4 and Figure 6.5). For example, fermentations at basic pH values and high protein to glucose ratio and are

interesting when acetate is the targeted VFA (Figure 6.3). On the contrary, acidic pH and at low protein to glucose protein ratio clearly favour n-butyrate yield, which attains a maximum value of 0.4 g n-butyrate/g substrate (Figure 6.4). Propionate has a different behaviour and its yield is maximised at neutral pH values at low protein to glucose ratios or at high protein to glucose ratios, regardless of the pH value (Figure 6.5). Other VFA are affected differently by both parameters. For example, n-valerate is positively correlated with protein concentration almost linearly and the pH has a very limited effect in its value (Figure A6.1).

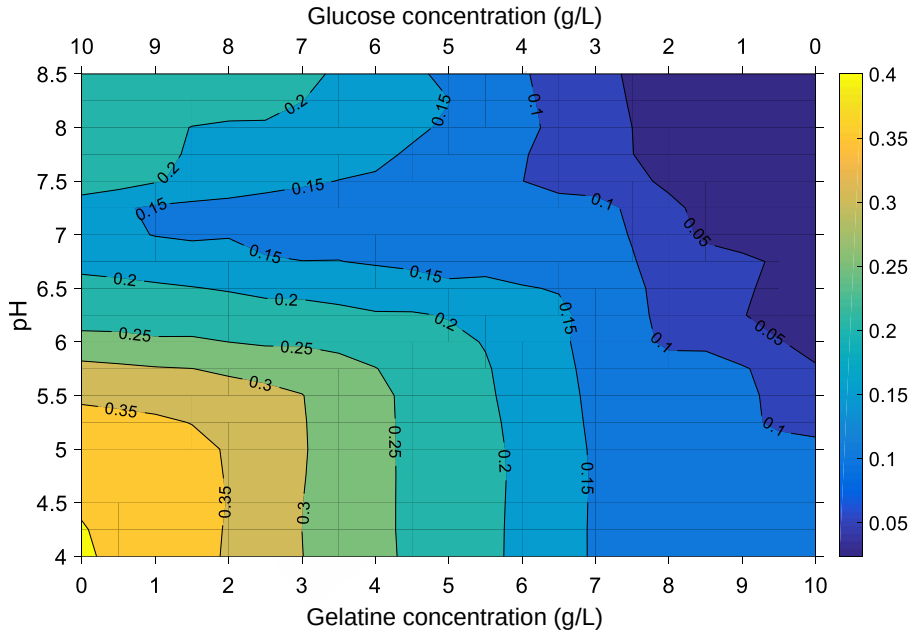

Figure 6.4. Predicted *n*-butyrate yield ($g_{VFA}/g_{Substrate}$) at different pH values (vertical axis) and at different glucose and gelatine concentrations in the feeding (horizontal axis).

Substrate conversion is also affected and varies between 99.8% and 95.3% for glucose and between 99.6% and 79.4% for protein in mass basis (Figure A6.2). Glucose conversion is mainly only affected by pH and it is maximum at neutral and high pH values since the low biomass concentration at acidic pH values limits the conversion. Overall glucose conversion is predicted to be almost complete regardless of the operational conditions, showing that glucose is a more energetic substrate than protein (its conversion provides more energy than protein and therefore it always consumed with priority). Protein conversion, on the contrary,

is both affected by pH and protein to glucose ratio (Figure A6.2). Its value is lower at medium protein to glucose ratio, as at these conditions some AA are not consumed catabolically due to energetic reasons, as discussed in Chapter 5. Finally, acidic pH values affect negatively protein conversion, for the same reason as for glucose. Overall, these values should be interpreted as the maximum values from a thermodynamic and bioenergetic point of view, as the model does not consider any kinetic inhibition affecting substrate conversion.

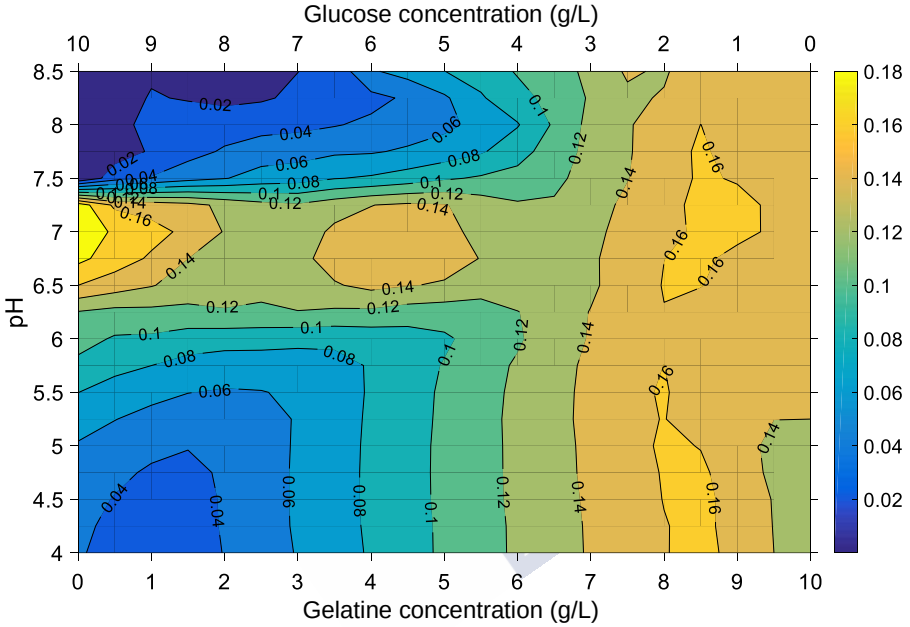

Figure 6.5. Predicted propionate yield ($g_{VFA}/g_{Substrate}$) at different pH values (vertical axis) and at different glucose and gelatine concentrations in the feeding (horizontal axis).

6.3.2. Why does substrate composition influence VFA selectivity?

Model simulations provide the insight needed to explain the different trends on VFA yield observed in the simulations as a result of changing glucose and protein proportions in the feeding. Protein and glucose concentrations will be referred in terms of mass percentage with respect to the total amount of protein and glucose in the feeding.

The yield of n-butyrate is shown to be clearly affected by the relative concentration of glucose and protein at a constant pH value (Figure 6.4). For example, at pH 6.5 its yield varies from 0.26 $g/g_{Substrate}$ (for 100% glucose) to 0.05

$g/g_{Substrate}$ (for 100% protein). This behaviour is directly explained by two associated phenomena: i) most of the butyrate comes from glucose and ii) the fraction of glucose converted into butyrate increases at high glucose to protein concentration ratios (Figure 6.6). On the contrary, acetate from glucose is higher a low glucose to protein concentration ratios.

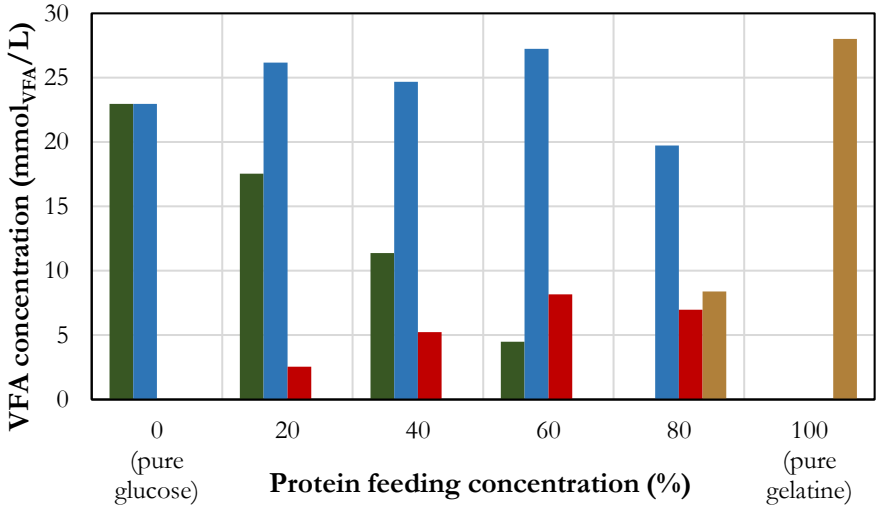

Figure 6.6. Acetate and n-butyrate concentration (mmol/L) due to glucose and glutamate conversion at pH 6.5 and at different substrate proportions. ■ butyrate from glucose ■ acetate from glucose ■ butyrate from glutamate ■ acetate from glutamate.

The AA with the highest presence in gelatine, glutamate, follows the opposite trend as glucose: its conversion to butyrate increases with protein concentration in the feeding (Figure 6.6). However, it cannot compensate the lower butyrate yields of glucose at high protein concentrations because, although the most abundant AA, it only represents 17% of the protein mass and therefore its individual conversion stoichiometry has a limited impact on the overall VFA yields.

The apparent link between these changes in the conversion stoichiometry of glucose and glutamate can be found in their respective metabolic networks. Glucose to acetate is the most favourable glucose conversion pathway as it has the highest ATP yield among the other most typical options (Table 6.3, reactions 1-3). However, it leads to a net NADH production that must be consumed in other pathways. When glucose is converted simultaneously with protein, this

NADH surplus can be consumed in some AA pathways and in this way glucose fermentation can be shifted towards acetate (Figure 6.6). Glutamate is one of these NADH-consuming AA. In protein monofermentation, it tends to be converted to acetate as this pathway has the highest ATP yield (Table 6.3, reactions 4-5). However, when glucose is also present, part of the glutamate is converted to butyrate, utilizing the glucose-related NADH excess (reaction 4 in Table 6.3). The ATP missed in the glutamate to butyrate conversion is compensated by the extra ATP gained in glucose conversion. At high protein to glucose ratios, all the glucose can be directed to acetate as the excess NADH can be absorbed in protein conversion. At low protein to glucose ratios, only part of the glucose that could have been converted to butyrate is shifted to acetate as the protein can only absorb part of the NADH surplus.

Table 6.3. Glucose, glutamate, isoleucine and valine conversion pathway ATP and NADH yields. Y_{ATP} and Y_{NADH} are the ATP and NADH production yields at pH 7 (mol mol_S^{-1}).

#	Reaction	$Y_{ATP/S}$	$Y_{NADH/S}$
1	Glucose→ But	3.3	0
2	Glucose→ 2Ac	4.0	2
3	Glucose→2 Pro	2.7	-2
4	Glutamate→But	0.67	-1
5	Glutamate→2Ac	1	0
6	Isoleucine→iVal	0.25	1
7	Valine→iBut	0.25	1

The model solution provides data on ATP and NADH production rates that include the effect of all the phenomena simulated (e.g. active transport or proton translocations) and in consequence they can describe more precisely the interactions between the substrates. Its analysis effectively shows that glutamate and glucose interact through the NADH production and consumption (Table 6.4). As already discussed, glucose conversion to acetate is the overall most favourable pathway but has a net NADH production that is absorbed in other pathways, as glutamate conversion to butyrate. However, at low protein to glucose ratios there is an equilibrium between transforming glucose through its most energetic pathway and the NADH absorption capacity of other pathways. For example, in the conditions of Table 6.4, converting glucose to butyrate has an ATP rate 17% lower than yielding acetate, with an opportunity cost of 0.26 mol ATP/mol NADH (i.e. for each NADH produced in the acetate pathway, 0.26 extra ATP are produced). To accommodate the extra NADH produced by

glucose some AA are rerouted through pathways with a lower ATP production. For example, glutamate is partially converted to butyrate (Table 6.4, reaction 4) when its conversion to acetate has a 41% higher ATP generation rate, with an opportunity cost of 0.26 mol ATP/mol NADH. These two changes in conversion pathways are in fact in equilibrium as they have the same value of opportunity cost (i.e. the extra ATP rate harvested in glucose conversion to acetate instead of butyrate is lost in glutamate conversion to butyrate instead to acetate).

Table 6.4. Steady state solution for pH 6.5, glucose concentration of 7 g/L and gelatine concentration of 3 g/L. r_{ATP} and r_{NADH} are the intracellular rates of ATP and NADH (mol L_x^{-1} h^{-1}).

#	Reaction	Z	r_{ATP}	r_{NADH}	Opportunity cost[1]
1	Glucose→ But	0.49	0.856	0	0.26
2	Glucose→ 2Ac	0.34	0.999	0.558	
3	Glucose→2 Pro	0.17	0.713	-0.558	
4	Glutamate→But	0.42	0.012	-0.032	0.26
5	Glutamate→2Ac	0.57	0.020	0	
6	Alanine→Pro	0	-0.003	-0.011	0.34
7	Alanine→But	0.99	0.001	0	
8	Isoleucine→iVal	0	0.070	0.683	0.15
9	Valine→iBut	0	0.100	0.473	0.15

[1]Opportunity cost is defined as the difference in r_{ATP} divided by the difference in r_{NADH} between two pathways ($\Delta r_{ATP}/\Delta r_{NADH}$).

Other AA are left unconsumed totally or partially in cofermentation scenarios as, for example, isoleucine or valine, since they are AA characterised by producing NADH in all their possible conversion pathways (Table 6.3). As acetate in glucose conversion also produces NADH and it is a more energetic pathway, it is favourable from a global energetic perspective not to consume these AA even though they would marginally produce ATP. This is represented in the solution analysis by a lower opportunity cost than that of glucose conversion to butyrate instead of acetate, they are left unconsumed (Table 6.4, reactions 8 and 9). Alanine, however, does not change its conversion pathway (Table 6.4, reactions 6 and 7) because the opportunity cost of changing it is higher than that of glucose and therefore it is not globally worthwhile to convert it to propionate instead of to butyrate.

NADH competition appears then as the mechanism to explain most of the interactions, not only among the AA that make up the protein substrate, but also between glucose and the rest of AA. It was shown that the glucose to protein ratio is a parameter with a direct link with the stoichiometry of the system.

Here, the interactions predicted between a particular set of the AA (i.e. the profile chosen for gelatine) and glucose are described. However, if the protein fermented is different, other AA can be the ones interacting with glucose. For example, serine and alanine are AA very abundant in keratin and albumin, respectively, and they behave similarly to glutamate: their preferred pathway is NADH-neutral, but they can yield other products (e.g. butyrate or ethanol) with concomitant NADH consumption but with lower ATP yield. In this way, they could have the role of glutamate in gelatine in our simulations and interact with glucose. Here lies one of the main advantages of the model since it is capable or simulating the cofermentation of any given protein with glucose straightforwardly. The only information needed for simulating the process is the protein profile on AA.

6.3.3. Validation with experimental data

The number of experimental data sets of protein and carbohydrate cofermentation with the needed information to validate our model is very limited. The experimental data set chosen (Breure et al., 1986b) is the only data set available in literature in which the product spectrum is reported in detail and methanisation is completely discarded. In these experiments, glucose (10 g/L) was added to the feeding of a CSTR at pH 7 after being fed only gelatine (5 g/L) until stabilisation at a dilution rate of 0.10, 0.15 and 0.20 h^{-1}. As part of the protein was not hydrolysed, as input for the model the AA concentration resulting from the actual protein hydrolysis is considered. The experimental results show significant deviations in the yield of some VFA (especially in cofermentation results) but they do not follow a pattern with the dilution rate and therefore it was decided to represent the average values for the sake of simplicity.

Simulations were done mimicking the different operational conditions of these experiments in both mono and cofermentation scenarios and compared with the experimental results (Figure 6.7). The model predicts satisfactorily well the product spectrum both in cofermentation and monofermentation experiments.

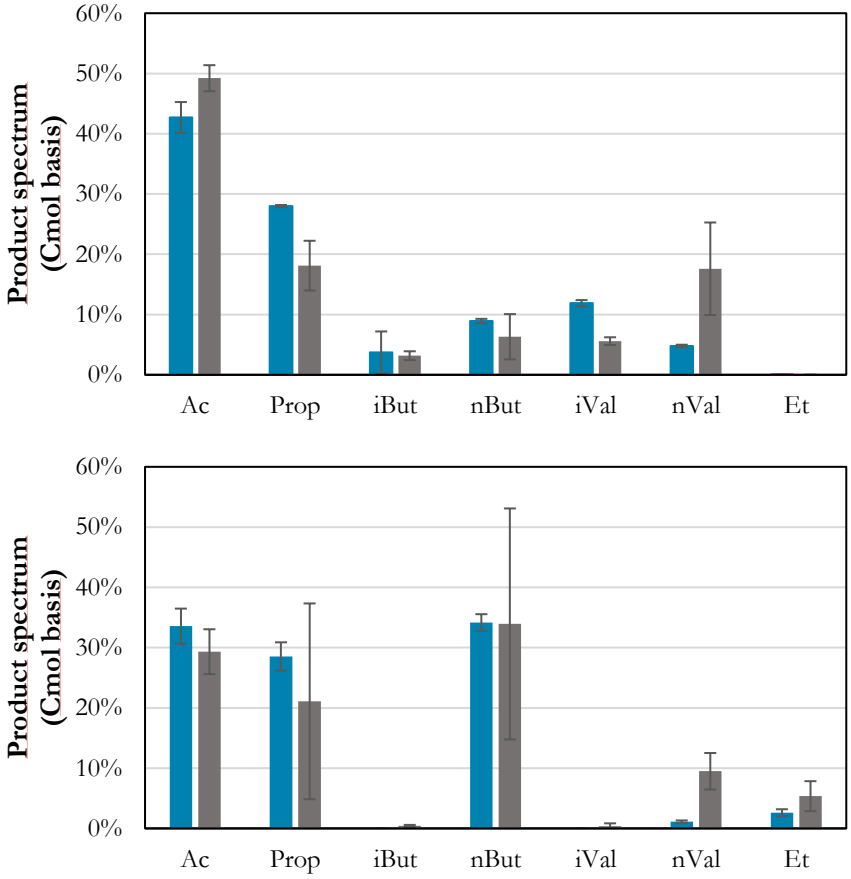

Figure 6.7. Product spectra of model and literature results at 3 different dilution ratios. Upper graph: gelatine monofermentation, bottom graph: cofermentation. ■ Model results ■ Literature results (Breure et al., 1986b).

Moreover, it is able to capture most part of the changes observed in product spectrum by the addition of glucose to the feeding:

i) The iso forms of butyrate and valerate disappear from the product spectrum during cofermentation experiments.
ii) The yield of n-butyrate increases significantly when glucose is present as well as the yield of ethanol.
iii) The propionate yield value does not change between mono and cofermentation in both the experimental data and the model results, but

a considerable deviation is present on the cofermentation experimental data. Propionate is always overpredicted by the model, which could be partially explained by an overrepresentation of the AA yielding propionate (e.g. threonine or aspartate) in the gelatine profile used in the simulation.

iv) The change in n-valerate yield is well estimated but the actual yields are underpredicted. It is likely that the fraction of arginine and proline in the gelatine used in the simulations is underestimated, as only these two AA can lead to valerate.

v) The acetate yield decreases in cofermentation in both simulated and experimental data and is overall well predicted.

vi) Apart from a partial hydrolysis inhibition, AA fermentation is also partially suspected to be inhibited by the presence of glucose as hinted by the systematically lower carbon recovery figures in the cofermentation experiments (AA are not measured and therefore if they are present in the outlet they are considered unidentified carbon), as observed as well in other experimental data set (Breure et al., 1986a). This decrease in AA conversion is only partially captured by the model as it drops from 91% to 85% in the cofermentation simulations. As abovementioned this model does not include any kinetic limitation due to the presence of glucose and therefore only captures the changes in conversion due to energetic or thermodynamic reasons (Liu et al., 2020).

6.3.4. Sources of uncertainty

NADH conservation in cofermentation scenarios. As the microbial community is assumed dominated by generalist microorganisms, protein and glucose consuming pathways will likely share common metabolites as, for example, NADH. The main implication of this assumption is how the NADH conservation constraint is described in the model. If the community is described as dominated by generalists, the NADH conservation constraint should be fulfilled by the glucose and protein catabolic reactions altogether, meaning that glucose or protein consumption can be non-neutral in terms of NADH. But, if the community was modelled as formed by a CH specialist consuming most of the glucose and a generalist, there would be two NADH conservation constraints: one for the generalist and other for the CH specialist. The outcome of the model would likely be different, since the NADH produced in glucose fermentation could not be consumed in protein fermentation reactions and its stoichiometry could not be

shifted towards acetate, as hypothesised in section 6.1. However, as pointed out in section 2.1 a generalist microbial community is more likely.

Ratio between glucose and AA maximum consumption rate. The ratio between the maximum consumption rate of glucose and AA was determined based on the assumption that a more thermodynamically favoured reaction is faster. Reliable data that would have allowed to determine more accurately this parameter were not available in literature. However, if this parameter is varied 50%, the main VFA yields vary less than 10% on average (data not shown), which shows a smaller sensitivity than, for example, the ratio between glucose and gelatine concentration in the feeding.

Unknown AA profile of the gelatine used in the literature experiments. The exact gelatine AA profile used in the literature experiments employed for model validation is not reported. As different gelatines have different AA profiles, this variation is transferred to the product spectrum simulated by the model (e.g. n-valerate is only predicted to be yielded by proline and therefore the predicted n-valerate concentration is directly linked to the proline concentration in the protein). Moreover, as pointed out in section 6.3.2 this also would affect glucose fermentation stoichiometry. The AA profile used in the simulations had then to be assumed. However, the dispersion related to the different AA profiles is reduced in the product spectrum as some AA have convergent pathways leading to the same products (Figure 6.8). In the case of an actual process design, the individual AA concentrations in the substrate would be measured.

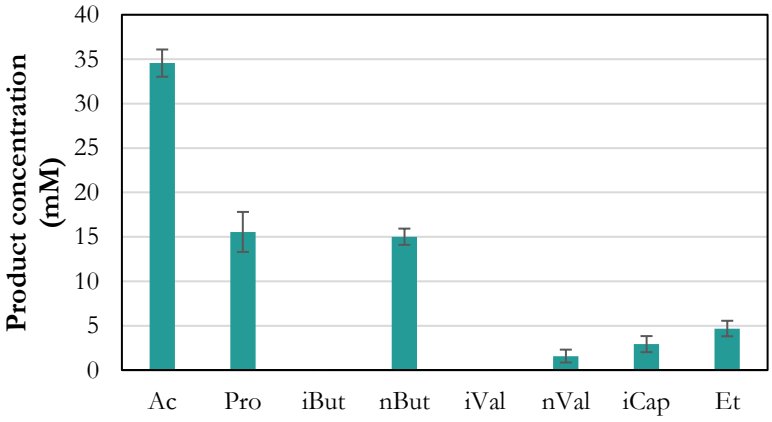

Figure 6.8. Product variability due to different AA profiles. Model simulations at 5 g/L of glucose and gelatine and at pH 7 for the 9 different gelatine AA profiles shown in section 5.6.1

6.4. USE AS PRODUCT DESIGN TOOL

This model is envisioned as a valuable tool in the design phase of cofermentation processes targeting the production of specific VFA. In this section, three design application scenarios with different purposes are presented.

6.4.1. Targeting VFA through design parameters

The information gathered in the exploration of the design space could also be used to design processes that maximise the production of the desired VFA. Now the pH value can be selected *a priori* or a feeding can be tailored to steer the process towards a particular VFA, given that a significant quantity of different wastes is available. As an example, and based on the information presented in section 6.3.1, different areas can be drawn schematically on the design parameter space to provide a quick guide to target the three major VFA for the system glucose-gelatine (Figure 6.9). Producing a corresponding figure for other protein sources (or protein mixes) would be straightforward with the model presented in this article, given the AA composition.

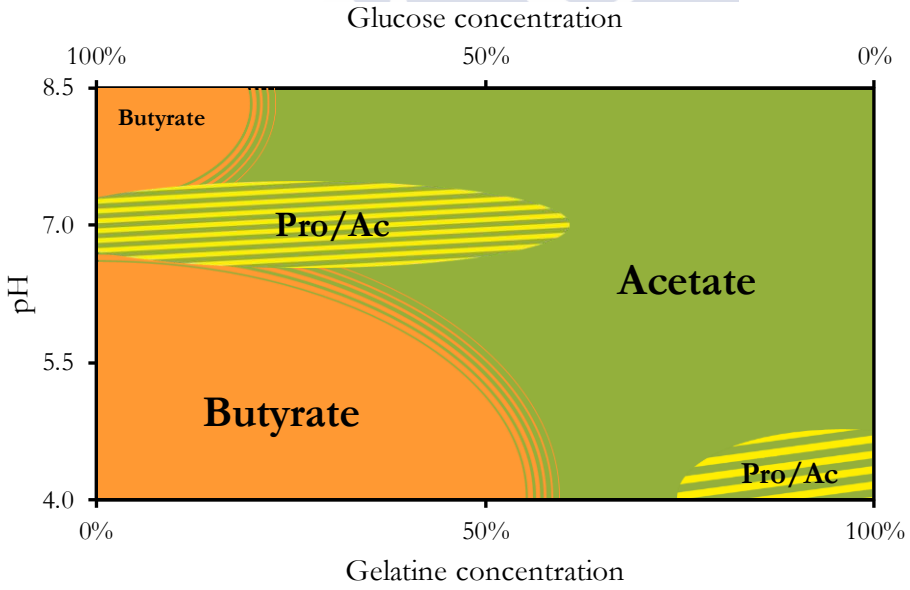

Figure 6.9. Operational parameter space areas that maximise the yield of three different VFA. ■ acetate ■ propionate ■ n-butyrate. Stripped areas correspond to zones in which the yield of two VFA is comparable.

6.4.2. Volatile fatty acids as substrates for polyhydroxyalkanoates production

VFA are the substrates in the microbial production of PHA, a family of bioplastics. In this process, some authors consider the ratio between odd and even-carbon VFA in the feeding an important operation parameter as it might determine to a significant extent some of the final properties of the bioplastic (Lemos et al., 2006; Zhang et al., 2014). This model could be used to design the VFA production step to target a specific odd to even-carbon VFA ratio value (Figure 6.10).

If a very low ratio of odd to even carbon VFA is to be avoided, carbohydrate-rich mixtures at acidic or basic pH values should be avoided. Intermediate values (from 0.3 to 0.5) are better attained by protein-rich mixtures of wastes, in which, in addition, the pH could be optimised following other objectives (e.g. maximum conversion) as its influence on the ratio value is very limited.

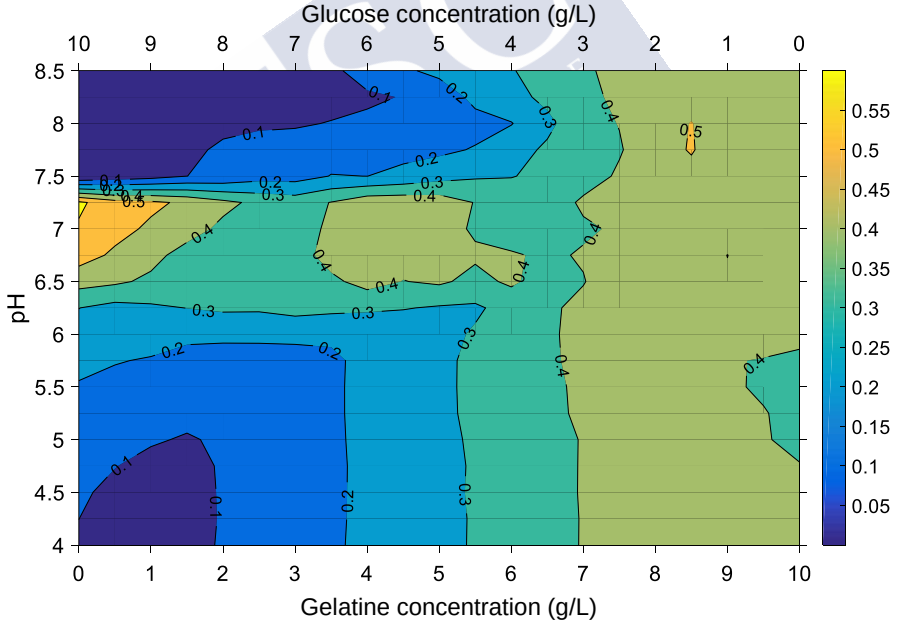

Figure 6.10. Odd to even carbon VFA ratio in the simulation results of section 3. Odd VFA: propionate and n-valerate. Even VFA: acetate, n-butyrate, i-butyrate, i-valerate, i-caproate and ethanol (Gameiro et al., 2015).

6.4.3. Production of volatile fatty acids from agro-industrial organic effluents

The model can also be used to design processes that valorise concrete effluent streams and to decide which stream is more adequate for our purposes. Cheese whey (CW) or canning industry wastewater are examples of waste streams with a high content of proteins and carbohydrates. As a proof of concept, the conversion of these two waste streams to VFA at two different pH values is simulated (tuna cooking wastewater (TCWW) with 7.3 g/L of gelatine and 0.85 g/L of glucose and CW with 1 g/L of casein and 4 g/L of glucose). As the relative concentration of glucose and protein is different in each effluent stream and they feature different proteins, both the stoichiometry and the pH effect are different (Figure 6.11).

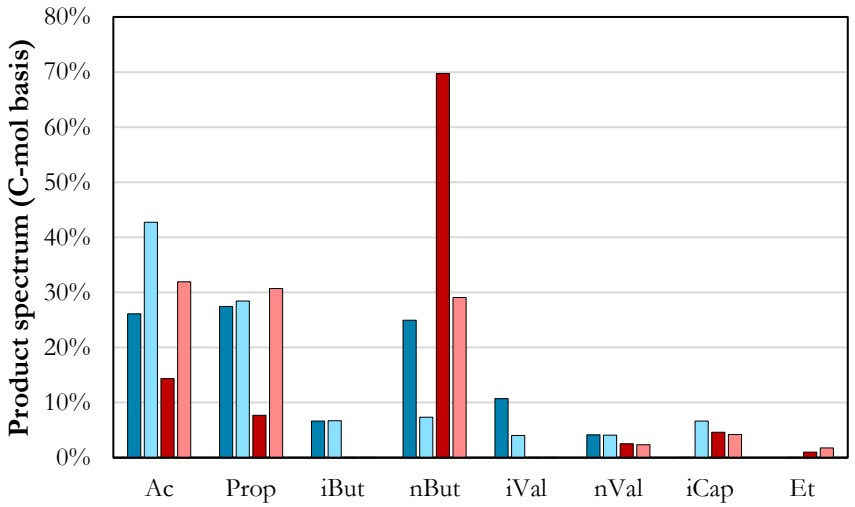

Figure 6.11. Model results for TCWW and CW MCF at a dilution rate of 0.1 h^{-1}. Dark and light colours represent results at pH 5 and 7, respectively. ■ TCWW ■ CW.

CW product spectrum at pH 7 has a high presence of n-butyrate, propionate and acetate and is clearly dominated by n-butyrate at acidic pH due to the high proportion of glucose, which is in line with the information of Figure 6.4. TCWW has a higher yield on acetate and, in general, the pH affects unevenly the yield of the different VFA. Propionate share remains almost constant as shown in Figure 6.5 for feedings with high protein presence. On the contrary, acetate yield decreases at low pH while n-butyrate is favoured at acidic pH, in agreement with

the tendencies observed in Figure 6.3 and Figure 6.4, respectively. This opens the possibility of choosing beforehand the most interesting waste depending on the targeted VFA. If we were interested in higher acetate or propionate productions, we would choose TCWW at neutral pH. On the other hand, if butyrate is the targeted VFA, CW at low pH is the best option between these two agro-industrial waste streams.

6.5. CONCLUSIONS

In this chapter, a mechanistic model for the cofermentation of proteins and carbohydrates by microbial mixed cultures was developed. It reproduces satisfactorily the expected product spectrum and the effect of adding glucose to gelatine monofermentation. Special emphasis was set on explaining mechanistically the effect of different protein to carbohydrate ratios in the feeding and of pH as these parameters have a marked effect on the conversion stoichiometries. The model shows that glucose and the amino acids conforming proteins do interact in their conversion, as previously hypothesised. The NADH conservation constraint is the most evident interaction as glucose and some amino acids compete for its production and consumption. Model validation was partially hampered by the scarcity of experimental data sets with the sufficient quality for this task. Expressly design experiments to study the proposed substrate interactions (e.g. cofermentation of specific amino acids with glucose) are needed to fully validate the model proposed in this chapter. The potential utility of the model as a product design tool was proved with several examples showing how to select optimally the operational parameters to target the production of specific VFAs.

6.6. ANNEX

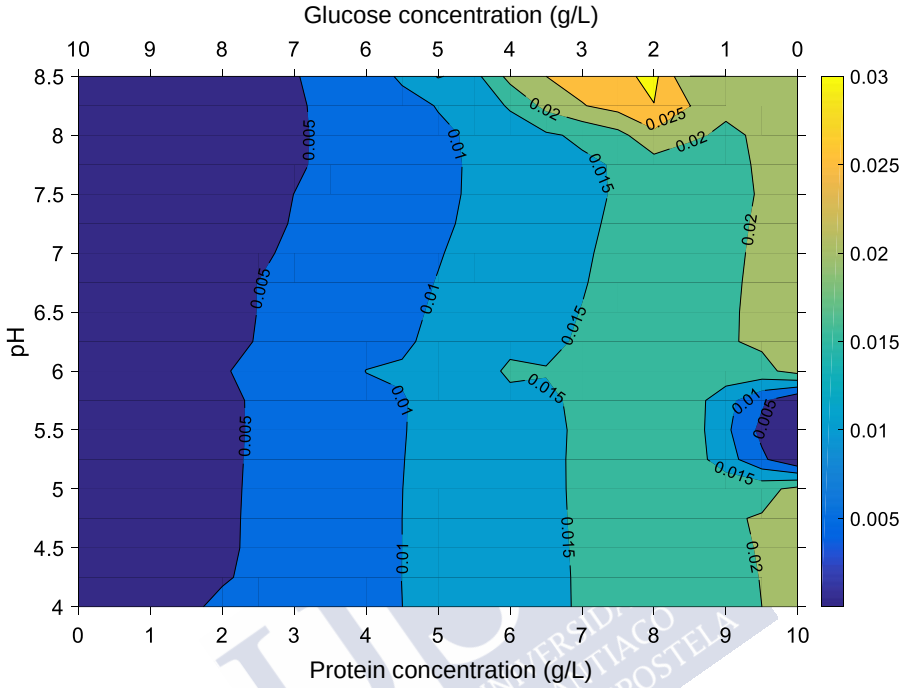

Figure A6.1. Predicted n-valerate yield (g VFA/g of substrate) at different pH values (vertical axis) and at different glucose and gelatine concentrations in the feeding (horizontal axis).

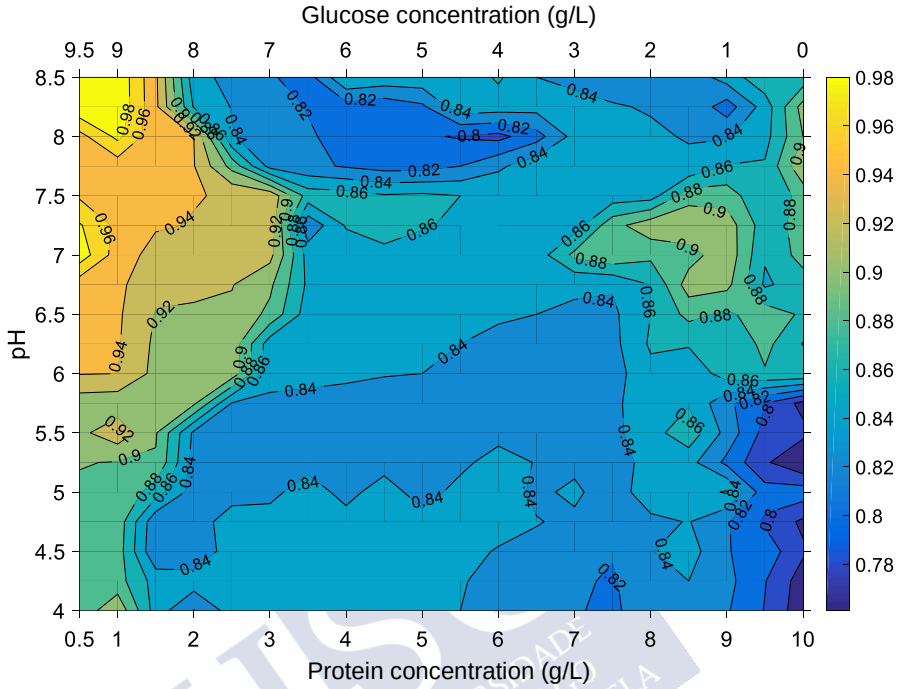

Figure A6.2. Predicted protein conversion (g consumed/g feeding) at different pH values (vertical axis) and at different glucose and gelatine concentration in the feeding (horizontal axis).

USC
UNIVERSIDADE
DE SANTIAGO
DE COMPOSTELA

CHAPTER 7

Kinetic modelling for protein mixed-culture fermentation process simulation

Summary

Available kinetic models are generally conceived for anaerobic digestion and therefore use parameters estimated in methanogenic environments and do not consider changes in the stoichiometry of the process with varying operational conditions, which limits strongly its application for designing fermentation process. In this chapter, a kinetic model specifically conceived for the production of volatile fatty acids in MCF from protein effluents is developed. Expressly designed experiments were carried out with casein and gelatine at different pH values to estimate accurate kinetic and stoichiometric parameters. The parameters show that pH exerts a marked influence on the parameters and that this effect depends also on the protein being fermented. Generally, neutral pH values lead to higher acidification rates while acidic values favour the production of reduced compounds, such as butyrate or valerate. Processes using casein as substrate have faster acidification rates and pH has a stronger influence on their kinetic and stoichiometric parameters. This model is envisioned as a tool to be used in the early-stage design or processes valorising industrial organic effluents and this utility was explored with a couple of deign case studies.

7.1. INTRODUCTION

In the previous chapters, mechanistic models were developed with the objective of predicting the VFA production stoichiometry of protein MCF at different pH values (Chapter 5) and the effect of the addition of a carbohydrate-based co-substrate (Chapter 6). However, to fully design a process, the kinetics of the system and the effect of environmental conditions on the VFA productivities also need to be addressed with kinetic models. In the case of MCF, kinetic models may be of great help to design processes that effectively suppress methanisation manipulating the hydraulic or solids retention times control while at the same time maximising VFA productivity.

Most of the available kinetic models for anaerobic mixed cultures processes are centred in anaerobic digestion as the well-known ADM1 (Batstone et al., 2002b). One of the intermediate reaction steps of anaerobic digestion is the production of VFAs from proteins. As the ultimate goal of the ADM1 is to predict methane production, the focus is not set on describing accurately the substrate conversion into the different VFAs and the description of the fermentative processes, in particular for substrates other than carbohydrates, results insufficient. A model intended to be applied in the production of VFA in MCF should use parameters obtained in fermentative environment as the environmental conditions differ significantly from methanogenic environments (e.g. radically different H_2 partial pressure or different VFA concentrations in the reactor). Also, the effect of the operational conditions and substrate characteristics on the stoichiometry of the system should be considered. Other models, even though they were developed specifically for protein MCF, also feature parameters estimated in methanogenic environments and are centred in describing the use of particulate substrates (Bai et al., 2017) or in modelling correctly inhibition processes (Tommaso et al., 2013). Moreover, they assume that the stoichiometry of the process is fixed and ignore the effect that different operational conditions have on VFA selectivity. It is well described in literature that different proteins or different pH values lead unequivocally to changes in the product spectrum of protein MCF (Bevilacqua et al., 2020a; Breure et al., 1986b; Ramsay and Pullammanappallil, 2001).

In this chapter, a kinetic model for protein mixed culture fermentation is presented. The kinetic parameters of the model are estimated from expressly designed and informative experiments under fermentative conditions at different pH values and using two proteins, casein and gelatine, given their relevance in industrial effluents. Special attention is paid to the influence of pH and the

protein amino acid composition on the kinetic parameters and product selectivity. This model is envisioned as a first step towards a benchmark model for the design of the production of volatile fatty acids in mixed-culture fermentation processes.

7.2. MATERIALS AND METHODS

The detailed description of the development of the kinetic model is covered in the general model development chapter of the thesis (section 2.3). This section contains only the description of the batch essays performed and of the parameter estimation procedure.

7.2.1. Batch essays

Batch protein fermentation experiments were carried out to generate information for the kinetic parameter estimation of the process. Bottles of 0.5 L of total volume (0.375 L of working volume) with rubber stoppers were used and placed in a temperature-controlled room at 25ºC and sparged with N_2 (approximately at a 10 mL/min rate). Two proteins hydrolysates, of casein (A2208,0500 PanReac) and gelatine (70951-1KG-F Sigma-Aldrich), were used as substrates in the essays (their composition on amino acids is available in the Annexes (Table A7.1). The following macronutrients were supplemented (g/L): NaCl (0.292), KH_2PO_4 (0.780), NH_4Cl (0.530), Na_2SO_4 (0.057), $MgCl_2 \cdot 6H_2O$ (0.120). The reactor pH was controlled with either HCl or NaOH 2M, except for one casein experiment in which the pH was naturally adjusted. The inoculum for the batch tests came from steady-state 2 L (1 L working volume) continuous reactors consuming the same protein and operated at the same pH value as the relative batch essay.

The initial biomass concentration was adjusted to an approximate value of 0.5 g VSS/L. Samples were taken at increasing time intervals (initially each 2-3 hours) and VFA concentration, total ammonia nitrogen (TAN) and biomass concentration (through optical density at 600 nm) were determined. The initial substrate concentration for all the pH-controlled experiments was adjusted to reflect a substrate to inoculum ratio (SIR) of approximately 10. In the casein experiment at free pH, three different SIR values were tested (5, 10 and 20) to determine whether the process presents product or ammonia inhibition. To vary the SIR value the biomass initial concentration was kept constant and the initial substrate concentration was adjusted in each of the experiments. The detailed description of the continuous reactors operation and of the analytical methods is available in (Bevilacqua et al., 2020a).

7.2.2. Parameter estimation

Parameters related with the amino acid consumption, biomass growth and decay and the stoichiometry of the system were estimated for each of the data sets generated in the batch essays at different pH and with casein and gelatine. Each data set consists of VFA, TAN and biomass concentration (through optical density at 600 nm) measurements for the same pH, substrate and SIR at increasingly wider time intervals (from 3 h at the beginning of the batch to daily measurements), until the conversion came to a halt. Complete conversion was considered when all the individual VFA measurements remained stable over time.

Hence, data sets were composed by a minimum of 10 and a maximum of 30 data points. Parameters for each data set were estimated by minimisation of the normalised root squared mean deviation (NRMSD) between the experimental data and the simulated data of the model (Eq. 7.1). The model is implemented in MATLAB (R2016a) and NRMSD minimisation is done with the command *lsqnonlin* (trust-region-reflective algorithm).

$$NRMSD = \frac{1}{p \cdot n \cdot m} \cdot \sqrt{\sum_{k=1}^{p} \sum_{j=1}^{n} \sum_{i=1}^{m} \left(\frac{\hat{y}_{k,j,i}(\theta) - y_{k,j,i}}{\sigma_{k,j}} \right)^2} \tag{7.1}$$

where m is the number of measurement times (between 9 and 16), n the number of experimentally measured compounds (in most cases 6), p the number of experiments at different SIR for the same substrate and pH, $\hat{y}$ is the simulated concentration value, y is the experimental concentration value, θ is the vector of parameters being estimated and σ is a normalisation factor meant to scale the residuals to comparable magnitudes (sigma is the range of the experimental values for all measurements except for biomass concentration in casein at pH 5 and 9, as its narrow range would have made extremely large residuals). The subscript i refers to a measurement over time of the compound j in the SIR and pH experiment k.

To ensure the robustness of the estimated parameter values and to avoid the model getting stuck at local minima, a bootstrap methodology, as described in (Gonzalez-Gil et al., 2018) was followed to determine the value and uncertainty interval of the estimated parameters. To check the convergence of the parameters estimated in the bootstrap methodology, the populations were divided in samples and their average value and standard deviations compared to check for divergences. The uncertainty of the kinetic parameters and of the initial compound concentrations in the model results (VFA, ammonia and biomass

concentrations), a Monte Carlo procedure was followed (Saltelli et al., 2008). A total of 500 iterations were performed using Latin Hypercube Sampling to ensure a maximum coverage of the parameter values space (Helton and Davis, 2003).

7.3. RESULTS AND DISCUSSION

7.3.1. Batch essays results

The length of the batch experiments spanned from 72 to 168 h when casein was the protein fermented and from 144 to 240 h when using gelatine as substrate. During the experiments TAN measurements were used to calculate the ammonification degree and to determine whether the fermentation process was complete. When the TAN concentrations remained stable, it was considered that VFA production complete and the reaction was stopped. Acidification degree, expressed as the percentage of substrate COD converted to measured VFA, ranged between 39.4% and 56.8% for casein fermentation without a particular trend with the pH value. In the case of gelatine, it peaked at pH 7 (71.5%), followed by the value at pH 9 (54.4%) and its minimum value was at pH 5 (29.5%). The results of the batch essays concerning the evolution over time of the concentration of VFAs, TAN and biomass is available in the Annexes (section 7.7.2).

The casein experiments at free pH were carried out at three different SIR values (5, 10 and 20), varying the substrate initial concentration, and showed virtually identical final acidification values. Therefore, it can be concluded that, in this range of substrate and product concentrations, there is no substrate nor product inhibition and it is not necessary to include in the model formulation product inhibition. Moreover, the parameters of the three experiments were estimated simultaneously and the estimated parameter set allows the model to accurately reproduce the three data sets (Figure 7.1). The pH of the experiments naturally adjusted to neutral values (between 7.2 and 7.4) because of the combined and opposite effect of VFA and ammonia and due to stripping of the produced CO_2 due to the continuous the nitrogen sparging.

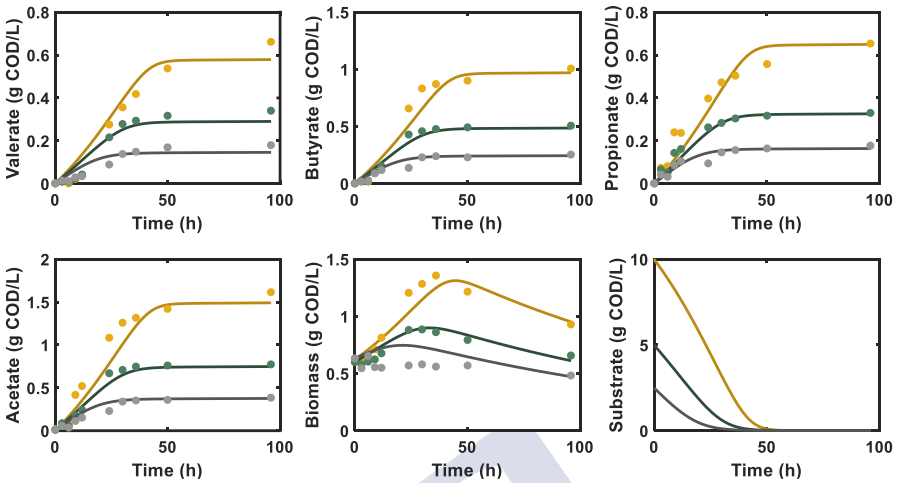

Figure 7.1. Experimental data (filled circles) and simulated data (lines) with the estimated parameters for the free pH batch casein fermentation. (—) SIR 20, (—) SIR 10, (—) SIR 5.

7.3.2. Estimated parameters

Overall, the experimental data allowed to estimate robust parameter sets and the resultant model could reproduce with satisfactory accuracy the experimental results. The NRMSD values for the different experimental data sets remained in all cases below 0.015 and the estimated uncertainty of the parameters is also narrow. As methanogenesis was not observed in the process, their parameters were not estimated and therefore this section only discusses parameters related with acidogenesis.

Thanks to the highly informative experimental data, the identification of a high number of parameters from the experiments was possible. This aspect is discussed in detail in the Annexes (section 7.7.3). An example of a fit between an experimental and simulated data with the propagation of the parameter uncertainties is shown in Figure 7.2.

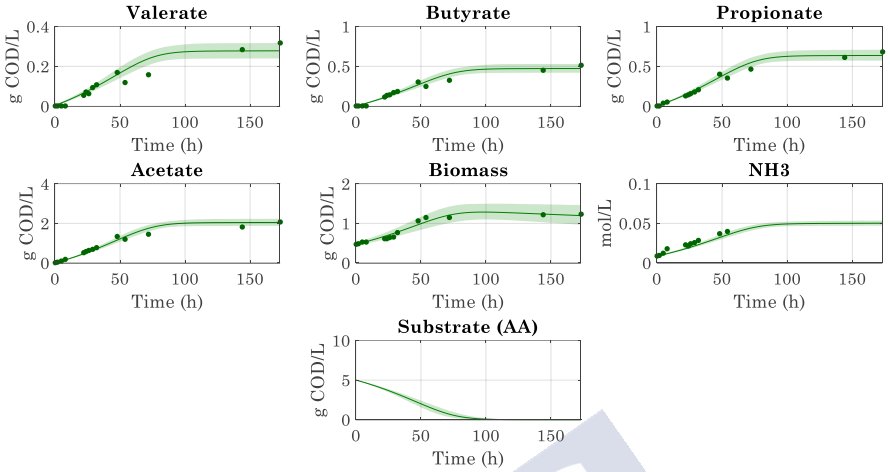

Figure 7.2. Fit between the experimental data (filled circles) and the model results (continuous lines) using the estimated parameters. The coloured areas represent the 95% interval confidence and were estimated with the kinetic and stoichiometric parameters and their confidence intervals following a Monte Carlo procedure.

7.3.2.1. Kinetic parameters

The estimated parameters show indeed that they are affected by the pH value of the experiment and also the substrate protein (Table 7.1). The estimated maximum acidification rate ($q_{Acid,max}$) presents its maximum value at pH 7 for both proteins, while acidic conditions (pH 5) slow down the process at a higher extent than alkaline conditions (pH 9). This effect is more pronounced in the case of casein than of gelatine. In the casein fermentation experiments at free pH, the q_{max} value is practically the same as the value for the pH 7 experiment, as expected by the very similar conditions of both experiments. Concerning the biomass yield, the influence of pH is different depending on the protein fermented. In the case of casein experiments, the free pH case presents the highest biomass yield very closely followed by the experiment at pH 7, which may have a mechanistic interpretation. At acidic and alkaline conditions, cells have to struggle against higher extracellular concentrations of free VFA and ammonia, respectively, increasing thus the energy needed to keep a homeostatic environment and lowering the biomass production per unit of substrate. Only values at pH 7 and 9 are available for gelatine. At alkaline conditions, the biomass yield value is considerably higher than at pH 7 and presents a very high value

compared to the correspondent casein experiment and considering that biomass yields at pH 7 were similar for both proteins.

Table 7.1. Estimated kinetic parameter values (mean value [estimated confidence interval with $\alpha = 0.05$]) for casein and gelatine fermentation at three controlled pH values (5, 7 and 9) and at naturally adjusted pH (free) only for casein fermentation. Some parameters under some conditions could not be estimated due to the lack of quality of the biomass measurements.

Parameter		Casein	Gelatine
$q_{Acid,max}$ (g_{COD} AA/g_{COD} BM·h)	pH 5	0.088 [0.082, 0.094]	0.081 [0.071, 0.091]
	pH 7	0.181 [0.173, 0.190]	0.115 [0.109, 0.122]
	Free	0.180 [0.170, 0.190]	N/A
	pH 9	0.139 [0.128, 0.150]	0.106 [0.098, 0.115]
Yield (g_{COD} BM/g_{COD} AA)	pH 5	0.167 [0.111, 0.223]	Not estimated
	pH 7	0.175 [0.149, 0.201]	0.163 [0.144, 0.185]
	Free	0.191 [0.169, 0.213]	N/A
	pH 9	0.134 [0.090, 0.172]	0.239 [0.214, 0.262]
μ_{max} (h^{-1})	pH 5	0.015 [0.009, 0.020]	0.015 [0.012, 0.018]
	pH 7	0.032 [0.027, 0.036]	0.019 [0.017, 0.021]
	Free	0.034 [0.030, 0.039]	N/A
	pH 9	0.019 [0.012, 0.024]	0.025 [0.023, 0.028]
k_{decay} (h^{-1})	pH 5	$2.7 \cdot 10^{-3}$ [0, $5.3 \cdot 10^{-3}$]	Not estimated
	pH 7	$6.7 \cdot 10^{-3}$ [$4.0 \cdot 10^{-3}$, $9.4 \cdot 10^{-3}$]	$9.0 \cdot 10^{-4}$ [0, $2 \cdot 10^{-3}$]
	Free	$6.6 \cdot 10^{-3}$ [$4.9 \cdot 10^{-3}$, $8.7 \cdot 10^{-3}$]	N/A
	pH 9	$5.6 \cdot 10^{-3}$ [$3.6 \cdot 10^{-3}$, $8.5 \cdot 10^{-3}$]	Not estimated
Inert fraction (%)	pH 5	36.2 [31.5 40.6]	67.8 [65.4 70.3]
	pH 7	32.3 [28.2, 36.0]	13.2 [7.6, 18.4]
	Free	44.7 [42.3, 47.0]	N/A
	pH 9	25.2 [20.0, 30.0]	36.7 [31.6, 42.4]

The maximum biomass specific growth (μ_{max}) values, determined by multiplication of the parameter populations of q_{max} and biomass yield value, describe the same trend as the biomass yield value. Decay constant values follow for both proteins the tendencies described by the biomass yields and is maximum at neutral pH for casein and at pH 9 for gelatine. However, in the case of gelatine experiments, the decay constant could be estimated only at pH 7 since the quality of the biomass measurements in the other cases was not enough to make an independent estimation, i.e. the parameter was non identifiable.

As already mentioned, amino acid acidification was not complete during the batch experiments, leading systematically to a fraction of non-converted substrate, reproducible during repetitions of the same experiment. The maximum production rate value of inerts was also estimated by the model and can be used to determine the extent of substrate converted to inert fraction (Table 7.1). These values follow, logically, the opposite trend as the acidification degree and the influence of the pH on them depends on the protein fermented. In the case of casein, the values of the inert fraction are very similar, except for the free pH experiments set, indicated by the overlapped confidence intervals. On the contrary, in the case of gelatine pH plays a marked influence. While the inert fraction is very low at pH 7 (13.9%), its value increases at pH 9 and is maximum at pH 5, where more than half of the substrate is converted to inerts.

The kind of the protein determines not only how the magnitude of the pH effect on the parameters, but it also influences the absolute value of the parameters. Casein presents at almost all conditions a higher $q_{Acid,max}$ and μ_{max} values (except for pH 9). At pH 7, casein consumption ($q_{Acid,max}$) is almost 60% faster than that of gelatine and the μ_{max} of casein fermenters exceeds that of gelatine fermenters in almost 70%, being this difference less pronounced at acidic conditions.

The few literature studies with available kinetic parameters for amino acid fermentation biomass generally report higher values. Angelidaki et al. (1999) assign in their model a value of 0.27 h^{-1} for amino acid fermenters μ_{max} and Flotats et al. (2006) and Siegrist et al. (2002) estimated values of 0.65 h^{-1} and 0.17 h^{-1}, respectively. However, in the case of Flotats et al. (2006) the uncertainty of the parameter is very large (its standard deviation is bigger than the parameter value) suggesting identifiability issues and Angelidaki et al. (1999) do not report under which conditions this parameter was estimated. Biomass yield values reported in literature also differ from the estimated in this work and are around 0.1 g_{COD} BM/g_{COD} AA (Batstone et al., 2002a; Flotats et al., 2006). However, if the expected ATP production per COD gram of amino acids is determined following the predicted stoichiometry reported in Chapter 5, it can be seen the values for a good share of them are similar to the value of glucose. Glucose ATP production is around 15 mmol ATP/$g_{COD\text{-}Glucose}$ (assuming an ATP yield of 3 ATP), while alanine and aspartate yield above 10 mmol ATP/$g_{COD\text{-}AA}$, serine around 12.5 ATP/$g_{COD\text{-}AA}$ and proline even has a higher number than glucose with 20.8 ATP/$g_{COD\text{-}AA}$. Hence, bioenergetic considerations suggest that the biomass yield may be similar when fermenting amino acids or carbohydrates.

7.3.2.2. VFA selectivity

The selectivity of the system on the different VFA is described by the estimated stoichiometric factors (Table 7.2) and as for the kinetic parameters, pH exerts a considerable influence. The two proteins result in different product spectra, justified by the different composition on amino acids (Bevilacqua et al., 2020a), but overall the pH effect on the product selectivity is independent of the protein used as substrate. Acetate share in the product spectrum increases with pH while butyrate and valerate share presents the opposite trend and its production is maximum at pH 5. Propionate production is slightly increased at neutral pH values and overall presents smaller variations with pH than the other VFA.

Table 7.2. Estimated stoichiometric factor values (mean value [estimated confidence interval with $\alpha = 0.05$]) for casein and gelatine fermentation at three controlled pH values (5, 7 and 9) and at naturally adjusted pH (free) only for casein fermentation.

		Casein	**Gelatine**
f_{Ac} (g_{COD} Ac/g_{COD} AA)	pH 5	0.066 [0.059, 0.073]	0.429 [0.396, 0.458]
	pH 7	0.264 [0.254, 0.273]	0.567 [0.552, 0.582]
	Free	0.335 [0.324, 0.346]	N/A
	pH 9	0.361 [0.346, 0.375]	0.663 [0.642, 0.682]
f_{Pro} (g_{COD} Pro/g_{COD} AA)	pH 5	0.076 [0.070, 0.081]	0.129 [0.117, 0.140]
	pH 7	0.123 [0.119, 0.127]	0.175 [0.165, 0.185]
	Free	0.140 [0.133, 0.147]	N/A
	pH 9	0.104 [0.095, 0.112]	0.074 [0.067, 0.082]
f_{But} (g_{COD} But/g_{COD} AA)	pH 5	0.294 [0.282, 0.305]	0.204 [0.186, 0.225]
	pH 7	0.189 [0.179, 0.199]	0.129 [0.120, 0.139]
	Free	0.221 [0.211, 0.231]	N/A
	pH 9	0.166 [0.159, 0.174]	0.123 [0.113, 0.134]
f_{Val} (g_{COD} Val/g_{COD} AA)	pH 5	0.395 [0.379, 0.410]	0.185 [0.161, 0.208]
	pH 7	0.257 [0.243, 0.271]	0.075 [0.067, 0.083]
	Free	0.135 [0.126, 0.143]	N/A
	pH 9	0.201 [0.190, 0.212]	0.090 [0.082, 0.098]

As with kinetic parameters, the magnitude of the pH effect differs on the two proteins and is overall higher for casein fermentation. For example, butyrate stoichiometric factor (f_{But}) increases 13% between pH 9 and pH 5 for casein, while for the same pH change f_{Ac} decreases in 30%. The same pH change provokes for gelatine an increase in f_{But} of 8% and a decrease of 23% in f_{Ac}. This difference in the magnitude of pH effect can be very well justified by the fact that when varying the pH only the stoichiometry of certain amino acids is affected.

For example, the increase in the fraction of butyrate due to a drop in pH is provoked mainly, according to the metabolic model of Chapter 5 for protein fermentation, by a change in the conversion stoichiometry of glutamate. Glutamate concentration is twice as much in the casein than in gelatine (Table A7.1), which could justify the higher increase in butyrate fraction in casein when the pH drops from alkaline to acidic conditions. Other amino acids particularly sensitive to the effect of pH in their conversion to VFA include aspartate, aspartate, histidine and leucine (Chapter 5).

At pH 5 the value of f_{Val} for casein is remarkably high and valerate is, in fact, the most abundant VFA in the product spectrum. A preferential consumption of those amino acids yielding valerate (arginine, proline, isoleucine and leucine) would justify its high stoichiometric factor or valerate might be also produced by chain elongation processes as a result of acetate and propionate condensation, which would explain the higher-than-possible f_{Val} value and as well the abrupt decrease in f_{Ac} of casein fermentation. However, since there are only limited evidences of chain elongation processes occurring in protein fermentation, it was decided not to incorporate them in the model developed in this work.

In comparison with literature information, gelatine fermentation experimental works report similar product spectra. In studies fermenting gelatine, acetate was always the main VFA with percentages in the product spectrum around 50% (molar basis), followed generally by butyrate and propionate (Breure et al., 1986b, 1986a; Breure and van Andel, 1984; Duong et al., 2019; Flotats et al., 2006). Valerate is reported to be the least VFA produced in some works (Duong et al., 2019; Flotats et al., 2006) but its share is higher and ranks second in others (Breure et al., 1986a; Breure and van Andel, 1984). Different pH values in literature affect VFA production in a similar way as in Table 7.2 and butyrate, or other reduced VFA, are favoured at acidic conditions. For example, butyrate increased its share in the product spectrum when switching the pH from 7 to 5.3 from 8% to 17% (Breure et al., 1986b) and from 7% to 19% in (Breure and van Andel, 1984). Works fermenting proteins other than gelatine and reporting data with the needed accuracy could not be found in literature.

7.4. A FRAMEWORK FOR PROTEIN FERMENTATION SIMULATION

As described previously, simulating the VFA production in protein MCF is a complex task due to the influence of both the substrate composition and the reactor conditions (pH in the case of this work). The aim of this section is to

reconcile the methodology proposed (the model) with the available information for casein and gelatine gathered in experimentation.

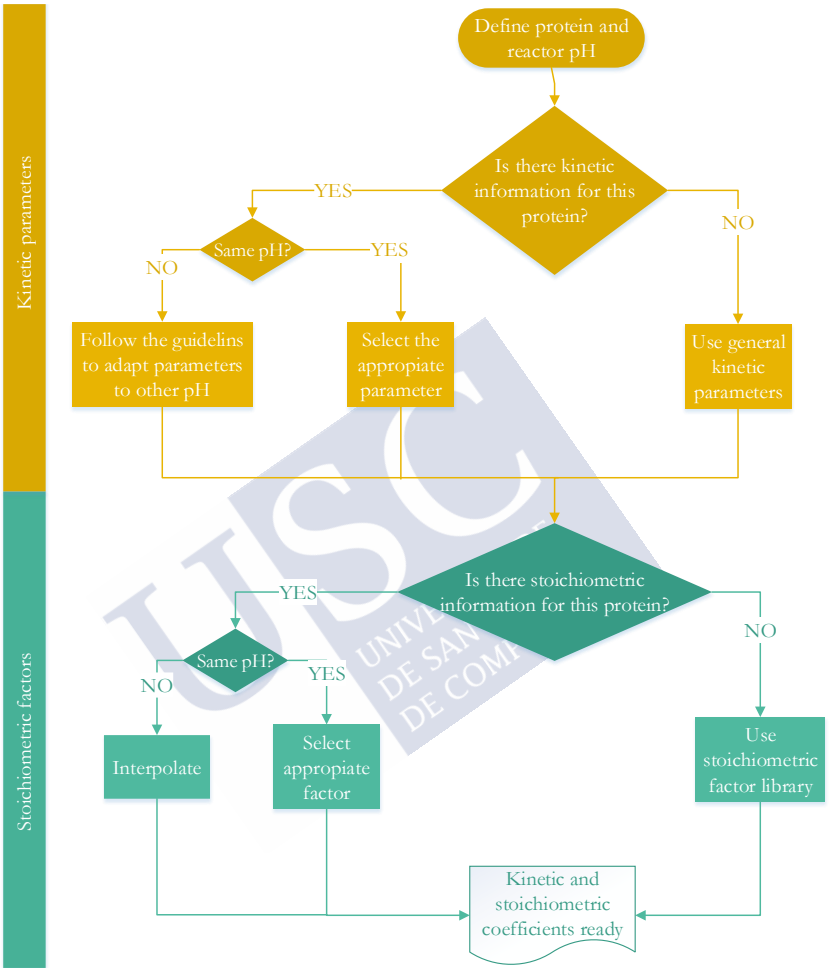

Figure 7.3. Flowchart for setting the appropriate kinetic parameter and stoichiometric factor values.

For that a series of guidelines are presented regarding the choice of the most adequate kinetic and stoichiometric parameters for simulating a particular scenario, which are graphically summarised in the flowchart of Figure 7.3. In the following subsections, a stepwise description of the flowchart is presented.

7.4.1. Selection of kinetic parameters

Here a series of guidelines are proposed in relation with the different kinetic parameters (q_{Acid}, biomass yield, k_{Decay} and inert fraction) to be used to simulate protein fermentation under different pH values.

The values of $q_{Acid,max}$ reported in Table 7.1 should be used in the model for simulating casein and gelatine fermentation processes. These values are reported only at three different pH values, while not precluding the simulation of systems at other pH conditions. In the case that the reactor to simulate is at other pH than the data available, the use of a pH inhibition function to describe its effect on $q_{Acid,max}$ is recommended. Since the pH effect on kinetic parameters is generally non-linear, the dependency of the maximum acidification rate ($q_{Acid,max}$) with the pH is described by a non-linear inhibition function (Eq. 7.2). This function allows to interpolate the value of $q_{Acid,max}$ of a protein at pH values between 5 and 9 by multiplying its maximum value (i.e. at pH 7) by the value of the function at the desired pH. This pH inhibition function was used before to describe the pH effect on kinetic parameters (Batstone et al., 2002a).

$$I = \frac{1 + 2 \cdot 10^{0.5 \cdot (pH_{LL} - pH_{UL})}}{1 + 10^{(pH - pH_{UL})} + 10^{(pH_{LL} - pH)}} \tag{7.2}$$

where I is the inhibition term expressed as the ratio between the $q_{Acid,max}$ values at a given pH value and its value at pH 7 and pH_{LL} and pH_{UL} are the lower and upper pH limits where the process is inhibited 50% with respect to pH 7. These two parameters modify the shape of the function and might do it asymmetrical.

The shape of this function describes a partial inhibition due to high and low pH values and has a value of one at pH 7 (i.e. no inhibition at this point). To make an inhibition function for casein or gelatine, its parameters (pH_{LL} and pH_{UL}) were estimated using the estimated kinetic parameters (Table 7.1). The experimental value of the inhibition function was determined by dividing the $q_{Acid,max}$ at pH values of 5 and 9 by the value at pH 7. The inhibition parameters were estimated by minimisation of the error norm using the trust-region-reflective algorithm implemented by the command *lsqnonlin* in MATLAB.

The resultant inhibition parameters (Table 7.3) produced the inhibition function form showed in Figure 7.4. It can be observed that the shape of the inhibition function is more pronounced for casein than for gelatine as pH exerts a stronger influence on $q_{Acid,max}$, as discussed in section 7.3.2.1, which is reflected on the estimated parameters values (Table 7.3).

Table 7.3. Parameters of the pH inhibition function (Eq. 3) for casein and gelatine and for a general case.

	pH_{LL}	pH_{UL}
Casein	5.01	9.51
Gelatine	4.62	10.08
General	4.83	9.73

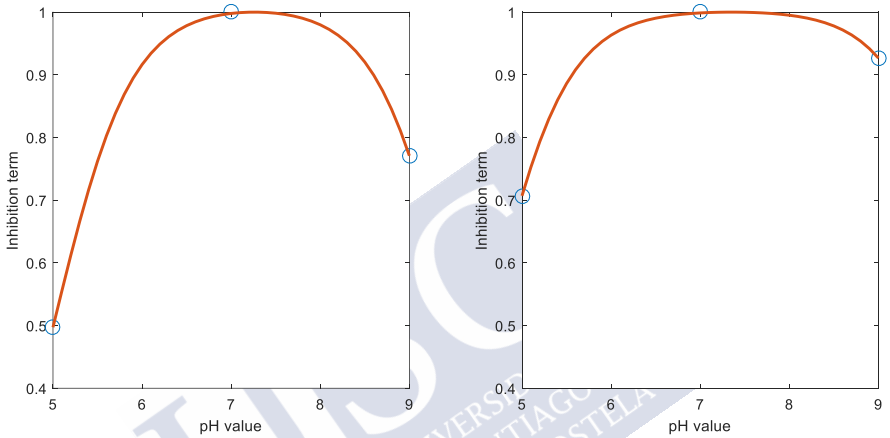

Figure 7.4. Estimated pH inhibition function for casein (left) and gelatine (right) fermentation as a function of the pH. Open circles represent the experimental values of the inhibition function and continuous lines represent the function with the estimated parameters.

In the case that the substrate is composed of other protein, or a casein or gelatine with a significantly different amino acid composition, an intermediate value of 0.150 g_{COD} AA/g_{COD} BM·h could be used as an initial estimation for $q_{Acid,max}$ at pH 7. In this case, to simulate processes at other pH values, it is recommended to use a general form of the inhibition function (Figure 7.5), which is estimated using the data from casein and gelatine kinetic parameters altogether (Table 7.3).

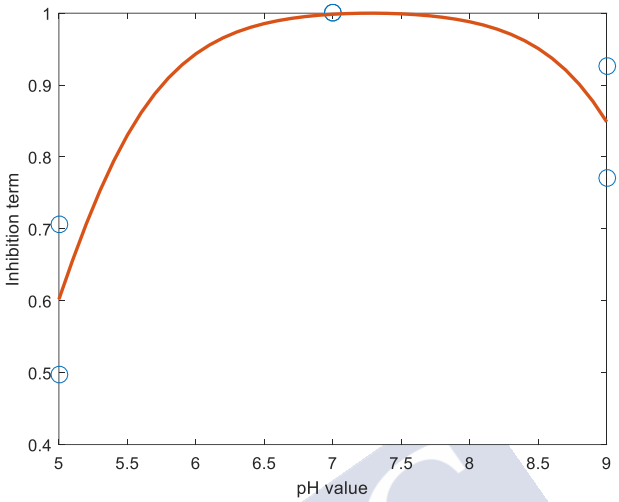

Figure 7.5. Estimated general pH inhibition function for protein fermentation as a function of the pH. Open circles represent the experimental values of the inhibition function and continuous lines represent the function with the estimated parameters.

The biomass yield values were overall less affected by the pH and the protein (Table 7.1). Although it is expected that a maximum is reached at neutral pH, the observed variation was limited and the error derived of using an average value is probably acceptable. In consequence, it is proposed to use a fixed value of 0.16 g_{COD} BM/g_{COD} AA, regardless of the pH of the reactor and the protein used as substrate. Although some differences can be drawn between the values from casein or gelatine, the use of a general value has a marginal impact in the VFA prediction as the difference between the biomass yields of gelatine and casein and the general value is very narrow (around 0.01 g_{COD} BM/g_{COD} AA).

The values of the decay constant are usually expressed as a percentage of the μ_{max} value to compare directly the importance of biomass decay processes with respect to its growth. The determined ratio between the decay constant and μ_{max} clearly show that casein fermenting biomass decay is more intense than in gelatine fermenting biomass (Table 7.4). This could be justified by the fact that. influenced by the protein fermented, two different bacterial populations with different characteristics (especially in its decay behaviour) dominated the microbial community. The values at pH 9 for both proteins are very high since usually decay represent around 10-20 % of the μ_{max}, which could be related with

the significantly higher concentration of free ammonia at pH 9 than at the rest of pH values.

Table 7.4. Ratio between k_{decay} and μ_{max} expressed as percentage.

	Casein	Gelatine
pH 5	16.0	6.0
pH 7	21.0	4.9
Free pH	19.3	N/A
pH 9	27.9	27.5

In the model simulations, it is suggested to use for the decay constant a pH-independent value for each of the proteins. Casein k_{decay} would be set to 20% of the value of the μ_{max} value of its fermenting biomass, while gelatine would have a 5% value. In case other proteins than casein or gelatine should be modelled, a conservative value of 10% should be used instead.

Regarding the inert fraction, it is recommended to employ the values estimated (Table 7.1), interpolating if necessary. In case of simulating the fermentation of other proteins than casein or gelatine, as an initial conservative approximate a value of 25% if proposed. The values of μ_{max} can be obtained as the product of $q_{Acid,max}$ and the biomass yield and hence recommendations are not needed.

7.4.2. Selecting stoichiometric coefficients

The stoichiometry of protein fermentation was shown to be different for casein and gelatine, but it is affected by the reactor pH in a similar way in both cases. The effect of pH can be briefly summarised as follows: acidic pH promotes the production of butyrate and valerate in detriment of acetate and alkaline values have not a marked effect. Propionate yield does not follow any clear tendency with pH and its variations are smaller.

Following the flowchart of Figure 7.3, if the protein used in the system to be designed is casein or gelatine, our proposal is to use the stoichiometry provided in Table 7.2, together with the aromatic VFA and H_2 stoichiometric coefficients reported in section 2.3.1, interpolating linearly between the given values if needed. Should another protein be used in the system or be the amino acid profile substantially different, the use of a library of stoichiometric factors is recommended. This library is built using the metabolic model of Chapter 5. This metabolic bioenergetic model is able to predict the stoichiometry of protein MCF at any given pH value given the composition on amino acids of the protein is

known. It proved to reproduce the observed stoichiometry of continuous protein fermentations by mixed cultures of microorganism and to capture accurately the effect of pH on the product spectrum. Although this metabolic model was developed expressly for continuous reactors, it was previously reported that the selectivity of the system is not much affected by the change in reactor configuration (Bevilacqua et al., 2020b, 2020a), which extends the applicability of this model to discontinuous reactors taking into consideration that the uncertainty of the stoichiometric factors would be higher. Therefore, we consider that this model stands as an appropriate tool to use when no experimental information of a particular system is available. As an example, a small library containing the stoichiometric factors for albumin and for a casein and gelatine, with a different amino acid profiles that the ones used in the batch experiments of this work, is available in the Annexes (7.7.4).

7.5. APPLICATION OF THE MODEL FOR BIOPROCESS DESIGN

This model is envisioned as a valuable tool for being used in the early-stage design of fermentation processes producing VFA from protein-rich wastes. In this section, two different application for the kinetic model developed in this work are presented to illustrate this aspect.

7.5.1. Optimising a continuous reactor fermentation process

Here the VFA production from gelatine and casein fermentation in a continuous stirred tank reactor (CSTR) at pH 7 is optimised. One of the critical design parameters in a continuous reactor is the hydraulic retention time (HRT), which in the case of not having a biomass retention system is equal to the solid retention time (SRT). Ideally, the HRT value would be as low as possible to increase the productivity of the system, but very low values might also result in lower VFA yields due to incomplete or no substrate conversion provoked by excessive biomass washing. On the contrary, high HRT values could allow for (partial) methanisation and hence lower VFA productivities. The model can be used to find an optimal HRT value that maximises VFA productivity or its yield from the substrate (Figure 7.6). Although higher conversions are attained at high HRT values (green lines in Figure 7.6), it might be more interesting to operate where the productivity is at its highest (yellow lines in Figure 7.6), which is around HRT values of 2.5 and 3.5 days for casein and gelatine, respectively. Gelatine top productivity is slightly higher than the one of casein since casein stoichiometric factors for aromatic VFA and H_2 are higher. However, casein fermentation

attains its maximum productivity at a lower HRT than gelatine as its fermentation is faster. In both cases, methane production was minimum and remained below 1% of the substrate COD even at the highest HRT values, as it was production was hampered by hydrogen accumulation and due to the significantly slower growth of methanogenic biomass.

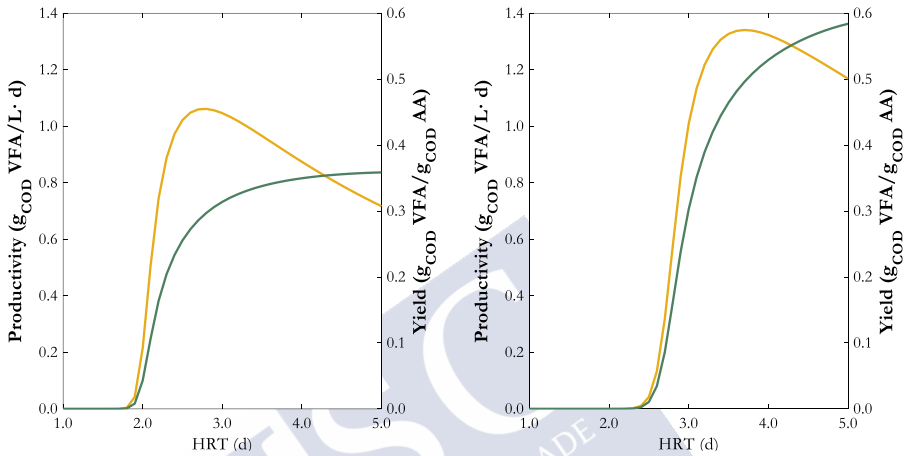

Figure 7.6. Simulated VFA productivity (yellow lines) and VFA yield (green lines) in casein (left graph) and gelatine (right graph) fermentation. Initial amino acid and biomass concentrations are 10 and 1 g_{COD}/L, respectively.

7.5.2. Optimising a sequential batch reactor

In this case, the acidification of casein in a sequential batch reactor (SBR) is simulated at two pH values (5 and 7) with the objective of optimising the production of butyrate and valerate, the most reduced and valuable VFA of the protein product spectrum. SBRs are an interesting configuration to boost volumetric productivities due to the increased solids retention time (SRT), which allows for a much higher biomass concentration in the reactor. In each of the cycles of an SBR most part of the liquid fraction is renovated with fresh substrate and usually the solids (i.e. mainly biomass if the feeding has low solids concentration) are mostly retained to ensure a high biomass concentration. Here the liquid and solid exchange ratio are defined as a measurement of the fraction of liquid and solids that are renovated each cycle. The solids exchange ratio can be controlled by the operator with the settling time before emptying the reactor or by the use of membranes to retain solids, for example.

To ensure a high productivity of the system, the model could be used to define an optimal cycle length and solid exchange ratio that maximise VFA productivity, while avoiding wasteful conversion of substrate to methane. In this example, the objective is the maximisation of the productivity of the most reduced VFA: butyrate and valerate. SBR were simulated at different cycle lengths and solid exchange ratio values at pH 7 (Figure 7.7) and pH 5 (Figure 7.8), with the same initial conditions as in the previous example and assuming that in each cycle 90% of the liquid is renovated.

The model results show that operating at high cycle length times low solid exchange ratio (the conditions of the right bottom corner of Figure 7.7) would lead to high conversion of the substrate to methane, while short cycle length times and high solids exchange ratio values (top left corner of Figure 7.7) lead to the washout of the fermentative biomass (Figure A7.10), resulting in lower or null VFA productivities. The reactor at pH 7 shows an optimal productivity of both butyrate and valerate when operated at cycle lengths between 6 and 9 h and at the lowest solids exchange ratio (Figure 7.7).

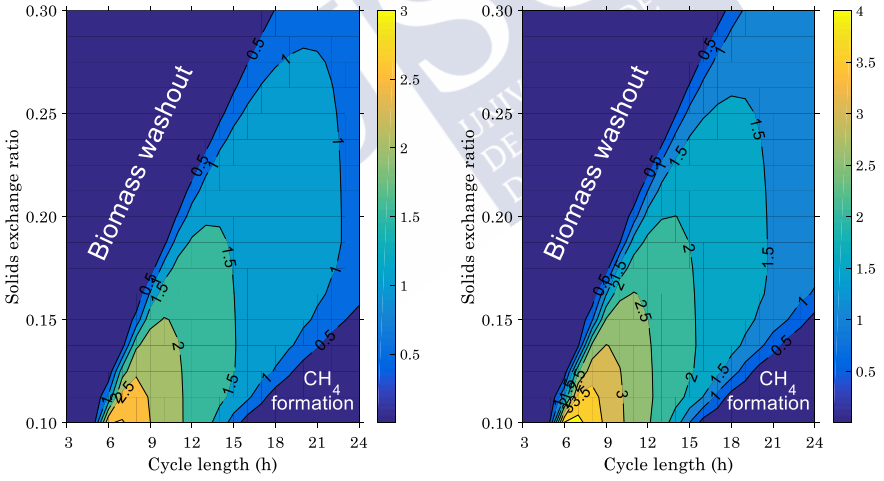

Figure 7.7. Individual butyrate (left) and valerate (right) productivities ($g_{COD}/L \cdot d$) in an SBR reactor under different cycle lengths (horizontal axis) and solids exchange ratio (vertical axes) for casein fermentation at pH 7. Each cycle 90% of the liquid is renovated.

Under these conditions the concentration of biomass is maximal in the reactor (Figure A7.10) and provides a high conversion capacity and the short cycle times boost the volumetric productivity. Methane production is effectively inhibited in this operational region due to methanogenic biomass washout since its growth is

slower than that of casein fermenters. However, if the fraction of non-converted substrate is considered (Figure A7.11), it would be better to operate at slightly longer cycle times (around 8h) to ensure full conversion of the substrate. At these conditions, butyrate and valerate productivities have a value of around 3 and 4 $g_{COD}/L \cdot d$, respectively.

At pH 5, it can be observed in Figure 7.8 that cycle length times should be longer than at pH 7 to avoid fermentative biomass being washed out since its growth is slower under acidic conditions (Table 7.1). In this case, methanogenesis is completely inhibited under all tested operational conditions space due to the much lower growth rate of methanogenic biomass at acidic conditions. Although the selectivity for butyrate and valerate is higher at pH 5 than at pH 7 (Table 7.2), their productivity is lower than at pH 7 due to the required longer cycle lengths. Overall, using an optimised SBR can increase up to ten times the global VFA productivity in comparison with a continuous reactor.

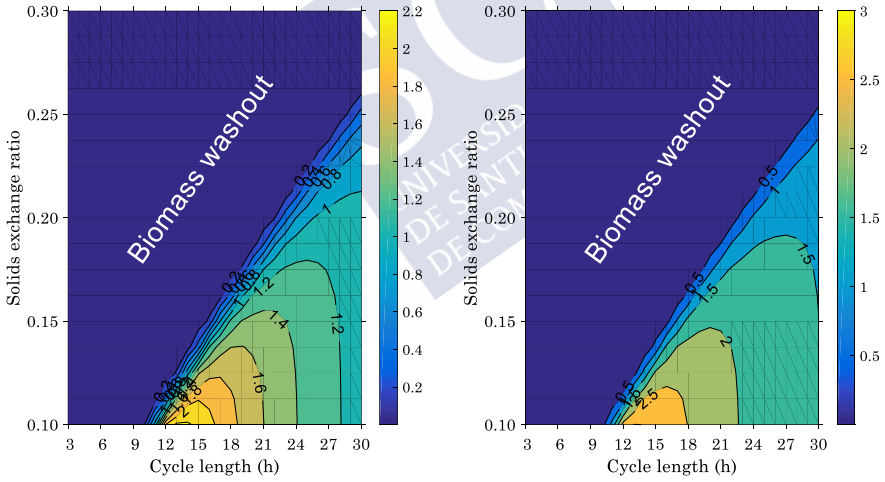

Figure 7.8. Individual butyrate (left) and valerate (right) productivities ($g_{COD}/L \cdot d$) in an SBR reactor under different cycle lengths (horizontal axis) and solids exchange ratio (vertical axes) for casein fermentation at pH 5. Each cycle 90% of the liquid is renovated

7.6. CONCLUSIONS

A kinetic model for the mixed-culture fermentation of proteins was developed. Kinetic and stoichiometric parameters were estimated from expressly designed experiments converting casein and gelatine at three pH conditions, covering the effect of pH and substrate on the process. This model is envisioned to be used

as an early-stage design tool with which optimise operational parameters and boost the productivity of fermentation system using protein-rich substrates. As a proof of concept, the model was used in two systems of interest to optimise some design parameters to maximise the overall or selective productivity of volatile fatty acids from casein and gelatine mixed-culture fermentations.

7.7. ANNEXES

7.7.1. Amino acid composition of the proteins used in the batch essays

Table A7.1. Molar-based composition on AA of the two protein hydrolysates used in the batch essays. For more information about the analytical method, see (Bevilacqua et al., 2020a).

	Casein	Gelatine
Aspartic acid	2.54	2.03
Serine	7.12	4.32
Glutamic acid	15.0	7.07
Glycine	2.80	34.5
Histidine	1.96	0.80
Arginine	3.83	5.11
Threonine	5.83	2.87
Alanine	7.64	13.5
Proline	13.9	16.1
Cysteine	0.00	0.00
Tyrosine	2.74	0.55
Valine	8.79	3.44
Methionine	0.93	0.49
Lysine	6.96	3.02
Isoleucine	5.94	1.33
Leucine	9.46	3.07
Phenylalanine	4.56	1.73

7.7.2. Batch essays results

In this section the results of the batch essays are shown. Firstly, the evolution over time of the concentration of VFAs, biomass and TAN for casein experiments at controlled pH is shown (Figure A7.1-A7.4).

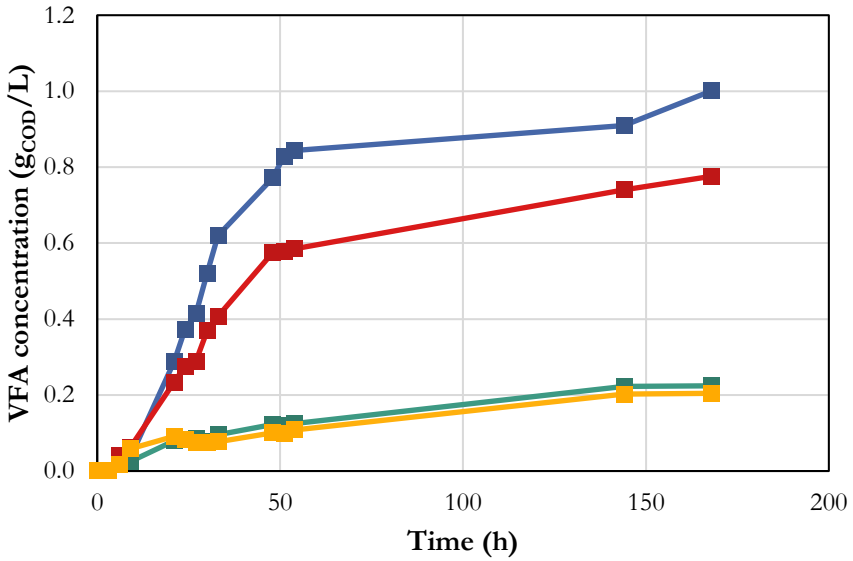

Figure A7.1. Evolution over time of the VFAs concentration (g_{COD}/L) in the batch essay of casein at pH 5. Valerate (—), butyrate (—), propionate (—) and acetate (—).

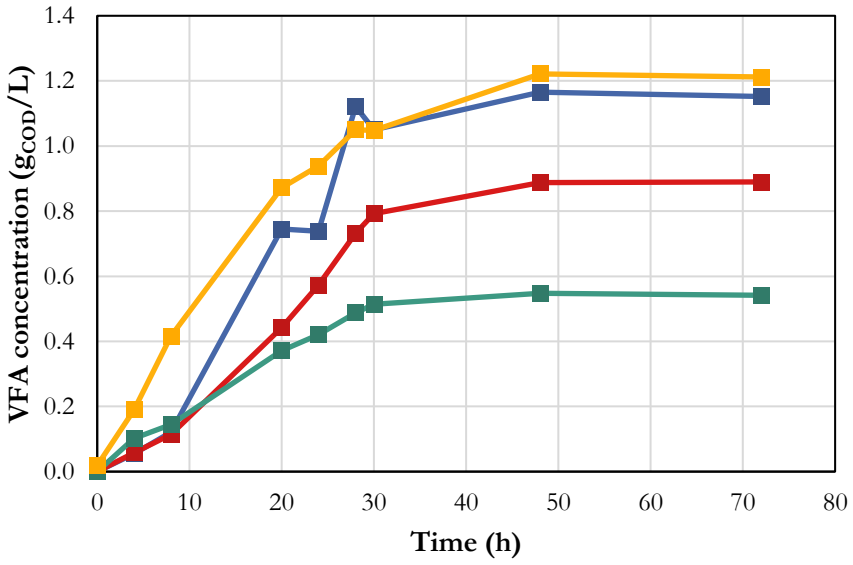

Figure A7.2. Evolution over time of the VFAs concentration (g_{COD}/L) in the batch essay of casein at pH 7. Valerate (—), butyrate (—), propionate (—) and acetate (—).

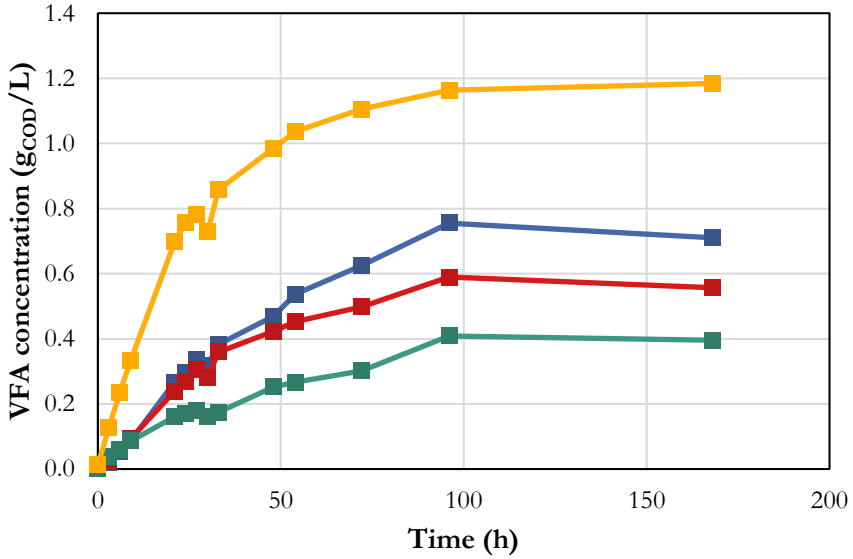

Figure A7.3. Evolution over time of the VFAs concentration (g_{COD}/L) in the batch essay of casein at pH 9. Valerate (—), butyrate (—), propionate (—) and acetate (—).

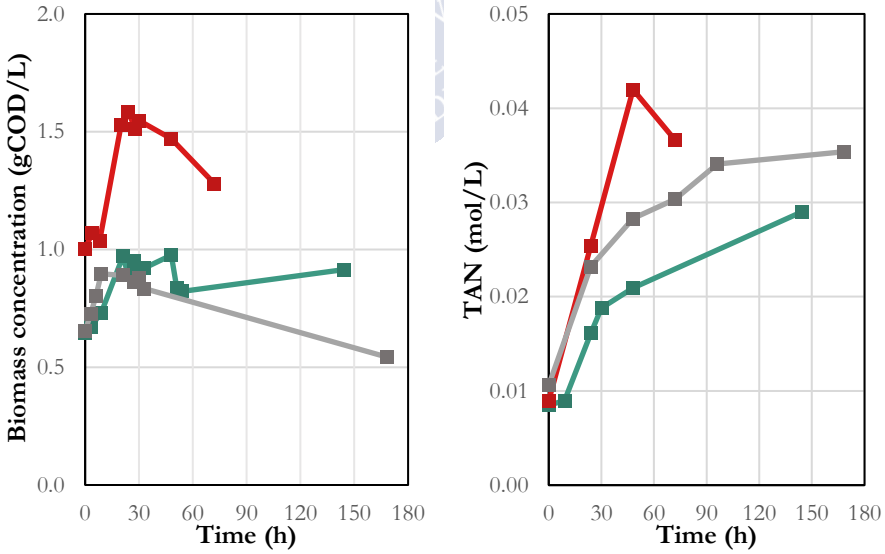

Figure A7.4. Evolution over time of the biomass concentration (left graph) and total ammonia nitrogen (TAN) concentration (right graph) in the batch essays of casein at pH 5 (—), pH 7 (—) and pH 9 (—).

Regarding the free pH experiments, only the biomass concentration over time for the different SIR values is shown in this section as the VFA data is shown in the main text and TAN measurements are not available (Figure A7.5).

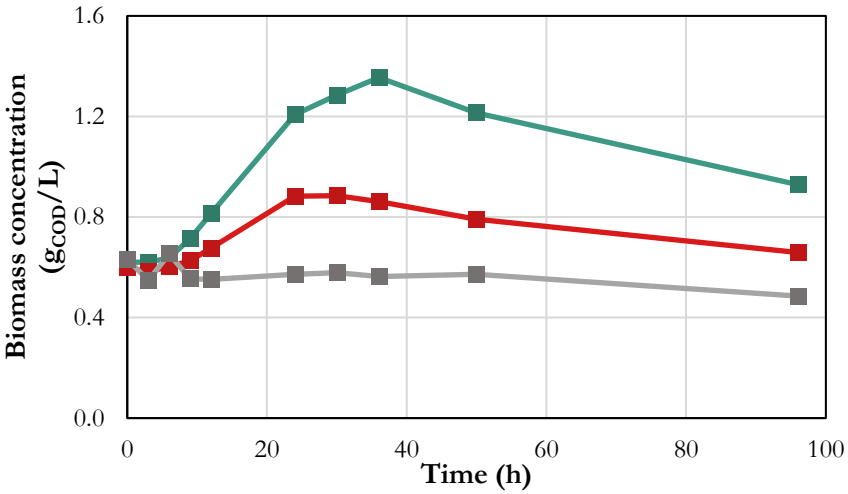

Figure A7.5. Evolution over time of the biomass concentration in the batch essays of casein at free pH at different substrate to inoculum (SIR) ratios. SIR 20 (—), SIR 10 (—) and SIR 5 (—).

Finally, the results of gelatine experiments are shown in Figures A7.6-A7.9.

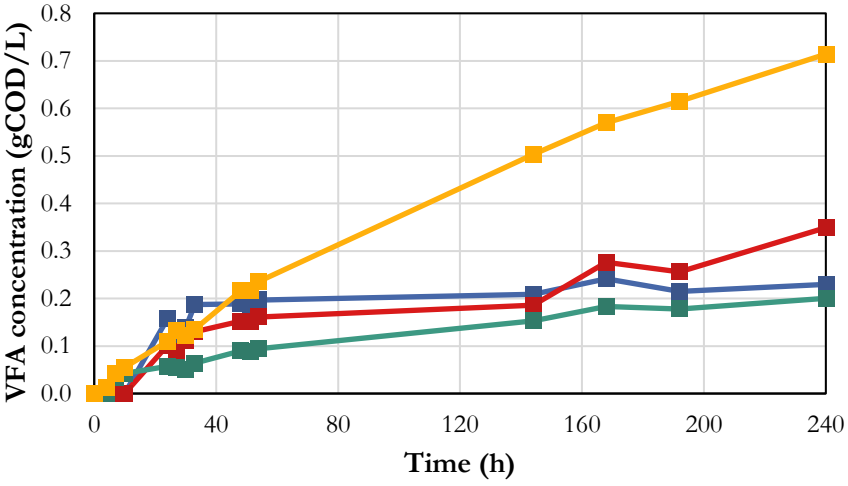

Figure A7.6. Evolution over time of the VFAs concentration (g_{COD}/L) in the batch essay of gelatine at pH 5. Valerate (—), butyrate (—), propionate (—) and acetate (—).

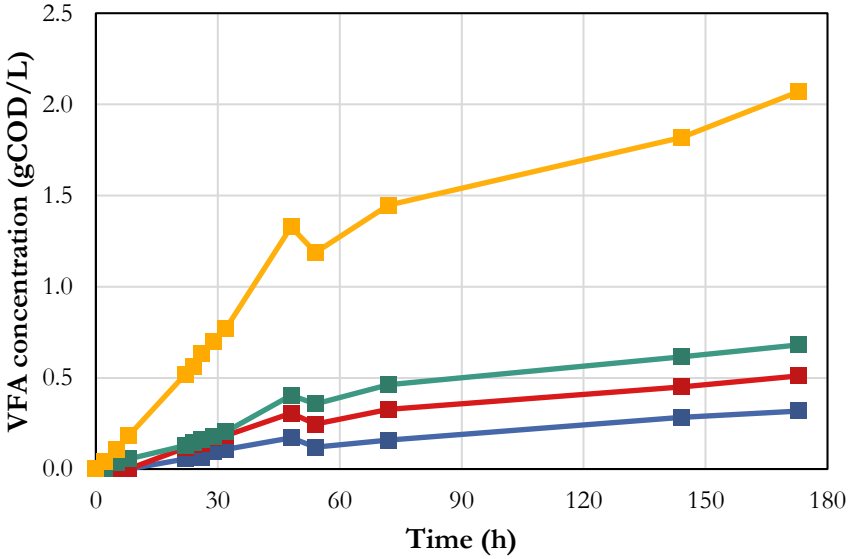

Figure A7.7. Evolution over time of the VFAs concentration (g_{COD}/L) in the batch essay of gelatine at pH 7. Valerate (—), butyrate (—), propionate (—) and acetate (—).

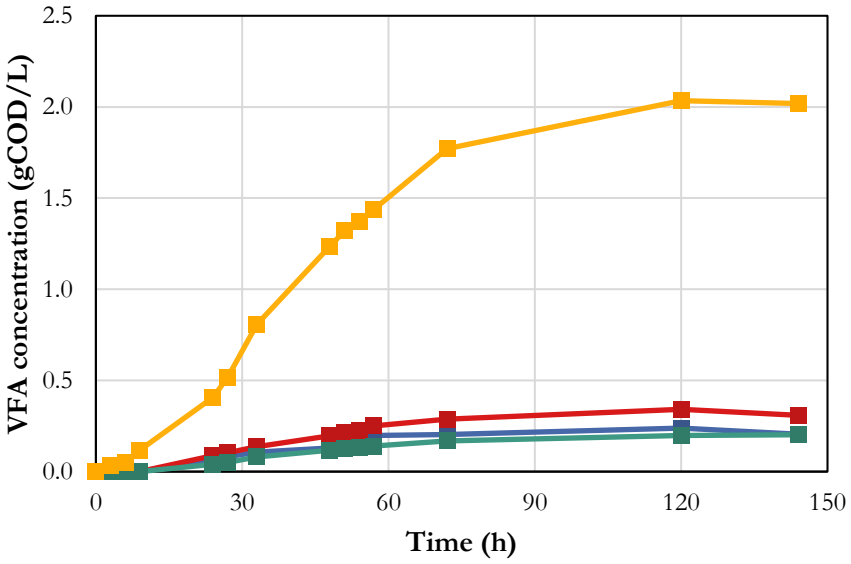

Figure A7.8. Evolution over time of the VFAs concentration (g_{COD}/L) in the batch essay of gelatine at pH 9. Valerate (—), butyrate (—), propionate (—) and acetate (—).

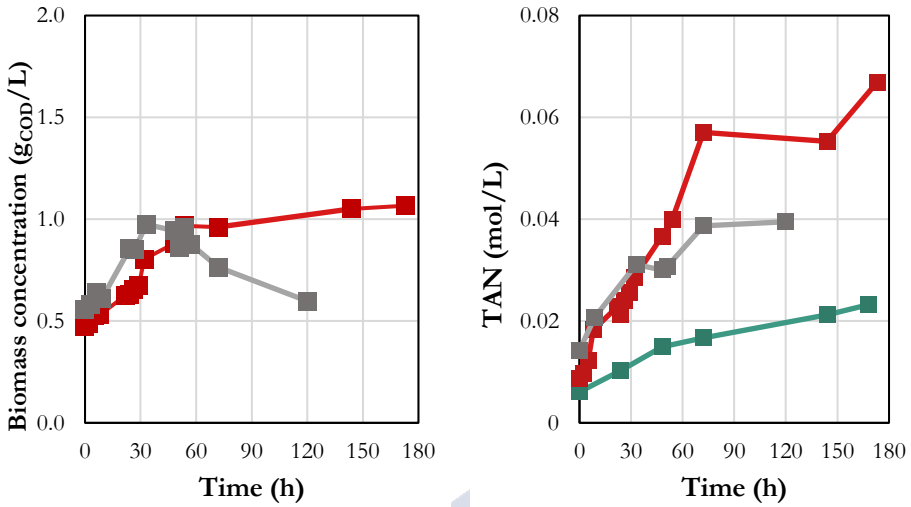

Figure A7.9. Evolution over time of the biomass concentration (left graph) and total ammonia nitrogen (TAN) concentration (right graph) in the batch essays of casein at pH 5 (—), pH 7 (—) and pH 9 (—).

7.7.3. Identifiability

To check if the quality of the experimental data is sufficient enough to determine with accuracy a given number of parameters, a factor of collinearity is determined For that, in the first place, the non-dimensional sensitivity matrix (the derivate of the model outputs with respect to the parameters estimated evaluated at the point of the estimated parameters) is calculated and normalised by multiplication by the estimated parameter value and divided by the average of each model output over time (Eq. A7.1). Then it is normalised again with its norm.

$$A_{i,j} = \frac{\frac{d\hat{y}_{i,k}}{d\theta_j} \cdot \frac{\theta_j}{mean(\hat{y}_i)}}{norm\left(\frac{d\hat{y}_i}{d\theta_j} \cdot \frac{\theta_j}{mean(\hat{y}_i)}\right)} \quad \text{(A7.1)}$$

where A is the non-dimensional sensitivity matrix, $\hat{y}_i$ is the ith model output (e.g. the concentration of a compounds at a given time of the batch) at time k and θ_j is the jth parameter of the model being estimated. The mean and the norm are determined for all time measurements of each compound.

The sensitivity among parameters is determined by matrix multiplication of the previous matrix by its transpose (AxA'). The diagonal of this matrix should be

filled with ones (the sensitivity of one parameter with itself is one). Finally, the collinearity factor is determined by the inverse of the squared root of the minimum value of the eigenvector of the parameter sensitivity matrix (Eq. A7.2). This factor value is inversely proportional to the collinearity among the parameters, i.e. if the parameters show linear dependency among them, it is not possible to identify with security a set of parameters since multiple lineal combinations of them will provide the same model output.

$$Collinearity\ factor = \frac{1}{\sqrt{\min\left(eig(A \times A')\right)}} \quad \text{(A7.2)}$$

A value inferior to 10 is considered to indicate a satisfactory identifiability of the estimated parameters. Considering the collinearity factor values obtained in the parameter estimations carried out in this work (Table A7.2), it can be said that all the parameter sets are composed of parameters showing a good identifiability.

Table A7.2. Collinearity factors of the estimated parameters in the different experiments.

	Casein	**Gelatine**
pH 5	4.83	4.00
pH 7	4.81	4.74
Free pH	8.92	N/A
pH 9	4.70	5.41

7.7.4. Stoichiometric coefficients library

The stoichiometric factors determined in the model of Chapter 5 for three proteins (albumin, gelatine and casein) are presented in Table A7.3 to A7.5, respectively. As the mentioned model does not incorporate the aromatic amino acids, there is no available stoichiometric factor for aromatic VFA.

Table A7.3. Simulated stoichiometric factors for 10 g/L albumin fermentation in a continuous reactor at different pH values.

	Reactor pH								
	5.0	**5.5**	**6.0**	**6.5**	**7.0**	**7.5**	**8.0**	**8.5**	**9.0**
F_{Ac} (g_{COD} Ac/g_{COD} AA)	0.17	0.17	0.17	0.17	0.26	0.31	0.28	0.28	0.28
F_{Pro} (g_{COD} Pro/g_{COD} AA)	0.12	0.12	0.12	0.13	0.08	0.09	0.12	0.12	0.14
F_{But}(g_{COD} But/g_{COD} AA)	0.39	0.40	0.40	0.38	0.34	0.27	0.26	0.26	0.21
F_{Val} (g_{COD} Val/g_{COD} AA)	0.26	0.26	0.26	0.26	0.26	0.26	0.26	0.26	0.29
F_{H2} (g_{COD} H_2/g_{COD} AA)	0.06	0.06	0.06	0.06	0.07	0.08	0.09	0.08	0.07

Table A7.4. Simulated stoichiometric factors for 10 g/L gelatine fermentation in a continuous reactor at different pH values.

	Reactor pH								
	5.0	**5.5**	**6.0**	**6.5**	**7.0**	**7.5**	**8.0**	**8.5**	**9.0**
F_{Ac} (g_{COD} Ac/g_{COD} AA)	0.29	0.29	0.50	0.50	0.50	0.50	0.50	0.50	0.49
F_{Pro} (g_{COD} Pro/g_{COD} AA)	0.16	0.16	0.16	0.16	0.16	0.16	0.16	0.16	0.16
F_{But} (g_{COD} But/g_{COD} AA)	0.34	0.34	0.11	0.11	0.11	0.11	0.11	0.11	0.12
F_{Val} (g_{COD} Val/g_{COD} AA)	0.16	0.16	0.16	0.16	0.16	0.16	0.16	0.16	0.16
F_{H2} (g_{COD} H_2/g_{COD} AA)	0.05	0.05	0.07	0.07	0.07	0.07	0.07	0.07	0.07

Table A7.5. Simulated stoichiometric factors for 10 g/L casein fermentation in a continuous reactor at different pH values.

	Reactor pH								
	5.0	**5.5**	**6.0**	**6.5**	**7.0**	**7.5**	**8.0**	**8.5**	**9.0**
F_{Ac} (g_{COD} Ac/g_{COD} AA)	0.18	0.18	0.22	0.24	0.27	0.33	0.31	0.30	0.29
F_{Pro} (g_{COD} Pro/g_{COD} AA)	0.11	0.11	0.13	0.11	0.11	0.10	0.12	0.14	0.14
F_{But} (g_{COD} But/g_{COD} AA)	0.36	0.37	0.30	0.30	0.26	0.20	0.19	0.19	0.18
F_{Val} (g_{COD} Val/g_{COD} AA)	0.30	0.29	0.29	0.29	0.30	0.30	0.30	0.30	0.31
F_{H2} (g_{COD} H_2/g_{COD} AA)	0.05	0.05	0.06	0.06	0.06	0.07	0.07	0.08	0.07

7.7.5. SBR case study

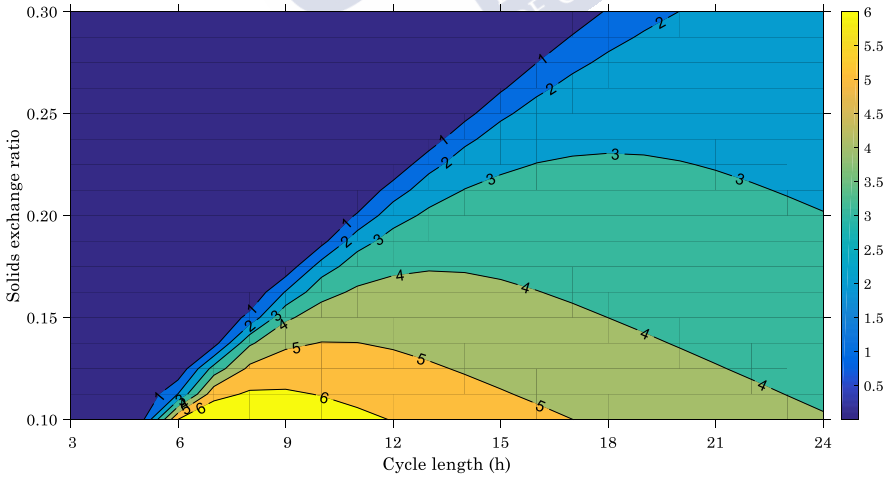

Figure A7.10. Casein fermentative biomass concentration (g_{COD}/L) at pH 7.

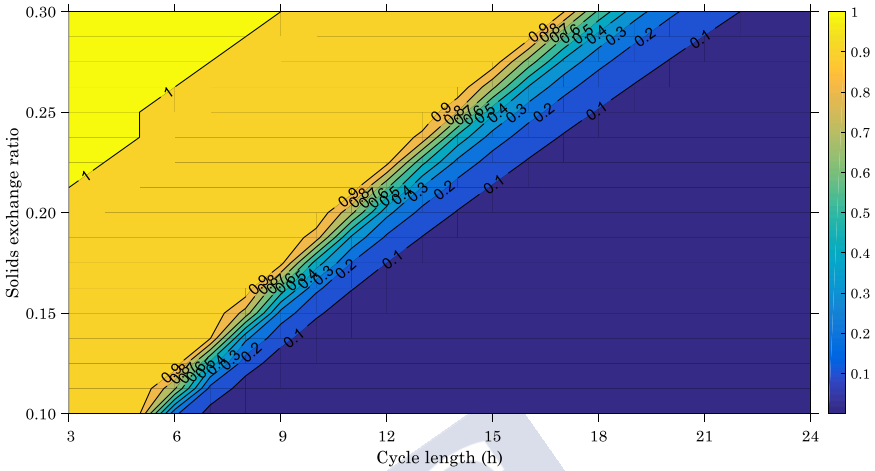

Figure A7.11. Fraction of non-consumed amino acids in casein fermentation at pH 7.

USC
UNIVERSIDADE
DE SANTIAGO
DE COMPOSTELA

CHAPTER 8

General discussion and conclusions

USC
UNIVERSIDADE
DE SANTIAGO
DE COMPOSTELA

8.1. GENERAL AND SPECIFIC CONCLUSIONS

The biorefinery carboxylate platform concept is set to become an important agent in the shift towards a more circular economy. In this production scheme, the substrates (ideally organic wastes) are transformed by mixed-culture anaerobic fermentations to short carboxylates, which are transformed in subsequent process to the final products of the biorefinery. One of the main issues deterring the establishment of the carboxylate platform biorefinery is the often low and variable product selectivity of anaerobic fermentations. The product spectrum is substantially influenced by environmental conditions and feeding characteristics without a clear, systematic and mechanistic interpretation (Chapter 1).Therefore, the development of predictive tools for a mechanistic understanding of the stoichiometry of anaerobic fermentations and for the design of processes with a high productivity of the desired product(s) has been the main objective of this thesis.

Carbohydrates constitute the most relevant substrates for fermentation and predicting accurately the stoichiometry of glucose conversion into VFA is essential in the development of biorefineries. A comprehensive metabolic understanding and description was achieved in Chapter 3 by including a novel biochemistry mechanism, electron bifurcation, in the metabolic network. An important product of carbohydrate rich biomass fermentation is lactic acid, which can only be produced at some specific conditions by MCF. The mathematical model developed in Chapter 4 incorporating concepts from the resource allocation theory, provided mechanistic understanding of lactate production from glucose in MCF only occurring under very specific environmental conditions.

The mathematical models developed in this thesis allow the prediction of the stoichiometry of protein MCF (Chapter 5) and of protein and carbohydrates mixed-culture co-fermentation (Chapter 6). The observed changes in product spectrum were mechanistically explained using the developed models. The predictive tools developed throughout the thesis have a direct utility as design tools and already allowed to identified strategies for controlling and directing product selectivity.

Focusing more on a process design perspective, a kinetic model for protein MCF was developed in Chapter 7. In this work, the link between operational conditions and kinetic behaviour of the fermentation processes was studied and

a guideline was proposed to choose the most appropriate kinetic parameters for the fermentation of proteins at different pH values. The predictive tools developed in this thesis have a strong potential to be used in design methodologies that may pave the way for the establishment of biorefinery as a sound and economically attractive production scheme.

In the introduction chapter of this thesis, broad research questions were identified according to the main objective to guide the research. In the following subsections, the specific conclusions of this thesis answering those questions are presented and discussed.

8.1.1. Substrate composition influences MCF outcome

One of the objectives of this thesis was to understand the effect of substrate composition on the outcome of MCF. In the case of proteins, the main goal was to understand mechanistically the differences in product spectrum when consuming different proteins and in cofermentation with glucose. Also, the effect of fermenting different proteins on the kinetics of the process was of interest for a process design perspective. Although there are models that predict how the glucose MCF product spectrum changes with operational conditions, the stoichiometry at some conditions is still not correctly predicted and does not reproduce the experimental observations.

The biochemical mechanism of electron bifurcation (EB) was proved in Chapter 3 as necessary to understand and describe accurately the observed glucose MCF stoichiometry (Mohd-Zaki et al., 2016; Temudo et al., 2007). Using a methodology based on performing NADH balances of experimental data sets, the results show that including EB mechanism in the butyrate pathway leads consistently to better NADH balance results (i.e. closer to zero). As the butyrate formation pathway (reverse beta oxidation) is always the same regardless of the initial substrate (i.e. it always starts from pyruvate), EB should be considered not only in glucose MCF but also in the butyrate-formation pathways coming from AA or other substrates. In consequence, butyrate pathways in the protein bioenergetic models (Chapter 5 and Chapter 6) included one description considering the EB mechanism. Including EB mechanism in glucose MCF implies that the H_2 to CO_2 ratio in the gas phase is no longer equimolar, since there is an additional H_2 production in the butyrate pathway (Buckel and Thauer, 2013).

It is obvious that the product spectrum of protein monofermentation is tightly related to its composition on AA, as each AA has a particular conversion stoichiometry. However, the bioenergetic model for protein MCF developed in Chapter 5 also showed that some AA interact with one another. Therefore, if the relative abundancies of the AA change, it is likely that the interaction will also be modified and consequently, the conversion stoichiometry of the involved AAs. The interactions were mechanistically identified, being the NADH conservation constraint of the model the main factor determining the interactions among AA. Those AA that produce NADH in their conversion compete or collaborate with other AA that produce or consume NADH, respectively. For example, the model results show that at pH 5.3 in gelatine fermentation, the glutamate most favourable conversion is the NADH-consuming production of n-butyrate, but not all glutamate follows this route since proline is competing for the needed NADH. The model predicts an equilibrium between the two NADH consuming reactions ruled by the marginal ATP production with respect to NADH consumption (i.e. the relative ATP production with respect to the NADH consumed). In the case of a higher glutamate abundance in the AA profile, its equilibrium with proline would likely be altered with the result of more n-butyrate being yielded from glutamate.

In cofermentation scenarios, the AA conforming a protein also interact with the cosubstrates, as shown in Chapter 6 for glucose and protein cofermentation. As for the interactions among AA, the consumption and production of NADH is the principal mechanism of interaction between the substrates and allows to explain the model predictions and the experimental data. The ratio between glucose and protein concentration in the feeding especially affected glucose and individual AA conversion stoichiometries and inflicted a similar or greater influence than pH in the product spectrum of cofermentation simulations as shown in Figure 8.1.

The fermented protein also proved to exert an influence on the kinetic behaviour protein MCF (Chapter 7). The estimated kinetic parameters using of two proteins, casein and gelatine, show indeed that overall casein fermentation is a faster process both in terms of uptake and biomass growth. The fate of lipids in anaerobic fermentation was not studied in this thesis. Extending the modelling framework presented in this thesis to lipids will greatly increase the applications of the present work.

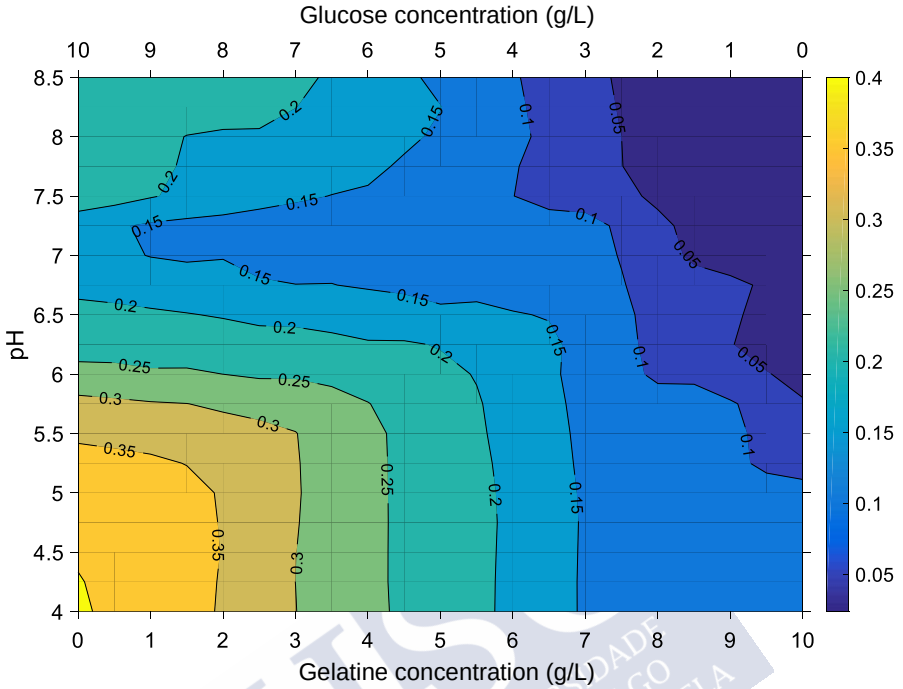

Figure 8.1. Predicted *n*-butyrate yield ($g_{VFA}/g_{Substrate}$) at different pH values (vertical axis) and at different glucose and gelatine concentrations in the feeding (horizontal axis). Areas with vertical contour lines show only dependency with the cosubstrate proportions and areas with horizontal contour lines show only dependency with the pH.

In summary, regarding the influence of substrate composition (AA profile and cosubstrates proportions) on the outcome of MCF, the work conducted in this thesis concludes that:

- EB is necessary to describe butyrate formation in glucose MCF and highlighted the importance of considering HA when predicting the yields of H_2 and CO_2.
- The cosubstrates in a cofermentation scenario interact with one another. Their relationship is strongly influenced by the NADH conservation constraint and the relative production of ATP by NADH consumed.
- The fermentation of a protein can be thought as a cofermentation of a number of AA. The relative abundances of AA (i.e. the AA profile of the protein) influence the individual AA conversion stoichiometries

since AA may interact with each other, mainly through NADH consumption and production.

- The kinetic behaviour of protein MCF is also dependant on the AA profile. The estimated kinetic parameters systematically indicate that casein fermentation is a faster process than gelatine fermentation.

8.1.2. Operational conditions determine the product spectrum of MCF

Operational conditions are known to affect substantially the product spectrum of MCF. For glucose MCF, the effect of the reactor pH is well documented and mechanistically interpreted but the effect of other parameters is still not fully understood. It is known that lactate production is fostered at high organic loadings or in discontinuous reactors, but the reasons are not fully understood yet. In the case of protein fermentation or cofermentation, the effect of pH on product selectivity was only described in experimental works. However, to build predictive tools a deeper and mechanistic knowledge is required.

The model developed in Chapter 4 incorporating concepts from the resource allocation theory proposed a mechanistic explanation for lactate production only occurring under specific conditions (discontinuous reactor and rich cultivation medium containing peptides and vitamins(Rombouts et al., 2020)). The model identified that the typical auxotrophy for amino acids of lactic acid bacteria (LAB) is a competitive advantage as allows them to attain a higher maximum specific growth rate even though lactate has a lower ATP yield than the other possible products. In consequence, those environments that select for fast growing microorganisms (i.e. with high substrate concentrations), as in batch reactors or a CSTR operated at high dilution rates, LAB are likely to dominate the microbial community with mainly lactate as product. Under other conditions, as in a low dilution rate CSTR in which the substrate residual concentration is kept low, the expected product spectrum follows the ATP maximisation perspective and is formed by the usual short carboxylates (i.e. butyrate, acetate or ethanol). Therefore, besides the reactor pH, the reactor configuration (i.e. discontinuous or continuous operation) has also a strong influence in the product spectrum of glucose MCF as it modifies which evolutive advantage prevails.

The effect of pH on the product spectrum was thoroughly studied in Chapter 5 and Chapter 6 using the bioenergetic models developed for protein mono and cofermentation with carbohydrates. The results undoubtedly indicate that conversion stoichiometry is strongly conditioned by this operational parameter

in both cases, as already suggested by the experimental information (Breure et al., 1986a; Breure and van Andel, 1984). In general terms, acidic pH values favour the production of n-butyrate while being detrimental to acetate production. Going from neutral to alkaline pH values has only a slight effect in protein monofermentation and has a limited effect in cofermentation scenarios. The yielding of other reduced VFA, such as isovalerate or propionate, may also be enhanced at acidic pH, but it depends on the AA profile of the protein and/or the cosubstrates ratio.

The bioenergetic models allowed for the mechanistic understanding of the pH effect on product spectrum of MCF. Cells create an electric and proton concentration gradient across their membranes and logically the energetics of this gradient are affected when the extracellular proton concentration varies. Consequently, the energetics of the processes related with proton transport across the membrane (charged species transport and proton translocations) are impacted. The energy related with proton translocations (i.e. the proton motive force, pmf) increases at acidic pH values, which means that reactions involved with a proton translocation are favoured since they allow the cell to conserve more energy in form of ATP. In the metabolic network there are protons translocations associated mainly with n-butyrate production (e.g. in the conversion of glutamate or glucose), which explains why this product is favoured under acidic conditions. Section 2.2.4.6 features in detail the pmf dependence with the external pH and how cells conserve energy from proton translocations.

Apart from influencing the stoichiometry of VFA production, the reactor pH also modifies the kinetics of protein MCF (Chapter 7). The estimated kinetic parameters show that independently of the protein, the process is faster at neutral pH values while alkaline and particularly acidic conditions slow the protein uptake rate.

Therefore, regarding the influence of the operational conditions of MCF, the following aspects can be concluded:

- The reactor configuration (i.e. discontinuous or continuous operation) has a strong impact on microbial selection in glucose MCF. Discontinuous reactors favour the presence of LAB as they can developed a higher uptake rate of the substrate. On the contrary, CSTR favour the presence of ATP efficient bacteria leading to product spectra dominated by acetate, butyrate or ethanol.

- The reactor pH exerts a strong influence in the product spectrum in MCF favouring generally the yield of n-butyrate at acidic conditions for glucose and gelatine mono- and co-fermentation. The mechanism responsible for this changed was identified to be the increase in the energy conserved by cells via proton translocations at low reactor pH values.
- The kinetics of protein conversion to VFA are also influenced significantly by the pH. Independently of the protein, faster consumption rates are attained at neutral pH values while alkaline and particularly acidic conditions lead to slower acidification rates.

8.1.3. MCF selectivity can be controlled with design parameters

Given the strong link between some operational parameters with the product selectivity of MCF processes, one of the immediate questions was whether modifying the environmental conditions of the reactor is a suitable strategy for directing the process towards specific product(s).

In the case of glucose MCF, there are sufficient evidences in literature from an experimental and modelling perspective (González-Cabaleiro et al., 2015; Temudo et al., 2007) that the product spectrum can be shifted completely from butyrate and acetate production at acidic pH values to acetate and ethanol production at alkaline conditions. In the case of protein MCF, pH was shown to be the design parameter controlling mostly the product spectrum, but overall, its variability is narrower than in glucose MCF (Chapter 5). For instance, although n-butyrate yield is affected particularly by pH, it never dominates exclusively the product spectrum neither it disappears from it. The case of protein cofermentation with glucose is an intermediate case, in which the influence of pH on the product spectrum is more pronounced than in the monofermentation but not as important as in glucose monofermentation (Chapter 6).

Co-substrate blending in cofermentation scenarios is also a parameter with potential to control the product spectrum of MCF. The product spectrum can be varied independently of the reactor pH by adjusting the composition of the feeding in glucose and protein (Chapter 6). If n-butyrate is the desired product, the feeding should be rich in glucose. If other compounds are of interest such as propionate or acetate, mixtures richer in protein are then more adequate. In the case of protein monofermentation the variability of the product spectrum is not as high (e.g. acetate is always one of the main products) and the process

stoichiometry is defined to a great extent by the AA profile of the protein. The composition of the feeding (the individual AA concentrations and the carbohydrate to protein ratio in the feeding) could be tailored to target specific products in the process, given that a sufficient and varied quantity of wastes is available.

The reactor configuration proved to be an important parameter in glucose MCF in the resource allocation model of Chapter 4. According to the model results, discontinuous reactors favour the domination of the microbial community by LAB, given that peptides are available in the medium, while CSTR operated under conditions ensuring complete substrate consumption select for bacteria producing butyrate, acetate or ethanol, as in the experiments reported by Temudo et al. (2007). Accordingly, depending on the desired product, the feeding regime (SBR, batch or continuous) will be selected.

The conclusions of the resource allocation model (Chapter 4) are in line with studies regarding labour division or cross feeding (Kreft et al., 2020). In these works, it is proposed that dividing a conversion process in two microbial groups allows them to attain higher maximum substrate consumption rates than single microbial groups performing the complete conversion. From a resource allocation theory, it is also logical that microorganisms requiring a lower overall enzyme concentration (as they perform only a part of the conversion) are capable of developing higher maximum substrate consumption than microorganisms performing the complete conversion. Thus, in scenarios favouring fast growers (i.e. discontinuous processes), the two microbial groups dividing the labour will likely dominate the community. Actually, lactate production can be also considered an intermediate of a two-step VFA production process, as it can be consumed to yield other VFA such as acetate, propionate or butyrate by other microbial groups (Ohnishi, 2015; Rombouts et al., 2020).

From the results obtained in this thesis, the next conclusions can be stated regarding the possibility of controlling product selectivity in MCF:

- Three variables with potential to drive MCF to the production of the desired products were identified: reactor pH, substrate composition and reactor configuration (only explored in glucose MCF).
- The reactor pH is an attractive parameter to control product selectivity since it has an important effect in changing product spectrum and it is easy to manipulate in an experimental setup.

- Substrate composition also allows to shift the product spectrum with glucose favouring the production of n-butyrate and protein the yield of acetate and propionate in general terms. However, this strategy is constrained by the number and composition of cosubstrates available.
- Lactate production in glucose MCF is promoted only if the reactor is run discontinuously and peptides are present in the cultivation medium.
- In general, the NADH conservation constraint imposes a limit to the effect of the strategy above mentioned. Strategies relaxing this constraint would theoretically increase the flexibility to steer the production towards the desired products.

8.2. LIMITATIONS OF THE BIOENERGETIC MODELS

8.2.1. Enzyme soup approach

The bioenergetic models developed in this thesis describe the mixed microbial community following an *enzyme soup* approach, which ignores completely the boundaries between microbial groups performing the different metabolic of the community functions (Perez-Garcia et al., 2016). One of its main implications is that all metabolites are shared among the community members and that the conservation constraints of intracellular moieties (e.g. NADH) are fulfilled considering all metabolic reactions altogether. Assuming a virtual microorganism capable of all functions is a way of placing boundaries on the metabolic capacity of the mixed culture (Biggs et al., 2015), which was our intention.

However, it is very likely that the real microbial community in a fermentation does not share all metabolites and that not all substrates can be metabolised by all members. Therefore, the predicted interactions among substrates via NADH (both among AA and AA with glucose) are likely to be overpredicted. For example, if AA would be degraded in groups, it could the case that the some of the AA predicted to interact in Chapter 5 at acidic pH, such as glutamate and proline, did not interact at all and did not compete for NADH. The strong interactions between some AAs as glutamate and glucose could also be affected if the microorganism using glutamate does not consume glucose.

In both cases, the results of the model would certainly be affected (Figure 8.2). Proline as a result of the NADH competition with glutamate was predicted to be consumed partially and glutamate was only converted partially to n-butyrate even though it was the most favourable conversion in terms of ATP. If these two AA

did not compete for NADH, they could be completely consumed or converted to n-butyrate, respectively, given that other AA providing AA are present.

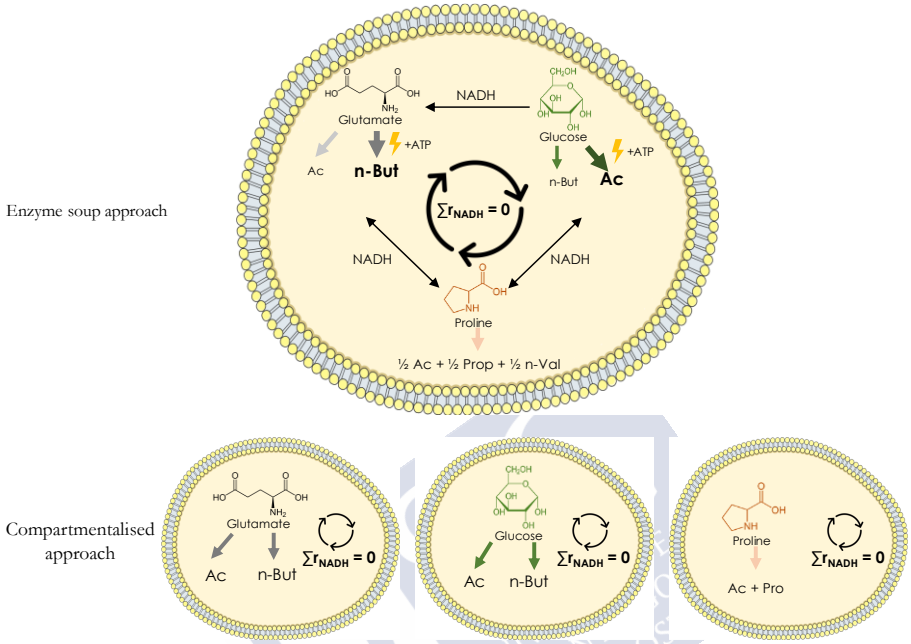

Figure 8.2. Interactions among substrates and their effect in the product spectrum in an enzyme soup approach (upper figure) and in a compartmentalised approach (bottom figures). In the enzyme soup approach, NADH is shared among the substrates and therefore the individual substrates can be transformed through the most energetic pathways (indicated with a lighting), while in the compartmentalised approach, NADH is not share among substrates and substrates cannot be channelled as much through the most energetic pathways.

In the case of glucose and protein cofermentation, part of the NADH produced in glycolysis is predicted to be absorbed by the conversion of glutamate to n-butyrate, even though it is not the most favourable pathway in terms of ATP. In case of a compartmentalised approach, glucose pathways would have to consume all the NADH produced in glycolysis and as a result glucose would yield less acetate.

To model more accurately the conversion of the substrates, microbiological and genetic information is needed to determine the species present and their metabolic capacities. In this way, the substrates (i.e. AA and glucose) can be grouped in clusters that are converted together and hence limit the substrates

that share metabolites, as NADH. However, this knowledge was not available at the moment of developing the metabolic models.

Moreover, the aim of these models was certainly to explore the metabolic capacity of a functionally diverse microbial community and how its catabolism is impacted by modifications in the environmental conditions. Even though the enzyme soup approach has certain limitations, we believe that it is the most adequate approach considering the model objective. Our vision is that the purpose of these models is to be used in the early-stage design of MCF or to provide guidelines on how to operate MCF reactors aiming at specific products and not as fine-tuning models.

8.2.2. Optimisation strategy

Other of the model main assumptions of the bioenergetic models how to translate into mathematical language the microbial community criterion to select which products are yielded. The approach followed assumes that the fittest microorganisms are those producing the compounds related with a higher ATP yield per unit of substrate. This approach only focuses in bioenergetic terms and implicitly assumes that the most efficient microorganisms will outcompete others in the microbial community. Accordingly, the parameters related with the uptake rate (i.e. the maximum uptake rate and the affinity constant) are set equal for the different substrates, meaning that the actual uptake rate only depends on the substrate concentration and all substrate can potentially be consumed at the same rate. Previous bioenergetic models that simulated with success glucose MCF in CSTR used this approach (González-Cabaleiro et al., 2015). Also, the results of the models of Chapter 5 and Chapter 6 on the stoichiometry of protein mono- and co-fermentation in a CSTR reproduced satisfactorily experimental results.

However, this approach might not be completely adequate for describing the stoichiometry when the reactor configuration is not a CSTR. For example, the production of lactate from glucose observed mainly in discontinuous fermenters would never be predicted following the ATP maximisation perspective, as lactate ATP yield is clearly inferior to other alternatives. The model developed in Chapter 4 showed that for correctly predicting lactate production in the conditions experimentally reported, other arguments related with the kinetics of the system must be also included. Being energy efficient in conditions of substrate excess appears not be enough and the focus is shifted towards being effective (i.e. fast) in consuming the substrate.

The conclusion is that the ATP yield optimisation perspective is well suited for substrate-limited conditions as typically found in well operated CSTRs. However, the use of the bioenergetic models of this thesis should be limited to CSTRs and extrapolation to other reactor configurations must be done cautiously, as the evolutive adaptation may select other dominant product spectra.

8.3. IMPLICATIONS OF THIS THESIS FOR PROCESS DESIGN

The mathematical models developed in this thesis had as main objective understanding the mechanisms governing MCF processes. However, they also have the potential to be process design tools, as discussed in their respective chapters and as well in the general and specific conclusions of the thesis. This section shows firstly how this work is integrated in a wider project, in second place some identified enhanced processes to have a higher control of the selectivity of the process are discussed and finally the process design potential of the work conducted in this thesis. As a proof of concept, a methodology for the early-stage design of processes producing VFA from proteins-rich wastes is proposed.

8.3.1. The BIOCHEM project

The work of this thesis was partially carried out in the context of the ERA-IB project BIOCHEM (Novel BIOrefinery platform methodology for a drive production of CHEMicals from low-grade biomass). The main objective of this project is to develop a model-aided methodology for designing bioprocesses using mixed microbial communities. In particular, the aim is to design processes with a high selectivity for the desired products and that achieve a high productivity to make the system economically feasible.

In this framework, the predictive tools developed in this thesis are envisioned to be a pillar of the BIOCHEM design methodology. Additionally, experimental data is being generated in MCF systems with a two-fold objective: to validate and refine the models developed in the project and to participate in the design methodology as described in Chapter 7. The design methodology is complemented in the project with in-situ product removal techniques to increase the productivity and also the possibility of engineering microbial communities (composed of associations of defined pure cultures) to maximise the yield of the desired products is studied and incorporated in the methodology.

8.3.2. Enhanced process configurations

In the conclusions, it was stated that that some operational variables (e.g. the reactor pH or substrate composition) have the potential to steer the product spectrum towards specific products. However, for all cases, the NADH conservation constraint, intrinsic to anaerobic fermentations, limits the extent to which the product spectrum can be steered by the pH or the substrate composition. For example, even though, the n-butyrate production from glutamate with concomitant NADH consumption is favoured in terms of ATP production at acidic pH, not all the glutamate can be directed towards butyrate production since not enough NADH is available (Chapter 5, section 5.3.3.2). Alternatively, glucose conversion to acetate is the preferred option for its high ATP yield but glucose can only be shifted completely to acetate at very high protein to glucose ratio, as only under these conditions protein consuming reactions can accommodate the NADH production related with glucose. This analysis suggests the possibility of altering artificially the NADH balance for achieving increased flexibility of the product spectrum. Additional electrons (i.e. NADH) can be pushed into the system with a cathode or indirectly via H_2, which can be either injected or produced in-situ electrochemically. In this way, to close the NADH balance, reactions consuming it (e.g. glutamate production of n-butyrate) will be favoured to absorb the additional reductive power. Conversely, if the objective is to shift the production towards acetate, an anode withdrawing reductive power from the system would theoretically promote reactions that are net producers of reductive power (i.e. NADH) such as glucose conversion to acetate.

The reactor configuration was proved to have a strong influence in the product spectrum of glucose MCF and it was concluded that discontinuous reactor configuration promote the production of lactate. Since this compound is a chain elongation promotor (Kucek et al., 2016), processes aiming at the production of medium chain fatty acids could be designed. A carbohydrate-rich waste would be converted to lactate in an SBR and then mixed with other wastes in a second reactor operated continuously. In this way, the short carboxylates produced by the fermentation of the second waste could be elongated to high-value compounds such as caproate or valerate.

8.3.3. Early-stage bioprocess design methodology

Here a methodology for the early-stage design of bioprocesses is presented with the aim of providing guidelines for defining the stoichiometry and for selecting the kinetic parameters to simulate the MCF of a given substrate(s) or mixture of them at a particular pH value. This methodology combines the use of predictive tools and experimental information, which is used to estimate the characteristic kinetic parameters of a system and is also stored in libraries to be used directly in the methodology.

The application of this methodology is generic but as the predictive tools developed in this thesis and the experimental information used focused in protein, the description of the methodology is centred in the process of protein MCF. However, the models can also be applied to other systems. The bioenergetics models for stoichiometry prediction are first-principle and therefore they have few parameters that are case-specific. In the case of the kinetic model, to be applied to other systems they only need a new set of parameters that can be found in literature or estimated from experimental information.

The first aspect covered by this methodology is how to simulate a novel bioprocess. In first place, the stoichiometry of the system is defined (Figure 8.3). If no experimental information is available for the desired protein, the stoichiometric coefficients should be predicted by the bioenergetic model. In the case it is suspected that the AA profile of the protein is significantly different than the protein in the library (even though they might have the same name), or if the substrate of the system is organic waste composed by unknown protein(s), the bioenergetic model should be also used. In all cases, the AA composition of the substrate must be determined as it is an input of the model. In the case that experimental information is available for the desired protein, the stoichiometry library should be used. The parameters for the desired pH value should be selected and in case this information is not available two options are possible: either interpolation, if the closest values are not very distinct, or using the bioenergetic model.

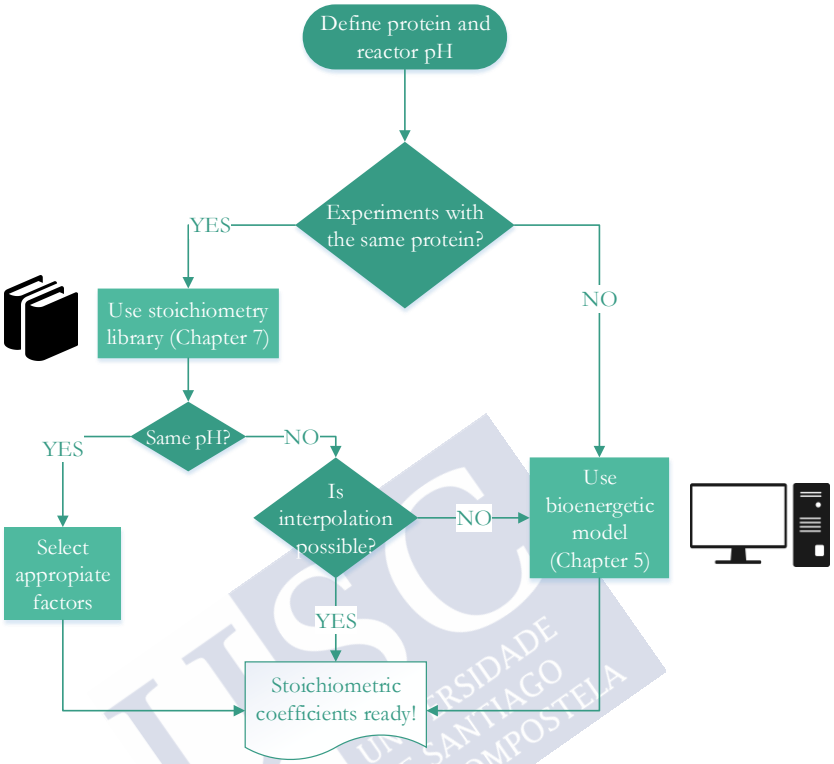

Figure 8.3. Flowchart for selecting the appropriate stoichiometric coefficients in the proposed design methodology.

Once the stoichiometric coefficients are set, the kinetic parameters need to be selected (Figure 8.4). As for the stoichiometry determination, using information stored in the kinetic library is preferred if it is available for the protein. If there is no available information for the selected pH of the system, the value of some kinetic parameters (e.g. maximum uptake rate or biomass yield) should be corrected, for example, with inhibition functions as proposed in Chapter 7.

In the case that the protein is different to the proteins of the library, or with a very distinct AA profile, the general values for kinetic values provided in Chapter 7 should be used as a starting value. In this case, it is recommended to perform experiments to validate and refine the model predictions both in terms of stoichiometry prediction and kinetics description.

The stoichiometric and kinetic libraries are expected to grow over time as they will incorporate the information generated in the experiments performed for

validating the model and for estimating kinetic parameters for other substrates under other operational conditions.

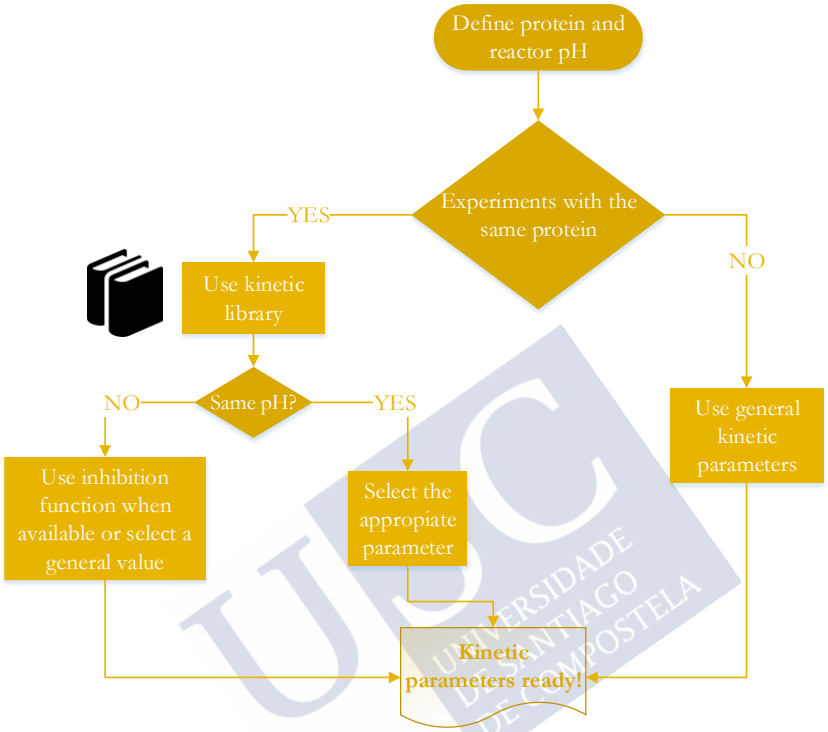

Figure 8.4. Flowchart for selecting the appropriate kinetic parameters in the proposed design methodology

The proposed methodology could also be used with design purposes, i.e. there is a targeted product and the substrate (e.g. a combination or organic wastes) and operational conditions need to be defined. Firstly, if there is information in the stoichiometry library regarding the potential proteins, the values are explored and the protein and the pH value are selected to ensure the highest stoichiometric coefficient possible for the desired products. If the stoichiometry library does not contain information for the available proteins, the bioenergetic model should be used to explore the operational space both in terms of pH and of possible substrate mixtures. Finally, once the substrate and pH value are defined, the appropriate kinetic parameters are selected accordingly using the flowchart of Figure 8.4.

8.4. FUTURE PERSPECTIVES ON COMPUTER-AIDED DESIGN

In this general discussion, the most immediate applications for process design of the models developed were discussed and condensed together in a bioprocess design methodology to serve as a starting point for designing protein MCF processes. We consider that integrating mathematical models with information gathered in expressly designed experiments is a very valid and sound approach that should be followed in bioprocess design methodologies. The development of the different kinds of model (e.g. bioenergetic or kinetic) should be done in parallel with experimental data generation to feed each other in a loop of information, as schematically described in Figure 8.5 as an example.

Experiments would provide information for developing and calibrating kinetics models (as done in Chapter 7) or would help in other modelling tasks such as building the metabolic network of a new substrate or refining model hypotheses. For example, microbiological and proteomic tests of the microbial community can help to analyse deeper the system. Knowing which microorganisms are present or which functions can be performed by the community may be of good help to describe accurately the microbial community in the models. Expressly design experiments with isotope labelled substrates would provide an excellent source of information for determining the metabolic pathways of a substrate.

Models have the potential of providing a good understanding of the system and therefore may help to identify mechanisms that are not obvious from a first analysis of the experimental data. In this sense, different operational conditions could be identified with model simulations that maximise a desired outcome of the system (e.g. maximisation of the yield of a compound or selection of a specific guild of microorganisms). For example, in a process performed by an engineered mixture of pure microbial species, the optimal inoculum volume of the different species could be set with the help of model simulations. Similarly, different ratio of co-substrates in a co-fermentation could be tested *in silico* and optimised depending on the desired product.

Also, additional experiments can be proposed in cases where not all the mechanisms or kinetic parameters can be estimated in a single round of experiments. A system with intermediate compounds that accumulate in the reactor, as for instance glucose conversion to VFA via lactate, is a good example of a process difficult to model, as the kinetic behaviour of the intermediate, lactate, is the result of two processes. In this case, for example, an experiment

with a lactate pulse at a specific time, determined by simulation, would help to have a better description of the process. Also, an exogenous additional of lactate could alter the product selectivity of the processes and this strategy could be optimised with the models to steer the product spectrum.

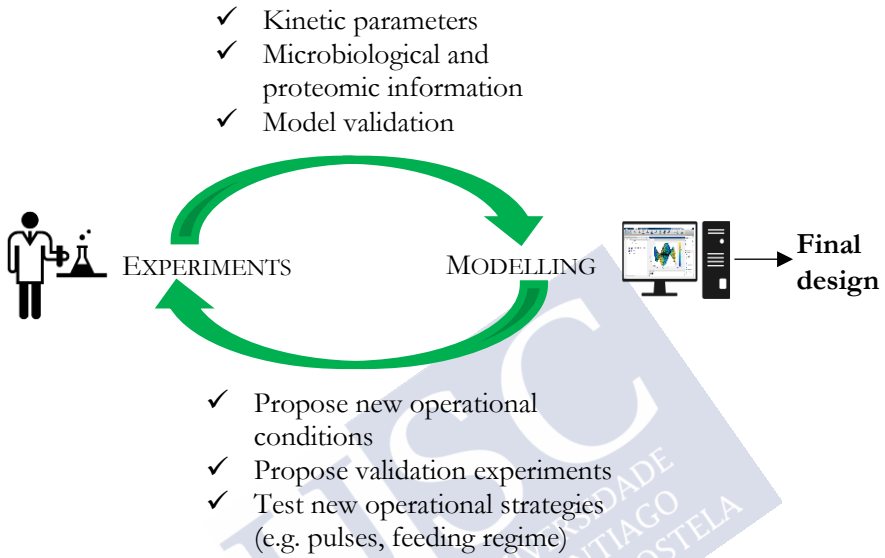

Figure 8.5. Proposed information flows between experimental information and model development in the envisioned design methodology.

This methodology has the additional advantage of continuous improving the accuracy of the model predictions, as with each new operational condition or strategy proposed, the model is tested in a different environmental condition. In this way, it is avoided that both the model and the experimental setup are centred in a very concise region of the environmental conditions space.

The examples of strategies given before would be a result of using the modelling tools and it is very likely that without using models they would not be envisioned. Likewise, the additional rounds of experiments would provide the needed confirmation and the opportunity to keep refining the model and of finding new strategies to accomplish the design objective. The strategies sketched here are just an example of the potential we envision of a design methodology that combines the richness of the experimental information with the power of predictive tools.

REFERENCES

USC
UNIVERSIDADE
DE SANTIAGO
DE COMPOSTELA

Agler, M.T., Wrenn, B.A., Zinder, S.H., Angenent, L.T., 2011. Waste to bioproduct conversion with undefined mixed cultures: the carboxylate platform. Trends Biotechnol 29, 70–78.

Alberty, R.A., 2010. Biochemical thermodynamics and rapid-equilibrium enzyme kinetics. J. Phys. Chem. B 114, 17003–17012.

Alberty, R.A., 2006. Biochemical Thermodynamics: Applications of Mathernatica. Wiley, Hoboken.

Alibardi, L., Cossu, R., 2016. Effects of carbohydrate, protein and lipid content of organic waste on hydrogen production and fermentation products. Waste Manag. 47, 69–77.

Alkaya, E., Kaptan, S., Ozkan, L., Uludag-Demirer, S., Demirer, G.N., 2009. Recovery of acids from anaerobic acidification broth by liquid-liquid extraction. Chemosphere 77, 1137–1142.

Alves de Oliveira, R., Komesu, A., Vaz Rossell, C.E., Maciel Filho, R., 2018. Challenges and opportunities in lactic acid bioprocess design—From economic to production aspects. Biochem. Eng. J. 133, 219–239.

Alves, M.M., Pereira, M.A., Sousa, D.Z., Cavaleiro, A.J., Picavet, M., Smidt, H., Stams, A.J.M., 2009. Waste lipids to energy: How to optimize methane production from long-chain fatty acids (LCFA). Microb. Biotechnol. 2, 538–550.

Andreesen, J.R., 1994. Glycine metabolism in anaerobes. Antonie Van Leeuwenhoek 66, 223–237.

Andreesen, J.R., Bahl, H., Gottschalk, G., 1989. Introduction to the Physiology and Biochemistry of the Genus Clostridium, in: Clarke, N.P.M. and D.J. (Ed.), Clostridia. Springer Science + Business Media New York, pp. 27–62.

Angelidaki, I., Ellegaard, L., Ahring, B.K., 1999. A comprehensive model of anaerobic bioconversion of complex substrates to biogas. Biotechnol. Bioeng. 63, 363–372.

Angenent, L.T., Karim, K., Al-Dahhan, M.H., Wrenn, B.A., Domíguez-Espinosa, R., 2004. Production of bioenergy and biochemicals from industrial and agricultural wastewater. Trends Biotechnol 22, 477–485.

Angenent, L.T., Kleerebezem, R., 2011. Crystal ball. Microb. Biotechnol. 4, 109–137.

Arslan, D., Steinbusch, K.J.J., Diels, L., Hamelers, H.V.M., Strik, D.P.B.T.B., Buisman, C.J.N., De Wever, H., 2016. Selective short-chain carboxylates production: A review of control mechanisms to direct mixed culture fermentations. Crit. Rev. Environ. Sci. Technol. 46, 592–634.

Atasoy, M., Owusu-Agyeman, I., Plaza, E., Cetecioglu, Z., 2018. Bio-based volatile fatty acid production and recovery from waste streams: Current status and future challenges. Bioresour. Technol. 268, 773–786.

Bachmann, H., Molenaar, D., Branco dos Santos, F., Teusink, B., 2017. Experimental evolution and the adjustment of metabolic strategies in lactic acid bacteria. FEMS Microbiol. Rev. 41, S201–S219.

Bai, J., Liu, H., Yin, B., Ma, H., 2015. Modeling of enhanced VFAs production from waste activated sludge by modified ADM1 with improved particle swarm optimization for parameters estimation. Biochem. Eng. J. 103, 22–31.

Bai, J., Liu, H., Yin, B., Ma, H., Chen, X., 2017. Modified ADM1 for modeling free ammonia inhibition in anaerobic acidogenic fermentation with high-solid sludge. J. Environ. Sci. (China) 52, 58–65.

Baldwin, S.A., Perham, R.N., Stribling, D., 1978. Purification and characterization of the class-II D-fructose 1,6-bisphosphate aldolase from Escherichia coli (Crookes' strain). Biochem. J. 169, 633–641.

Bar-Even, A., Flamholz, A., Noor, E., Milo, R., 2012. Thermodynamic constraints shape the structure of carbon fixation pathways. Biochim. Biophys. Acta - Bioenerg. 1817, 1646–1659.

Barker, H.A., 1981. Amino Acid Degradation by Anaerobic Bacteria. Annu. Rev. Biochem. 50, 23–40.

Barker, H.A., D'Ari, L., Kahn, J., 1987. Enzymatic reactions in the degradation of 5-aminovalerate by Clostridium aminovalericum. J. Biol. Chem. 262, 8994–9003.

Basan, M., Hui, S., Okano, H., Zhang, Z., Shen, Y., Williamson, J.R., Hwa, T., 2015. Overflow metabolism in Escherichia coli results from efficient proteome allocation. Nature 528, 99–104.

Bastidas-Oyanedel, J.R., Bonk, F., Thomsen, M.H., Schmidt, J.E., 2015. Dark fermentation biorefinery in the present and future (bio)chemical industry. Rev. Environ. Sci. Biotechnol. 14, 473–498.

Bastidas-Oyanedel, J.R., Schmidt, J.E., 2018. Increasing profits in food waste biorefinery-a techno-economic analysis. Energies 11.

Batstone, D.J., Keller, J., Angelidaki, I., Kalyuzhnyi, S. V., Pavlostathis, S.G., Rozzi, A., Sanders, W.T.M., Siegrist, H., Vavilin, V.A., 2002a. Anaerobic Digestion Model No.1 (ADM1). IWA Publishing, London.

Batstone, D.J., Keller, J., Angelidaki, I., Kalyuzhnyi, S. V, Pavlostathis, S.G., Rozzi, A., Sanders, W.T., Siegrist, H., Vavilin, V.A., 2002b. The IWA Anaerobic Digestion Model No 1 (ADM1). Water Sci Technol 45, 65–73.

Bauer, E., Thiele, I., 2018. From Network Analysis to Functional Metabolic Modeling of Human Gut Microbiota. Nov. Syst. Biol. Tech. 3, e00209-17.

Berger, E.A., 1973. Different mechanisms of energy coupling for the active transport of proline and glutamine in Escherichia coli. Proc. Natl. Acad. Sci. U. S. A. 70, 1514–8.

Bevilacqua, R., Regueira, A., Mauricio-iglesias, M., Lema, J.M., Carballa, M., 2020a. Protein composition determines the preferential consumption of amino acids during anaerobic mixed-culture fermentation. Water Res. *Under review.*

Bevilacqua, R., Regueira, A., Mauricio-iglesias, M., Lema, J.M., Carballa, M., 2020b. Steering protein fermentation with pH to target the production of specific volatile fatty acids. *In preparation.*

Biddle, A.S., Leschine, S., Huntemann, M., Han, J., Chen, A., Kyrpides, N., Markowitz, V., Palaniappan, K., Ivanova, N., Mikhailova, N., Ovchinnikova, G., Schaumberg, A., Pati, A., Stamatis, D., Reddy, T., Lobos, E., Goodwin, L., Nordberg, H.P., Cantor, M.N., Hua, S.X., Woyke, T., Blanchard, J.L., 2014. The complete genome sequence of Clostridium indolis DSM 755T. Stand. Genomic Sci. 9, 1089–1104.

Biesterveld, S., Kok, M.D., Dijkema, C., Zehnder, A.J., Stams, A.J., 1994. D-xylose catabolism in Bacteroides xylanolyticus X5-1. Arch Microbiol 161, 521–527.

Biggs, M.B., Medlock, G.L., Kolling, G.L., Papin, J.A., 2015. Metabolic network modeling of microbial communities. Wiley Interdiscip. Rev. Syst. Biol. Med. 7, 317–334.

Bonnarme, P., Lapadatescu, C., Yvon, M., Spinnler, H.E., 2001. L-methionine degradation potentialities of cheese-ripening microorganisms. J. Dairy Res. 68, 663–674.

Bonnarme, P., Psoni, L., Spinnler, H.E., 2000. Diversity of L-Methionine catabolism pathways in cheese-ripening bacteria. Appl. Environ. Microbiol. 66, 5514–5517.

Booth, I.R., 1985. Regulation of cytoplasmic pH in bacteria. Microbiol. Rev. 49, 359–378.

Borodina, I., Nielsen, J., 2014. Advances in metabolic engineering of yeast Saccharomyces cerevisiae for production of chemicals. Biotechnol. J. 9, 609–620.

Bosdriesz, E., Molenaar, D., Teusink, B., Bruggeman, F.J., 2015. How fast-growing bacteria robustly tune their ribosome concentration to approximate growth-rate maximization. FEBS J. 282, 2029–2044.

Box, G.E.P., 1979. Robustness in the Strategy of Scientific Model Building, Robustness in Statistics. ACADEMIC PRESS, INC.

Box, G.E.P., 1976. Science and Statistics. J. Am. Stat. Assoc. 71, 791–799.

Breure, A.M., Beeftink, H.H., Verkuijlen, J., Andel, J.G. Van, 1986a. Acidogenic fermentation of protein / carbohydrate mixtures by bacterial populations adapted to one of the substrates in anaerobic chemostat cultures. Appl. Microbiol. Biotechnol. 23, 245–249.

Breure, A.M., Mooijman, K.A., van Andel, J.G., 1986b. Protein degradation in anaerobic digestion: influence of volatile fatty acids and carbohydrates on hydrolysis and acidogenic fermentation of gelatin. Appl. Microbiol. Biotechnol. 24, 426–431.

Breure, A.M., van Andel, J.G., 1984. Hydrolysis and acidogenic fermentation of a protein, gelatin, in an anaerobic continuous culture. Appl. Microbiol. Biotechnol. 20, 40–45.

Breure, A.M., van Andel, J.G., Burger-Wiersma, T., Guijt, J., Verkuijlen, J., 1985. Hydrolysis and acidogenic fermentation of gelatin under anaerobic conditions in a laboratory scale upflow reactor. Appl. Microbiol. Biotechnol. 21, 50–54.

Broer, S., kramer, R., 1990. Lysine uptake and exchange in Corynebacterium glutamicum. J. Bacteriol. 172, 7241–7248.

Buchanan, B.B., Arnon, D.I., 1970. Ferredoxins-chemistry and function in photosynthesis, nitrogen fixation, and fermentative metabolism, in: Adv Enzymol Relat Subj Biochem. Interscience Publishers, New York, pp. 119–176.

Buckel, W., 2001. Unusual enzymes involved in five pathways of glutamate fermentation. Appl. Microbiol. Biotechnol. 57, 263–273.

Buckel, W., 1998. Anaerobic Energy Metabolism, in: Joseph W. Lengeler, G.D. and H.G.S. (Ed.), Biology of the Prokaryotes. Blackwell Science Ltd, Oxford, UK, pp. 278–326.

Buckel, W., Barker, H.A., 1974. Two Pathways of Glutamate Fermentation by Anaerobic Bacteria. J. Bacteriol. 117, 1248–1260.

Buckel, W., Thauer, R.K., 2018. Flavin-based electron bifurcation, ferredoxin, flavodoxin, and anaerobic respiration with protons (Ech) or NAD+(Rnf) as electron acceptors: A historical review. Front. Microbiol. 9.

Buckel, W., Thauer, R.K., 2013. Energy conservation via electron bifurcating ferredoxin reduction and proton/Na+ translocating ferredoxin oxidation. Biochim. Biophys. Acta - Bioenerg. 1827, 94–113.

Bundhoo, M.A.Z., Mohee, R., 2016. Inhibition of dark fermentative bio-hydrogen production: A review. Int. J. Hydrogen Energy 41, 6713–6733.

Carballa, M., Regueiro, L., Lema, J.M., 2015. Microbial management of anaerobic digestion: exploiting the microbiome-functionality nexus. Curr. Opin. Biotechnol. 33, 103–111.

Carr, F.J., Chill, D., Maida, N., 2002. The lactic acid bacteria: A literature survey. Crit. Rev. Microbiol. 28, 281–370.

Carvajal-Arroyo, J.M., Candry, P., Andersen, S.J., Props, R., Seviour, T., Ganigué, R., Rabaey, K., 2019. Granular fermentation enables high rate caproic acid production from solid-free thin stillage. Green Chem. 21, 1330–1339.

Cavaleiro, A.J., Pereira, M.A., Guedes, A.P., Stams, A.J.M., Alves, M.M., Sousa, D.Z., 2016. Conversion of Cn-Unsaturated into Cn-2-Saturated LCFA Can Occur Uncoupled from Methanogenesis in Anaerobic Bioreactors. Environ. Sci. Technol. 50, 3082–3090.

Ceze, M., Fidkowski, K.J., 2015. Constrained pseudo-transient continuation. Int. J. Numer. Methods Eng. 102, 1683–1703.

Chen, Y., Jiang, S., Yuan, H., Zhou, Q., Gu, G., 2007. Hydrolysis and acidification of waste activated sludge at different pHs. Water Res. 41, 683–689.

Costa, E., Pérez, J., Kreft, J.U., 2006. Why is metabolic labour divided in

nitrification? Trends Microbiol. 14, 213–219.

D´Alessio, G., Josse, J., 1971. Glyceraldehyde Phosphate Dehydrogenase of Escherichia coli. J. Biol. Chem. 246, 4326–4333.

Dauner, M., Sauer, U., 2001. Stoichiometric growth model for riboflavin-producing Bacillus subtilis. Biotechnol. Bioeng. 76, 132–143.

Davila-Vazquez, G., Arriaga, S., Alatriste-Mondragón, F., de León-Rodríguez, A., Rosales-Colunga, L.M., Razo-Flores, E., 2008. Fermentative biohydrogen production: trends and perspectives. Rev. Environ. Sci. Bio/Technology 7, 27–45.

de Jong, E., Jungmeier, G., 2015. Biorefinery Concepts in Comparison to Petrochemical Refineries, Industrial Biorefineries and White Biotechnology. Elsevier B.V.

de Kok, S., Meijer, J., van Loosdrecht, M.C., Kleerebezem, R., 2013. Impact of dissolved hydrogen partial pressure on mixed culture fermentations. Appl Microbiol Biotechnol 97, 2617–2625.

de Vries, M.C., Vaughan, E.E., Kleerebezem, M., de Vos, W.M., 2006. Lactobacillus plantarum-survival, functional and potential probiotic properties in the human intestinal tract. Int. Dairy J. 16, 1018–1028.

Dennis, P.P., Bremer, H., 2008. Modulation of Chemical Composition and Other Parameters of the Cell at Different Exponential Growth Rates. EcoSal Plus 3.

Dharmadi, Y., Murarka, A., Gonzalez, R., 2006. Anaerobic fermentation of glycerol by Escherichia coli: A new platform for metabolic engineering. Biotechnol. Bioeng. 94, 821–829.

Dinamarca, C., Bakke, R., 2009. Apparent hydrogen consumption in acid reactors: observations and implications. Water Sci. Technol. 59, 1441–1447.

Dinamarca, C., Ganan, M., Liu, J., Bakke, R., 2011. H2 consumption by anaerobic non-methanogenic mixed cultures. Water Sci Technol 63, 1582–1589.

Driessen, A.J.M., Kodde, J., De Jong, S., Konings, W.N., 1987. Neutral amino acid transport by membrane vesicles of Streptococcus cremoris is subject to regulation by internal pH. J. Bacteriol. 169, 2748–2754.

Driessen, A.J.M., Van Leeuwen, C., Konings, W.N., 1989. Transport of basic

amino acids by membrane vesicles of Lactococcus lactis. J. Bacteriol. 171, 1453–1458.

Duong, T.H., Grolle, K., Nga, T.T.V., Zeeman, G., Temmink, H., Van Eekert, M., 2019. Protein hydrolysis and fermentation under methanogenic and acidifying conditions. Biotechnol. Biofuels 12, 1–10.

Dürre, P., 2008. Fermentative butanol production: Bulk chemical and biofuel. Ann. N. Y. Acad. Sci. 1125, 353–362.

Elbehti, A., Brasseur, G., Lemesle-Meunier, D., 2000. First evidence for existence of an uphill electron transfer through the bc1 and NADH-Q oxidoreductase complexes of the acidophilic obligate chemolithotrophic ferrous ion-oxidizing bacterium Thiobacillus ferrooxidans. J. Bacteriol. 182, 3602–3606.

Elsden, S.R., Hilton, M.G., 1978. Volatile acid production from threonine, valine, leucine and isoleucine by clostridia. Arch. Microbiol. 117, 165–172.

Excherichia, I.N., 1972. Mechanisms of Active Transport Bacterial Membrane Vesicles in Isolated. J. Biol. Chem. 248, 7858–7863.

Fang, H.H.P., Liu, H., 2002. Effect of pH on hydrogen production from glucose by a mixed culture. Bioresour. Technol. 82, 87–93.

Fang, H.H.P., Yu, H., 2002. Mesophilic acidification of gelatinaceous wastewater. J. Biotechnol. 93, 99–108.

Fernández, A., Huang, S., Seston, S., Xing, J., Hickey, R., Criddle, C., Tiedje, J., 1999. How stable is stable? Function versus community composition. Appl. Environ. Microbiol. 65, 3697–3704.

Fernández, F.J., Villaseñor, J., Infantes, D., 2011. Kinetic and stoichiometric modelling of acidogenic fermentation of glucose and fructose. Biomass and Bioenergy 35, 3877–3883.

Flamholz, A., Noor, E., Bar-Even, A., Milo, R., 2012. EQuilibrator - The biochemical thermodynamics calculator. Nucleic Acids Res. 40, 770–775.

Flotats, X., Palatsi, J., Ahring, B.K., Angelidaki, I., 2006. Identifiability study of the proteins degradation model, based on ADM1, using simultaneous batch experiments. Water Sci. Technol. 54, 31–39.

Fonknechten, N., Chaussonnerie, S., Tricot, S., Lajus, A., Andreesen, J.R., Perchat, N., Pelletier, E., Gouyvenoux, M., Barbe, V., Salanoubat, M., Le Paslier, D., Weissenbach, J., Cohen, G.N., Kreimeyer, A., 2010. Clostridium sticklandii, a specialist in amino acid degradation:Revisiting its metabolism through its genome sequence. BMC Genomics 11.

Gameiro, T., Sousa, F., Silva, F.C., Couras, C., Lopes, M., Louros, V., Nadais, H., Capela, I., 2015. Olive oil mill wastewater to volatile fatty acids: Statistical study of the acidogenic process. Water. Air. Soil Pollut. 226.

Gary, C., Frossard, J., Chenevard, D., 1995. Heat of combustion, degree of reduction and carbon content: 3 interrelated methods of estimating the construction cost of plant tissues. Agronomie 15, 59–69.

Garza-ramos, G., Perez-montfort, R., Rojo-dominguez, A., Gomez-puyou, M.T. De, Gomez-puyou, A., 1996. 1996-Garza-Ramos_Species-specific inhibition of homologous enzymes 120, 114–120.

Gaskell, W.H., 1886. On the Structure, Distribution and Function of the Nerves which innervate the Visceral and Vascular Systems. J. Physiol. 7, 1-80.9.

Geer, L.Y., Marchler-Bauer, A., Geer, R.C., Han, L., He, J., He, S., Liu, C., Shi, W., Bryant, S.H., 2010. The NCBI BioSystems database. Nucleic Acids Res. 38, 492–496.

Gernaey, K. V., 2015. A Perspective on PSE in Fermentation Process Development and Operation, Computer Aided Chemical Engineering. Elsevier.

Goelzer, A., Fromion, V., 2011. Bacterial growth rate reflects a bottleneck in resource allocation. Biochim. Biophys. Acta - Gen. Subj. 1810, 978–988.

Gombert, A.K., Nielsen, J., 2000. Mathematical modelling of metabolism. Curr. Opin. Biotechnol. 11, 180–186.

Gommers, P.J.F., Vanschie, B.J., Vandijken, J.P., Kuenen, J.G., 1988. Biochemical Limits to Microbial-Growth Yields - an Analysis of Mixed Substrate Utilization. Biotechnol Bioeng 32, 86–94.

Gonçalves, M.R., Costa, J.C., Pereira, M.A., Abreu, A.A., Alves, M.M., 2014. On the independence of hydrogen production from methanogenic suppressor in olive mill wastewater. Int. J. Hydrogen Energy 39, 6402–6406.

González-Cabaleiro, R., Lema, J.M., Rodríguez, J., 2015. Metabolic Energy-Based Modelling Explains Product Yielding in Anaerobic Mixed Culture

Fermentations. PLoS One 10, e0126739.

González-Cabaleiro, R., Lema, J.M., Rodríguez, J., Kleerebezem, R., 2013. Linking thermodynamics and kinetics to assess pathway reversibility in anaerobic bioprocesses. Energy Environ. Sci. 6, 3780–3789.

Gonzalez-Gil, L., Mauricio-iglesias, M., Carballa, M., Lema, J.M., 2018. Why are organic micropollutants not fully biotransformed ? A mechanistic modelling approach to anaerobic systems. Water Res. 142, 115–128.

Groeger, C., Wang, W., Sabra, W., Utesch, T., Zeng, A.-P., 2017. Metabolic and proteomic analyses of product selectivity and redox regulation in Clostridium pasteurianum grown on glycerol under varied iron availability. Microb. Cell Fact. 16, 64.

Guidotti, G.G., Borghetti, A.F., Gazzola, G.C., 1978. The Regulation Of Amino Acid Transport in Animal Cells. Biochim. Biophys. 515, 329–366.

Guo, X.M., Trably, E., Latrille, E., Carrère, H., Steyer, J.-P., 2010. Hydrogen production from agricultural waste by dark fermentation: A review. Int. J. Hydrogen Energy 35, 10660–10673.

Hallenbeck, P.C., Ghosh, D., 2009. Advances in fermentative biohydrogen production: the way forward? Trends Biotechnol 27, 287–297.

Hanselmann, K.W., 1991. Microbial energetics applied to waste repositories. Cell. Mol. Life Sci. 47, 645–687.

Helton, J.C., Davis, F.J., 2003. Latin hypercube sampling and the propagation of uncertainty in analyses of complex systems. Reliab. Eng. Syst. Saf. 81, 23–69.

Herrmann, G., Jayamani, E., Mai, G., Buckel, W., 2008. Energy conservation via electron-transferring flavoprotein in anaerobic bacteria. J Bacteriol 190, 784–791.

Heyne, R.I., de Vrij, W., Crielaard, W., Konings, W.N., 1991. Sodium ion-dependent amino acid transport in membrane vesicles of Bacillus stearothermophilus. J. Bacteriol. 173, 791–800.

Hoehler, T.M., Jørgensen, B.B., 2013. Microbial life under extreme energy limitation. Nat. Rev. Microbiol. 11, 83–94.

Hoelzle, R.D., Virdis, B., Batstone, D.J., 2014. Regulation Mechanisms in Mixed and Pure Culture Microbial Fermentation. Biotechnol. Bioeng. 111, 2139–

2154.

Horiuchi, J.I., Shimizu, T., Tada, K., Kanno, T., Kobayashi, M., 2002. Selective production of organic acids in anaerobic acid reactor by pH control. Bioresour. Technol. 82, 209–213.

Hu, H.W., He, J.Z., 2017. Comammox—a newly discovered nitrification process in the terrestrial nitrogen cycle. J. Soils Sediments 17, 2709–2717.

Hugo, H. v., Schoberth, S., Madan, V.K., Gottschalk, G., 1972. Coenzyme specificity of dehydrogenases and fermentation of pyruvate by clostridia. Arch. Mikrobiol. 87, 189–202.

Hui, S., Hwa, T., Erickson, D.W., Wang, J., Williamson, J.R., Silverman, J.M., Basan, M., Chen, S.S., 2015. Quantitative proteomic analysis reveals a simple strategy of global resource allocation in bacteria. Mol. Syst. Biol. 11, e784–e784.

Infantes, D., González del Campo, A., Villaseñor, J., Fernández, F.J., 2012. Kinetic model and study of the influence of pH, temperature and undissociated acids on acidogenic fermentation. Biochem. Eng. J. 66, 66–72.

Jackson, B.E., McInerney, M.J., 2002a. Anaerobic microbial metabolism can proceed close to thermodynamic limits. Nature 415, 454–456.

Jackson, B.E., McInerney, M.J., 2002b. Anaerobic microbial metabolism can proceed close to thermodynamic limits. Nature 415, 454–456.

Jänisch, T., Reinhardt, S., Pohsner, U., Böringer, S., Bolduan, R., Steinbrenner, J., Oechsner, H., 2019. Separation of volatile fatty acids from biogas plant hydrolysates. Sep. Purif. Technol. 223, 264–273.

Jansen, M.L.A., Bracher, J.M., Papapetridis, I., Verhoeven, M.D., de Bruijn, H., de Waal, P.P., van Maris, A.J.A., Klaassen, P., Pronk, J.T., 2017. Saccharomyces cerevisiae strains for second-generation ethanol production: from academic exploration to industrial implementation. FEMS Yeast Res. 17, 1–20.

Jiang, Y., Marang, L., Kleerebezem, R., Muyzer, G., van Loosdrecht, M.C.M., 2011. Polyhydroxybutyrate production from lactate using a mixed microbial culture. Biotechnol. Bioeng. 108, 2022–2035.

Johnson, K., Jiang, Y., Kleerebezem, R., Muyzer, G., Loosdrecht, M.C.M. Van, 2009. Enrichment of a Mixed Bacterial Culture with a High Polyhydroxyalkanoate Storage Capacity. Biomacromolecules 10, 670–676.

Jones, M.E., 1985. Conversion of glutamate to ornithine and proline: Pyrroline-5-carboxylate, a possible modulator of arginine requirements. J. Nutr. 115, 509–515.

Jungermann, K., Thauer, R.K., Leimenstoll, G., Decker, K., 1973. Function of reduced pyridine nucleotide-ferredoxin oxidoreductases in saccharolytic Clostridia. Biochim. Biophys. Acta - Bioenerg. 305, 268–280.

Kaminskas, E., Kimhi, Y., Magasanik, B., 1970. Urocanase and N-formimino-L-glutamate formiminohydrolase of Bacillus subtilis, two enzymes of the histidine degradation pathway. J. Biol. Chem. 245, 3536–3544.

Kapdan, I.K., Kargi, F., 2006. Bio-hydrogen production from waste materials. Enzyme Microb. Technol. 38, 569–582.

Kappler, O., Janssen, P.H., Kreft, J., Schink, B., 1997. Effects of alternative methyl group acceptors on the growth energetics of the 143, 1105–1114.

Karadag, D., Puhakka, J.A., 2010. Direction of glucose fermentation towards hydrogen or ethanol production through on-line pH control. Int. J. Hydrogen Energy 35, 10245–10251.

Kleerebezem, R., Joosse, B., Rozendal, R., Loosdrecht, M.C.M., 2015. Anaerobic digestion without biogas? Rev. Environ. Sci. Bio/Technology 14, 787–801.

Kleerebezem, R., Rodriguez, J., Temudo, M.F., van Loosdrecht, M.C., 2008. Modeling mixed culture fermentations; the role of different electron carriers. Water Sci Technol 57, 493–497.

Kleerebezem, R., van Loosdrecht, M.C.M., 2007. Mixed culture biotechnology for bioenergy production. Curr. Opin. Biotechnol. 18, 207–212.

Kleerebezem, R., Van Loosdrecht, M.C.M., 2010. A Generalized Method for Thermodynamic State Analysis of Environmental Systems. Crit. Rev. Environ. Sci. Technol. 40, 1–54.

Klein, B.C., de Mesquita Sampaio, I.L., Mantelatto, P.E., Filho, R.M., Bonomi, A., 2019. Beyond ethanol, sugar, and electricity: a critical review of product diversification in Brazilian sugarcane mills. Biofuels, Bioprod. Biorefining 13, 809–821.

Koonin, E. V., Wolf, Y.I., 2012. Evolution of microbes and viruses: a paradigm shift in evolutionary biology? Front. Cell. Infect. Microbiol. 2, 119.

Krämer, R., Kanbert, C., Hoischen, C., Ebbighausen, H., 1990. Uptake of glutamate in Corynebacterium glutamicum. Eur. J. Biochem. 194, 929–935.

Kreft, J.U., Griffin, B.M., González-Cabaleiro, R., 2020. Evolutionary causes and consequences of metabolic division of labour: why anaerobes do and aerobes don't. Curr. Opin. Biotechnol. 62, 80–87.

Kreimeyer, A., Perret, A., Lechaplais, C., Vallenet, D., Médigue, C., Salanoubat, M., Weissenbach, J., 2007. Identification of the last unknown genes in the fermentation pathway of lysine. J. Biol. Chem. 282, 7191–7197.

Kruger, N.J., Von Schaewen, A., 2003. The oxidative pentose phosphate pathway: Structure and organisation. Curr. Opin. Plant Biol. 6, 236–246.

Kubitschke, J., Lange, H., Strutz, H., 2014. Carboxylic Acids, Aliphatic. Ullmann's Encycl. Ind. Chem., Major Reference Works.

Kucek, L.A., Nguyen, M., Angenent, L.T., 2016. Conversion of L-lactate into n-caproate by a continuously fed reactor microbiome. Water Res. 93, 163–171.

Kuenen, J.G., 1983. The Role of Specialists and Generalists in Microbial Population Interactions, in: Blanch, H.W., Papoutsakis, E.T., Stephanopoulos, G. (Eds.), Foundations of Biochemical Engineering. American Chemical Society, pp. 229–251.

Kumar, G., Ponnusamy, V.K., Bhosale, R.R., Shobana, S., Yoon, J.J., Bhatia, S.K., Rajesh Banu, J., Kim, S.H., 2019. A review on the conversion of volatile fatty acids to polyhydroxyalkanoates using dark fermentative effluents from hydrogen production. Bioresour. Technol. 287, 121427.

Landeweerd, L., Surette, M., van Driel, C., 2011. From petrochemistry to biotech: A European perspective on the bio-based economy. Interface Focus 1, 189–195.

Lane, N., 2015. The vital question: why is life the way it is? Profile Books LTD, London.

LaRowe, D.E., Dale, A.W., Amend, J.P., Van Cappellen, P., 2012. Thermodynamic limitations on microbially catalyzed reaction rates. Geochim. Cosmochim. Acta 90, 96–109.

Lee, W.S., Chua, A.S.M., Yeoh, H.K., Ngoh, G.C., 2014. A review of the production and applications of waste-derived volatile fatty acids. Chem. Eng. J. 235, 83–99.

Lee, Y.J., Jeong, K.J., 2015. Challenges to production of antibodies in bacteria and yeast. J. Biosci. Bioeng. 120, 483–490.

Lemos, P.C., Serafim, L.S., Reis, M.A.M., 2006. Synthesis of polyhydroxyalkanoates from different short-chain fatty acids by mixed cultures submitted to aerobic dynamic feeding. J. Biotechnol. 122, 226–238.

Lengeler, J.W., Gerhart, D., Schlegel, H.G., Georg, T. V, Thieme, G., 1999. Biology of the Prokaryotes, 1st ed. Stuttgart.

Li, B., Taniguchi, D., Gedara, J.P., Gogulancea, V., Gonzalez-Cabaleiro, R., Chen, J., McGough, A.S., Ofiteru, I.D., Curtis, T.P., Zuliani, P., 2019. NUFEB: A massively parallel simulator for individual-based modelling of microbial communities. PLoS Comput. Biol. 15, e1007125.

Li, F., Hinderberger, J., Seedorf, H., Zhang, J., Buckel, W., Thauer, R.K., 2008. Coupled ferredoxin and crotonyl coenzyme A (CoA) reduction with NADH catalyzed by the butyryl-CoA dehydrogenase/Etf complex from Clostridium kluyveri. J Bacteriol 190, 843–850.

Li, Z., Nimtz, M., Rinas, U., 2014. The metabolic potential of Escherichia coli BL21 in defined and rich medium. Microb. Cell Fact. 13, 1–17.

Lim, S.J., Kim, B.J., Jeong, C.M., Choi, J. dal rae, Ahn, Y.H., Chang, H.N., 2008. Anaerobic organic acid production of food waste in once-a-day feeding and drawing-off bioreactor. Bioresour. Technol. 99, 7866–7874.

Lin, Y., de Kreuk, M., van Loosdrecht, M.C.M., Adin, A., 2010. Characterization of alginate-like exopolysaccharides isolated from aerobic granular sludge in pilot-plant. Water Res. 44, 3355–3364.

Liu, J., Rost, B., 2001. Comparing function and structure between entire proteomes. Protein Sci. 10, 1970–1979.

Liu, K., Atiyeh, H.K., Pardo-Planas, O., Ezeji, T.C., Ujor, V., Overton, J.C., Berning, K., Wilkins, M.R., Tanner, R.S., 2015. Butanol production from hydrothermolysis-pretreated switchgrass: Quantification of inhibitors and detoxification of hydrolyzate. Bioresour. Technol. 189, 292–301.

Liu, N., Santala, S., Stephanopoulos, G., 2020. ScienceDirect Mixed carbon substrates : a necessary nuisance or a missed opportunity ? Curr. Opin. Biotechnol. 62, 15–21.

Loddeke, M., Schneider, B., Oguri, T., Mehta, I., Xuan, Z., Reitzer, L., 2017. Anaerobic Cysteine Degradation and Potential Metabolic Coordination in Salmonella enterica and Escherichia coli. J. Bacteriol. 199, 1–16.

Mahadevan, R., Edwards, J.S., Doyle, F.J., 2002. Dynamic flux balance analysis of diauxic growth. Biophys. J. 83, 1331–1340.

Mans, R., Daran, J.M.G., Pronk, J.T., 2018. Under pressure: evolutionary engineering of yeast strains for improved performance in fuels and chemicals production. Curr. Opin. Biotechnol. 50, 47–56.

Martin, W.F., 2012. Hydrogen, metals, bifurcating electrons, and proton gradients: The early evolution of biological energy conservation. FEBS Lett. 586, 485–493.

McCarty, P.L., 2007. Thermodynamic electron equivalents model for bacterial yield prediction: Modifications and comparative evaluations. Biotechnol. Bioeng. 97, 377–388.

Meinecke, B., Bertram, J., Gottschalk, G., 1989. Purification and characterization of the pyruvate-ferredoxin oxidoreductase from Clostridium acetobutylicum. Arch. Microbiol. 152, 244–250.

Meister, A., 2016. On the Enzymology of Amino Acid Transport Published by : American Association for the Advancement of Science Stable URL : http://www.jstor.org/stable/1735289 Linked references are available on JSTOR for this article : - On tlle Enzymology of Amino Acid Tr 180, 33–39.

Melendez-Hevia, E., 1990. The game of the pentose phosphate cycle: A mathematical approach to study the optimization in design of metabolic pathways during evolution. Biomed. Biochim. Acta 49, 903–916.

Millat, T., Janssen, H., Thorn, G.J., King, J.R., Bahl, H., Fischer, R.J., Wolkenhauer, O., 2013. A shift in the dominant phenotype governs the pH-induced metabolic switch of Clostridium acetobutylicumin phosphate-limited continuous cultures. Appl. Microbiol. Biotechnol. 97, 6451–6466.

Mnif, S., Chamkha, M., Labat, M., Sayadi, S., 2011. Simultaneous hydrocarbon biodegradation and biosurfactant production by oilfield-selected bacteria. J. Appl. Microbiol. 111, 525–536.

Mohd-Zaki, Z., Bastidas-Oyanedel, J., Lu, Y., Hoelzle, R., Pratt, S., Slater, F., Batstone, D., 2016. Influence of pH Regulation Mode in Glucose

Fermentation on Product Selection and Process Stability. Microorganisms 4, 2.

Molenaar, D., Van Berlo, R., De Ridder, D., Teusink, B., 2009. Shifts in growth strategies reflect tradeoffs in cellular economics. Mol. Syst. Biol. 5, 1–10.

Mori, M., Hwa, T., Martin, O.C., De Martino, A., Marinari, E., 2016. Constrained Allocation Flux Balance Analysis. PLoS Comput. Biol. 12, 1–24.

Mosey, F.E., 1983. Mathematical modelling of the anaerobic digestion process: Regulatory mechanisms for the formation of short-chain volatile acids from glucose. Water Sci. Technol. 15, 209–232.

Nielsen, J., Villadsen, J., 1994. Bioreaction Engineering Principles, First. ed. Springer US, New York.

Nilsson, A., Nielsen, J., 2016. Metabolic Trade-offs in Yeast are Caused by F1F0-ATP synthase. Sci. Rep. 6, 1–11.

Ningthoujam, S.S., Talukdar, A.D., Sarker, S.D., Nahar, L., Choudhury, M.D., 2018. Prediction of Medicinal Properties Using Mathematical Models and Computation, and Selection of Plant Materials, Computational Phytochemistry. Elsevier Inc.

Noor, E., Haraldsdóttir, H.S., Milo, R., Fleming, R.M.T., 2013. Consistent Estimation of Gibbs Energy Using Component Contributions. PLoS Comput. Biol. 9, e1003098.

O'Malley, M.A., 2008. "Everything is everywhere: but the environment selects": ubiquitous distribution and ecological determinism in microbial biogeography. Stud. Hist. Philos. Sci. Part C Stud. Hist. Philos. Biol. Biomed. Sci. 39, 314–325.

Octave, S., Thomas, D., 2009. Biorefinery: Toward an industrial metabolism. Biochimie 91, 659–664.

Oh, S.T., Martin, A.D., 2007. Thermodynamic equilibrium model in anaerobic digestion process. Biochem. Eng. J. 34, 256–266.

Ohnishi, A., 2015. Megasphaera as lactate-utilizing hydrogen-producing bacteria, in: Kalia, V.C. (Ed.), Microbial Factories: Biofuels, Waste Treatment: Volume 1. Tokyo, pp. 47–71.

Oxender, D.L., Christensen, H.N., 1963. Distinct Mediating Amino Systems for the Transport Acids by the Ehrlich Cell * of Neutral 238.

Padan, E., Zilberstein, D., Schuldiner, S., 1981. pH homesstasis in bacteria. BBA - Rev. Biomembr. 650, 151–166.

Pavlostathis, S.G., Giraldo-Gomez, E., 1991. Kinetics of anaerobic treatment: A critical review. Crit. Rev. Environ. Control 21, 411–490.

Payot, S., Guedon, E., Gelhaye, E., Petitdemange, H., 1999. Induction of lactate production associated with a decrease in NADH cell content enables growth resumption of Clostridium cellulolyticum in batch cultures on cellobiose. Res. Microbiol. 150, 465–473.

Peekhaus, N., Conway, T., 1998. What ' s for Dinner ?: Entner-Doudoroff Metabolism in Escherichia coli. Society 180, 3495–3502.

Perez-Garcia, O., Lear, G., Singhal, N., 2016. Metabolic network modeling of microbial interactions in natural and engineered environmental systems. Front. Microbiol. 7.

Peters, J.W., Miller, A.F., Jones, A.K., King, P.W., Adams, M.W.W., 2016. Electron bifurcation. Curr. Opin. Chem. Biol. 31, 146–152.

Peters, V., Janssen, P., Conrad, R., 2006. Efficiency of hydrogen utilization during unitrophic and mixotrophic growth of Acetobacterium woodii on hydrogen and lactate in the chemostat.

Petitdemange, H., Cherrier, C., Raval, R., Gay, R., 1976. Regulation of the NADH and NADPH-ferredoxin oxidoreductases in clostridia of the butyric group. Biochim Biophys Acta 421, 334–337.

Pfeiffer, T., Bonhoeffer, S., 2004. Evolution of cross-feeding in microbial populations. Am. Nat. 163.

Pfeiffer, T., Schuster, S., Bonhoeffer, S., 2001. Cooperation and competition in the evolution of ATP-producing pathways. Science (80-.). 293, 1436.

Poole, R.J., 1978. Energy Coupling for Membrane Transport. Annu. Rev. Plant Physiol. 29, 437–460.

Poolman, B., Driessen, A.J., Konings, W.N., 1987. Regulation of solute transport in streptococci by external and internal pH values. Microbiol. Rev. 51, 498–508.

Prusiner, S., Milner, L., 1970. A rapid radioactive assay for glutamine synthetase,

glutaminase, asparagine synthetase, and asparaginase. Anal. Biochem. 37, 429–438.

Rafrafi, Y., Trably, E., Hamelin, J., Latrille, E., Meynial-Salles, I., Benomar, S., Giudici-Orticoni, M.T., Steyer, J.P., 2013. Sub-dominant bacteria as keystone species in microbial communities producing bio-hydrogen. Int. J. Hydrogen Energy 38, 4975–4985.

Rai, R., Keshavarz, T., Roether, J.A., Boccaccini, A.R., Roy, I., 2011. Medium chain length polyhydroxyalkanoates, promising new biomedical materials for the future. Mater. Sci. Eng. R Reports 72, 29–47.

Ramsay, I.R., 1997. Modelling and Control of High-Rate Anaerobic Wastewater Treatment Systems. The University of Queensland.

Ramsay, I.R., Pullammanappallil, P.C., 2001. Protein degradation during anaerobic wastewater treatment: Derivation of stoichiometry. Biodegradation 12, 247–257.

Rasmussen, H., Sørensen, H.R., Meyer, A.S., 2014. Formation of degradation compounds from lignocellulosic biomass in the biorefinery: Sugar reaction mechanisms. Carbohydr. Res. 385, 45–57.

Reddy, M.V., Mohan, S.V., Chang, Y.C., 2018. Medium-Chain Fatty Acids (MCFA) Production Through Anaerobic Fermentation Using Clostridium kluyveri: Effect of Ethanol and Acetate. Appl. Biochem. Biotechnol. 185, 594–605.

Ren, N.-Q., Zhao, L., Chen, C., Guo, W.-Q., Cao, G.-L., 2016. A review on bioconversion of lignocellulosic biomass to H2: Key challenges and new insights. Bioresour. Technol. 215, 92–99.

Rodriguez, J., Kleerebezem, R., Lema, J.M., van Loosdrecht, M.C., 2006. Modeling product formation in anaerobic mixed culture fermentations. Biotechnol Bioeng 93, 592–606.

Rombouts, J.L., Kranendonk, E., Regueira, A., Weissbrodt, D., Kleerebezem, R., van Loosdrecht, M.C.M., 2020. Selecting for lactic acid producing and utilising bacteria in anaerobic enrichment cultures. Biotechnol Bioeng 117, 1281-1293.

Rombouts, J.L., Mos, G., Weissbrodt, D.G., Kleerebezem, R., van Loosdrecht, M.C.M., 2019a. Diversity and metabolism of xylose and glucose fermenting microbial communities in sequencing batch or continuous culturing. FEMS

Microbiol. Ecol. 95.

Rombouts, J.L., Mos, G., Weissbrodt, D.G., Kleerebezem, R., Van Loosdrecht, M.C.M., 2019b. The impact of mixtures of xylose and glucose on the microbial diversity and fermentative metabolism of sequencing-batch or continuous enrichment cultures. FEMS Microbiol. Ecol. 95, 1–10.

Saady, N.M.C., 2013. Homoacetogenesis during hydrogen production by mixed cultures dark fermentation: Unresolved challenge. Int. J. Hydrogen Energy 38, 13172–13191.

Sabra, W., Zeng, A.P., Deckwer, W.D., 2001. Bacterial alginate: Physiology, product quality and process aspects. Appl. Microbiol. Biotechnol. 56, 315–325.

Sakai, S., Nakashimada, Y., Inokuma, K., Kita, M., Okada, H., Nishio, N., 2005. Acetate and ethanol production from H2 and CO2 by Moorella sp. using a repeated batch culture.

Saltelli, A., Ratto, M., Andres, T., Campolongo, F., Cariboni, J., Gatelli, D., Saisana, M., Tarantola, S., 2008. Global Sensitivity Analysis: The Primer. John Wiley & Sons, Ltd, West Sussex.

Satpute, S.K., Banat, I.M., Dhakephalkar, P.K., Banpurkar, A.G., Chopade, B.A., 2010. Biosurfactants, bioemulsifiers and exopolysaccharides from marine microorganisms. Biotechnol. Adv. 28, 436–450.

Saum, S.H., Müller, V., 2007. Salinity-dependent switching of osmolyte strategies in a moderately halophilic bacterium: Glutamate induces proline biosynthesis in Halobacillus halophilus. J. Bacteriol. 189, 6968–6975.

Sawers, G., 1998. The anaerobic degradation of L-serine and L-threonine in enterobacteria: Networks of pathways and regulatory signals. Arch. Microbiol. 171, 1–5.

Schomburg, I., Chang, A., Hofmann, O., Ebeling, C., Ehrentreich, F., Schomburg, D., 2002. BRENDA: A resource for enzyme data and metabolic information. Trends Biochem. Sci. 27, 54–56.

Schuetz, R., Kuepfer, L., Sauer, U., 2007. Systematic evaluation of objective functions for predicting intracellular fluxes in Escherichia coli. Mol. Syst. Biol. 3.

Schumacher, R., 2018. Metabolic trade-offs arising from increased free energy conservation in Saccharomyces cerevisiae. Delft University of Technology.

Scott, M., Klumpp, S., Mateescu, E.M., Hwa, T., 2014. Emergence of robust growth laws from optimal regulation of ribosome synthesis. Mol. Syst. Biol. 10, 747.

Seeliger, S., Janssen, P.H., Schink, B., 2002. Energetics and kinetics of lactate fermentation to acetate and propionate via methylmalonyl-CoA or acrylyl-CoA. FEMS Microbiol. Lett. 211, 65–70.

Seif, Y., Sonal, K., Hefner, Y., Anand, A., Yang, L., 2020. Metabolic and genetic basis for auxotrophies in Gram-negative species.

Shen, C.R., Lan, E.I., Dekishima, Y., Baez, A., Cho, K.M., Liao, J.C., 2011. Driving forces enable high-titer anaerobic 1-butanol synthesis in Escherichia coli. Appl. Environ. Microbiol. 77, 2905–2915.

Shi, E., Li, J., Zhang, M., 2019. Application of IWA Anaerobic Digestion Model No. 1 to simulate butyric acid, propionic acid, mixed acid, and ethanol type fermentative systems using a variable acidogenic stoichiometric approach. Water Res. 161, 242–250.

Shilling, M., Matt, L., Rubin, E., Visitacion, M.P., Haller, N.A., Grey, S.F., Woolverton, C.J., 2013. Antimicrobial effects of virgin coconut oil and its medium-chain fatty acids on clostridium difficile. J. Med. Food 16, 1079–1085.

Siegrist, H., Vogt, D., Garcia-Heras, J.L., Gujer, W., 2002. Mathematical model for meso- and thermophilic anaerobic sewage sludge digestion. Environ. Sci. Technol. 36, 1113–1123.

Simon, H., Bader, J., Günther, H., Neumann, S., Thanos, J., 1985. Chirale Verbindungen durch biokatalytische Reduktionen. Angew. Chemie 97, 541–555.

Sims, G.K., Sommers, L.E., Konopka, A., 1986. Degradation of pyridine by Micrococcus luteus isolated from soil. Appl. Environ. Microbiol. 51, 963–968.

Singhania, R.R., Patel, A.K., Christophe, G., Fontanille, P., Larroche, C., 2013. Biological upgrading of volatile fatty acids, key intermediates for the valorization of biowaste through dark anaerobic fermentation. Bioresour. Technol. 145, 166–174.

Smid, E.J., Lacroix, C., 2013. Microbe-microbe interactions in mixed culture food fermentations. Curr. Opin. Biotechnol. 24, 148–154.

Spirito, C.M., Richter, H., Rabaey, K., Stams, A.J.M., Angenent, L.T., 2014. Chain

elongation in anaerobic reactor microbiomes to recover resources from waste. Curr. Opin. Biotechnol. 27, 115–122.

Stams, A.J.M., Plugge, C.M., 2009. Electron transfer in syntrophic communities of anaerobic bacteria and archaea. Nat. Rev. Microbiol. 7, 568–577.

Steinbusch, K.J.J., Hamelers, H.V.M., Plugge, C.M., Buisman, C.J.N., 2011. Biological formation of caproate and caprylate from acetate: Fuel and chemical production from low grade biomass. Energy Environ. Sci. 4, 216–224.

Stouthamer, A.H., 1973. A theoretical study on the amount of ATP required for synthesis of microbial cell material. Antonie Van Leeuwenhoek 39, 545–565.

Straub, M., Demler, M., Weuster-Botz, D., Dürre, P., 2014. Selective enhancement of autotrophic acetate production with genetically modified Acetobacterium woodii. J. Biotechnol. 178, 67–72.

Strazzera, G., Battista, F., Garcia, N.H., Frison, N., Bolzonella, D., 2018. Volatile fatty acids production from food wastes for biorefinery platforms: A review. J. Environ. Manage. 226, 278–288.

Taffs, R., Aston, J.E., Brileya, K., Jay, Z., Klatt, C.G., McGlynn, S., Mallette, N., Montross, S., Gerlach, R., Inskeep, W.P., Ward, D.M., Carlson, R.P., 2009. In Silico approaches to study mass and energy flows in microbial consortia: A syntrophic case study. BMC Syst. Biol. 3, 1–16.

Taherzadeh, M.J., Keikhosro, K., 2008. Bioethanol: Market and Production Processes, in: Nag, A. (Ed.), Biofuels Refining and Performance. The McGraw-Hill Companies, Inc., pp. 69–106.

Tan, R., Miyanaga, K., Uy, D., Tanji, Y., 2012. Effect of heat-alkaline treatment as a pretreatment method on volatile fatty acid production and protein degradation in excess sludge, pure proteins and pure cultures. Bioresour. Technol. 118, 390–398.

Temudo, M.F., Kleerebezem, R., van Loosdrecht, M., 2007. Influence of the pH on (open) mixed culture fermentation of glucose: A chemostat study. Biotechnol. Bioeng. 98, 69–79.

Temudo, M.F., Mato, T., Kleerebezem, R., Van Loosdrecht, M.C.M., 2009. Xylose anaerobic conversion by open-mixed cultures. Appl. Microbiol. Biotechnol. 82, 231–239.

Temudo, M.F., Muyzer, G., Kleerebezem, R., Van Loosdrecht, M.C.M., 2008a. Diversity of microbial communities in open mixed culture fermentations: Impact of the pH and carbon source. Appl. Microbiol. Biotechnol. 80, 1121–1130.

Temudo, M.F., Poldermans, R., Kleerebezem, R., Van Loosdrecht, M.C.M., 2008b. Glycerol fermentation by (open) mixed cultures: A chemostat study. Biotechnol. Bioeng. 100, 1088–1098.

Thauer, R.K., Jungermann, K., Decker, K., 1977. Energy conservation in chemotrophic anaerobic bacteria. Bacteriol. Rev. 41, 100–180.

Thomas, T.D., Ellwood, D.C., Longyear, V.M.C., 1979. Change from homo- to heterolactic fermentation by Streptococcus lactis resulting from glucose limitation in anaerobic chemostat cultures. J. Bacteriol. 138, 109–117.

Tobajas, M., Garcia-Calvo, E., 1999. Determination of biomass yield for growth of Candida utilis on glucose: Black box and metabolic descriptions. World J. Microbiol. Biotechnol. 15, 431–438.

Tommaso, G., Domingues, M.R., Ribeiro, R., Varesche, M.B.A., Zaiat, M., Foresti, E., 2013. Anaerobic degradation of protein: Simplified kinetic modelling and microbial dynamics. Water. Air. Soil Pollut. 224.

Tuck, C.O., Pérez, E., Horváth, I.T., Sheldon, R.A., Poliakoff, M., 2012. Valorization of Biomass : Deriving More Value from Waste. Science (80-.). 337, 695–699.

Uematsu, H., Sato, N., Hossain, M.Z., Ikeda, T., Hoshino, E., 2003. Degradation of arginine and other amino acids by butyrate-producing asaccharolytic anaerobic Gram-positive rods in periodontal pockets. Arch. Oral Biol. 48, 423–429.

Unden, G., Strecker, A., Kleefeld, A., Kim, O. Bin, 2013. C4-Dicarboxylate Utilization in Aerobic and Anaerobic Growth. EcoSal Plus.

Vangsgaard, A.K., Mauricio-Iglesias, M., Gernaey, K. V., Smets, B.F., Sin, G., 2012. Sensitivity analysis of autotrophic N removal by a granule based bioreactor: Influence of mass transfer versus microbial kinetics. Bioresour. Technol. 123, 230–241.

Vazquez, A., Oltvai, Z.N., 2011. Molecular crowding defines a common origin

for the warburg effect in proliferating cells and the lactate threshold in muscle physiology. PLoS One 6, 1–9.

Venkata Mohan, S., Nikhil, G.N., Chiranjeevi, P., Nagendranatha Reddy, C., Rohit, M. V., Kumar, A.N., Sarkar, O., 2016. Waste biorefinery models towards sustainable circular bioeconomy: Critical review and future perspectives. Bioresour. Technol. 215, 2–12.

Wang, Y., Tashiro, Y., Sonomoto, K., 2015. Fermentative production of lactic acid from renewable materials: Recent achievements, prospects, and limits. J. Biosci. Bioeng. 119, 10–18.

Waygood, B.E., Sanwal, B.D., 1974. The Control of Pyruvate Kinases of Escherichia. J. Biol. Chem. 249, 265–274.

Wei, D., Xue, X., Yan, L., Sun, M., Zhang, G., Shi, L., Du, B., 2014. Effect of influent ammonium concentration on the shift of full nitritation to partial nitrification in a sequencing batch reactor at ambient temperature. Chem. Eng. J. 235, 19–26.

White, D., Drummond, J., Fuqua, C., 2012. The physiology and biochemistry of prokaryotes, 4th ed. Oxford University Press, New York.

Yin, J., Yu, X., Wang, K., Shen, D., 2016. Acidogenic fermentation of the main substrates of food waste to produce volatile fatty acids. Int. J. Hydrogen Energy 41, 21713–21720.

Yu, H.G., Fang, H.H., 2002. Acidogenesis of dairy wastewater at various pH levels. Water Sci. Technol. 45, 201–206.

Yu, H.Q., Fang, H.H.P., 2003. Acidogenesis of gelatin-rich wastewater in an upflow anaerobic reactor: influence of pH and temperature. Water Res. 37, 55–66.

Yu, H.Q., Fang, H.H.P., Gu, G.W., 2002. Comparative performance of mesophilic and thermophilic acidogenic upflow reactors. Process Biochem. 38, 447–454.

Yu, H.Q., Mu, Y., 2006. Biological hydrogen production in a UASB reactor with granules. II: Reactor performance in 3-year operation. Biotechnol. Bioeng. 94, 988–995.

Zacharof, M.P., Lovitt, R.W., 2014. Recovery of volatile fatty acids (VFA) from complex waste effluents using membranes. Water Sci. Technol. 69, 495–503.

Zeng, H., Yang, A., 2019. Modelling overflow metabolism in Escherichia coli with flux balance analysis incorporating differential proteomic efficiencies of energy pathways. BMC Syst. Biol. 13, 1–18.

Zhang, F., Zhang, Y., Chen, M., van Loosdrecht, M.C., Zeng, R.J., 2013. A modified metabolic model for mixed culture fermentation with energy conserving electron bifurcation reaction and metabolite transport energy. Biotechnol Bioeng 110, 1884–1894.

Zhang, M., Wu, H., Chen, H., 2014. Coupling of polyhydroxyalkanoate production with volatile fatty acid from food wastes and excess sludge. Process Saf. Environ. Prot. 92, 171–178.

Zhuang, K., Izallalen, M., Mouser, P., Richter, H., Risso, C., Mahadevan, R., Lovley, D.R., 2011. Genome-scale dynamic modeling of the competition between Rhodoferax and Geobacter in anoxic subsurface environments. ISME J. 5, 305–316.

Zoetemeyer, R.J., van den Heuvel, J.C., Cohen, A., 1982. pH influence on acidogenic dissimilation of glucose in an anaerobic digestor. Water Res. 16, 303–311.

Zomorrodi, A.R., Islam, M.M., Maranas, C.D., 2014. D-OptCom: Dynamic Multi-level and Multi-objective Metabolic Modeling of Microbial Communities. ACS Synth. Biol. 3, 247–257.

Zomorrodi, A.R., Maranas, C.D., 2012. OptCom: A multi-level optimization framework for the metabolic modeling and analysis of microbial communities. PLoS Comput. Biol. 8.

USC
UNIVERSIDADE
DE SANTIAGO
DE COMPOSTELA

LIST OF PUBLICATIONS

Scientific journals

- R. Bevilacqua, A. Regueira, M. Mauricio-Iglesias, J. M. Lema, M. Carballa. Protein composition determines the preferential consumption of amino acids during anaerobic mixed-culture fermentation. *Water Research*. Submitted.
- A. Regueira, R. Bevilacqua, M. Mauricio-Iglesias, M. Carballa, J. M. Lema. Computer aided design of protein anaerobic fermentation into volatile fatty acids. *Water Researcch*. Submitted. **Chapter 7** is based on this publication.
- A. Regueira, J. L. Rombouts, S. A. Wahl, M. Maurico-Iglesias, J. M. Lema, R. Kleerebezem. Resource allocation explains lactic acid production in mixed-culture anaerobic fermentations. *Biotecehnology and Bioengineering*. Submitted. **Chapter 4** is based on this publication.
- J. L. Rombouts, E. M. M. Kranendonk, A. Regueira, D. G. Weissbrodt, R. Kleerebezem, M. C. M. Van Loosdrecht. Selecting for lactic acid producing and utilising bacteria in anaerobic enrichment cultures. *Biotechnology and Bioengineering*, 117(5) 1281-1293.
- A. Regueira, R. Bevilacqua, J. M. Lema, M. Carballa, M. Mauricio-Iglesias (2020). A metabolic model for targeted volatile fatty acids production by cofermentation of carbohydrates and proteins. *Bioresource Technology*, 298, 122535. **Chapter 6** is based on this publication.
- A. Regueira, J. M. Lema, M. Carballa, M. Mauricio-Iglesias (2020). Metabolic modeling for predicting VFA production from protein-rich substrates by mixed-culture fermentation. *Biotechnology and Bioengineering,* 117(1) 73-84. **Chapter 5** is based on this publication.
- A. Regueira, R. Bevilacqua, J. M. Lema, M. Carballa, M. Mauricio-Iglesias (2019). Targeted conversion of protein and glucose waste streams to volatile fatty acids by metabolic models. *IFAC-PapersOnLine*. 52 (26), 175-180.

- A. Regueira, R. González-Cabaleiro, I. D. Ofiteru, J. Rodríguez, J. M. Lema (2018). Electron bifurcation mechanism and homoacetogenesis explain products yields in mixed culture anaerobic fermentations. *Water Research*. 141, 349-356. **Chapter 3** is based on this publication.

Congress proceedings

Oral contributions

- A. Regueira, R. Bevilacqua, J. M. Lema Rodicio, M. Carballa, M. Mauricio-Iglesias. Targeted conversion of protein and glucose waste streams to volatile fatty acids by metabolic models. *8th IFAC Conference on Foundations of Systems Biology in Engineering (FOSBE 2019)*. València (Spain), October 2019.
- R. Bevilacqua, A. Regueira, M. Mauricio-Iglesias, J. M. Lema, M. Carballa. Targeting specific volatile fatty acid production through pH shifts during protein fermentation. *3rd IWA Resource Recovery Conference*. Venice (Italy), September 2019.
- R. Bevilacqua, A. Regueira, M. Mauricio-Iglesias, J. M. Lema, M. Carballa. Evaluation of protein composition influence on yields and selectivity of volatile fatty acids production. *16th IWA World Conference on Anaerobic Digestion (AD16)*. Delft (The Netherlands), June 2019.
- A. Regueira, R. Bevilacqua, J. M. Lema Rodicio, M. Carballa, M. Mauricio-Iglesias. Modelling VFA production kinetics from protein-rich industrial wastes. *16th IWA World Conference on Anaerobic Digestion (AD16)*. Delft (The Netherlands), June 2019.
- A. Regueira, R. Bevilacqua, J. M. Lema Rodicio, M. Carballa, M. Mauricio-Iglesias. Modelling the production of VFA from proteins by mixed-culture fermentations. *Congreso Nacional de Biotecnología (BIOTEC 2019)*. Vigo (Spain), June 2019.
- A. Regueira, S. Tejedor-Sanz, M. Mauricio-Iglesias, A. Esteve-Núñez, J. M. Lema. Insights into the effect of a biocathode on driving mixed-culture fermentations under low electron recovery. *4th European Meeting*

of the International Society for Microbial Electrochemistry and Technology (EU-ISMET 4). Newcastle upon Tyne (United Kingdom), September 2018.

- A. Regueira, R. González-Cabaleiro, D. Ofiteru, J. Rodríguez, J. M. Lema. Electron bifurcation mechanisms and homoacetogenesis explain producto yields in mixed culture anaerobic fermentations. *15th IWA World Conference on Anaerobic Digestion (AD15)*. Beijing (China), October 2017.

- A. Regueira, M. Mauricio-Iglesias, M. Carballa, J. M. Lema. BIOCHEM: A new methodology for designing mixed-culture bioprocesses assisted with bioenergetic models. *10th World Congress of Chemical Engineering (WCCE 10)*. Barcelona (Spain), October 2017.

Poster contributions

- A. Regueira, J. L. Rombouts, S. A. Wahl, M. Mauricio-Iglesias, J. M. Lema, R. Kleerebezem. AN insight on the production of lactic acid form carbohydrate-rich wastewaters. *4th International Conference on Biogas Microbiology*. Braga (Portugal), September 2020.

- R. Bevilacqua, A. Regueira, M. Mauricio-Iglesias, J. M. Lema, M. Carballa. Steering volatile fatty acids production during protein fermentation by adjusting substrate composition and pH. *Congreso Nacional de Biotecnología (BIOTEC 2019)*. Vigo (Spain), June 2019.

- A. Regueira, R. Bevilacqua, M. Mauricio-Iglesias, J. M. Lema, M. Carballa. Designing mixed-culture bioprocesses by means of bioenergetics models. *Symposium Novel Anaerobes 2017*. Braga (Portugal), November 2017.

- A. Taboada-Santos, A. Regueira, I. Rodríguez-Verde, A. Sánchez, M. Carballa, J. M. Lema. Steering transition from anaerobic mono-digestion of sewage sludge to co-digestion. *15th IWA World Conference on Anaerobic Digestion (AD15)*. Beijing (China), October 2017.